THE UNIVERSITY
of EDINBURGH

Coordination of cell differentiation and mitochondrial development in *Trypanosoma brucei*

Gloria Amegatcher

Doctor of Philosophy

The University of Edinburgh

2019

Abstract

Trypanosomes are unicellular parasites of humans and livestock, characterised by a single mitochondrion and a highly complex mitochondrial DNA network, the kinetoplast. *Trypanosoma brucei* causes human African trypanosomiasis (HAT, or sleeping sickness) and Nagana in animals, often lethal diseases transmitted by tsetse flies in sub-Saharan Africa. The trypanosome mitochondrial respiratory system involved in energy production comprises of the five classical complexes (I-V); and in addition, a type 2 NADH:ubiquinone oxidoreductase, a glycerol-3-phosphate dehydrogenase and a trypanosome alternative oxidase. Some subunits for respiratory complexes I, III, IV and V are encoded in the kinetoplast DNA. *T. brucei* encodes genes for complex I; null mutants of complex I (cI) in monomorphic bloodstream form background and RNAi in procyclic cells have not shown any growth defects. Akinetoplastic stumpy cells have shorter life span which could be due to absence of mitochondrially encoded subunits and thus cannot express functional NADH dehydrogenase. Moreover, BF parasites in adipose tissue appear to upregulate pathway for beta-oxidation, which is expected to increase demand for NADH dehydrogenase activity. Little is known about the metabolism and bioenergetics of cI in stumpy forms. Mitochondrial activity changes across the life cycle stages of the parasite. The parasite life stages include slender and stumpy forms (found in the mammalian bloodstream) and procyclic form (found in the tsetse fly). The mammalian bloodstream stage parasite does not express respiratory complexes III and IV and generates most if not all ATP via glycolysis; the insect stage parasite generates most ATP mitochondrially. Thus, coordination of the expression patters for nuclearly and mitochondrially encoded respiratory chain subunits is essential for parasite life cycle progression. In organisms such as yeast, mammals and plants, 'mitochondrial retrograde signalling' pathways, including the 'unfolded protein response (UPR^{mt}), convey information on the functional status of this organelle to the nucleus and modulate expression of nuclear genes accordingly. It is not known if similar signalling pathways exist in trypanosomes.

This thesis investigated two questions:

1. Does complex I play an important role in stumpy and/or in cells residing in adipose tissue?

2. Does retrograde signalling pathway exists in *T. brucei*, lack of mitochondrial genome results in changes in nuclear gene expression?

To address the first question, the goal was to generate genetic null mutants for key nuclearly encoded cI subunits (*NUBM* or *NUKM*) in pleomorphic (i.e. differentiation competent) *Trypanosoma brucei brucei* cell line EATRO 1125. Next, the ability of these knockout cell lines to differentiate and to reside in adipose issue would be monitored. Unfortunately, I could not generate a cI null mutant in pleomorphic background as I subsequently determined that the parental cell line used was not fully pleomorphic in mice.

Even though the null mutant generated for complex I were not fully pleomorphic, I still investigated their survival in adipose tissue. Results showed that these null mutants were able to reside in adipose tissue. I further probed this by using pleomorphic cell lines devoid of mitochondrial DNA (akinetoplastic cell lines (AK)), which are also cI deficient as all seven mitochondrially encoded subunits of this complex are absent. These AK were able to differentiate in both blood and adipose tissue. The AK seems to present more in the adipose tissue when compared with the wild type. Coinfection with AK and WT together in mice showed that they both migrate from blood into adipose tissue. I observed that the ratio of WT/AK in blood is much higher than in adipose tissue. Moreover, blood/AT balance in AK is shifted towards AT, compared to WT.

To explore potential retrograde signalling pathways in *T. brucei,* we compared the nuclear transcriptome of a wild type strain with an AK mutant, before and after differentiation from the slender to the stumpy form (a transitional stage on route to differentiation to the insect stage). This was done by RNA-sequencing.

In WT and AK parasites, genes showed significant upregulation in stumpy forms (we considered a difference of $\geq$ 2-fold with a p-value $\leq$ 0.05 as significant) in comparison to WT. Most of these genes were hypothetical proteins. Genes involved in the glycolytic pathway were generally downregulated in stumpy cells. We also observed robust downregulation in stumpy cells of numerous histones and of two genes involved in kinetoplast maintenance, mitochondrial DNA ligase LIG k alpha (Tb927.7.610) and cysteine peptidase *PNT1* (Tb927.11.6550). Other changes in akinetoplastic stumpy cells concerned a hypothetical

protein (~3-fold upregulated) and a putative adenylosuccinate lyase (~3-fold downregulated), but overall, we observed only a limited number of robust changes (13 up, 9 down).

This study suggests that the absence of the mitochondrial genome has a surprisingly limited effect on the levels of nuclearly encoded messenger RNA needed to make proteins in bloodstream stage of *T. brucei*.

In summary, this will provide a comprehensive view of the potential effects of mitochondrial dysfunction on nuclear gene expression in these parasites. Also, my work will give understanding of metabolism and bioenergetics of cI in stumpy and adipose tissue forms of *T. brucei*.

Lay summary

Trypanosomes are protozoan (single-cell) parasites of humans and livestock. They have a single mitochondrion called the kinetoplast, which is the cell component responsible for energy production. *Trypanosoma brucei* causes human African trypanosomiasis (sleeping sickness) and Nagana in animals, often lethal diseases transmitted by tsetse flies in sub-Saharan Africa. The fly bites its host and sucks blood, and in the process, the trypanosome parasite within the fly's saliva swims out and enters either the human or animal host. These parasites then swim into the host bloodstream, survive, grow and divide to produce many of its kind. Some of them are then taken up by a fly during feeding and transferred to a new host. This is the mechanism of spreading the disease. It has been difficult to cure this disease and stop its spread because there are only few drugs available to treat affected people. Moreover, there has been high rates of drug resistance which is very worrying.

Mitochondrial respiratory complex comprises of five sub-complexes (I-V) which are involved in energy production. Some subunits for respiratory complexes I, III, IV and V are encoded in the kinetoplast DNA. *T. brucei* encodes genes for complex I; null mutants of complex I (cI) in monomorphic bloodstream form (BF) background and RNAi in procyclic cells have not shown any growth defects. Akinetoplastic stumpy cells have shorter life span which could be due to absence of mitochondrially encoded subunits and thus cannot express functional NADH dehydrogenase. Moreover, BF parasites in adipose tissue appear to upregulate pathway for beta-oxidation, which is expected to increase demand for NADH dehydrogenase activity. Little is known about the metabolism and energy relationships and transformation of cI in stumpy forms. Mitochondrial activity changes across the life cycle stages of the parasite. The parasite life stages include slender and stumpy forms (found in the mammalian bloodstream) and procyclic form (found in the tsetse fly). The mammalian bloodstream stage parasite does not express complexes III and IV so generates most, if not all, its energy through the glycolysis (i.e. breakdown of food into energy). In organisms such as yeast, mammals and plants, 'mitochondrial retrograde signalling' pathways convey information on the functional status of mitochondrion to the nucleus and modulate expression of nuclear genes accordingly. It is not known if similar signalling pathways exist in trypanosomes.

My thesis investigates how lack of a mitochondrial genome results in changes in nuclear gene expression to know whether retrograde signalling pathways exists in *T. brucei*. I compared the nuclear transcriptome of a wild type strain with strain without a kinetoplast, (AK) before and after differentiation from the 'slender' to the 'stumpy' form using RNA sequencing. In WT and AK parasites, genes showed significant upregulation in stumpy forms (we considered a difference of $\geq$ 2-fold with a p-value $\leq$ 0.05 as significant) in comparison to WT. Most of these genes were hypothetical proteins. Genes involved in the glycolytic pathway were generally downregulated in stumpy cells.

Subsequently, my research explored to know the role that complex I plays in stumpy forms and/or in cells residing in adipose tissue, two cI subunit genes were knocked in cell line that can differentiate from slender to stumpy. Unfortunately, I could not generate a complex I null mutant in pleomorphic background as I determined that the parental cell line used could not differentiate. Even though the null mutant generated for complex I were not fully pleomorphic, I still investigated their survival in adipose tissue. Results showed that these null mutants resided preferentially in adipose tissue. I further probed this by using pleomorphic cell lines without mitochondrial DNA (akinetoplastic cell lines (AK)), which are also complex I deficient as all seven mitochondrially encoded subunits of this complex are absent. These AK were able to differentiate in both blood and adipose tissue.

In summary, my work will give a comprehensive view of the potential effects of mitochondrial dysfunction on nuclear gene expression in these parasites. Also, showing that AK cells are able to differentiate and reside in adipose tissue will be a platform for further studies to be done in respect to fatty acid metabolism.

Declaration

I declare that I have wholly undertaken the study reported herein and that except portions where references have been duly cited, this thesis is the outcome of my research. No part of this thesis has been submitted to another institution for any other degree or professional qualification.

……..

Gloria Amegatcher

2019

Acknowledgements

My sincere gratitude to Professor Achim Schnaufer and Professor Keith Matthews for giving me the opportunity to take on this project and for their support throughout. I appreciate the guidance, encouragement and opportunities provided. I am fortunate to have had a great lab group for their friendship and lending advice and help whenever I was in need. I would like to thank all members of the Schnaufer and Matthews's laboratory, both past and present, for all the ideas they have contributed to this project. I would particularly like to thank Caroline Dewar for training me when I first started, and for giving me her cell lines to work with.

I would like to express my appreciation to our collaborator Dr Luisa Figueiredo and her lab group especially Tiago for making me feel extremely welcome upon my visit to IMM in Lisboa for their contribution towards the mice infection for some of the data generated for chapter 4. I would like to thank Julie Young and Julie Wallis for the training on animal handling and moral support. I will also want to thank Dr Alasdair Ivens for his help on bioinformatics, Petra Schneider for advice concerning qRT-PCR methods and Martin Waterfall for assistance with flow cytometry.

I am highly indebted to The Darwin Trust of Edinburgh for funding my PhD studentship, and to the Trustees of the James Rennie Bequest and British Society for Parasitology for supporting me with travel grants to attend conferences to talk about my research. Special thanks also go to the Centre for Immunity, Infection & Evolution for investing into my RNA-Seq analysis.

On a more personal note, I would like to thank Julie Young my bestie for her affection, generosity and cheerful moments; your friendship means a lot to me. I also thank Dr Matheiu Cayla aka 'Guru' for the time and effort he spent in mentoring me, and for the support and feedback throughout. I also thank all my friends and acquaintances in Ashworth laboratory at the King's Buildings for the laughter, all the 'kks' and great company.

I would also like to thank my parents and the entire family for their support. To my husband Samuel and daughter Mariam, you have been my inspiration to come this far and I dedicate this thesis to you. Thank you for your understanding and undying love.

Most importantly, all thanksgiving, praises and appreciation go to God Almighty for bringing me this far to make a dream come true.

Abbreviations

A6	Subunit a of *T. brucei* F_1F_o ATPase
AAC	ATP/ADP carrier
AAT	Animal African Trypanosomiasis
AK	Akinetoplastic
ATF	Adipose tissue form
ATOM	Archaic translocase of the outer mitochondrial membrane
ATP	Adenosine triphosphate
BARP	Bloodstream alanine-rich proteins (misnomer)
BBB	Blood-brain barrier
BSD	Blasticidin
BLE	Phleomycin
BSA	Bovine serum albumin
BSF	Bloodstream form
bZip	Basic-leucine zipper
cAMP	Cyclic adenosine monophosphate
CCA	Cis aconitate/citrate
CDK	Cyclin dependent kinases
CKO	Conditional knock-out
CI	Complex I
COX	Cytochrome oxidase subunit
DAPI	4', 6-diamidino-2-phenylindole
DHAP	Dihydroxyacetone phosphate
DK	Dyskinetoplastic
E. coli	*Escherichia coli*
EP	Glutamate-proline repeat containing protein
ES	Expression site
EtBr	Ethidium bromide

ETC	Electron transport chain
FACS	Fluorescence activated cell sorting
FAD	Flavin adenine dinucleotide
FAZ	Flagellar attachment zone
FC	Fold change
FCS	Fetal calf serum
Fe/S	Iron sulfur centre
FMN	Flavin mononucleotide
G-3-P	Glyceraldehyde-3-phosphate
G3PDH	Glycerol-3-phosphate dehydrogenase
gDNA	Genomic DNA
Gly-3-P	Glycerol-3-phosphate
GPEET	Glycine-proline-glutamate threonine pentapeptide repeat-containing - protein
GPI	Glycosylphosphatidylinositol
gRNA	Guide RNA
HAT	Human African Trypanosomiasis
HpHbR	Haptoglobin-haemoglobin receptor
HPR	Haptoglobin-related protein
Hyg	Hygromycin
IFA	Immunofluorescence assay
IM	Inner mitochondrial membrane
kDNA	Kinetoplast DNA
kDNA+	Cells retaining their kDNA
L262P	Lysine to proline substitution at amino acid position 262
LipDH	Lipoamide dehydrogenase
MtDNA	Mitochondrial DNA
NAD+	Nicotinamide adenine dinucleotide (oxidised)
NADH	Nicotinamide adenine dinucleotide (reduced)
NDH2	Alternative NADH dehydrogenase

NECT	Nifurtimox-eflornithine combination therapy
Neo	Neomycin
OM	Outer membranes
OSCP	Oligomycin sensitivity-conferring protein (misnomer)
PAD1	Protein associated with differentiation
PAGE	Polyacrylamide gel electrophoresis
PCF	Procyclic form
PCR	Polymerase chain reactions
Puro	Puromycin
PV	Proventriculus
PVDF	Polyvinylidene fluoride
qPCR	Quantitative polymerase chain reaction
qRT-PCR	Quantitative reverse transcriptase-polymerase chain reaction
RT-PCR	Reverse transcriptase Polymerase Chain Reaction
RIT-seq	RNA interference target–sequencing
RNAi	RNA interference
S. cerevisiae	*Saccharomyces cerevisiae*
SDS	Sodium dodecyl sulfate
SIF	Stumpy induction factor
SKO	Single knockout
SL	Slender
SS	Stumpy
T. b. gambiense	*Trypanosoma brucei gambiense*
T. b. brucei	*Trypanosoma brucei brucei*
T. b. equiperdum	*Trypanosoma brucei equiperdum*
T. b. evansi	*Trypanosoma brucei evansi*
T. b. rhodesiense	*Trypanosoma brucei rhodesiense*
T. brucei	*Trypanosoma brucei*
T. congolense	*Trypanosoma congolense*

T. vivax	*Trypanosoma vivax*
TAC	Tripartite attachment complex
TAO	Trypanosome alternative oxidase
TCA	Tricarboxylic acid
TLF	Trypanosome lytic factor
TMD	Transmembrane domain
UPR^{mt}	Mitochondrial unfolded protein response
UTR	Untranslated region
VSG	Variable surface glycoprotein
WHO	World Health Organisation
WT	Wild type
WTγ	Wild type with ATPase subunit γ
γGS	Glutamate-γ-semialdehyde
Δψm	Mitochondrial membrane potential

Contents

List of figures

List of tables

1 Introduction

1.1 Trypanosomes as a pathogen

Trypanosomatid parasites cause several neglected tropical diseases globally, which put about half a billion people and over 60 million livestock at risk of infection (Fèvre et al., 2008a). These trypanosomatids include *Leishmania spp*., responsible for leishmaniasis; *Trypanosoma cruzi*, which causes Chagas disease mainly in Central and South America; salivarian *Trypanosoma brucei*, the cause of African trypanosomiasis in both humans and animals, including the subspecies *T. brucei* which cannot infect human but infects only livestock and wildlife; *Trypanosoma vivax* and *Trypanosoma congolense*, which causes disease in animals (Abdi et al., 2017; Meyer et al., 2016). It has been reported that *T. vivax* and *T. congolense* infections result in adverse effect on animal production and health deterioration in humans living in sub-Saharan Africa (Auty et al., 2015; Giordani et al., 2016; Morrison et al., 2016). These subspecies belong to the taxonomic order Kinetoplastida and phylum *Euglenozoa*. Moreover, they have a densely intercatenated network of circular DNA forming a major component of their mitochondrial genome which characterises all kinetoplastids (Meyer and Porter, 1954; Steinert, 1960; Steverding, 2008).

These organisms are biologically intriguing due to the vast differences in their molecular and cellular biology compared to other eukaryotes. In addition to its being an infectious pathogen, trypanosomes are intrinsically useful organisms for investigating many aspects of fundamental eukaryotic and kinetoplastid-specific cell biology. For example, *T. brucei* has become an attractive model to study the assembly and the functions of cilia and flagella (Santi-Rocca et al., 2015). Studying this parasite also helps to understand developmental regulation in trypanosomatids in general. *T. brucei* is amenable to reverse genetic approaches, such as gene knockout by homologous recombination, or RNA interference (RNAi)-mediated downregulation of gene expression (Serricchio and Bütikofer, 2011). The energy metabolism of bloodstream of *T .brucei* serves as kinetic metabolic model in systems biology (Bakker et al., 2011). *T. brucei* molecular and cellular features such RNA editing and

the GPI anchor, which were first discovered in African trypanosomes, has made these parasites an interesting model organism for these processes (Ferguson et al., 1988).

1.1.1 Animal trypanosomiasis

Animal African Trypanosomiasis (AAT) also known as Nagana, is spread by about 30 species of tsetse flies found in tropical Africa. Livestock breeders have indicated that the disease prevents sustainable farming in most parts of sub-Saharan Africa, thereby drastically reducing meat and milk production (http://www.fao.org) and necessitates constant administering of trypanocidal drugs. The disease causes US$4 billion in loss of crop and livestock production in sub-Saharan Africa (http://www.fao.org). Moreover, the disease retards usage of these animals for agricultural activities such as ploughing, thereby limiting food cultivation, local transport, and ultimately socio-economic development (Franco et al., 2014b; Meyer et al., 2016).

Nagana infection can either be acute or chronic, with the chronic infection being more common. The pathological symptoms associated with Nagana infection include: fever, emaciation, loss of hair, listlessness, discharge from the eyes, oedema, severe anaemia, and paralysis (Steverding, 2008). The reported incidence of Nagana may be affected by several factors such as accessibility of reservoir hosts, periodic seasons of the disease vector, flies' behaviour in densely populated areas, the specificity and accuracy of analytical techniques, the infection phase, method of collecting specimen, and other human actions (Albert et al., 2015; Majekodunmi et al., 2013; Odeniran and Ademola, 2018). For instance, Nagana infection is rampant in Nigeria because about 80% of the nation's landforms are populated with tsetse flies (Anene et al., 1991; Odeniran and Ademola, 2018). Despite the disease prevalence in tropical Africa, the method of diagnosing Nagana infection is mostly rudimentary.

Identification of the parasite using reliable diagnostic tools underpins efficient control of the disease (Aksoy et al., 2017). The routine diagnostic approach usually relies on detection of

parasites via the use of a microscope, even though the technique is extremely insensitive (Takeet et al., 2013).

Currently, researchers have adopted the use of polymerase chain reaction, serological testing and immunodiagnostic techniques to improve diagnostic efficiency of the disease (Majekodunmi et al., 2013; Odeniran and Ademola, 2018). Efficient eradication of the disease could be boosted by adopting the use molecular methods to diagnose Nagana infection.

Recently, the first-line drug for treatment of late-stage animal trypanosomiasis is organo-arsenical tryparsamide combined with suramin (Steverding, 2008). Drugs originally used for treatment of Nagana infection were phenanthridines homidium bromide (also known as ethidium bromide), isometamidium chloride, quinapyramine and aromatic diamidine diminazene aceturate (Dolan et al., 1990; Kinabo, 1993). Resistance to these drugs have led to an extensive spread of the disease within sub- Saharan Africa (Chitanga et al., 2011). In addition to chemotherapy, control of the vector is another effective way of controlling the disease (subsection 1.1.3 of Chapter 1).

1.1.2 Human African trypanosomiasis

Human African trypanosomiasis (HAT) is recognized as a serious public health concern. It is classified by the WHO as a neglected tropical disease that is caused by two subspecies of the protozoan parasite *T. brucei*: *T. b. rhodesiense* and *T. b. gambiense*. The distribution of African trypanosomes is restricted to 36 countries in sub-Saharan Africa. The epidemiology of the disease is determined by the distribution of the vector (tsetse fly), with over 95% of cases attributed to *T. b. gambiense* infection and the remaining 5% to *T. b. rhodesiense* infection (Franco et al., 2014a). A number of epidemics of the disease have occurred during the 20th century, resulting in the death of approximately 700,000 natives of Africa. In response to these epidemics, surveillance of affected individuals and control of the disease vector have resulted in drastic reduction of HAT cases (Franco et al., 2017).

In 2017, the number of new cases of HAT reported to WHO was reduced to about 1500 (WHO, 2017) compared with 11,382 cases reported in 2006 (Fèvre et al., 2008b).

HAT is usually fatal when left untreated. The disease can be divided into two clinical stages, correlating with the location of the parasite and the associated symptoms: the early haemolymphatic stage and the later neurological stage. In the early stage of the disease, symptoms include intermittent fever, headache, severe itching of the skin (also known as pruritus), adenopathy, swollen lymph nodes and joint pain. The central nervous system (CNS) stage of the disease is accompanied by neurological symptoms including mental and sleep anomalies (Kennedy, 2004). The sleep anomalies indicate that sleeping sickness may be a circadian clock rhythm disorder (Rijo-Ferreira et al., 2018). Countries such as Uganda, Malawi, Nigeria, Cameroon, Kenya and Ghana have fewer cases of trypanosomiasis due to provision of funding for surveillance, drug donations by pharmaceutical companies and implementation of control programs (Simarro et al., 2008). In 2013, the World Health Organization and the Bill and Melinda Gates Foundation agreed to implement novel surveillance policies to reduce disease caused by *T. b. gambiense* (WHO, 2013).

Previous studies have found that *T. b. rhodesiense* occurs in Southern and South-Eastern Africa and is associated with acute disease (as described in the haemolymphatic stage of the disease) in humans. *T. b. gambiense* is found in West and Central Africa and causes chronic disease, which is associated with persistent or otherwise long-lasting neurological disorder in humans (Goodhead et al., 2013; Pays and Vanhollebeke, 2009; Simarro et al., 2011). Trypanosomiasis occurs in humans when the host immune system is incapable of eliminating the parasite infection because of rapid parasite growth and parasite antigenic variation (Horn and McCulloch, 2010). In mouse models, trypanosomes have been shown to sequester in tissues or organs (Capewell et al., 2016; Trindade et al., 2016).

Ultimately, these phenomena result in evasion of the host immune system by the parasite and concomitant parasitaemia waves, thereby serving as a vital survival strategy for the parasite, as the parasite auto-regulates parasitaemia and antigenic variation (Horn, 2014;

MacGregor et al., 2011). The mechanisms for parasite evasion and survival is described in section 1.2.1 of Chapter 1.

1.1.3 Vector control

Tsetse flies, of the genus *Glossina,* are the vectors that harbour and transmit the trypanosome parasite. A better comprehension of the complex biology and mitochondrial oxidative regulation processes within the parasite is essential for development of Trypanosomatid-targeting chemotherapy (Menna-Barreto and de Castro, 2014).

Tsetse flies are categorised into three main taxonomic groups: morsitans, palpalis and fusca, depending on their habitation, preference of host and morphology of external genitalia (Vreysen et al., 2013). Out of these groups, palpalis and morsitans are of economic importance since they transmit most cases of African animal and human trypanosomiasis (Esterhuizen et al., 2011; Vreysen et al., 2013). Flies belonging to the palpalis group transmit about 90% of HAT cases, whiles palpalis subspecies are known for transmission of animal trypanosomiasis in western and central Africa (Esterhuizen et al., 2011; Omolo et al., 2009). The morsitans group on the other hand transmits both HAT and AAT in southern and eastern Africa (Vreysen et al., 2013). These insects are expanding their geographical coverage in search for food, to boost reproduction, in search for a new niche to evade eradication, or migrating from treated regions to colonise an untreated area and migration driven by climate change (Cuisance et al., 1984; Getahun et al., 2014; Moore et al., 2012).

Tsetse fly vector control is considered an appropriate way of controlling trypanosomiasis (Bouyer et al., 2010). The use of genetics techniques to understand and quantify gene flow among subpopulations of tsetse flies can be used to control fly population. Techniques employed to control the vector include the use of biconical traps, targets impregnated with insecticide, progressive airborne spraying, and male insect sterility (Joja and Okoli, 2001; Kgori et al., 2006; Vreysen et al., 2000). Alternative approaches include the use of electric nets to catch flies in flight (Packer and Brady, 1990) and the paratransgenic approach (Haines et al.,

2003). The latter technique attempts to reduce the competence of vectors to sustain and transmit disease by expressing parasite inhibitory molecules in the vector symbiont. Tsetse species belonging to the morsitans group are receptive to host odours, such that targets and traps treated with insecticide or baits containing artificial mixtures of these odours can control these tsetse populations (Vale et al., 1988). The chemicals used to attract morsitans-group tsetse are ineffective when used on Palpalis-group species of tsetse (Green, 1994).

1.1.4 Diagnosis and current therapy for HAT

The HAT disease is diagnosed primarily through usage of the card agglutination test for trypanosomiasis (CATT), which is a serological screen for antibodies produced in response to one of the many trypanosome's surface antigen types (Checchi et al., 2011). The sensitivity of CATT is highly variable, and complete diagnosis requires identification of parasites in either the lymph or blood using a compound microscope (Chappuis et al., 2005). The choice of drug for treatment of the disease is dependent on the stage of infection. Parasite identification via lumbar puncture is critical for diagnosing the second stage of the disease (Bonnet et al., 2015). *T. b. rhodesiense* and *T. b. gambiense* are morphologically identical to each other even though they have separate geographical locations.

In case of suspected co-infection with both parasites, microscopy and other simple techniques are less efficient in diagnosis and more advance techniques are required. For example, the genes encoding serum resistance-associated (SRA) protein is present only in the genome of *T. b. rhodesiense* but not *T. b. gambiense* and *T. b. brucei* (Radwanska et al., 2002); thus detection of this gene by molecular techniques is the preferred diagnostic approach. There are only few available active drugs for the treatment of HAT.

Pentamidine, Suramin, Eflornithine and Melarsoprol, although a fifth, Nifurtimox, is increasingly used in combination with Eflornithine. These drugs are associated with toxicity and the drug of choice depends on the infecting species and the stage of disease (Figure 1.1).

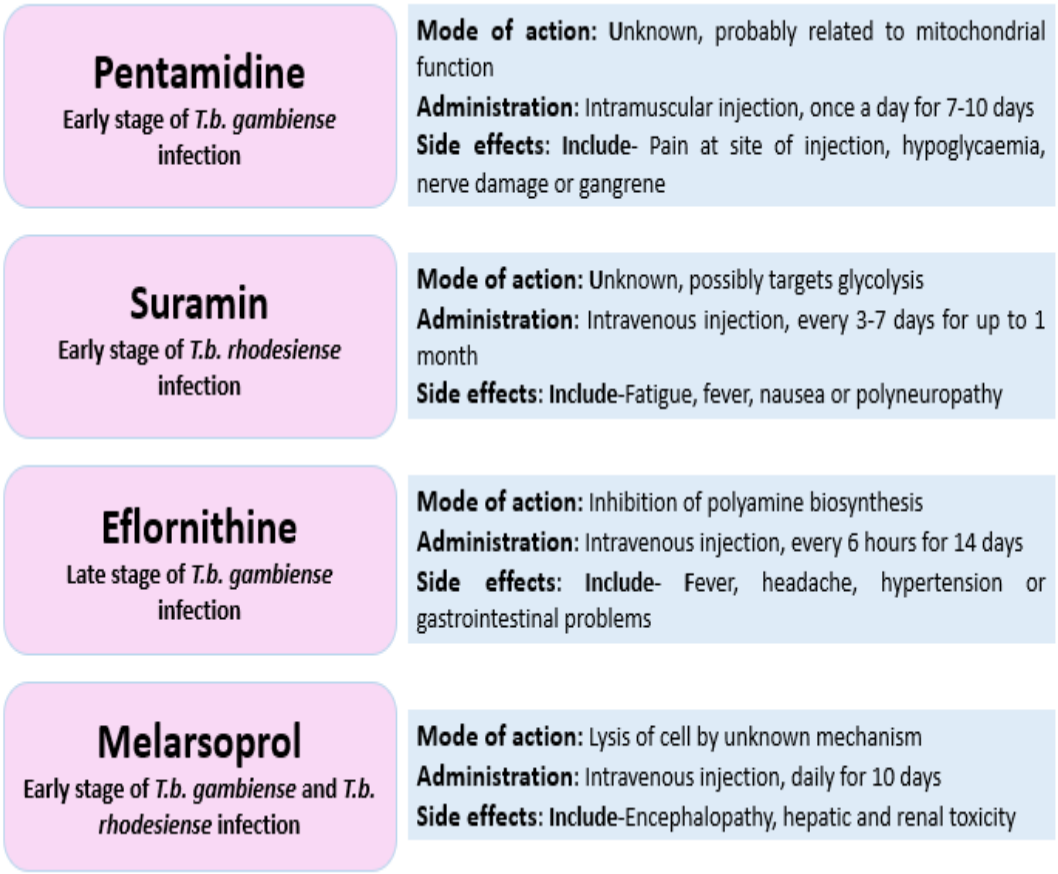

Figure 1.1 Drugs currently licensed for use against HAT. Figure generated from data gathered in (Blum et al., 2001; Burri and Blum, 1996; Coulaud et al., 1975).

The nifurtimox-eflornithine combination therapy (NECT) was introduced in 2009. NECT is ineffective against *T. b. rhodesiense* infections (Stich et al., 2013). Despite the high risk associated with this drug, it is still used for treatment of HAT since the disease will always lead to death if left untreated. Therefore, there is an urgent need to discover new medications and drug targets to curb the epidemics associated with *T. brucei* infections.

1.1.5 Drug resistance

T. brucei is capable of developing resistance to drugs through genetic mutations. Resistance has been recorded against all available drugs, even though the mechanisms underlying resistance to all these drugs is yet to be fully understood. Melarsoprol and pentamidine resistance is known to be caused by point mutations in TbAT1, a purine nucleoside transporter, and TbAQP2, an aquaporin. The loss of TbAT1 does not solely account for the high level of resistance to melarsoprol and pentamidine (Stewart et al., 2010). Moreover, deletion or rearrangements of TbAQP2 has been found to be present in strains resistant to both drugs (Munday et al., 2014). The AQP2 protein mediates high affinity drug uptake and is a genetic marker for predicting drug-resistant strains of trypanosomes (Fairlamb and Patterson, 2018).

The loss of a single non-essential amino acid within the transporter gene, TbAAT6, in genetically modified cell lines was shown to be a consequence of eflornithine resistance (Vincent et al., 2010). TbAAT6, an amino acid transporter, controls the uptake of eflornithine. Gene deletion causes drug resistance, and re-expression of the gene causes restoration of sensitivity to eflornithine (Vincent et al., 2010).

Due to the privatization of veterinary services in most parts of Africa, farmers can easily access these drugs; and hence misuse has led to drug resistance (Delespaux et al., 2008, 2002; Van den Bossche et al., 2000). Resistance to these drugs has been reported in many countries, especially within the endemic areas (Delespaux and de Koning, 2007; Tchamdja et al., 2017).

Suramin resistance is linked to expression switch of one of the VSG (Wiedemar et al., 2018). The invariant surface glycoprotein, ISG75, shows reduction of *T. brucei* susceptibility to suramin when genome-scale RNA interference (RNAi) target sequencing (RIT-Seq) screen was performed (Alsford et al., 2013, 2012).

New therapies that are safer and easier to administer is needed to minimise the side effect of drug toxicity of the current trypanocides. At present, there are no existing vaccines for the treatment of trypanosomiasis. The development of a vaccine is limited by using mice as a

model organism for the study of trypanosomiasis (La Greca and Magez, 2011). The use of non-pathogenic trypanosome species is also being explored as a possible vaccine. These non-pathogenic trypanosomes are being manipulated to serve as vehicles for establishing an immune response to specific antigens, or as delivery vehicles for therapeutics (Mott et al., 2011). The available drugs for treating the disease are associated with poor efficacy, major side effects and increasing levels of resistance (Fairlamb et al., 2016).

Recently, West and colleagues reported three novel and versatile approaches for synthesizing ascofuranones, which together with the structure-activity relationship, resulted in improved yields compared to previous synthetic approaches. These novel synthetic methods also allowed late stage modification of the crucial aromatic head group of ascofuranone, which is responsible for enzyme-compound affinity and the non-drug-like functionality of the compound (West et al., 2017). From a library of oxaboroles, the benzoxaborole 6-carboxamides were particularly active against *T. brucei* and following a lead optimization programme, SCYX-7158 was selected as a clinical candidate for HAT (Jacobs et al., 2011).

Benzoxaboroles, which are boron-containing compounds, have been reported as potential drugs against several diseases caused by viruses, fungi, bacteria and parasites (Goldstein et al., 2013; Mahalingam et al., 2011; Markham, 2014; Zhang et al., 2015). In the case of HAT, the two compounds currently in clinical trials, fexinidazole and the oxaborole SCYX-7158, were both derived from phenotypic approaches (Field et al., 2017). In general, oxaboroles have demonstrated to be potent against all *T. brucei* subspecies, with low potential for cytochrome P450 CYP450 inhibition and high permeability (Nare et al., 2010). The oxaborole, SCYX-7158, which is an orally active benzoxaborole, is also effective, safe and active for treatment of stage 2 HAT (Jacobs et al., 2011). The phase I clinical study with SCYX-7158 for treatment of human African trypanosomiasis was completed in 2015, and the phase II/III trial started in 2016 (Carneiro et al., 2017).

Extracts from plant sources are also sources of bioactive molecules with novel chemotherapeutic potentials against trypanosomes. Notably, extracts from plants which were collected from different parts of North America exhibited antitrypanosomal activity

against the bloodstream form of *T. brucei*. Plants that have produced antitrypanosomal extracts include: *Alnus rubra, Hoita macrostachya, Salvia spathacea, Sabal minor, Ribes montigenum, Quercus alba, Leea rubra, Coccoloba pubescens, Rhus integrifolia* and *Nuphar luteum*. It is anticipated that further studies with these extracts would provide novel compounds that are useful for treatment of HAT (Jain et al., 2016).

1.2 Cell biology of *T. brucei*

The biology of trypanosomes is beginning to unveil the links between the structure of the genome and the understanding of the parasitology of trypanosomes (Daniels et al., 2010). The study of the various aspects of the parasite's cell biology include structure and morphology of the cell, positioning of the organelles, cell division and transfer of protein across the cell to other organelles (Matthews, 2005). There are several examples of kinetoplastid-specific cell biology, a few of which are described in detailed below.

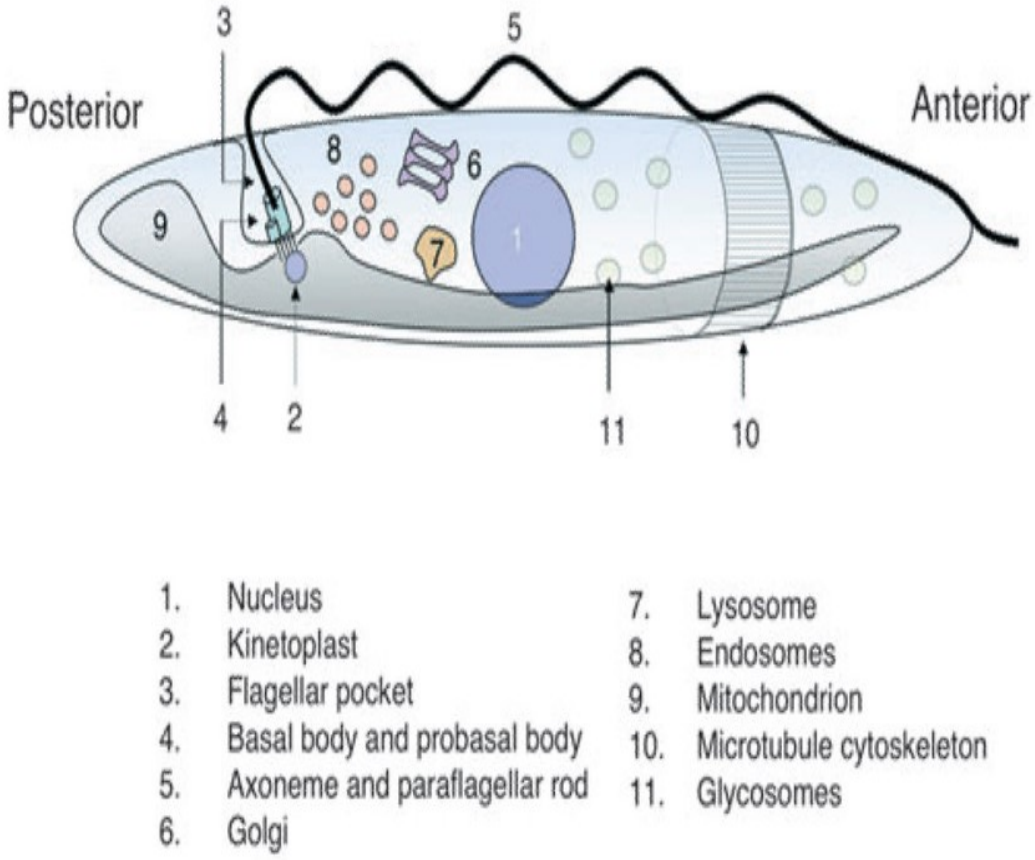

Figure 1.2. **Schematic of the cellular architecture of *T. brucei* (Matthews, 2005).**

Trypanosomes use hydrodynamic flow to eliminate surface bound immunoglobulins in order to increase cell survival and disease transmission (Engstler et al., 2007). The surface of the parasite is covered by variant surface glycoproteins (VSG) that act as a blockade to the alternative pathway of complement (Ferrante and Allison, 1983) and also allows the parasite population to evade host immunoglobulins by antigenic variation (Schwede and Carrington, 2010). This precludes the development of vaccines against HAT and thus chemotherapy remains the only option for disease intervention. It has been shown that the trypanosome surface coat proteins undergo antigenic variation via expression of only one of the pool of hundreds of VSG genes within the genomic repertoire (Horn, 2014).

Trypanosomes also use the haptoglobin-haemoglobin receptor (HpHbR) protein, which binds haptoglobin-haemoglobin complexes, to acquire haem from their host (Lane-Serff et al., 2016).

In human blood, two complexes of lipid-rich particles called trypanosome lytic factors (TLFs) 1 and 2 contain a lipid-binding protein, apolipoprotein L1 (ApoL1) and haptoglobin-related protein (HPR), which binds haemoglobin (Raper et al., 1999; Thomson et al., 2009). According to Pays (2014), the uptake of TLF-1 into *T. b. brucei* via parasite haptoglobin-haemoglobin receptor (HpHbR) causes their lysosome to swell when ApoL1 is released into the lysosome and embeds in the membrane, ultimately leading to lysis of *T. b. brucei*. However, the mechanism of *T. b. brucei* death by TLFs is not clear at the molecular level. *Trypanosoma brucei gambiense* and *Trypanosoma brucei rhodesiense* are the only two subspecies that counteract the effect of trypanolytic factors, and hence can cause Human African Trypanosomiasis (Pays et al., 2014; Vanhamme et al., 2003).

1.2.1 The life cycle of *T. brucei*

T. brucei survives extracellularly, in the mammalian bloodstream, and within the tissues. The parasite is transmitted by tsetse flies. Vector-transmitted pathogens acclimatise to periodic changes in their environment in order to survive the drastic change in environmental conditions during their life cycle (Figure 1.3) (Silvester et al., 2017). Like other eukaryotic parasites, *T. brucei* encounters different surroundings as they migrate between the mammalian host and the tsetse fly. Therefore, these parasites undergo differentiation, when necessary, to facilitate survival and transmission. This involves modulation of gene expression, as well as immunological, metabolic and morphological changes that are indispensable for successful progression through the life cycle (Matthews, 2005).

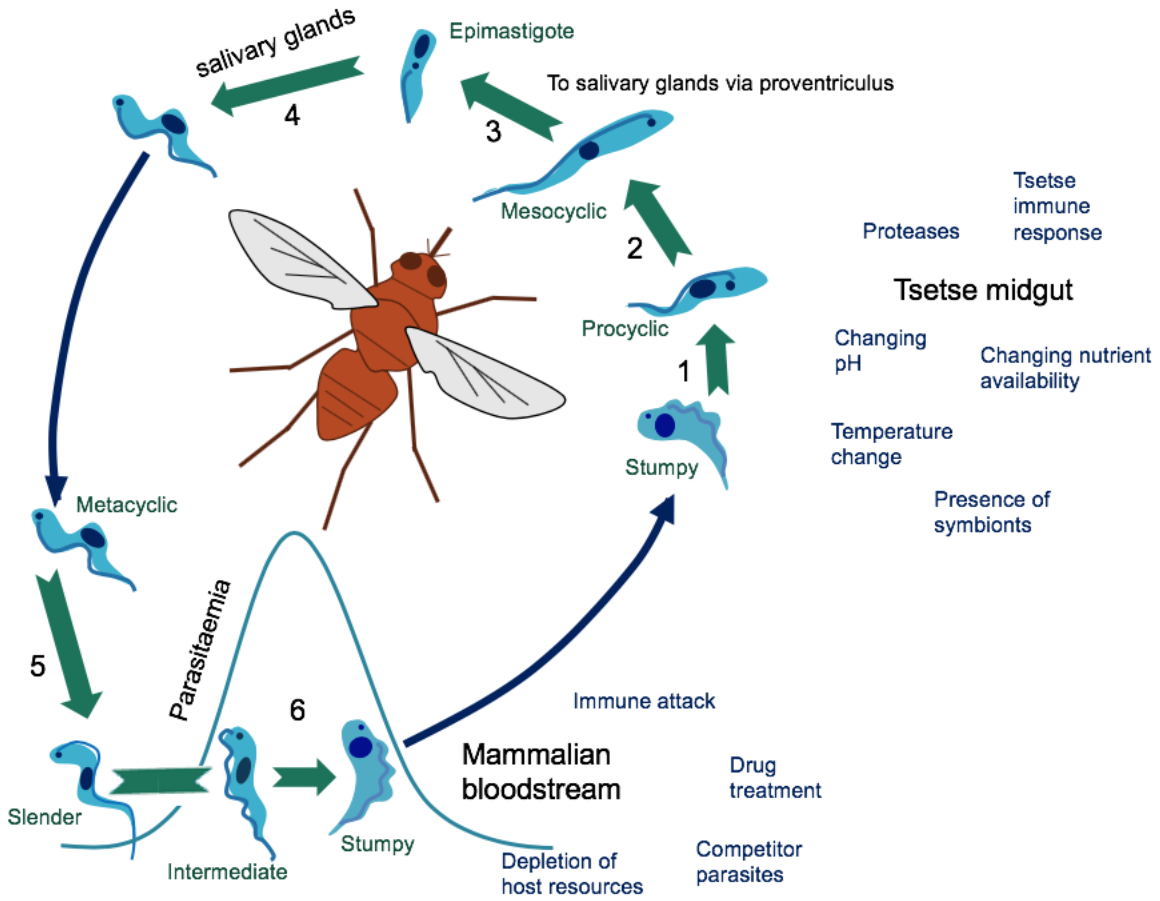

Figure 1.3. The life cycle of *Trypanosoma brucei*. The cyclic events of the *T. brucei* life cycle. (1) *T. brucei* stumpy forms ingested from an infected mammalian host differentiate to procyclic cells within the midgut of the tsetse fly. (2) Procyclic cell body and flagellum are continuously elongated further the midgut to assume the mesocyclic form. (3) Following differentiation, the mesocyclic forms migrate to the proventriculus. (4) The epimastigotes undergo further differentiation into metacyclic cells, which is the infective stage in the salivary gland. (5) Metacyclics are transferred to a mammalian host by the tsetse fly during a blood meal and differentiate to bloodstream forms in the new host. (6) The stumpy form of *T. brucei* must survive a reasonable duration of time in the bloodstream of the mammalian host in order to be transmitted. The parasite must also survive within the tsetse midgut to enable differentiation, which is essential for establishing infection. Image adapted from (Silvester et al., 2017) and modified by Gloria Amegatcher.

1.2.2 Bloodstream form stages

In the bloodstream of mammalian hosts, parasites are routinely attacked by the host immune system to control possible infection. Trypanosomes have various strategies of evading the host defence mechanisms. These include auto regulation of parasitaemia and antigenic variation. Antigenic variation involves consecutive expression of discrete VSGs, which are linked to the surface membrane of the parasite by a glycosylphosphatidylinositol (GPI) anchor (Pays et al., 2004). There are approximately 20 VSG expression sites in the genome of *T. brucei* (Gottesdiener et al., 1991). VSG is the main surface protein that protects other surface proteins from detection by the host's immune system. This is due to a rapid turnover of the surface VSG, which is aided by motility of the parasites.

Slender forms of the parasite evade the host immune response by switching the expression of VSG coat (Horn, 2014; MacGregor et al., 2011; Vickerman, 1978). Even though the repertoire of potential VSG genes and pseudogenes is over 1000 (Berriman et al., 2005), only one VSG is expressed, at any time per cell (Callejas et al., 2006; Hertz-Fowler et al., 2008), with antigenic variation occurring either by a new VSG gene recombining with the expressed VSG gene or by activation of another VSG expression site (ES) (Cross et al., 1998; Vanhamme et al., 2001).

A switch in the expression of a specific VSG can be facilitated by either gene conversion, telomere exchange or dynamic expression site switching (Horn and Cross, 1997; Taylor and Rudenko, 2006). The frequency of occurrence of switches in the expression of VSG genes ranges from 2.2×10^{-7} to 2.6×10^{-6}, *in vitro*, in *T. brucei* (Lamont et al., 1986). Recognition of antibodies by the VSG triggers a lytic response in the slender forms and stumpy forms, though stumpy forms are relatively resistant (Amiguet-Vercher et al., 2004).

In the bloodstream of the mammalian host, the cell population cycles between proliferative slender bloodstream forms, the intermediate forms and the cell cycle-arrested (G0/G1) stumpy form.

The slender forms respond to a signal molecule, known as the stumpy induction factor (SIF), which is released constantly by the parasite. SIF accumulates with increase in the population of the slender forms, thereby triggering differentiation of slender forms to stumpy cells (Vassella et al., 1997).

Growth is halted in stumpy cells as parasitaemia peaks, and hence prolong infection by preventing further increase in parasitaemia. Stumpy forms dominate the late stage of infection and they do not switch their VSG. As a result, the host immune system can clear the infection since stumpy forms have a limited lifespan (Dewar et al., 2018). Because all the parasite population do not undergo differentiation, the few slender bloodstream forms that are able to switch their VSG evade immune clearance and proliferate to initiate repeat waves of infection.

In the laboratory, the strains that can undergo differentiation from slender to stumpy forms are called pleomorphic. Monomorphic slender bloodstream forms are generated through a series of *in vivo* or *in vitro* passages, rendering them unable to differentiate to stumpy forms. These monomorphic cells are virulent and lethal to the host (Ashcroft, 1960; Turner, 1990). Unlike pleomorphic slender forms, monomorphic cells are unable to sense the presence of SIF (Vassella et al., 1997).

Even though monomorphic trypanosomes respond ineffectively to SIF *in vivo*, they could be exposed to cell-permeable cAMP and AMP analogues, that bypass SIF signalling, to generate a ‘stumpy-like’ forms *in vitro* (Breidbach et al., 2002, 2002; Vassella et al., 1997). Surprisingly, the identity of SIF remains unknown (MacGregor et al., 2011; Vassella et al., 1997). As a consequence of the signal, mRNA expression of PAD proteins, encoding carboxylate transporters, increases once the parasites are committed to differentiation and have undergone cell cycle arrest (Dean et al., 2009). Genome-wide RNAi screening has been used to demonstrate that several RNA binding proteins, kinases and phosphatases are involved in the stumpy induction pathway (Mony et al., 2014).

1.2.3 The insect stages

Following ingestion, the stumpy form of trypanosomes adapts and differentiates into an 'early' procyclic form in the tsetse fly midgut (Vassella et al., 2000) (figure 1.3). Many factors can influence the success of transmission from the mammalian bloodstream to the midgut of the insect. These factors include the age of the fly, number of previous blood meals of the fly, the tsetse immune response and gut conditions (Dyer et al., 2013). Trypanosomes are exposed to different temperature conditions between the mammalian host and the tsetse fly vector.

The temperature within the mammalian bloodstream is 37 °C, whereas tsetse flies survive at an optimum temperature of approximately 27 °C. In the evenings, and at dawn, flies are exposed to lower temperatures (approximately 20 °C) during the uptake of their blood meal (Makumi et al., 1998). The PAD1 protein is involved in citrate cis-aconitate (CCA)-mediated differentiation, which is upregulated in stumpy forms; the PAD2 protein is elevated at low temperatures and it potentially signals the initiation of differentiation stimulated by blood citrate (Dean et al., 2009). The addition of 6 mM citrate/cis-aconitate to SDM79 culture medium can also drive *in vitro* differentiation of stumpy to procyclic forms at 27 °C (Brun and Schonenberger, 1981; M. Engstler and Boshart, 2004).

The intracellular signalling pathway that responds to cis aconitate/citrate (CCA) has been deduced. TbPTP1, a protein phosphatase, acts downstream of PAD1 to prevent differentiation of stumpy forms to the procyclic form whilst in the bloodstreams (Szoor et al., 2006). In the presence of CCA, *T. brucei* phosphotyrosine phosphatase (TbPTP1) is inactivated, and leads to phosphorylation and activation of its substrate called PTP1-interacting protein (TbPIP39), which is trafficked to the glycosome to initiate differentiation.

In addition to expression of PAD proteins, stumpy forms of *T. brucei* show upregulation of the nucleoside transporter 10 gene (*TbNT10*) (Sanchez et al., 2004). *T. brucei* is incapable of synthesizing purines de novo, and thus depends on transport of purine nucleosides across the plasma membrane, which is aided by specific permeases (Berens et al., 1995). The expression

of TbNT10 may promote transformation to procyclic forms in the tsetse fly (Sanchez et al., 2004). Moreover, RNA-Seq analysis has shown upregulated expression of adenylate cyclases in stumpy forms (Naguleswaran et al., 2018), as well as 12 additional genes that encode components of the inositol metabolic pathway (Cordeiro et al., 2017). Lipoamide dehydrogenase (LipDH) also shows increased activity in the stumpy form (Tyler et al., 1997) and can be used to detect differentiation in stumpy form. Indeed, the stumpy surface receptor marker PAD1, which is expressed exclusively in stumpy forms (Dean et al., 2009), and a secretory protein called expression site associated genes (ESAG9) (Monk et al., 2013), are the markers used in this project to confirm differentiation from slender to stumpy forms.

In addition to exposure to CCA, differentiation from stumpy forms to procyclic forms can be stimulated in various ways, *in vivo*. For instance, digestive proteases within the midgut of the fly have been shown to induce differentiation into the procyclic forms, *in vitro* (Aksoy et al., 2003; Yabu and Takayanagi, 1988). Stumpy forms can tolerate a constant cytoplasmic pH of 6.9, which is encountered within the protease-rich environment of the midgut. In *Leishmania* and *T. cruzi*, acidic stress can contribute to differentiation of promastigotes into amastigotes *in vitro* and *in vivo* (Bates et al., 1992). Similarly, mild acid treatment can stimulate the differentiation of stumpy forms to procyclic forms (Rolin et al., 1998) the signalling pathway underlying the acid-mediated differentiation of stumpy forms is shared with the CCA-based signalling (Szoor et al 2013).

Within the third day of post infection, procyclic forms are found in the ectoperitrophic space, and by the sixth day, they migrate through the proventriculus (PV) to the anterior of the gut (Sharma et al., 2009).

Subsequently, mesocyclic trypomastigotes emerge, and are usually mobile because they possess long flagella. In the lumen of the PV, the mesocyclic trypomastigotes initiate differentiation into epimastigotes, with a concomitant reversal of the positions of the kinetoplast and nucleus (Sharma et al., 2008). Long epimastigotes divide asymmetrically into long and short epimastigotes, and the latter enter the salivary gland (Van Den Abbeele et al., 1999).

The epimastigotes that are attached to the epithelium of the salivary glands undergo proliferation and colonise the salivary gland (Sharma et al., 2009). These epimastigotes undergo a subsequent division into trypomastigotes and finally to metacyclics (Rotureau et al., 2012). The cell cycle-arrested forms can be injected into the mammalian host upon a tsetse bite, where they differentiate to slender forms to complete the life cycle.

The surface proteins of the forms found in the fly stages can be used as differentiation and stage-specific markers. For example, in procyclic forms the VSG-coat is substituted with the surface glycoproteins, glutamate-glutamate-threonine repeat containing protein (GPEET) and glutamate-proline repeat (EP) procyclin (Ruepp et al., 1997). Three forms of closely-related EP procyclin (EP1-1, EP1-2, EP1-3) exhibit similarity across their entire coding regions but have distinct 3' UTRs (Vassella et al., 2001a). The EP procyclin is usually found in the midgut and the proventricular stages. 'Early' (which express GPEET predominantly) and 'late' (which express EP predominantly) procyclic forms can be sustained in culture, *in vitro*.

Moreover, addition of glycerol to the culture medium extends GPEET expression, which upon removal, results in the cells undergoing a temporal growth arrest and suppression of GPEET expression (Vassella et al., 2000). GPEET-negative cells can re-express GPEET in glucose-depleted culture medium, or spontaneously, without glycerol induction (Morris et al., 2002; Vassella et al., 2004). An alanine-rich protein (BARP) is expressed exclusively by epimastigotes in the salivary glands (Urwyler et al., 2007).

VSG is expressed on the metacyclic forms which enables them to be resistant to existing humoral immunity to VSGs (Barry et al., 1998) and complement activated by the alternative pathway.

1.2.4 The cell cycle of *T. brucei*

The mitotic cell division cycle in eukaryotes is a conserved process whereby a cell duplicates and separates newly synthesized cellular components to the two daughter cells. The synthesis

and degradation, as well as activation and silencing of regulatory proteins, regulate the sequential events that must occur for cell division to proceed properly (Crozier et al., 2018). The trypanosome cell division cycle is divided into four sequential stages: Gap 1 (G1), where metabolic changes prepare the cell for division; DNA synthesis (S), where nuclear and kinetoplast DNA are replicated; Gap 2 (G2), where metabolic changes gathers cytoplasmic materials required for mitosis and cytokinesis; and mitotic (M) phase, where replicated DNA separates into the daughter cells. These events occur once per cell cycle in the described sequential order (Elledge, 1996). This requires coordination between the cell cycle and the parasite life cycle regulation (Matthews and Gull, 1994a) (section 1.3 of this thesis). Kinetoplast DNA replication initiates prior to nuclear DNA replication in S phase. Thus, at the onset of the G1 phase of the cell cycle, each cell has a single kinetoplast and nucleus (1K1N) (Woodward and Gull, 1990).

The cell cycle regulatory machinery of *T. brucei* has some similarities and differences with other eukaryotic organisms. The genome of *T. brucei* consist of genes encoding several cyclins and Cdc2-related kinases (CRKs) (Elledge, 1996), which are essential for the cellular changes occurring between the G1/S and G2/M-phases (Hammarton et al., 2004; Tu and Wang, 2004). The spindle assembly checkpoint, which is important for cell division in other eukaryotes, is yet to be identified in trypanosomatid species (Hammarton, 2007; Li, 2012).

Since trypanosomes comprise several single-copy organelles such as the basal body, the flagellum, the mitochondrion and the kinetoplast (mitochondrial DNA), organelle replication and segregation must be tightly regulated and integrated in the cell cycle (Steinert and Van Assel, 1967).

During the G1 phase, eukaryotic cells respond to environmental cues, which determine whether to multiply, differentiate or go into quiescence. Current data suggest that trypanosomes regulate G1 phase progression through different mechanisms (Hammarton, 2007). For example, *T. brucei* lacks receptor-linked tyrosine kinases and G-protein coupled receptors. Additionally, the organism has only one phosphoinositide 3-kinase (Vps34), which is vital for Golgi segregation in *T. brucei* but not for development across G1 (Hall et al., 2006).

However, the CRKs (cyclin-related kinases) are required for progression through G1 phase in (Hall et al., 2006).

During the nuclear S-phase, the replicated mitochondrial genomes segregate into two kinetoplasts (generating a 2 kinetoplast, 1 nucleus, '2K1N', configuration of DNA containing organelles). The basal body extends and develops a new daughter basal body close to the existing basal body (Sherwin and Gull, 1989). A new flagellum also begins to obtrude from the daughter basal body, extending within the flagellar pocket (Lacomble et al., 2010) and then externally. Bloodstream forms have no flagellar connector (a structure in procyclic forms that tethers the flagellar tip along the cell body as it extends; Moreira-Leite et al., 2001), thereby allowing flexibility for growth to occur (Briggs et al., 2004). The binding of the flagellum attachment zone (FAZ) between the flagellar tip and the base of the flagellum causes a relocation of the daughter basal body to the posterior of the cell.

The relocation event is also influenced by growth and movement of the daughter flagellum (Absalon et al., 2007). Segregation of the kinetoplast is aided by the connection of basal bodies to the kDNA by the tripartite attachment complex (TAC; Ogbadoyi et al., 2003); the movement is driven by migration of the basal body (Robinson and Gull 1991).

Transition to the G2/M phase in *T. brucei* is controlled by the mitotic cyclin dependent kinases (CDK). This is performed by the cyclin related kinase (CRK3), which is homologous to the mammalian CDK1. Formation of a complex between CRK3 and the cyclin-like gene, CYC6, ensures initiation of mitosis (Li and Wang, 2003; Tu and Wang, 2004). Cells in G2 phase have 2K1N due segregation of the replicated kinetoplast, but not the nuclear DNA. Progression to the M phase causes segregation of chromosomal DNA (Sharma et al., 2008). After mitosis, and just prior to cytokinesis, the cells contain two kinetoplasts and two nuclei (2K2N; Woodward and Gull, 1990).

Cytokinesis occurs following cleavage at the anterior end (Kohl et al., 2003), which progresses towards the posterior end between the two flagella (Vaughan and Gull, 2003). In the procyclic forms, the arrangement is KNKN, (Figure 1.4) while in the bloodstream form its arranged as

KKNN (Briggs et al., 2004). Cellular checkpoints exist in the bloodstream forms and procyclic forms to ensure that mitosis will only take place after the nucleus has undergone S phase; however, cytokinesis can occur in the absence of mitosis, generating anucleate cytoplasts ('zoids';) (Robinson et al., 1995).

There does not, however, appear to be a mitosis-dependent cytokinesis checkpoint in trypanosomes, with cytokinesis progressing even if mitosis fails (Ploubidou et al., 1999; Robinson et al., 1995). The mechanism controlling coordination between DNA duplication and segregation is not well understood. Specifically, change in a single amino acid in the nuclearly encoded F_1F_O–ATPase subunit γ can compensate for complete loss of kDNA in the bloodstream form of *T. brucei* (Dean et al., 2013). The ATP synthase γ mutation that compensates for kDNA loss in bloodstream forms is not able to compensate for kDNA loss in procyclic forms.

This observation precludes a potential kDNA replication checkpoint for cell cycle completion, suggested by (Ploubidou et al., 1999), but indicates that the checkpoint is DNA independent, perhaps being enacted at the level of the basal bodies. Pleomorphic *T. brucei* with and without kDNA (selected after expressing mutant γ in strain AnTat1.1 90:13) can also differentiate to stumpy forms. However, these akinetoplastic cells showed a decreased lifespan, suggesting a critical role for a kDNA-encoded product in stumpy form (Dewar et al., 2018). These akinetoplastic and pleomorphic cell line was used in this study to generate RNA-Seq data in Chapter 3.

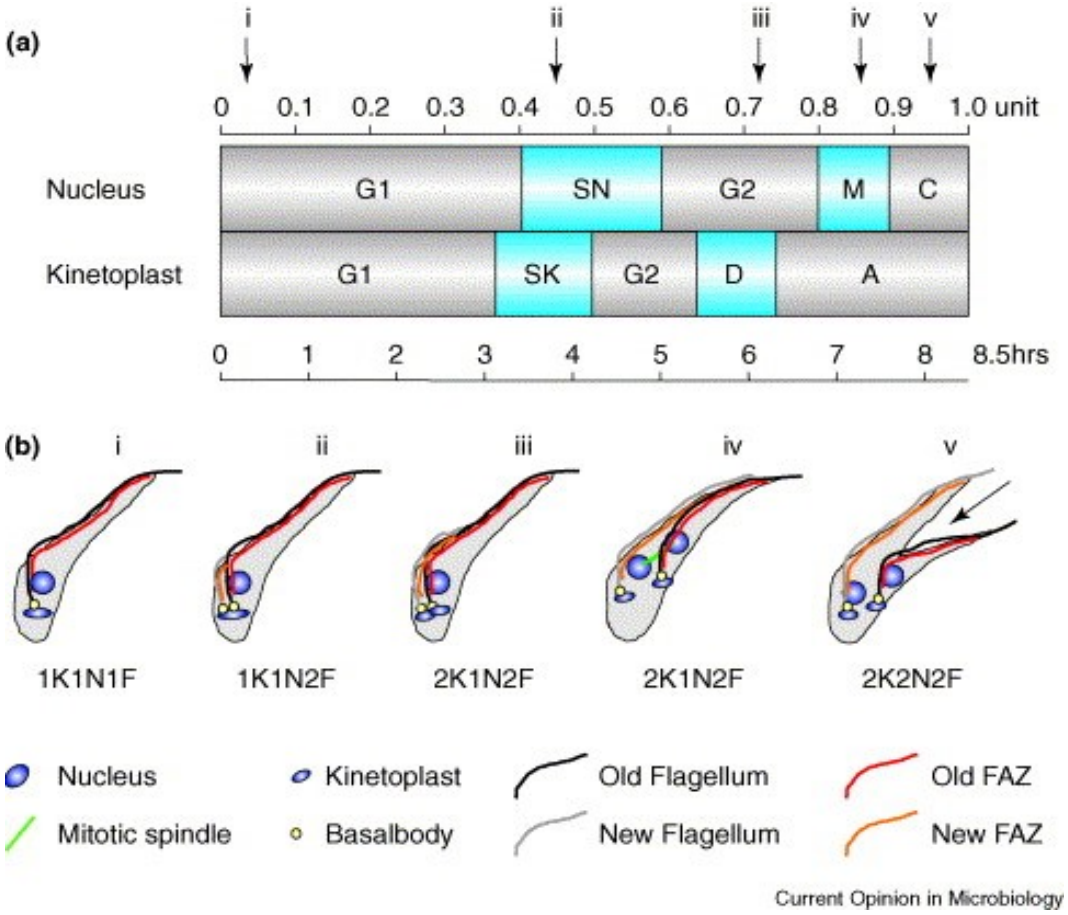

Figure 1.4. Cell cycle showing the major morphological events of *T. brucei* procyclic forms. (a)The trypanosome cell cycle categorised under nuclear and kinetoplast components of DNA replication (S). Kinetoplast DNA replication initiates before nuclear DNA replication. The latter is relatively shorter and is followed by kinetoplast segregation (D), which preceed nuclear mitosis (M). 'A' refers to the 'apportioning' phase during which basal bodies move away from each other. (b) Schematic representations of the formation of daughter cells through the cell cycle. The black arrow indicates the direction and position of the cleavage groove (McKean, 2003).

1.2.5 Glycosomes

Glycosomes are peroxisome-like organelles found in trypanosomatids. They are responsible for sequestering enzymes needed for β- oxidation of fatty acids, lipid biosynthesis and purine salvage. Also, most enzymes involved in the glycolytic pathway are found within the glycosome, even though other organisms have these enzymes localized within the cytosol (Haanstra et al., 2016; Opperdoes, 1987).

T. brucei has a range of proteins which are used for preserving the glycosome population to maintain a well-organized energy production system (Furuya et al., 2002; Michels et al., 2006). Glycosomes are indispensable for survival of the parasite. The composition of glycosome is dependent on the life cycle of the parasite. For the bloodstream form of the parasite, ATP is generated solely by glycolysis, the components of which comprise approximately 90% of glycosomal proteins (Haanstra et al., 2016). On the contrary, the procyclic forms of the parasite generate ATP via glycolysis in the presence of glucose, but switches to amino acid-based metabolism in the absence of glucose (Lamour et al., 2005). Unlike the bloodstream forms, procyclics have a fully functional mitochondrion and specific proteins which are involved in the production of ATP (details on ATP production by the mitochondrion is provided in section 1.3.5). Moreover, activation and upregulation of the mitochondrion in the procyclic form are relevant for metabolism of proline and threonine, the electron transport chain and the tricarboxylic acid (TCA) cycle (Haanstra et al., 2016; Misset et al., 1986).

1.2.6 Gene Expression

Gene expression is regulated at different stages, which includes transcription, mRNA stability, translation and protein stability (Jeacock et al., 2018). *T. brucei* is an interesting model organism for studying gene expression because of the presence of GT-rich RNA polymerase II (pol-II) promoters, which are responsible for driving constitutive polycistronic transcription. However, they lack regulators of RNA polymerase II promoters for protein-coding genes (Wedel et al., 2017).

Unlike other eukaryotes, where RNA polymerase I solely transcribes ribosomal RNA (rRNA), in *T. brucei* this enzyme also transcribes genes encoding the variant surface proteins of the bloodstream forms and the procyclin genes of procyclin forms of the parasite (Günzl et al., 2003). Most protein-encoding genes in kinetoplastids are arranged as polycistronic units of dozens of genes that are transcribed from a common promoter into long mRNA precursors

(Martínez-Calvillo et al., 2003). Mature mRNA is generated via post-transcriptional processing, including trans-splicing (Liang et al., 2003).

Trypanosomes have only two genes with known introns (Tb927.3.3160 and Tb927.8.1510 (Koch et al., 2016), and each mRNA has an identical sequence *trans*-spliced onto the 5'-end (Clayton, 2016; Mair et al., 2000); the mature mRNA is obtained via post-transcriptional processing (Liang et al., 2003). However, the 3'-untranslated sequences are responsible for translational control, mRNA stability and interactions with RNA-binding proteins (Clayton, 2013). In yeast, a single mRNA can generate 4000 protein molecules (Futcher et al., 1999). In contrast, the ratio of mRNA to protein in *T. brucei* procyclic forms is 1:550 (Kolev et al., 2010).

1.3 Energy metabolism and mitochondrial biology of trypanosomes

Trypanosomes have a single mitochondrion, unlike many other eukaryotes which usually have multiple mitochondria per cell. The trypanosome mitochondrial DNA contains an incompletely characterised genome that is organised into a single, discrete structure, called kinetoplast DNA (kDNA). The kDNA comprises giant genetic elements of thousands of concatenated circular DNA, classified as maxicircles and minicircles (Kolev et al., 2010). A cell of *T. brucei* contains 30-50 copies of maxicircles and about 200-400 copies of minicircles, which makes kDNA replication a complex process (Verner et al., 2015). The population of minicircles in *T. brucei* is heterogeneous, with each minicircle encoding between two to five guide RNAs (Pollard et al., 1990). These guide RNAs are responsible for RNA editing (Aphasizhev et al., 2016; Hajduk and Ochsenreiter, 2010).

RNA editing is essential in *T. brucei*, and is currently being explored as a potential drug target (Schnaufer et al., 2001). RNA editing is performed by the 20S editosome (Mehta et al., 2015; Simpson et al., 2017). The process of RNA editing can either be repair of frameshifts, insertion of uridine at the 5’ end of the mRNA to generate a start codon, or formation of an entire open reading frame (ORF) by insertion or deletion of several uridines. RNA editing is

a sequential process, which occurs in the 3' - 5' direction (Maslov and Simpson, 1992; Panigrahi et al., 2003).

The maxicircles and minicircles are intertwined to form a large disc-shaped network that is connected to the basal body of the flagellum. Kinetoplast histone-like associated proteins (KAP1-KAP4) are involved in stabilizing the kDNA network to form a regular disk (Xu et al., 1996). The kDNA is linked to the base of the flagella and the basal body by a membrane-bound so-called tri-partite attachment complex (TAC). The TAC consist of three regions; the first region connects the kDNA network to the inner mitochondrial membrane (IM), the second region is a segment tightly enclosing a detergent-resistant differentiated IM and outer membranes (OM) and the third region comprise the final (exclusion zone) filaments that form a link between the OM and the basal body (Povelones, 2014; Robinson and Gull, 1991).

Currently, the identified components of the TAC include the p166, which contains a single transmembrane domain (TMD) and is not essential for localization of the complex (Zhao et al., 2008). The TAC102 constitute unilateral filaments while p196 and TAC65 have been shown to localize to the exclusion zone filaments (Gheiratmand et al., 2013; Kaser et al., 2016; Trikin et al., 2016). TAC40, a β-barrel protein of the mitochondrial porin family was found to be confined to the TAC whiles the peripheral archaic translocase of the OM 36 protein (pATOM36) was detected throughout the OM (Käser et al., 2016).

Procyclic and bloodstream form *T. brucei* depend on their mitochondrion and, normally, their kDNA for survival. However, as described above (section 1.2.4), some akinetoplastic (AK, cells without kDNA) and dyskinetoplastic (DK, cells that have lost functionally critical parts of kDNA) *T. brucei* bloodstream form mutants do exist (Schnaufer et al., 2001). Specific mutations in the nuclearly encoded subunit γ of the F_OF_1-ATPase enable AK or DK cells of the bloodstream form to survive (Dean et al., 2013), but viable AK or DK insect forms have not been reported (Schnaufer et al., 2002; Stuart, 1971). Loss of kDNA can be induced with kDNA-intercalating drugs or by down-regulation of proteins required for kDNA replication or segregation (Schnaufer et al., 2002, Wang and Englund, 2001).

1.3.1 Structure and expression of trypanosome mitochondrial genome

The mitochondrion is an indispensable organelle in most eukaryotes, though some organisms can survive without it. In addition to production of energy, the mitochondrion triggers signalling, cell death and cell proliferation (McBride et al., 2006). The mitochondrion possess its own genome, which is organized for transcription, replication and translation (Borst, 1972; Schatz et al., 1964), even though most proteins are encoded by the nuclear DNA, translated in the cytosol and imported into the mitochondrion (Chacinska et al., 2009).

One of the characteristics of the *T. brucei* life cycle is the regulation of mitochondrial activity. Control of mitochondrial activity through the life cycle, in particular with respect to energy metabolism, is central to fulfilling the metabolic requirements of the trypanosome. Alternating between extreme niche environments requires vast morphological and metabolic adaptations. The slender bloodstream form of the parasite uses ATP generated by glycolysis, with oxidative phosphorylation absent.

The mitochondrion of bloodstream forms does not have detectable cytochromes and lack several key enzymes of the citric acid cycle (such as pyruvate dehydrogenase, a-ketoglutarate dehydrogenase, citrate synthetase, and succinate dehydrogenase) that are required for oxidative phosphorylation. Hence the mitochondrion is not involved in energy production in the bloodstream forms (Priest and Hajduk, 1994; Vickerman Keith, 1965). However, the mitochondrion has roles in iron-sulphur centre (Fe/S) biogenesis (Kovarova et al., 2014), fatty acid biosynthesis (Clayton et al., 2011) and production of thymidine monophosphate (dTMP) (Roldan et al., 2011).

Differentiation of stumpy form prepares the activation of mitochondrion for energy production in the procyclic form (Priest and Hajduk, 1994; Vickerman Keith, 1965). The mitochondrion is a single elongated and stretched tube (Tyler et al., 2001) as shown in Figure 1.5. Activation of the mitochondrion involves expansion and remodeling of the inner membrane to form cristae (Gilkerson et al., 2003; Vickerman Keith, 1965). Furthermore, the

entire organelle is enlarged and forms a complex network throughout the cell (Figure 1.5) (Priest and Hajduk, 1994).

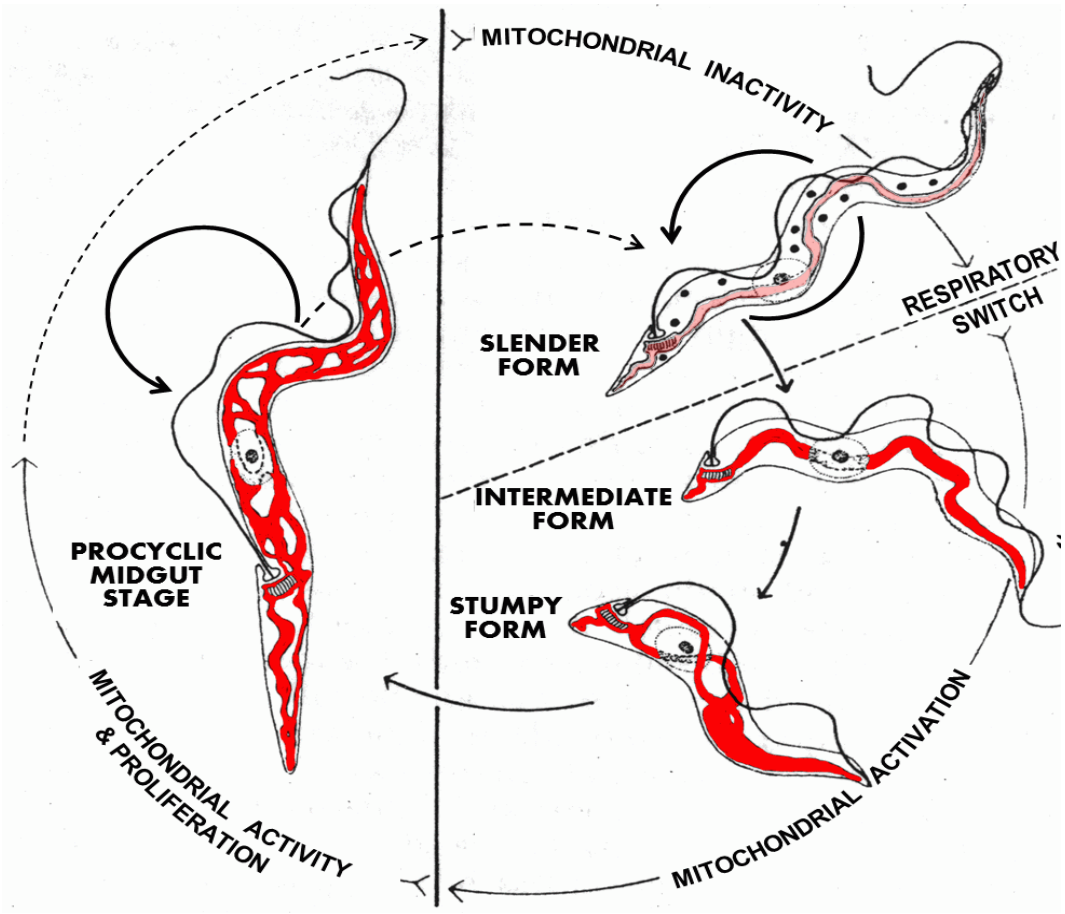

Figure 1.5. The life cycle of *Trypanosoma brucei* and mitochondrial function. The mitochondrial activity changes across the life cycle stages of *T. brucei.* Mitochondrion is inactive for oxidative phosphorylation in slender forms (the mitochondrion is shown in pale pink). Differentiation from intermediate to stumpy forms causes upregulation of mitochondrion activity in preparation for oxidative phosphorylation (mitochondrion is shown in red). In the procyclic form, mitochondrion is active for oxidative phosphorylation. This image is adapted from Vickerman (1965) after modification by A. Schnaufer.

The *T. brucei* ETC consists of five classic multi-subunit complexes (cI-cV) (Figure 1.6). Complex I is discussed in detail in section 1.3.6, whereas complexes II, III, IV and V are explained in this section. There are three additional enzymes that provide alternative pathways for the flow of electrons between UQ and UQH_2. These enzymes are: (i) glycerol-3-phosphate oxidase (GPO, Figure 1.7), which oxidizes glycerol-3-phosphate (G-3-P) to dihydroxyacetone phosphate (DHAP) (Guerra et al., 2006); (ii) a rotenone-insensitive NADH:Q oxidoreductase (NDH2) (Fang and Beattie, 2002); (iii) the trypanosome alternative oxidase (TAO), which catalyzes the reduction of O_2 to H_2O (Chaudhuri et al., 2002). The TAO is absent in the mammalian host. None of these enzymes contribute to ΔΨm, as they do not pump protons. In the bloodstream form, these three complexes together with complexes I and V are present in the inner mitochondrial membrane (Surve et al., 2012). It has been hypothesized that cI activity can be fully replaced by NDH2 to regenerate NAD^+ (Fang and Beattie, 2002). However, when NADH was applied externally to digitonin-permeabilised procyclic cells to ascertain whether the NADH binding site of NDH2 has the correct orientation to contribute to mitochondrial NAD+ regeneration, oxygen consumption was detected (Verner et al., 2013). The mitochondrial membrane is resistant to NADH, suggesting that NDH2 is oriented towards the cytosol in the mitochondrial membrane.

In bloodstream forms, the first seven steps of glycolysis occur in the glycosome, which is associated with mitochondrial respiration through the glycerol-3-phosphate:dihydroxyacetone phosphate shuttle (G3P:DHAP). The shuttle consists of two enzymes; GPO in the inner mitochondrial membrane (see above and Figure 1.7) and NAD-dependent glycerol-3-phophate dehydrogenase (NAD-G3PDH), which is positioned within the glycosomes (Opperdoes et al., 1977). NAD^+ is produced from the G3P:DHAP in bloodstream and procyclic forms. Alternatively it can be generated from the succinate-producing glycosomal pathway in procyclic forms to maintain an NAD+/NADH balance in the glycosome (Michels et al., 2006). In bloodstream forms, GPO transfers electrons from G3P to ubiquinol in the mitochondrial IM. Subsequently, ubiquinone is produced following oxidation by the TAO.

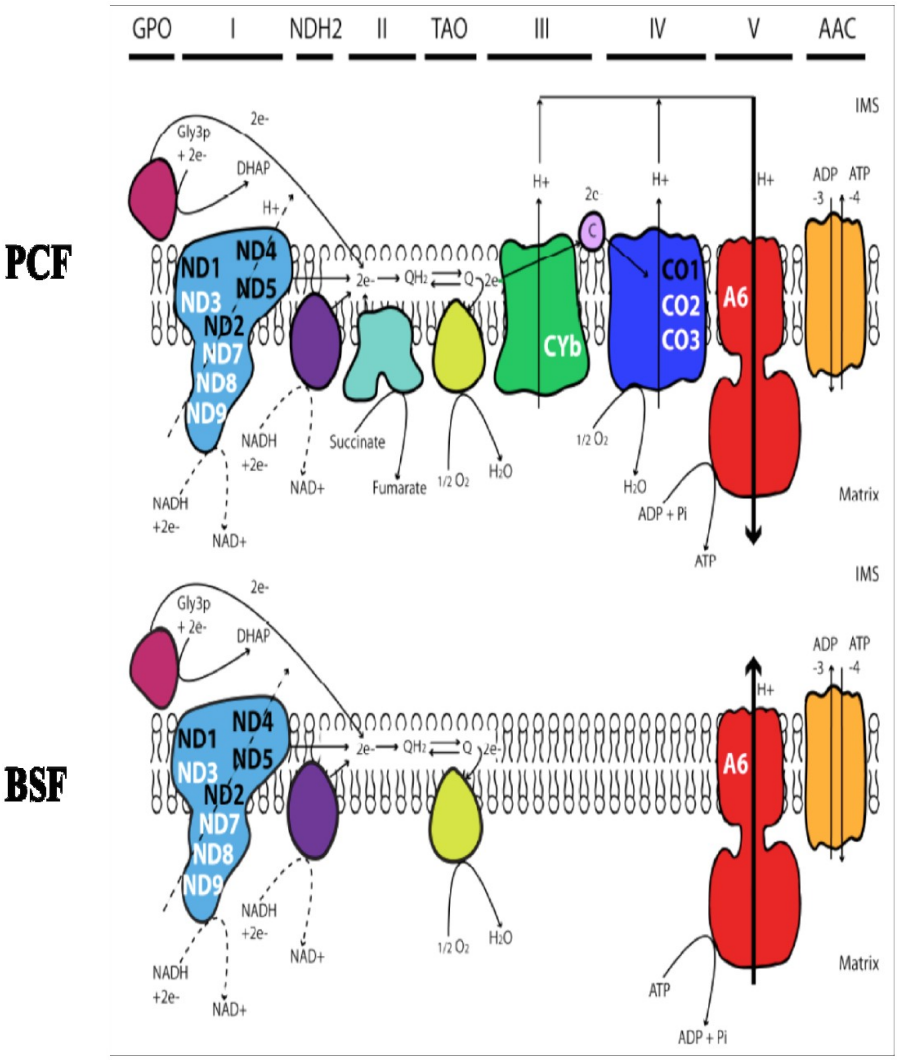

Figure 1.6. Composition of the respiratory chain varies across the life cycle of *T. b. brucei*. Complexes I, III, IV and V contain kDNA-encoded subunits. These are labelled; black = never-edited, white = edited. Key: GPO = glycerol-3-phosphate oxidase, NDH2 = alternative NADH:ubiquinone dehydrogenase, TAO = trypanosome alternative oxidase, AAC = ADP/ATP antiporter (Figure produced by L. Jeacock and A. Schnaufer).

1.3.1.1 Complex II

Complex II has been shown to be non-essential in procyclic forms in the presence of abundant glucose, but it is essential in glucose-depleted conditions (Coustou et al., 2008). In the absence of glucose, proline catabolism is used to generate ATP in the mitochondrion. Interestingly, the *T. brucei* complex II is larger than in other eukaryotes, having additional but non-canonical subunits (Acestor et al., 2011). Complex II may also be present in the stumpy bloodstream forms, although its activity or role is yet to be determined (Gunasekera et al., 2012).

1.3.1.2 Complex III

Complex III (cIII) is a multisubunit transmembrane protein encoded by both the mitochondrial (subunit apocytochrome b, CyB) and the nuclear genomes. In bloodstream forms, the levels of CyB transcript are very low (Michelotti and Hajduk, 1987). Translation of this subunit cannot occur in this parasitic stage, as unedited CyB mRNA lacks an AUG codon that is generated by the editing of the transcript only in procyclic forms (Feagin et al., 1987). Genetic knock-down of two nuclearly-encoded subunits of cIII (Rieske protein and subunit I) in procyclic forms (Horváth et al., 2005) resulted in retardation of cell growth, as well as in a decrease of cytochrome c reductase activity and $\Delta\psi m$. These observations are in accordance with complex III having a classical role in the procyclic respiratory chain.

1.3.1.3 Complex IV

Complex IV or cytochrome c oxidase (COX) has three mitochondrially and fifteen nuclearly-encoded core subunits. Complex IV also has multiple accessory proteins whose functions are currently unknown (Zíková et al., 2008). Messenger RNAs for two of the mitochondrially-encoded subunits, COX II and III, are edited in procyclic forms (Priest and Hajduk, 1994).

Silencing of three novel subunits of complex IV by RNAi in procyclic forms showed no lethal growth defects, even though there was drastic decrease in RNA level as well as cytochrome c oxidase activity (Gnipova et al., 2012). Complex IV has a traditional role in the procyclic respiratory chain. Hence, knocking down subunits of the complex reduces the Δψm and the cytochrome c oxidase activity. In the bloodstream form, complex IV is absent (Figure 1.6) and is induced upon differentiation to the procyclic form (Mayho et al., 2006; Priest and Hajduk, 1994).

1.3.1.4 Complex V

Complex V or ATP synthase (F_1F_O ATPase) uses transmembrane protonmotive force, which is generated via electron flow to O_2, to synthesise ATP from ADP and inorganic phosphate in a process called oxidative phosphorylation (Boyer, 1997,

Baradaran et al., 2013; Berrisford and Sazanov, 2009; Friedrich and Bottcher, 2004). The structure of ATP synthase consists of an extrinsic domain, F_1, and an intrinsic membrane domain, F_O, which are linked by two stalks (Boyer, 1997). A connecting central stalk contains subunits δ, ε, and γ; the latter subunit contacts both F_1 and F_O. The enzyme functions as a reversible H^+-transporting ATPase via coupling of F_1 and F_O. In yeast, the mitochondrial ATP synthase consist of thirteen different subunits.

The F_1 segment comprises subunits α, β, γ, δ and ε, and the F_O sector subunits 6, 8, 9, β, δ, f, h and OSCP (Spannagel et al., 1997). In *T. brucei*, complex V has a stoichiometry of $\alpha_3\beta_3\gamma_1\delta_1\varepsilon_1p18_1$ for the F_1 subunits. The F_O complex is composed of one each of subunits 6 (a) and 4 (b) and a ring of multiple subunits 9 (c). The catalytic sites of ATP synthase are within the β subunits, with three active sites per complex. All three active sites need to be occupied for optimal catalysis (Amano et al., 1996). The subunits b, OSCP, F6 and d make up the peripheral stalk. During ATP synthesis, the movement of protons across the concentration gradient into the matrix occurs through the F_O segment by successive protonation and

deprotonation of aspartate 6 in subunit c, thereby driving rotation of the c ring (Girvin and Fillingame, 1995; Kuruma et al., 2012). This causes rotation of γ within the α/β hexamer, which results in a conformational change within the β active sites to drive ATP synthesis (Rastogi and Girvin, 1999). A complete revolution of γ within the $\alpha_3\beta_3$ core produces three ATP molecules (Stock et al., 1999).

The A6 is a subunit of F_O ATPAse subunit 6; it is encoded by the mitochondrion and is involved in proton translocation (Kuruma et al., 2012). The A6 transcript is pan-edited in both bloodstream and procyclic forms. Specific point mutations within the nuclearly-encoded γ subunit of the mitochondrial F_1 F_O - ATPase allow survival in the absence of kDNA in the slender bloodstream forms of *T. brucei* (Dean et al., 2013).

In the bloodstream form of *T. brucei*, ATPase generates Δψm during ATP hydrolysis, and the ADP/ATP carrier (AAC) supplies the mitochondrion with ATP from glycolysis (Schnaufer et al., 2005). The ADP/ATP carrier plays an essential role in sustaining the cellular ATP homeostasis by exchanging mitochondrial ATP for cytosolic ADP. The enzyme fuels the substrate level phosphorylation and oxidative phosphorylation in procyclic cells by providing the mitochondrion with ADP and the rest of the cell with mitochondrially-produced ATP. AAC activity in procyclic forms is driven by Δψm. This observation is supported by RNAi studies performed on TbMCP5 (Peña-Diaz et al., 2012). Moreover, the AAC inhibitor, carboxyatractyloside (CATR), strongly reduced mitochondrial ATP production, confirming that the exchange of mitochondrial ATP for cytoplasmic ADP is entirely aided by AAC activity (Peña-Diaz et al., 2012).

1.3.2 Mitochondrial Protein Import in Trypanosomes

In *T. brucei*, as in other eukaryotes, most mitochondrial proteins are encoded in the nucleus. These proteins must be imported into the mitochondrion to perform their functions. TOM40 is a typical protein import channel within the mitochondrial outer membrane (Gabriel et al., 2001; Neupert, 1997).

The OM protein translocase of *T. brucei* called archaic translocase of the outer mitochondrial membrane (ATOM) has 7 subunits (ATOM40, ATOM19, ATOM14, ATOM12, ATOM11, ATOM69 and ATOM46) and also aid membrane translocation (Desy et al., 2016). Except for ATOM46, the remaining six subunits are essential for mitochondrion protein import (Harsman and Schneider, 2017).

Only two ATOM subunits, ATOM40 and ATOM14, have been shown to be homologous to the yeast TOM subunits (Mani et al., 2016). Until now, no orthologues of the other five ATOM subunits have been found outside the kinetoplastid lineage. *T. brucei* contains a SAM complex within the mitochondrial OM, and the core subunit (Sam50/Tob55) is conserved (Sharma et al., 2010).

1.3.3 Metabolism in slender bloodstream form

In bloodstream form, ATP is mainly produced via glycolysis; pyruvate is generated as the end product (Creek et al., 2015), along with some production of succinate, acetate and alanine (Mazet et al., 2013). Trypanosomatids partially oxidize pyruvate, succinate, alanine and acetate, which are secreted as end products from energy metabolism (Mazet et al., 2013). All trypanosomatids studied so far generate acetate, which vary across their life cycle stages (Cazzulo, 1992; VanHellemond et al., 1997) and is dependent on the species and environmental conditions.

Conversion of glucose to 3-phosphoglycerate occurs within the glycosome, with pyruvate conversion occurring in the cytosol. There is a fine balance between ATP production and usage, as well as NADH/NAD^+ balance, which must be maintained within the glycosome under aerobic conditions for efficient ATP production. Aldolase generates two 3-carbon intermediates, DHAP and G3P. DHAP is converted to G3P within the glycosome, with glycosomal NAD^+ maintaining the metabolism of G3P to pyruvate. (Figure 1.7). In the mitochondrion, pyruvate is converted by the pyruvate dehydrogenase complex into acetyl-CoA and then into acetate. Two ATPs are generated by pyruvate kinase from glycolysis

(Michels et al., 2006). Under anaerobic conditions, DHAP is metabolised to glycerol, thereby producing one ATP molecule within the glycosome (Figure 1.7).

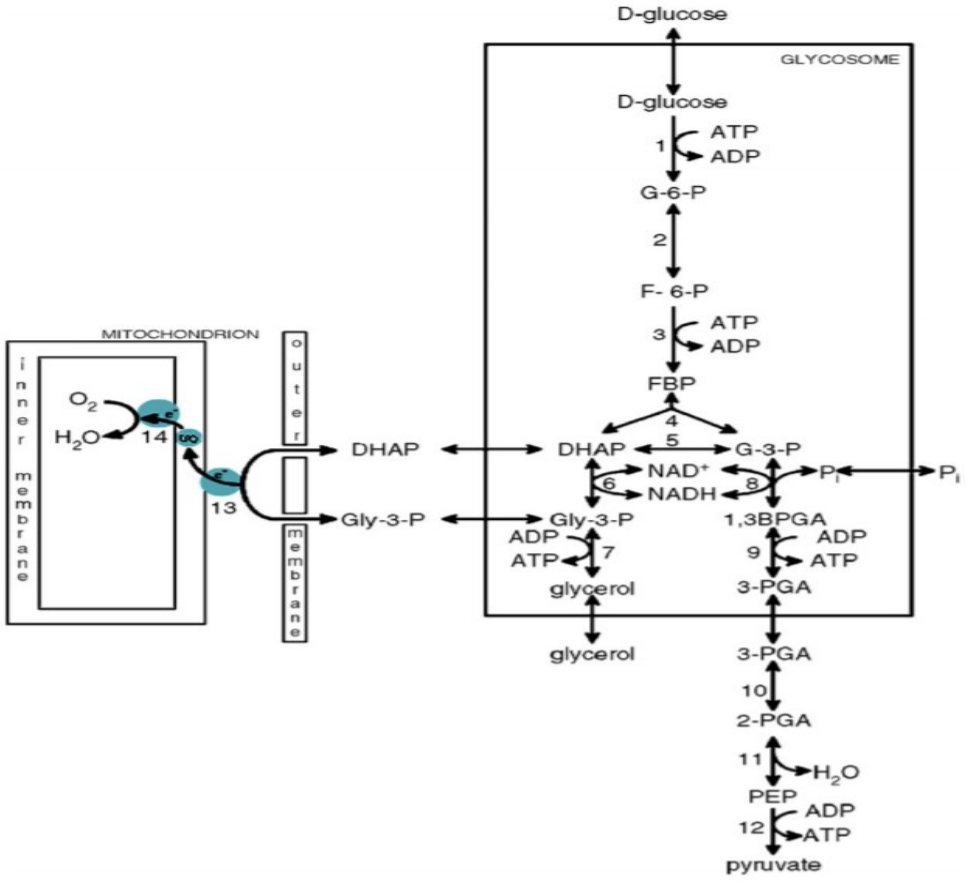

Figure 1.7 Glycolytic pathway in bloodstream form of *T. brucei.* This pathway shows the aerobic and anaerobic conditions, leading to pyruvate and glycerol production respectively. Key for abbreviations and enzymes involved in the pathways are listed: 1,3 BPGA = 1,3 bisphosphoglycerate, DHAP, dihydroxyacetone phosphate, F6P = fructose-6-phosphate, G3P = glyceraldehyde-3-phosphate, G6P = glucose-6-phosphate, Gly-3-P= glycerol-3-phosphate, PEP = phosphenolpyruvate, 3PGA = 3-phosphoglycerate, Pi = inorganic phosphate, UQ = ubiquinone pool. Enzymes: 1. hexokinase, 2. G6P isomerase, 3. phosphofructokinase, 4. aldolase, 5. triosephosphate isomerase, 6. G3P dehydrogenase, 7. glycerol kinase, 8. G3P dehydrogenase, 9. phosphoglycerate kinase, 10. phosphoglycerate mutase, 11. enolase, 12. pyruvate kinase, 13. glycerol3-phosphate dehydrogenase, 14. alternative oxidase. The image is adapted from (Michels et al., 2006).

1.3.4 Metabolism in stumpy bloodstream form

The stumpy forms adapt to the procyclic midgut upon entry into the tsetse fly. This adaptation also corresponds to metabolic changes occurring within the parasite during differentiation from slender to stumpy forms. Stumpy bloodstream form show increase in complex I, II and V activities, whilst complex III and IV activities attain their peak in the procyclic forms. Stable isotope labelling by amino acids in cell culture (SILAC), followed by quantitative proteomic analysis has been used to demonstrate that stumpy forms have abundant mitochondrial proteins compared to slender forms when the fold change (log_2) was analysed between the different life cycle stages (Gunasekera et al., 2012). The production of acetate from acetyl-CoA is catalysed by either ASCT or acetyl coA thioesterase (Figure 1.8) (Mazet et al., 2013). Moreover, stumpy forms can utilise glucose and α-ketoglutarate as energy sources (Vickerman Keith, 1965). Complex V is believed to act in the directionality of ATP synthase in the stumpy form (Dewar et al., 2018). It has been reported that SCoAS and ASCT levels in stumpy forms and procyclic are similar (Gunasekera et al., 2012).

1.3.5 Metabolism in procyclic forms

The mitochondrion of procyclic forms can produce ATP through three different pathways (Besteiro et al., 2005) (Figure 1.9). Under conditions of glucose deficiency, the carbon sources that are used for ATP production are proline, an amino acid abundant in the fly midgut, and threonine. Metabolism of proline produces alanine, glutamate, CO_2 and succinate in glucose-deficient medium (van Weelden et al., 2005) whiles the end products of threonine metabolism are acetate and glycine (Linstead et al., 1977; van Weelden et al., 2005).

A metabolic switch occurs as the stumpy forms in the mammalian bloodstream transit to the midgut of tsetse fly and differentiate into procyclic forms (Fenn and Matthews, 2007). Conversion of proline to glutamate is mediated by enzymatic and non-enzymatic steps. Firstly, proline is oxidized to Δ^1-pyrroline-5-carboxylate (P5C) by a FAD-dependent proline

dehydrogenase (TbProDH) (Lamour et al., 2005). The P5C ring opens to produce glutamate-γ-semialdehyde (γGS) through a non-enzymatic process.

Finally, the γGS carbonyl moiety is oxidized to glutamic acid by a P5C dehydrogenase (TbP5CDH). The final step is associated with reduction of $NAD(P)^+$ to NAD(P)H (Mantilla et al., 2015).

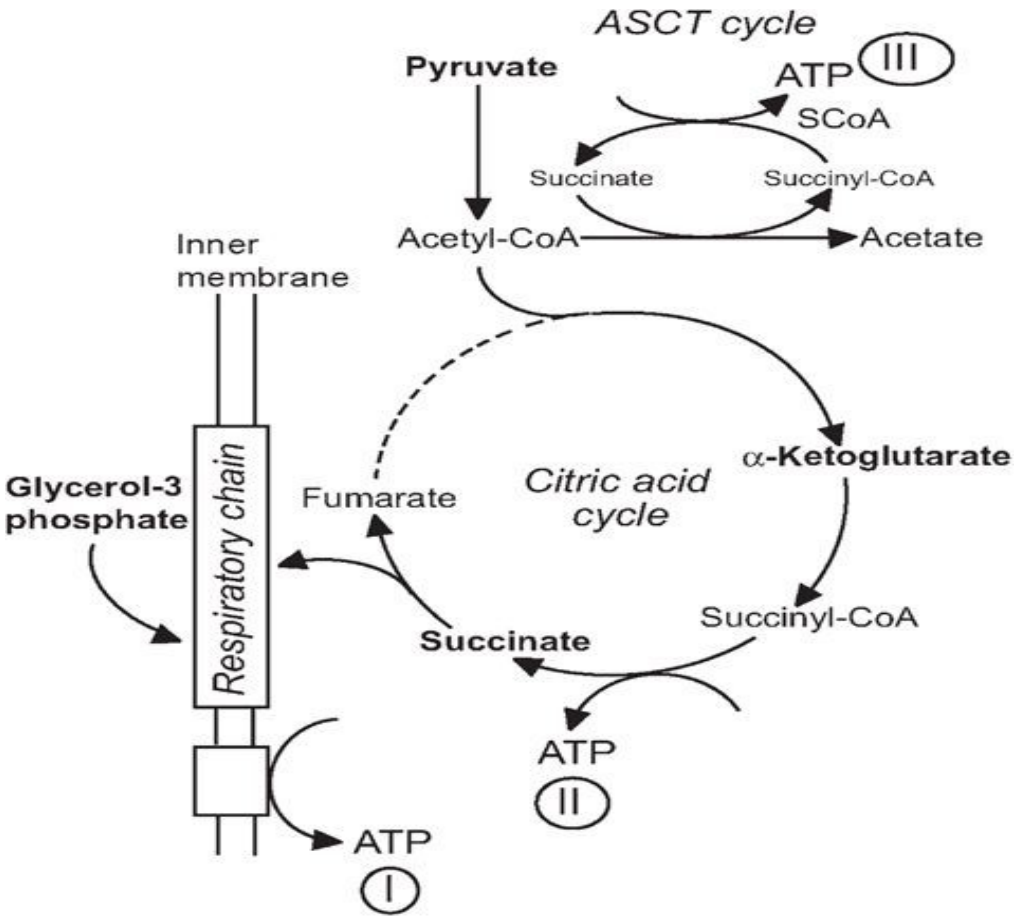

Figure 1.8 Mitochondrial ATP production in procyclic forms of *T. brucei.* The three ATP production pathways are the respiratory chain, the citric acid cycle, and the ASCT cycle. The sites of ATP production are I: corresponds to OXPHOS; II and III correspond to SUBPHOS (Schneider et al., 2007).

The acetate:succinate CoA-transferase/SCoAS cycle (ASCT cycle) produces ATP, coupling ATP generation with acetate formation (Bochud-Allemann and Schneider, 2002). It can function in anaerobic conditions, which is a possible adaptation to hypoxic conditions in the fly. Mitochondrial ATP can be generated by SUBPHOS in an aerobic condition where acetate is formed using the acetate:succinate coenzyme A (CoA) transferase/SCoAS cycle (ASCT cycle) (see Figure 1.8) (Van Hellemond et al., 1998). Proline metabolism generates α-ketoglutarate as an intermediate causes flux through this pathway (Bochud-Allemann and Schneider, 2002).

This enzyme is essential in the presence of glucose; the interruption of SCoAS eliminates mitochondrial ATP production via the substrate level phosphorylation pathways (Figure 1.8). ASCT is expressed in procyclic forms but is not important in the presence of glucose because acetyl-CoA thioesterase is able to generate acetate (Zíková et al., 2017). Production of ATP using substrate level phosphorylation is approximately 3 times higher in glucose-rich media compared to glucose-depleted media, due to ASCT (Bringaud et al., 2006). The ASCT cycle occurs in the mitochondria of trypanosomatids and some helminths and is also present in the hydrogenosomes of trichomonads and some fungi (Schneider et al., 2007).

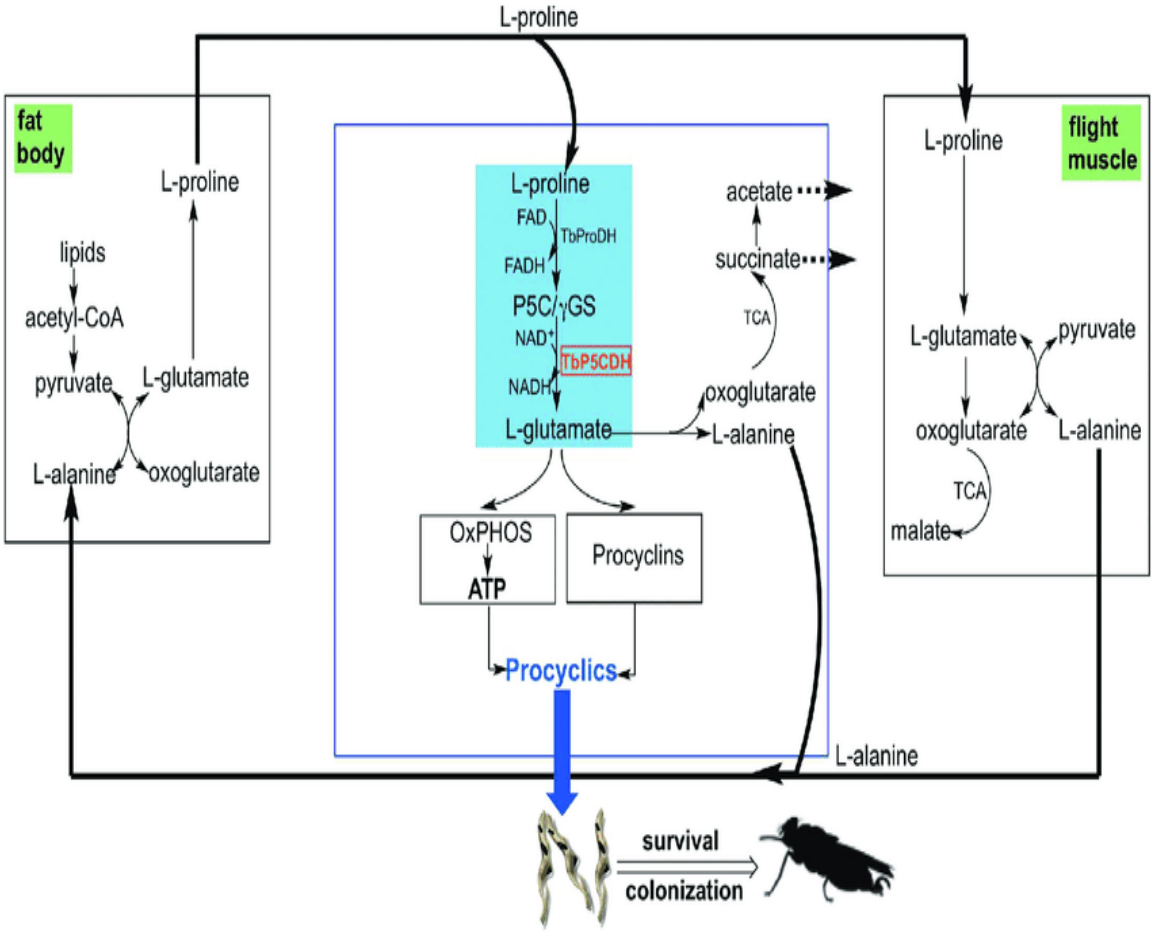

Figure 1.9 Proline-alanine cycle between *T. brucei*, tsetse tissue, fat body and flight muscles. Proline combustion produces alanine as the main end product in tsetse flight muscle (right panel). Alanine is conveyed to the fat body by the hemolymph (left panel). Alanine and lipids are the main sources for proline production in the fat body. Alanine amino group (-NH2) is transported to oxoglutarate to generate glutamate and pyruvate. Pyruvate can be carboxylated to form oxaloacetate and acetyl-CoA for β-oxidation of lipids. The fat body TCA cycle goes from citrate to oxoglutarate. Proline fuels the respiratory capacity to synthesize ATP driven by OxPHOS. Midgut procyclics depend on proline degradation for survival within tsetse fly. TbP5CDH (in red) is important for establishment within the tsetse (Mantilla et al., 2015).

1.3.6 Complex I of *T. brucei*

The presence and role of complex I (NADH dehydrogenase) in energy metabolism in trypanosomatid has been debated (Opperdoes and Michels, 2008). Eukaryotic complex I consists of about 46 subunits; 14 of these subunits are bacterial core subunits and 21 subunits are eukaryotic core subunits. The *Trypanosoma* complex I has 19 subunits which are homologous to both eukaryotes and prokaryotes. Homology search of *T. brucei* indicates 12 core homologues and 7 conserved accessory subunits within five members of the trypanosomatid family; these proteins are encoded by genes in the mitochondrial and nuclear genomes (Acestor et al., 2011; Panigrahi et al., 2009). The trypanosomatid complex I has four bacterial homologues and seven subunits encoded by the trypanosomatid mitochondrial genome, as well as six nuclearly-encoded subunits (Opperdoes and Michels, 2008). Aside the core subunits of complex I in trypanosomatids, proteomic studies have identified other core components of complex I (Panigrahi et al., 2009). Two core subunits thought to be essential for proton pumping, NADH dehydrogenase subunits 4L (ND4L) and 6 (ND6), were not found using bioinformatic or proteomic analysis.

This observation suggests that complex I does not participate in generation of $\Delta\psi m$ (Opperdoes and Michels, 2008) or that the subunits could be present in diverged form. Thus, some of the mitochondrial 'C-rich' (CR) genes and unidentified reading framed (MURFs) may represent some of the 'missing' subunits. Indeed, one of these has since been tentatively identified as ND2 (Kannan and Burger, 2008).

There has been much debate about the role of complex I in *T. brucei* even though NADH oxidation occurring within the mitochondrion of *T. brucei* is well known (Fang and Beattie, 2003; Horváth et al., 2005). The function of complex I has been reported to be neither significant nor important in the bloodstream forms (Surve et al., 2012). Moreover, the impact of complex I in procyclic forms is still unclear. Individual knock-down of three complex I core subunits (*NUBM, NUKM* and *NUEM*) in procyclic forms via RNA interference suggested that complex I only contributes 20% of the total mitochondrial NADH:ubiquinone oxidoreductase activity and is not required for growth *in vitro* (Verner et al., 2011). The authors also observed

that knockdown of the complex I core subunits had no effect on Δψm (Verner et al., 2011). Unlike procyclic forms, no reduction of NADH oxidation activity was seen in monomorphic bloodstream forms (Surve et al., 2012). This observation has also been reported for *Phytomonas serpens*, a pathogen of plants, which is devoid of complexes III and IV (Maslov et al., 2002) but has a complex I similar to *T. brucei* (Cermáková et al., 2007).

Research on the role of complex I is complicated by the presence of a second 'type 2' NADH:ubiquinone oxidoreductase, *NDH2*, in *T. brucei* which contributes to respiration (Fang and Beattie, 2003). *NDH2* is composed of a single subunit confined to the mitochondrion (Surve et al., 2017). Additionally, *NDH2* is insensitive to rotenone, is nuclearly-encoded and contributes partially to rotenone-insensitive respiration (Fang and Beattie, 2003; Horváth et al., 2005). A previous report has indicated that rotenone-sensitive Δψm is present in the stumpy bloodstream form of *T. brucei* (Bienen et al., 1991).

It has been hypothesized that NDH2 facilitates rapid growth of procyclic forms , and also facilitates NAD^+ regeneration for other mitochondrial dehydrogenases, instead of complex I (Fang and Beattie, 2003). However, there is debate as to whether the NADH binding site of *NDH2* is correctly-oriented for regenerating mitochondrial NAD^+. When NADH was tested on digitonin-permeabilised procyclic cells, mitochondrial G3PDH activity was increased with a corresponding reduction in respiration (Verner et al., 2013). RNAi targeting *NDH*2 produced growth retardation and decreased ΔΨm in procyclic forms (Verner et al., 2013). However, there was no significant change in activity of NADH:Q2 oxidoreductase in NDH2 knockdown cells (Verner et al., 2013).

The mitochondrial membrane is not permeable to NADH and hence *NDH2* could be oriented towards the cytosol from the mitochondrial membrane; it is not certain whether *NDH2* would be able to compensate for complex I activity. Generation of an *NDH2* mutant in slender bloodstream form of *T. brucei* lacking the *NUBM* gene showed strong defects in growth phenotype in parasites lacking cI function (Surve et al., 2017). Using proton nuclear magnetic resonance (H-NMR) spectrometry, the study also demonstrated that there was no difference in pyruvate and alanine levels, but there was a strong reduction in acetate levels in *NDH2* null

mutants and in the uninduced *NUBM NDH2* conditional knockout cell line (Surve et al., 2017). The reduction in the level of acetate also resulted in a shift in fatty acid composition of the cell line with *NDH2* knockdown in the *NUBM* background. These data imply that *NDH2* is present but non-essential for sustaining mitochondrial redox balance in slender bloodstream forms (Surve et al., 2017). Recent studies have shown that adipose tissue is a reservoir for *T. brucei*. The bloodstream form of *T. brucei* in the adipose tissue upregulate the pathway for beta-oxidation, which is expected to increase the demand for NADH dehydrogenase activity (Trindade et al., 2016). It was hypothesized in this study that NADH dehydrogenase is involved in the pathway for beta oxidation but not energy production. This hypothesis was tested in chapter 4 of this thesis.

1.3.7 Compensation for mitochondrial DNA function in dyskinetoplastic *T. brucei*

Balanced production of proteins and gene regulation is crucial to trypanosomes. During the life cycle stages, there are modulations of gene expression and metabolic adjustment to suit environmental changes and ensure progression of the life cycle (as discussed section 1.2.1). As previously reported, the developmental regulation of mitochondrial activity requires coordination between the nucleus and kinetoplast (Schneider, 2001). In this thesis, the nuclearly-encoded subunit of cytochrome oxidase *COX VI*, which has been extensively studied (Matthews and Gull, 1998), was used to investigate whether absence of the kinetoplast influences regulation of nuclear gene expression.

Cytochrome oxidase has 10 nuclearly-encoded and 3 mitochondrially-encoded subunits. RNA interference of three subunits of cytochrome c oxidase (TbCOX VII, TbCOX X and TbCOX 6080) in procyclic forms caused reduced mitochondrial membrane potential and decreased production of ATP (Gnipova et al., 2012). The cytochrome-containing complexes, complexes

III and IV, are not present in short stumpy forms but mRNA expression of their nuclearly-encoded subunits was increased by approximately 2-fold (Priest and Hajduk, 1994). The cytochrome oxidase complex is developmentally regulated in *T. brucei*. COX VI expression has been shown to be enriched at the protein levels in procyclic forms (Tasker et al., 2001). Additionally, COX VI mRNA has been reported to be 2.5-fold higher in procyclic forms compared to bloodstream forms (Mayho et al., 2006).

To investigate the potential crosstalk between the nuclear and mitochondrial genome during the events of differentiation, expression of a nuclear-encoded component of the cytochrome oxidase (*COX*) complex was disrupted by RNA interference in dyskinetoplastid cells lacking a mitochondrial genome. This allows the ablation of mRNA of the *COX VI* to turn off its expression. The result showed that dyskinetoplastic cells were able to express nuclear Cox VI and thus, the regulation of COX VI gene is independent of kinetoplast (Timms et al., 2002).

Coordination between mitochondrion and nucleus have been studied in organisms like yeast and mammals. The mitochondrion communicates with the nucleus if there is a dysfunction of the mitochondrion; the process is termed retrograde signalling. Retrograde signalling was first observed by independent studies conducted by (Butow and Avadhani, 2004; Kirchman et al., 1999; Laun et al., 2001). Retrograde regulation is triggered in response to changes in the functional state of the mitochondrion. An example is the existence of metabolic readjustments for the maintenance of glutamate supplies in respiratory-deficient yeast cells (Butow and Avadhani, 2004). Retrograde response has also been shown to account for longevity, as extension of life span was reversed by inactivation of retrograde target (RTG) genes (Butow and Avadhani, 2004). Mitochondrion dysfunction leads to a reduction in membrane potential, which triggers RTG in the nucleus to promote longevity in yeast cells (Jazwinski, 2013).

In yeast, the role of RTG genes in communication between mitochondria and the nucleus are also required for expression of genes encoding peroxisomal proteins. During mitochondrial dysfunction, there are recruitment of a series of signal transduction proteins that induces a wide range of nuclear target genes (Jazwinski, 2013; Kirchman et al., 1999; Kotiadis et al., 2014). This response plays a vital role in maintaining mitochondrial function and cell integrity. To date, there is no evidence of retrograde response in trypanosomes during stringent regulation of mitochondrial activity. Is *T. brucei* capable of sensing the absence of mitochondrial genome to relay information to the nucleus to compensate for the defect? In chapters 3 and 4 of this thesis, the effect of absence of mitochondrial genome on gene regulation during differentiation from slender to stumpy forms was investigated both *in vitro* and *in vivo*. A typical signalling response to mitochondrion misfolded proteins for eliciting nuclear response to resolve the defect is shown in Figure 1.10.

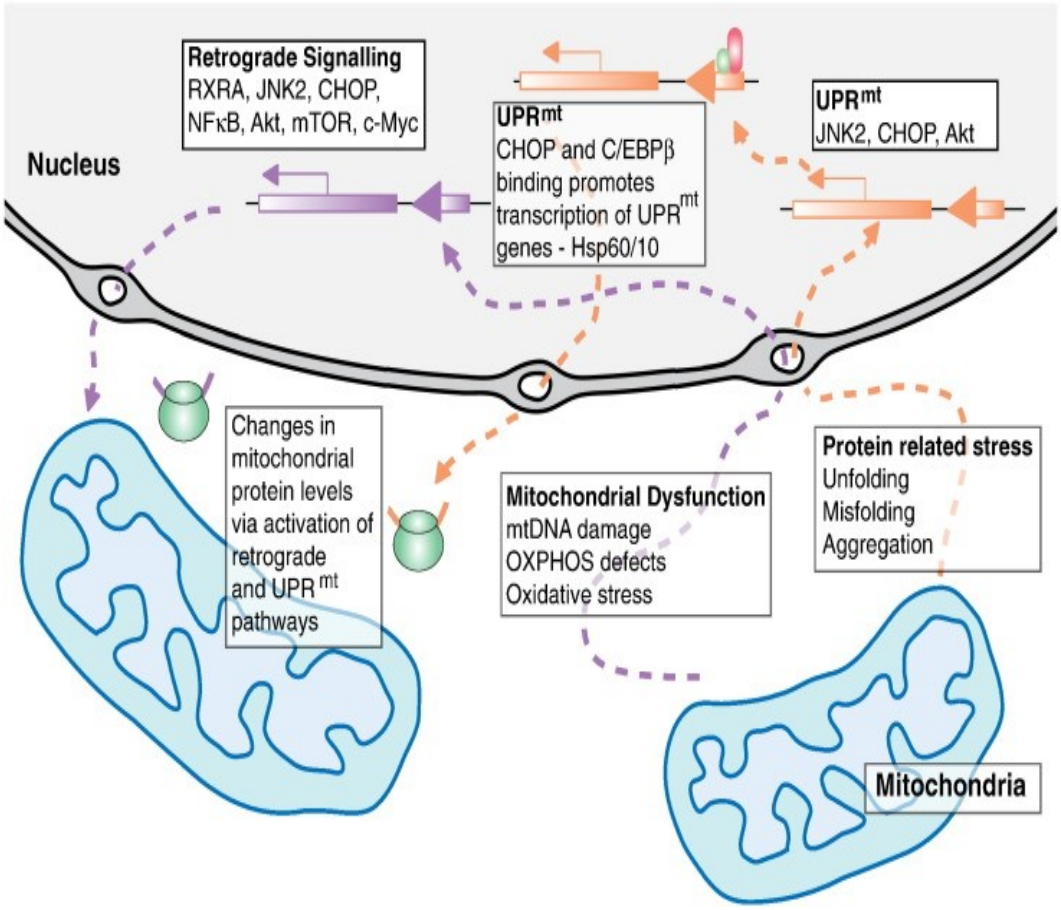

Figure 1.10 Factors Involved in Mitochondrial Retrograde Signalling and UPR^{mt} mitochondrion-nuclear crosstalk is triggered under mitochondrial stress in yeast. Activation of the UPR^{mt} signalling pathway occurs when proteins aggregate or misfold and accumulate in the mitochondrial matrix. This two-step pathway involves activation of transcription factors, including the CCAAT-enhancer-binding protein homologous protein (CHOP). This leads to transcription of mitochondrial quality control genes including Hsp60/10. Retrograde signalling is activated by dysfunction of the mitochondrion and triggers activation of cytosolic signalling pathways which lead to activation of transcription factors including (RXRA, JNK2, CHOP, NKκB,) and transcription of nuclear genes that produce adaptive changes in mitochondrial protein levels. The image was adapted from (Kotiadis et al., 2014).

1.4 Aims

The aims of this thesis are to investigate the consequences of mitochondrial dysfunction:

(i) on temporal and spatial differentiation of bloodstream form of *T. brucei*

(ii) on nuclear gene expression, to uncover potential retrograde signalling pathways in these parasites.

Why will *T. brucei* invest energy in the biogenesis of complex I if it does not contribute to its growth in both bloodstream and procyclic forms? An akinetoplastic cell line that had spontaneously lost its mitochondrial DNA and expresses ATPase subunit γL262P, a WTγ cell line containing the complete kDNA but otherwise being isogenic, and complex I null mutant cell lines were used to address the following:

1. Do retrograde signalling pathways exists in *T. brucei*? Does lack of a mitochondrial genome result in changes in nuclear gene expression?
2. Does complex I play an important role in stumpy forms and/or in cells residing in adipose tissue?
3. Are complex I null mutant stumpy cells capable of differentiating and survive in the adipose tissue?

2 Materials and methods

2.1 Trypanosome cultures

2.1.1 Cell lines

All bloodstream form cell lines (see Table 2.1) were cultured in HMI-9 medium (Hirumi and Hirumi, 1989) and incubated at 37 °C with 5% CO_2. Akinetoplastic cell line (WT/L262Pγ) and one wild type gamma mutant (WT/WTγ) strain of *T. brucei* EATRO 1125 AnTat1.1 90:13 were donated by Caroline Dewar and Sinclair Cooper, Schnaufer's laboratory, University of Edinburgh. The mutant cell lines were generated by replacing one allele of the nuclear-encoded F_1F_O-ATPase subunit γ with an L262P mutation (L262Pγ) to functionally uncouple the F_1F_o synthase part in the pleomorphic cell line *T. brucei* EATRO 1125 (AnTat1.1 90:13). The isogenic control (WT/WTγ), otherwise referred to as WTγ was generated by introducing a wild type version of gamma ATPase subunit γ into the same parental cell line, thus controlling for changes associated with transfection and selection of transgenic parasites. These cell lines were cultivated in the presence of 2.5 µg/ml hygromycin and 1.25 µg/ml G418 to maintain expression of the T7-polymerase and the tetracycline repressor. Culture-adapted pleomorphic *T. brucei* EATRO 1125 AnTat1.1 (Markus Engstler and Boshart, 2004) (Table 2.1) was cultured in methylcellulose (Sigma-94378) containing HMI-9 medium supplemented with 10% heat-inactivated foetal calf serum (FCS) (Invitrogen), prior to transfection (Hirumi and Hirumi, 1989). The AnTat 1.1 refers to serodeme/VSG. *UBP1*/2 RNAi cell lines (Hartmann et al., 2007) and *PNT1* RNAi cells (courtesy of Dr Claudia Schaffner, Schnaufer lab) were induced by adding 100 ng/ml tetracycline to the cell cultures. Purite water that was used throughout the experimental designs in this thesis was purified by reverse osmosis.

Table 2.1 Cell lines used and /or generated in this study

Cell line	Parental strain	Genotype	Description
WT/L262Pγ	Lister 427SM	*ATPγ/Δatpγ::atpγL262P PURO*	*T. b. brucei* Lister 427 with one ATPγ allele replaced with PURO and constitutively expressing an additional L262P mutant *ATPγ* gene replaced with WT *ATPγ*
427 WT	Lister 427SM	Not applicable	WT *T. b. brucei* strain Lister 427
WT/WTγ	Lister 427SM	ATPγ/Δatpγ::atpγWT *PURO*	*T. b. brucei* Lister 427 with one *ATPγ* allele replaced with *PURO* and constitutively expressing WT *ATPγ* gene
NUKM CKO	Lister 427SM	*Δnukm::NEO/Δnukm ::HYG*	*T. b. brucei* Lister 427 with both alleles replaced with *NEO* and *HYG* and constitutively expressing *NUKM*- mutant complex I gene
NUBM CKO	Lister 427SM	*NUBM*^{Ti} *BLE Δnubm::T7RNAP+NEO /Δnubm::TETR+HYG*	*T. b. brucei* Lister 427 with both alleles replaced with *NEO* and *HYG* and constitutively expressing *NUBM*- mutant complex I gene
EATRO 1125 AnTat1.1	Not applicable	Not applicable	WT *T. b. brucei* strain AnTat 1.1
EATRO 1125 AnTat1.1 90:13	Not applicable	T7RNAP::NEO P_{T7}::TETR::HYG	WT *T. b. brucei* strain AnTat 1.1 90:13
WT/WTγ	AnTat1.1 90:13	*ATPγ/Δatpγ::NEO/ atpγWT::HYG*	*T. b. brucei* AnTat 1.1 90:13 with both *ATPγ* alleles replaced with *NEO* and *HYG* and constitutively expressing an additional WT *ATPγ* gene
WT/L262Pγ (AK)	AnTat1.1 90:13	*ATPγ/Δatpγ::NEO/ atpγL262P::HYG*	*T. b. brucei* AnTat 1.1 90:13 with both *ATPγ* alleles replaced with *NEO* and *HYG* and constitutively expressing an additional *L262P* mutant *ATPγ*. This cell line spontaneously lost mitochondrial DNA (mtDNA) without treatment
WT/L262Pγ (aAK)	AnTat1.1 90:13	*ATPγ/Δatpγ::NEO/ atpγL262P::HYG*	*T. b. brucei* AnTat 1.1 90:13 with both *ATPγ* alleles replaced with *NEO* and *HYG* and constitutively expressing an additional *L262P* mutant *ATPγ*. This cell

			line treated with acriflavine to devoid it of kinetoplast
NUKM SKO	AnTat1.1 90:13	*Δnukm/NUKM*	*T. b. brucei* AnTat 90:13 with one *NUKM* allele replaced with *BSD*
NUKM SKO	AnTat1.1	*Δnukm/NUKM*	*T. b. brucei* AnTat 1.1 with one *NUKM* allele replaced with *NEO*
NUBM SKO	AnTat1.1	*Δnubm/NUBM*	*T. b. brucei* AnTat 1.1 with one *NUBM* allele replaced with *NEO*
NUKM DKO	*NUKM* SKO	*Δnukm::NEO/Δnukm ::HYG*	*T. b. brucei* AnTat 1.1 with both alleles replaced with *NEO* and *HYG* and constitutively expressing *NUKM*- mutant complex I gene
NUBM DKO	*NUBM* SKO	*Δnubm::NEO/Δnubm ::HYG*	*T. b. brucei* AnTat 1.1 with both alleles replaced with *NEO* and *HYG* and constitutively expressing *NUBM*- mutant complex I gene
NUKM Addback	*NUKM* DKO	*Δnukm::NEO/Δnukm ::HYG*	*T. b. brucei* AnTat 1.1 with both *NUKM* alleles deleted. The addback of *NUKM* is inserted in β tubulin locus to constitutively express *NUKM* complex I gene
NUBM PCF	*NUBM* DKO	*Δnubm::NEO/Δnubm ::HYG*	*T. b. brucei* AnTat 1.1 with *NUBM* alleles replaced with *NEO* and *HYG* and constitutively expressing *NUBM*- mutant complex I gene differentiated to procyclic using cis aconitate

Systemic TriTrpDB IDs: *NUBM* (Tb927.5.450)
NUKM (Tb927.11.1320)
ATPase subunit γ (Tb927.10.180)

2.1.2 Transfection of bloodstream form cells

Bloodstream forms were transfected as described (Schumann Burkard et al., 2011). 10 µg plasmid DNA was used per transfection. DNA was linearized by restriction enzyme NotI. After confirming linearization via gel electrophoresis, DNA was ethanol precipitated and the final pellet was resuspended in 20 µl MilliQ water (Sigma). Cells in the logarithmic stage of growth were centrifuged at 1300 g for 10 min; 5 x 10^7 cells were used per transfection.

Cell pellets were resuspended in 100 µl nucleofection solution (90 mM NaH_2PO_4, 5 mM KCl, 0.15 M $CaCl_2$, 50 mM HEPES, pH 7.3) (Schumann Burkard et al., 2011). Cells in methylcellulose were removed from the cultures by diluting the culture in 1:4 with sterile TDB and followed same protocol to transfect 5 x 10^7 trypanosomes with 10 µg of linearized plasmid DNA.

A mock transfection of parental cells without DNA was done to serve as a control to confirm that the selective drugs inhibited growth of untransfected cells. For the transfection, the AMAXA Nucleofector® II was used with Program Z-001 (Schumann Burkard et al., 2011). After nucleofection, cells were recovered in a pre-warmed 25 ml culture medium supplemented with FCS for at least 6 hours at 37 °C, 5% CO_2. After the 6-hour incubation, selective drugs were added, and the cells were plated in 24-well plates in 10-fold serial dilutions and in 48-well plates in 1:30 and 1:100 dilutions.

Drugs to maintain selection for transgenes were: G418 (2.5 µg/ml for bloodstream forms, 15 µg/ml for procyclin forms) (Invitrogen), hygromycin (5 µg/ml for bloodstream forms, 50 µg/ml for procyclic forms) (Invitrogen), and puromycin (1 µg/ml for bloodstream forms and procyclic) (Sigma).

The genomic DNA (gDNA) of these clones was extracted using GenElute Mammalian gDNA miniprep kit (Sigma) for downstream analyses (e.g. PCR) to allow direct Sanger sequencing of the selected clones.

2.1.3 Differentiation to the stumpy stage

For a generation of density-induced stumpy parasites, slender cells at a seeding density of 5 x 10^5 cells/ml were cultivated without dilution for 48 hours in methylcellulose containing HMI-9 medium supplemented with 10% v/v heat-inactivated FCS and 5% v/v serum plus (94378, Sigma). This allowed the accumulation of SIF that consequently developed into stumpy cells. Cultures were incubated at 37 °C and 5% CO_2. To harvest the cells, methylcellulose was removed from the cultures by diluting the cultures at least 1:4 with sterile trypanosome dilution buffer (TDB; 5 mM KCl, 80 mM NaCl, 1 mM $MgSO_4$, 20 mM Na_2HPO_4, 2 mM NaH_2PO_4,

20 mM glucose, pH 7.6). The diluted culture was filtered (MN 615 1/4, Macherey-Nagel, Germany) using sterile conditions and centrifuged (1500*g*, 15 min, RT) prior to differentiation to PCF.

2.1.4 Differentiation to Procyclic Forms

Bloodstream stage trypanosomes were induced to differentiate to procyclic forms by seeding 1.5×10^7 cells into 5 ml of HMI-9 with 50 µl of 6 mM cis-aconitate and a shift in temperature from 37 °C to 27 °C and 5% CO_2. After 24 hr incubation, the cells were washed from HMI-9 and transferred into the SDM-79 medium (Brun and Schonenberger, 1981). The differentiated population was assessed by the expression of EP by immunoblotting (Section 2.12).

2.2 Growth analysis *in-vitro*

Cell lines were grown to measure the growth effect of the absence of cI *NUBM in-vitro*. Cells were grown in HMI-9 media (Invitrogen) (Hirumi and Hirumi, 1989) containing 10% v/v FCS. Cell counts were performed daily for 14 days using the Neubauer counting chamber; cells were diluted to starting concentration (2 x 10^6cells/ml) every 24 hours.

2.3 Animal experiment and parasite purification

Animal experiments were carried out according to the United Kingdom Animals Act (Scientific Procedures) under a licence PPL70/8734 issued by the United Kingdom Home Office and approved by the University of Edinburgh local ethics committee. Unless otherwise indicated, all infections were performed in wild-type male C57BL/6J mice, which were 6–10 weeks old (Charles River, France) and MF1 mice that were at least 10 weeks old (SCRM, Edinburgh) by intraperitoneal injection of 2,000 *T. brucei* AnTat 1.1 and EATRO 1125 AnTat 1.1 ·90:13 parasites without any immunosuppressants. Parasitaemia was monitored daily from day three post-infection with a tail snip being performed, and cells were examined from a drop of

blood compressed under a cover slip on a microscope slide at the 40x objective. Cell numbers per field of view were estimated by examining at least 10 fields of view from the wet smears using the Herbert and Lumsden rapid matching method (Herbert and Lumsden, 1976). The cell morphology was also scored qualitatively from these wet smear slides. Slender cells are longer, thinner with a long flagellum at the posterior end whiles stumpy cells are shorter, wider, with an extremely short attached flagellum. Slender or stumpy cells depending on the experiment were harvested via a cardiac puncture to collect the infected blood in a 2 ml syringe containing 200 µl of 2% sodium citrate (anticoagulant). Trypanosome parasites were purified from blood using DEAE-cellulose DE52 (Whatman anionic exchange cellulose, Z742600) at pH 7.8 (Lanham, 1968) that were preincubated with phosphate saline glucose (PSG) (44 mM NaCl, 57 mM Na_2HPO_4, 3 mM KH_2PO_4, 55 mM glucose, pH 7.8) pre-warmed at 37 °C. Blood was loaded onto the column, and the column was continuously topped up with warm PSG, and the eluate was collected. The density of the cells was measured using a Beckmann Z2 Coulter counter.

2.3.1 Perfusion and parasite isolation from adipose tissue and solid organs

Anesthetized mice were laid on their back on a dissecting board placed on the procedural stage. Forelimbs were spread to secure each paw to the rack with a pin. A pair of dissecting scissors was used to open the skin to expose the chest cavity. An incision with a scalpel was then made through the abdomen, along the length of the diaphragm, with a sharp scissor and cut through the connective tissue at the bottom of the diaphragm to access the rib cage. About 500 µl of blood was collected from the right ventricle using a 27G insulin syringe. Prewarmed (37 °C) heparinized saline (50 ml phosphate buffered saline (PBS) with 250 µl of 5000 I.U./mL) was passed through the left ventricle using a syringe and needle. The right atrium was cut with a pair of sharp scissors, making sure solution was freely flowing through the organs and tissues. After a successful perfusion, organs and tissues were collected and

washed quickly in 1x PBS. The pre-weighed organs were transferred into 1.5 ml eppendorf tubes and snap froze in liquid nitrogen and then transferred to -80 °C. Adipose tissue form (ATF) parasites were collected from gonadal fat depot by agitated at 150 rpm in HMI-9 at 37 °C for up to 1 hour to enable parasites to be harvested from the fat tissue.

2.4 DNA Manipulation

2.4.1 Polymerase chain reaction

Polymerase chain reactions (PCR) were carried out in 0.2 ml PCR tubes (Axygen 321-10-051) in PeqSTAR 96 Universal Gradient thermo-cycler (95-96002, PeQLab Biotechnology). GoTaq® Flexi DNA polymerase (Promega) was used for routine PCR reactions to confirm the presence or absence of a gene or DNA fragment of interest. PCR primers were designed using Primer3 Plus Design software (Untergasser et al., 2007) and all primers were manufactured by Sigma Aldrich (Appendix A). PCR reactions were performed on 50 ng *T. b. brucei* gDNA. A 50 µl reaction in sterile water consisted of 10 µl 5x reaction buffer, 3 µl 25 mM $MgCl_2$, 2 µl 10 mM dNTP mix, 2 µl 10 µM Forward primer, 2 µl 10 µM Reverse primer, 0.5 µl Taq Polymerase (5 units/µl) and 29.5 µl MilliQ water. The reaction was performed with the following condition: 95 °C for 5 min and [95 °C 30 s, (Tm-5) °C 30 s, 72 °C 1 min/kb] for 35 cycles and 72 °C for 10 min.

2.4.2 Agarose gel electrophoresis

Gel electrophoresis was used to visualise DNA as well as for separating different length DNA fragments by restriction digest, gel purification of fragments of interest and to assess the amplicons from PCR reactions. Gel electrophoresis was carried out at 80 V for 1 hour using 1% (w/v) agarose gels in 1x TAE buffer (40 mM Tris-Acetate, 1 mM EDTA, pH 8). For the nucleic acid stain, ethidium bromide (10 mg/ml, Sigma) was added during the preparation of agarose gels to enable the visualisation of the separated DNA fragments in a dilution of 1:100, 000. Gels were viewed under a UV lamp (G:Box; Syngene, by Syngene United Kingdom) and the

size of the DNA fragments of interest was estimated using DNA ladders from New England Biolabs.

2.4.3 Bacterial transformation

For transformation, chemically competent laboratory stocks of XL-1 blue *E. coli* cells (C7373-03) stored at -80 °C were used. One microliter of prepared plasmid was added to 100 µl of competent bacteria and the mixture incubated on ice for 30 min. The cells were heat shocked at 42 °C for 30 seconds in a water bath. To allow the cells to recover before selection, 800 µl of Luria broth (LB) broth was added to the cells and incubated at 37 °C for 45 min while shaking. The cells were then plated onto selective LB agar plates (1 mg/ml ampicillin or 1 mg/ml kanamycin) and incubated at 37 °C overnight. All plasmids used in this thesis contain ampicillin or kanamycin resistance genes. Only cells with the plasmid with formed colonies were seen the following day. The colonies were then used to prepare DNA (Section 2.4.4) to confirm that they have obtained a plasmid and that plasmid contains the appropriate sequence.

2.4.4 Preparation of plasmid DNA

For plasmid DNA preparation, a mini-prep was carried out. A discrete colony of interest on an LB agar plate was picked with a sterile pipette tip and used to inoculate 5ml of LB broth. In all, Ampicillin or kanamycin drug (1 mg/ml) was added to the culture. The culture was grown overnight at 37 °C with shaking. On the following day, 2 ml of culture is transferred to a 2 ml eppendorf tube and centrifuged at 16,000 g for 5 min at room temperature. The extraction was done using the Monarch Plasmid Miniprep Kit (NEB T1010). The supernatant was removed and 200 µl of plasmid resuspension buffer (B1) was added to the pellet. The pellet was resuspended by rapping the eppendorf along a rack and 200 µl of plasmid lysis buffer (B2) added. The sample in the tube was mixed by inversion and 400 µl of pre-chilled plasmid neutralization buffer (B3) was added and the mixture mixed by inverting the tube and then

incubated for 2 min at room temperature. The sample was then centrifuged at 16,000 g for 5 min at room temperature.

The supernatant was transferred to a spin column and centrifuged for 1 min. The flow through was discarded and column re-inserted column in the collection tube and added 200 µl of plasmid wash buffer 1 and centrifuged for 1 min.

This was followed by adding 400 µl of plasmid wash buffer 2 and centrifuged for 1 min. The column was transferred into a clean 1.5 ml microfuge tube and added 30 µl of DNA Elution Buffer. After 1 min of incubation at room temperature, the sample was spun for 1 min to elute DNA. and stored at -20 °C.

2.4.5 Plasmids and Constructs

To generate knock-out constructs for complex I (cI) subunits *NUBM* and *NUKM*, about 500 bp of the 5' and 3' intergenic regions from *NUKM* and *NUBM* were amplified using *NUBM* 5' and 3' UTR and *NUKM* 5' and 3' UTR forward and reverse primers listed in Appendix A and cloned into pGEM-T Easy (Promega). Knockout constructs using pLew 13 and pLew 90 were generated as described by (Ochatt et al., 1999). The constructs used in this study are listed in Table 2.2. The open reading frames of *NUBM* and *NUKM* (Tb927.5.450 and Tb927.11.1320 respectively) were PCR amplified with forward and reverse primers for *NUBM* and *NUKM* (Appendix A). The amplified PCR products were cloned into expression vector pLew 79-3V5-PAC as described (Surve et al., 2012) to generate expression vector for the two genes. An example of one of the many plasmids used is shown in figure 2.1. The remaining plasmid maps used in this thesis are shown in Appendix B.

To generate the synthetic knockout construct for *NUKM*, about 200 bp proximal of the 5' and 3' intergenic regions from *NUKM* gene with 3' aldolase used as housekeeping gene. The selectable marker used here was phleomycin (KO_*NUKM*_proximal_phleo_3Aldo). For KO_*NUKM*_distal_blast_5Aldo construct, the 200 bp was distal to the 5' and 3' intergenic regions from *NUKM* gene with 5' aldolase used as housekeeping gene. Here, blasticidin was

used as drug marker (Table 2.2). For plasmids used for making probes for northern analysis, *COX VI* (Tb927.10.280) coding sequence was inserted into the multiple cloning sites of pBluescript sk+ by *in silico* cloning using Seqbuilder software (version 14, DNASTAR). Direct integration of *COX VI* into the vector was confirmed using M13 forward and reverse primers (Appendix A) and *COX VI* PCR product used to prepare riboprobe for northern blot analysis. The Sanger sequencing reaction was set-up using the BigDye® Terminator v3.1 Cycle-Sequencing Kit (Applied Biosystems) using ABI 3730XL capillary sequencing instrument at the Edinburgh Genomic facility to confirm plasmids.

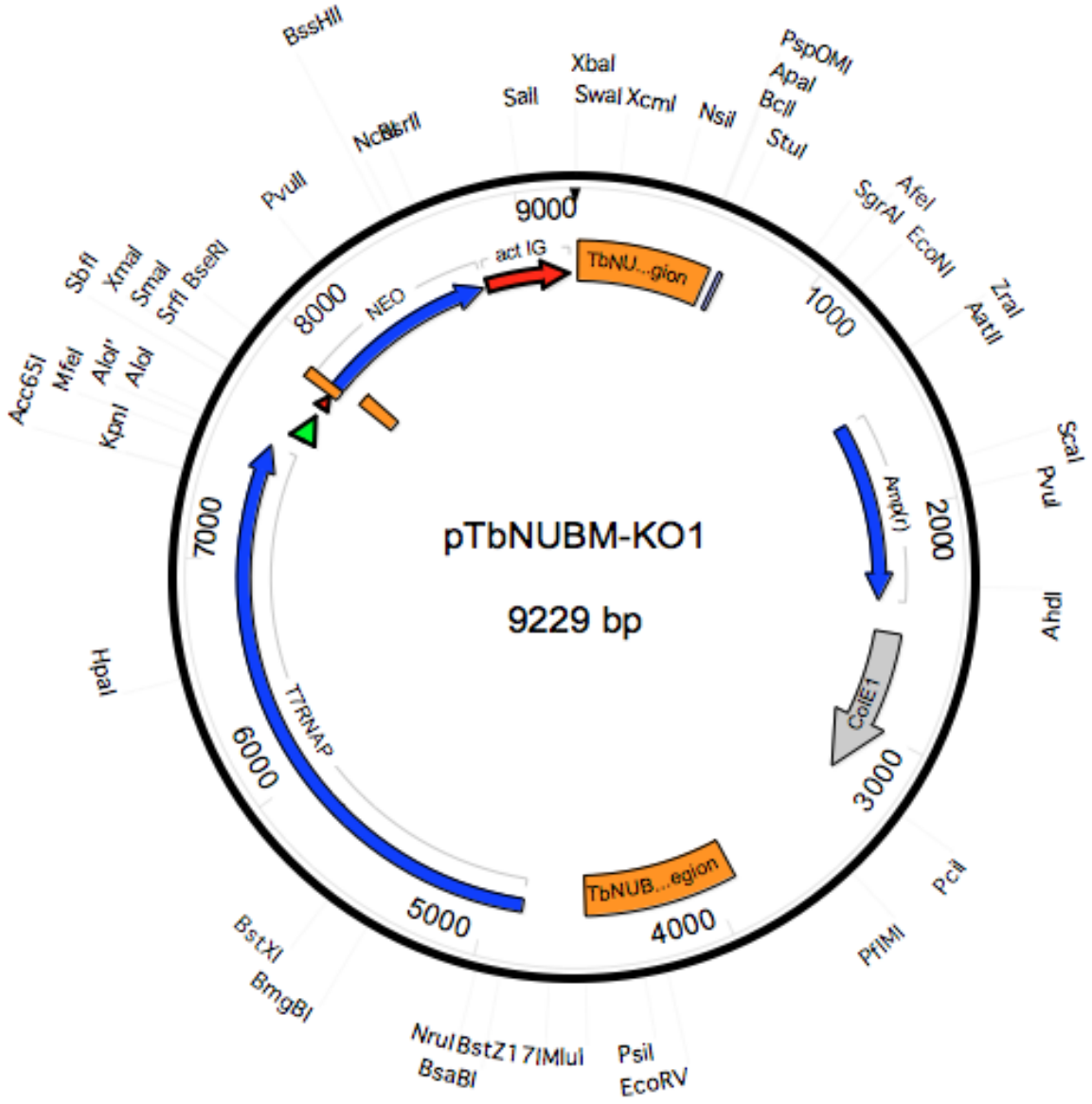

Figure 2.1 pLew 13 vector with T7 RNA polymerase and neomycin gene. The bacterial resistance is ampicillin and the target locus is tubulin. This plasmid served as the backbone to generate the knockout construct lacking cI subunits.

Table 2.2 List of constructs used in this study

Name of plasmid	Resistance Markers
pTbNUBM-KO1 (pLew 13)	Neomycin (NEO)
pTbNUBM-KO2 (pLew 90)	Hygromycin (HYG)
pTbNUKM-KO1 (pLew 13)	Neomycin (NEO)
pTbNUKM-KO2 (pLew 90)	Hygromycin (HYG)
pHD1344-tubNUKM (pHD1344-tub)	Puromycin (PAC)
pEX-K4 NUKM- 1_	Blasticidin (BSD)
pEX-K4 NUKM- 2	Phleomycin (BLE)
COX VI pBluescript sk+	Ampicillin (AMP)

2.5 Microscopy

For 4, 6-diamidino-2-phenylindole (DAPI) (Life Technologies) staining, *T. brucei* cells were washed in PBS after harvesting at 1 × 10^6 cells/ml and concentrated by centrifuging at 5000 x g for 3 min. The pellet was resuspended in 50 µl of 1× PBS and smeared onto poly-L-lysine slides (VWR, 631-0107) and allowed it to air-dry. The adhered cells on the slides were fixed in ice cold methanol stored at -20 °C. The cells were then incubated with 20 µl of 10 µg/ml DAPI for 2 min to stain the nuclei and the mitochondrial DNA, followed by three washes with 1x PBS. Slides were mounted with a coverslip by application of Mowiol (6 g glycerol, 2.4 g Mowiol, 12 ml 0.2 M Tris, pH 8.5 (Harlow Chemical, Kent, United Kingdom) containing 4 µl p-Phenylenediamine (PDA, Sigma) to a final concentration of 1 mg/ml. The slides were examined under a microscope (Leica DMR, Mannheim/Germany) using a 100× oil immersion objective.

2.5.1 Indirect immunofluorescence assay (IFA)

Differentiation of *T. brucei* cells into stumpy forms was assessed by IFA using a *PAD1* antibody (Dean et al., 2009). A drop of blood from the tail vein of an infected mouse was smeared on a polysine-covered slide (VWR; 631-0107). It was then allowed to air dry and fixed in ice-cold methanol at least overnight. The fixed slides were rehydrated in 1x PBS for 5 mins in a glass slide box and blocked for 30 min with 2% bovine serum albumin (BSA, Sigma) in PBS at 37 °C

in a humidity chamber. Slides were washed once in PBS then incubated with 50 µl of α-*PAD1* antibody (courtesy of Professor Keith Matthews) diluted in 2% BSA in PBS, 1:1000 for 1 hr at 37 °C in a humidity chamber. Slides were washed three times in PBS, incubated with secondary antibody diluted in 2% BSA PBS (anti-rabbit Alexa Fluor 488 goat anti-rabbit IgG ref A11008; lot 1408830 1:500).

The slides were then washed once in PBS for 10 min and slides stained with 50 µl of 10 µg/ml DAPI in PBS for 2 min in the dark to highlight the nuclei and kinetoplast of the cells.

The slides were mounted with Mowiol containing 2.5% DABCO (1, 4-diazabicyclo [2.2.2] octane) and analysed on a Zeiss Axioskop 2 plus or Zeiss Axio Imager Z2 and images captured on QCapture Suite Plus Software (version 3.1.3.10, https://www.qimaging.com). Cropping of images and adjustment of contrast and brightness were done using ImageJ software (Schneider et al., 2012).

2.6 RNA Sample Preparation

To ensure a completely sterile and RNase-free working area for RNA work, benches and pipettes were cleaned thoroughly with 70% ethanol and RNase ZAP (Ambion), and filter tips were used to reduce RNase contamination. RNA samples were prepared from 30 ml of logarithmically growing cell culture to obtain at least 1 x 10^7 cells. The cells were centrifuged at 800 x g for 10 min and the cell pellet was resuspended in 600 µl RLT buffer from a QIAGEN RNeasy Mini Kit (74106) supplemented with 10 µl -mercaptoethanol/ml to lyse the cells. The lysate was then stored at -80 °C until processing. Upon thawing, the lysate was homogenised by vortexing at full speed for 1 minute. The RNA was then extracted using QIAGEN RNeasy Mini Kit, which uses an RNeasy spin column, according to manufacturer's instructions. RNA was eluted into 30 µl of water. DNase treatment was added after RNA extraction using an Ambion TURBO DNA-free kit (Applied Biosystems AM1907) according to manufacturers' instructions. RNA was stored at -80 °C. Repetitive freeze-thaw of samples was avoided and samples were always thawed on ice.

2.7 Nano Agilent analysis of RNA

The integrity of the DNase-treated RNA was assessed using the Agilent Bioanalyzer nanochip kit. Briefly, the chip priming station was set to 'C', and an RNA Nano chip was positioned in the station. 1 µl Nano dye concentrate was mixed with 65 µl of spin filtered (1500 x g for 10 minutes) Nano gel matrix, and vortexed thoroughly. 9 µl was pipetted into the 'G' well for the RNA Nano chip and was dispensed by pressing down of the plunger for 30 seconds.

9 µl of the gel-dye mix was then pipetted into the two wells above well 'G', 5 µl Nano marker was pipetted into all remaining wells and 1 µl heat-denatured RNA ladder (70 °C for 2 minutes) was pipetted into the ladder well. 1 µl of each sample was loaded into each of the sample wells before the chip was vortexed for 60 seconds at 2400 rpm. The chip was inserted into the Agilent 2100 Bioanalyzer to start the run.

2.8 Reverse transcription of *T. b. brucei* RNA

Reverse transcription was performed using SuperScript III (Life Technologies) protocol. The reaction was set up using 500 ng RNA and 11 µl dH2O was mixed with 1 µl of 10 mM dNTPs and 1 µl of 200 ng/µl random hexamer primers (NEB). The sample mixture was incubated at 65 °C for 5 min and then put on ice for at least 1 min. This was followed by adding 4 µl of 5x first strand buffer, 1 µl of 0.1 M DTT, 1 µl RNaseOUT (40 units/µl) (Invitrogen) and either 1 µl Superscript III Reverse Transcriptase (+RT) or 1 µl dH2O (-RT). The reaction condition used was 25 °C 5 min, 50 °C 60 min and 70 °C 15 min. After the stated incubations, 1 µl RNase H (NEB) was added, and the mixture incubated at 37 °C for 20 min to remove RNA. The temperature was increased to 90 °C for 10 min to stop the reaction.

2.9 Parasite quantification by quantitative PCR (qPCR)

To quantify parasites, 25 mg of tissue was weighed into a 1.5 ml tube. The Nzytech kit (MB13503) was used to extract gDNA according to manufacturer's protocol and quantified

using Nanodrop ND-1000 (Thermo Scientific). The Tachyon ROX SYBR 2X Master Mix dTTP blue (UF-RSMT-B0101, Neurogenetic) was used for the qPCR estimation with *T. brucei* 18S rDNA primers (Appendix A). Reactions were carried out in a Stephone™ Real-Time PCR machine (4376600, Applied Biosystems). To each well of a 96 well plate the following components were added and mixed: 10 µl 2 x SYBR Green PCR Master Mix, 8 µl 1.5 µM primer mix, and 2.0 µl diluted DNA. Template DNA was diluted 1:10 for investigating gene and 1:50 for internal control. Each reaction was done in triplicate.

Thermocycler condition used was: 50 °C 2 min, 95 °C 10 min, [95 °C 15 s, 60 °C 1 min] x 40. A melt curve was added to the end of PCR reaction to ensure that there was only one amplification product. Melt curve stage: 95 °C 15 s, 60 °C 1 min, 95 °C 15 s. Results were analysed via the CT method (Carnes and Stuart, 2007). The data was analysed using the ABI Stephone software version 2.

2.10 Quantitative reverse transcriptase PCR (qRT -PCR)

The quality of the RNA was checked on the Agilent 2100 Bioanalyzer (see Section 2.7) and the RNA quantified with Qubit fluorometer (Q32857, Invitrogen). Quantitative PCR reactions were performed in a total volume of 20 µl, with the same protocol and reagent, equipment and calculation described in Section 2.9. Primers used are listed in Appendix A. The cDNA was 1:10 for investigating genes and 1:50 for the GPI8, a stable housekeeping transcript was used as endogenous loading control. Mock reverse transcribed RNA ('-RT cDNA') was used as a negative control with each primer set. The internal reference used was the WT/WTγ or WT AnTat 1.1 90:13 cell line of the same strain for each analysis.

2.11 Northern blot

2.11.1 Probe preparation

Riboprobes were prepared by performing standard PCR (see Section 2.4.1) on *COX VI* pBluescript sk+ plasmid to amplify *COX VI* gene using M13 forward and reverse primers. DNA was purified using Qiagen column and estimated DNA was used to prepare riboprobes following manufacturer's protocol (Roche). DNA was then purified before the riboprobe reaction was set up using DIG RNA labelling Kit (SP6/T7) (Roche). The reaction was set up using 1 µg of DNA and incubated with 2 µl of 10x NTP labelling mixture (10 mM ATP, 10 mM CTP, 10m MGTP, 6.5 mM UTP, 3.5 mM DIG-11_UTP, pH 7.5), 5 mM DTT, 20 units RNase inhibitor to prevent RNA degradation during the reaction, 1x transcription buffer and 40 units of T7 RNA polymerase. The reaction was incubated at 37 °C for 3 hr, after which 20 U of DNase 1, RNase-free was added, and followed by further incubation for 15 min at 37 °C. The reaction was stopped by adding 2 µl of 200 mM ethylenediaminotetraacetic acid (EDTA), pH 8.0. The probe was then precipitated with 100 mM LiCI and three volumes of cold 100% ethanol at -80 °C for 1 hr. The sample was centrifuged at 12,000 x g for 15 min, and the pellet was washed once with 70% ethanol and allowed to air dry after discarding the supernatant. The pellet was resuspended in 50 µl of nuclease-free water supplemented with 20 U RNase inhibitor (Thermo Fisher Scientific, UK). The *ESAG9* (Tb927.5.4620) riboprobe was a kind gift from Dr Eva Rico, (former postdoc in Keith Matthews lab).

2.11.2 RNA gel preparation and running method

RNA agarose gels were prepared by dissolving 1.8 g of agarose in 130.5 ml of distilled water and microwaved. 15 ml of 10 x MOPS (23.13 g MOPS, 10 ml of 2.5M sodium-Acetate (pH 7.0), 10 ml of 0.5 M EDTA in 500 ml; autoclaved) was added to make 1x MOPS final concentration and swirled when cooled. Additionally, 4.5 ml of 37% formaldehyde was added in the chemical hood before the gel was cast and left to set in the hood. An equal quantity of 1 µg RNA from each sample in a volume less than 6 µl was added to 9 µl formamide, 3 µl of 37% formaldehyde, 2 µl of 10x MOPS and 2 µl of RNA gel loading buffer. The sample was then

heated to 65 °C for 5 min to remove any secondary structure. The samples were loaded into the agarose gel and run at 150 Volts in 1x MOPS running buffer for 90 min. The gel was stained with 20 µl of 10 mg/ml ethidium bromide in 200 ml of 1x MOPS for 15 min with shaking to check for equal loading. The gel was then de-stained by washing at least twice in purite water for 30 min with shaking. The gel was then visualised and photographed using a Syngene G:box UV transilluminator (Syngene United Kingdom). This allowed visualisation of the ribosomal RNA within the samples, allowing the identification of under or overloaded lanes.

2.11.3 Northern blot setup

Northern blotting was performed using capillary transfer onto a positively charged nylon membrane. A plastic tray was filled with 10x saline-sodium citrate (SSC) up to about 2 cm the height of the plastic tray. A sandwich box was placed upside down in the tray and a square plastic, same size as that used to cast the RNA agarose gel was then placed on the sandwich box. A piece of chromatography paper (Fisher CHR200) pre-wet in 10x SSC (1.5 M NaCl, 150 mM tri-sodium citrate) was placed over the gel tray and down into the 10x SSC in the plastic tray to create a wick for buffer transfer.

The RNA agarose gel was then placed upside down onto the chromatography paper and clingfilm wrapped around the gel and over the plastic tray to prevent evaporation to the environment. A piece of positively charged nylon membrane (Roche 11 417 240 001) pre-wet in 10x SSC was placed on top of the gel and this was rolled flat using a 10 ml serological pipette to remove any bubbles between the gel and the membrane. The membrane was handled using plastic tweezers. Two pieces of chromatography paper, pre-wet in 2x SSC were placed on top of the membrane making sure all bubbles were removed. A pile of paper towels, four inches thick were placed on top of two pieces of paper and a large area flat piece of plastic placed on top to hold the heavyweight catalogue. The blot was left to transfer overnight and next day, nylon membrane was taken from the setup and allowed to dry. The RNA was UV cross-linked to the membrane using a UV cross-linker CL-508 (0.120 joules, 254 nm) (Uvitec Ltd, UK). The blot was then stored at room temperature prior to hybridisation.

2.11.4 Hybridization of the blot

The membrane was pre-hybridised in 10 ml of pre-warmed hybridisation buffer in a hybridisation tube at 68 °C for 1 hour in a hybridisation oven (Techne Hybridiser HB-1D) with rotation. To 100 µl of hybridisation buffer, 2 µl of riboprobe was added and heated at 99 °C for 5 min. The heated probe in the buffer was added to 7 ml of hybridisation buffer pre-warmed to 68 °C. The pre-hybridisation buffer was removed and the probe in the hybridisation buffer added to the membrane. The membrane was then hybridised overnight at 65 °C with rotation.

2.11.5 Detection of mRNA in Samples

After an overnight hybridisation, the blot was washed at 68 °C twice in 100 ml of 2x SSC with 0.1% SDS for 30 min and then once in 100 ml 0.5x SSC with 0.1% SDS for 30 min.

The membrane was removed from the hybridisation tube and subsequent steps performed in sandwich boxes. The membrane was rinsed in 100 ml of RNA wash buffer (1x maleic acid with 0.3% Tween 20) for 1 minute at room temperature. The membrane was then blocked in 50 ml Maleic Acid buffer (100 mM maleic acid, 150 mM NaCl, pH 7.5) with 1% DIG blocking reagent (Roche 11 096 176 001) for 1 hour at room temperature with shaking. After pouring off the blocking solution, the membrane was then incubated in 50 ml of Maleic Acid buffer with 1% DIG block and 1.5 U of Anti-DIG (Anti-Digoxigenin-AP Fab Fragments Roche 11 093 274 910) for 30 min at room temperature with shaking. The membrane was washed again three times in RNA wash buffer for 10 min before being incubated in 50 ml of RNA detection buffer (100 mM Tris HCl and 100 mM NaCl; pH 9.5) for 2 min, both at room temperature. The membrane was placed in a sleeve of heat sealable polyethylene (Bag W) and 10 µl of 25 mM CDP-Star Chemiluminescence substrate (Roche 11 685 627 001) in 1 ml of RNA detection buffer was applied evenly over the surface and left for 2 min. The Bag W was closed over the membrane and excess CDP-Star was removed using paper towels to drive the solution out from between the sleeve of Bag W. The sleeve was then sealed with a Hulme Martin Impulse heat sealer and incubated at 37 °C for 15 min. The blot was visualised by X-ray film by placing

the membrane in an X-ray cassette in the dark. Once in a dark room, an Amersham Hyper film ECL (GE Healthcare, UK) was placed in the cassette on top of the membrane and exposed for 1 min initially and the film developed in a Compact X2 X-ray processor. Further films were exposed for either a longer or shorter duration depending on the result from the first exposure.

2.12 Western blot analysis

Sodium dodecyl sulphate–polyacrylamide gel electrophoresis (SDS–PAGE) and immunoblotting were performed as described earlier (Tasker et al., 2000, Breidbach et al., 2000). Monoclonal antibodies used were: *T. brucei* procyclin (purchased from Cedarlane, Canada), *PAD1* (courtesy of Professor Keith Matthews), anti-*PNT1* (a kind gift from Jeremy Mottram, University of York, United Kingdom) (Grewal et al., 2016) and *UBP1* antibody (donated by Alejandro Cassola's laboratory; Argentina) (Cassola et al., 2015). Anti-elongation factor 1-alpha antibody (Merck Millipore; 05-235) at a 1:7000 dilution was used as loading control. To prepare whole cell protein samples for analysis, 2×10^6 cells were pelleted, washed in 1x PBS and resuspended in 10 µl of 2x sodium dodecyl sulphate (SDS) sample buffer (4% SDS, 20% glycerol, 120 mM Tris-HCl, pH 6.8, 0.2% bromophenol blue, 200 mM DTT). These extracts were then resolved on a precast NuPAGE 4-12% Bis-Tris Gel (Novex Life Technologies), run at 150 V with 500 ml ice-cold 1x MOPS SDS running buffer (25 ml 20 x MOPS SDS running buffer + 475 ml d H_2O) (Invitrogen), using 1 L ice-cold 1x transfer buffer (200 ml methanol, 700 ml purite water and 100 ml of 10x transfer buffer (390 mM glycine, 480 mM Tris, 0.36% SDS), and run at 90 V for 90 min. This was followed by blocking with 5% w/v skimmed milk in 1x Tris- Buffered Saline Tween (TBST) (10 mM Tris-HCl,150 mM NaCl and 0.05% Tween-20) for 1 hr at room temperature. The membranes were then incubated with primary antibody at dilutions of 1: 1000 for *PAD1*, 1:3000 for *EP* procyclin, 1:1000 for *PNT1* or 1:500 for *UBP1* in 5% skimmed milk outlined above. The incubation was done overnight at 4 °C under shaking. Membranes were then washed thrice for 10 min each in 0.05% TBST. Both anti-mouse (IRDye® 680 goat anti-mouse, Licor) and anti-rabbit (goat anti-rabbit IgG (H+L)

Dylight 800, Thermo Scientific) secondary antibodies were diluted 1:7,500 and incubated 1 h at room temperature. Secondary antibodies were diluted in 50% PBS and 50% Licor blocking buffer.

The PNT1 secondary antibody was anti-chicken diluted in 1:2000 in 5% skimmed milk. Washes were repeated after secondary labelling, washed three times for 10 min each in TBST, and then placed in 1× Tris- Buffered Saline (TBS) (NaCl-81.8 g, Tris- 12.1g in 1L litre dH_2O) prior to developing. Membranes were imaged using a Licor Odyssey CLx scanner.

2.13 Southern blotting

Probes were designed and produced to detect the *NUKM* (Tb927.11.1320) or *NUBM* (Tb927.5.450) coding sequence (to confirm presence or absence of the gene) and *NUBM* 5' or *NUKM* 5' intergenic region (to confirm the correct integration of constructs). Probes were prepared using the DIG High Prime DNA labelling and detection starter kit II (Roche; 11585614910). For each sample, 1 µg of a double-stranded DNA template produced by either PCR or restriction digestion, according to the manufacturer's instructions.

For each sample, 1 µg of gDNA was digested with *pst1* restriction enzyme (Promega; R6111) for a minimum of three hours at 37 °C and run on a 1% (w/v) agarose gel at 20 V overnight. The gel was soaked in Depurination Solution (0.25 M HCl) for 15 min with agitation. It was then denatured using a denaturation solution (1.5 M NaCl/0.5 M NaOH) 2 times, 15 mins each with agitation and then neutralised using neutralization solution (1M Tris and 1.5M NaCl; pH 7.4) before the DNA was transferred to a nylon membrane (Amersham Hybond-XL, GE Healthcare Bio-Sciences Corp., Piscataway, NJ, USA) overnight. The membrane was removed the next day and cross-linked using a UV cross-linker CL-508 (0.120 joules, 254nm) (Uvitec Ltd, UK).

Hybridization was carried out overnight at 44 °C for the 5' *NUKM* or 48 °C for 5' *NUBM* intergenic region probe respectively. To probe for *NUKM* gene, the hybridization temperature was 48 °C and that of *NUBM* was 48 °C. The DIG-labelled DNA probe was added to DIG Easy Hyb Buffer (Roche; 11603558001) and incubated with membrane overnight.

After 16 hr of incubation, the membrane was washed twice for 5 mins with 2x SSC / 0.1% SDS at room temperature, and then twice for 15 mins with pre-warmed 0.5x SSC/0.1% SDS at 65 °C. The membrane was rinsed in maleic acid buffer with 0.3% Tween 20 for one min at room temperature. The membrane was blocked in 1% DIG block (Roche) in the maleic acid buffer for one hour at room temperature with agitation and then incubated with Anti Digoxigenin-AP Fab Fragments (Roche) in 1% DIG block/maleic acid buffer for 30 mins. Maleic acid buffer with 0.3% Tween 20 was used to wash the membrane three times for 10 mins. The blot was soaked in the detection buffer (100 mM Tris pH 9.5, 100 mM NaCl) for two mins and then placed between two sheets of polyethylene followed by addition of 10 µl of 25 mM CDP-Star chemiluminescent substrate (Roche, 11685627001) diluted 1:100 in the detection buffer for two mins. Excess substrate was removed, and the polythene sealed using a heat sealer before incubation at 37 °C for 15 mins. The blot was then exposed to X-ray film and developed as described (Section 2.11.5).

2.14 Bioinformatics

2.14.1 RNA-Seq analysis:

For RNA-Seq (Wang et al., 2009) analysis, mice were infected with two pleomorphic *T. brucei* AnTat1.1 90:13 cell lines. An akinetoplastic (AK) cell line expressing ATPase subunit L262Pγ that had lost all mitochondrial DNA spontaneously and a WTγ cell line with complete kDNA but otherwise being isogenic. Slender cells were harvested on day four post-infection whereas short stumpy forms were harvested on day seven post-infection when most of the population had differentiated and purified (Section 2.3).

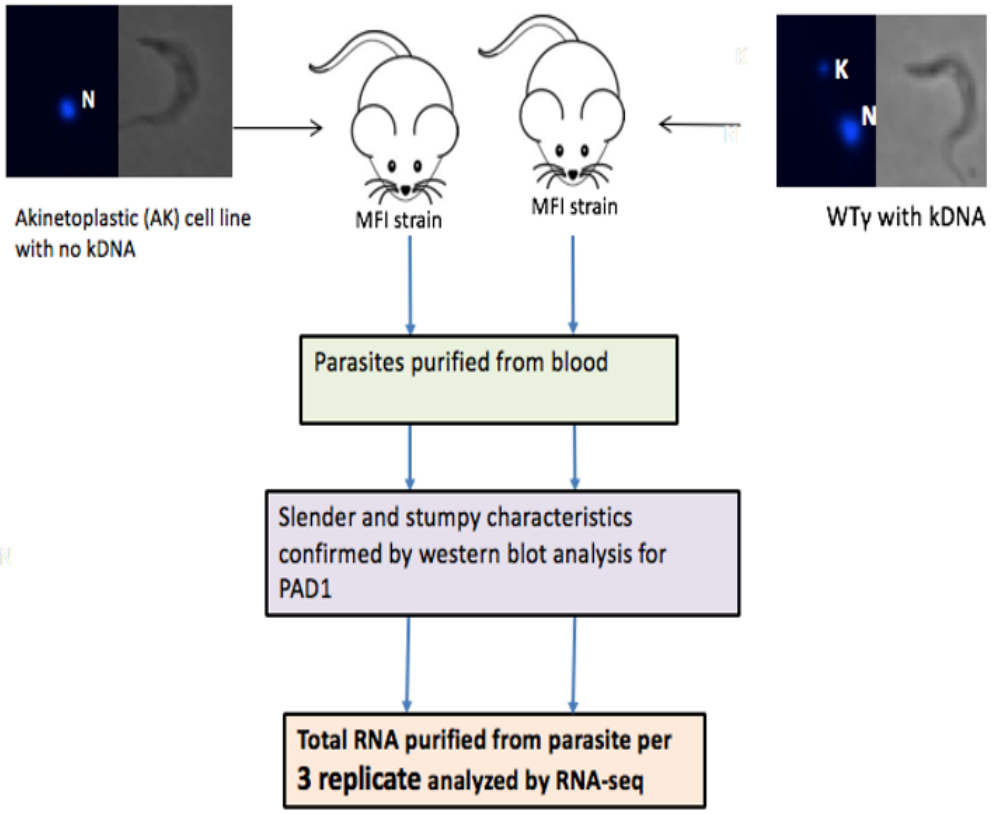

Figure 2.2 Schematic diagram showing sample preparation for RNA-seq analysis. Mice were infected with two pleomorphic *T. brucei* AnTat1.1 90:13 cell line. The akinetoplastic (AK) cell line expresses ATPase subunit L262Pγ that had lost all mitochondrial DNA spontaneously and the isogenic WTγ cell line has complete kDNA.

The slender and stumpy characteristics of parasites were confirmed by western blot analysis for *PAD1 (*Section 2.12*)* and IFA for *PAD1* (Section 2.5.1). Total RNA was purified from parasite per three replicate (Section 2.6) and analysed by RNA-sequencing. Total RNA was reverse transcribed (Section 2.8) and library generated using oligo dT priming containing the Illumina-specific Read 2 linker sequence. After the first strand synthesis, the RNA was removed, and the second strand synthesis initiated by random priming and a DNA polymerase. The second

strand synthesis was followed by a purification step rendering the protocol compatible with automation. Library amplification was followed which required step sequences for cluster generation. Next-generation sequencing (NGS) reads were generated towards the poly(A) tail to directly correspond to the mRNA sequence. The presence and quantity of RNA in the biological samples were sequenced by Beijing Genomics Institute (BGI). High-throughput sequencing of cDNA libraries by the Illumina HiSeq 4000 sequencer generated compressed fastq files with a characteristic length of each DNA read of 100 bp. Fastq formatted sequences were downloaded from the BGI website. The raw sequences were quality assessed using FASTQC. Based on the output of the FASTQC analysis, the raw fastq sequences required no further pre-processing to remove contaminating primers. These files were decompressed and mapped to the *T. b. brucei* TREU927 genome and annotation, downloaded in gff format from ftp.sanger.ac.uk/pub/project/pathogens/gff3/CURRENT**/** in February 2015. Alignments to the reference set were performed using bowtie2 (version 2.2.7) software, requirement for concordant read pair mapping was applied, and all other alignments discarded. The Sequence Alignment Map (SAM) files that were generated by the mapping of the DNA reads to the reference genome were converted to sorted and indexed Binary Alignment Map (BAM) files using the Samtools program. Read counts for each of the predicted protein-coding regions were determined. The counts data were subsequently normalized to the sample with the lowest number of alignments, counts converted to $\log_2$, and then quantile normalized. Pairwise comparisons of sample groups were performed on the normalized tag counts using linear modelling (Bioconductor *limma* package). Analyses of the RNA-Seq data were performed by Dr Alasdair Ivens, Director of Bioinformatics, CIIE, University of Edinburgh, United Kingdom. Statistical analysis of graphs was done in GraphPad Prism 7 software. In all cases, a p-value of less than 0.05 was significant (i.e. given the null hypothesis, the probability of observing the data is less than 5%).

3 The consequences of kDNA loss on nuclear gene expression

3.1 Background and rationale

The regulation of mitochondrial activity in different developmental stages of trypanosomes requires coordination between the nucleus and kinetoplast (Schneider, 2001). An example of this regulation is seen with the cytochrome oxidase (*COX*) complex. This enzyme complex has ten nuclear-encoded and three kinetoplastid-encoded (*COX I, II*, and *III*) subunits. RNA editing of the cytochrome oxidase complex is restricted to the *COX II* and *III* subunits (Feagin and Stuart, 1988). The *COX VI* has been extensively studied compared to the other nuclear-encoded components (Matthews and Gull, 1998). The *COX VI* mRNA is upregulated in stumpy forms and is more abundant in the procyclic forms, the stage where *COX VI* protein expression occurs (Tasker et al., 2001).

Mitochondrial retrograde signalling is a pathway for communication from mitochondrion to nucleus, thereby influencing many cellular activities (Butow and Avadhani, 2004). Coordination between the nucleus and mitochondrial genome has been studied in organisms such as yeast, mammals and plants. In yeast, mitochondrial dysfunction causes the nucleus to modulate gene expression to compensate for the defect (Knorre et al., 2016). Though successful completion of the life cycle of *T. brucei* depends on stringent regulation of mitochondrial activity, it is not known if similar signalling pathways exist in these parasites.

Analysis of the genome sequence of *T. brucei* genome projected over 9000 predicted genes; 1700 were specific to *T. brucei* with about 900 being pseudogenes (Berriman et al., 2005).

Little is known about global changes at the transcriptional level (Matthews et al., 2004; Wheeler et al., 2011), even though the transcriptome of bloodstream and insect procyclic forms are about 30% diverse (Nilsson et al., 2010). A number of transcripts which are

developmentally regulated have been attributed to differences in mRNA stability (Clayton and Shapira, 2007). Various techniques have been used to assess gene expression in the different life cycle stages of trypanosome parasites, including microarray analysis, nimbelgen profiling and massively parallel signature sequencing (MPSS) (Harbers and Carninci, 2005; Reinartz et al., 2002). Nevertheless, these techniques have limitations which hinder detailed and accurate study aimed at fully understanding the transcriptome of trypanosome parasites. The RNA-Seq technology has being used to provide extensive knowledge on parasite biology and host interactions (Geiger et al., 2011). Moreover, RNA-Seq can be used to elucidate the precise sequence of nucleotide transcripts and their relative abundance within a biological sample (Fiebig et al., 2015).

The coordination of cell differentiation and gene regulation between the nuclear and mitochondrial genome in *T. brucei* has been studied. For example, the ability of bloodstream form parasites devoid of a mitochondrial genome to differentiate into procyclic forms has been determined (Timms et al., 2002). Reduction in the copy number of the nuclear-encoded *COX VI* transcript by RNAi showed that neither the other *COX* mRNAs encoded by the nucleus nor the mitochondrion were altered (Timms et al., 2002). This knock-down experimental procedure was carried out to determine whether the loss of a nuclear-encoded subunit transcript would influence the regulation of the kinetoplast-encoded subunits of the same enzyme complex. However, the study did not demonstrate coordinated regulation between the nucleus and mitochondrion during differentiation (Timms et al., 2002). In this thesis, the ability of akinetoplastic stumpy cells to upregulate *COX VI* mRNA following differentiation was investigated.

Specifically, the RNA-Seq technology was used to obtain *in vivo* transcriptome data of akinetoplastic (AK) and wild type (WT) *T. brucei* cell lines before and after differentiation from slender to stumpy forms. Comparison of the transcriptome data from these two cell lines was used to obtain an overview of differentially expressed genes in the bloodstream forms of *T. brucei*.

3.1.1 Hypotheses

1. The lack of a mitochondrial genome results in changes in nuclear gene expression in *T. brucei*, similar to retrograde signalling in organisms like yeast.
2. The transcriptome of wild type and akinetoplastic cell lines of *T. brucei* changes during differentiation from slender to stumpy forms.

3.2 Result

3.2.1 Akinetoplastic cells express stumpy differentiation markers

The *PAD1* (Dean et al., 2009) and *ESAG9* (Monk et al., 2013) proteins have previously been shown to be markers for stumpy forms of *T. brucei*. Wild type (WT) procyclic, WT/WTγ (WTγ) and WT/L262Pγ (kDNA^0) (aAK) cell lines were used for the RNA analysis to probe for these stumpy markers in differentiated cells. The akinetoplastic slender cells were made kDNA independent by the introduction of L262P gamma mutation (See Section 2.1.1 and Table 2.1). The WT/L262Pγ cell line was treated with acriflavine to obtain two akinetoplastic clones; the acriflavine dye concentrates within the kinetoplast to inhibit kDNA synthesis (Dean et al., 2013). The L262Pγ mutation was shown to render the bloodstream slender forms of *T. brucei* to be independent of the kDNA (Dean et al., 2013). To obtain an isogenic control, the wild type version (WTγ) was also introduced into the parental strain and was identified as the WT/WTγ strain (Dewar et al., 2018).

The isogenic WT/WTγ strain and the akinetoplastic WT/L262Pγ strain were both generated by Caroline Dewar (Dewar et al., 2018). For this current study, the isogenic WT/WTγ strain and the akinetoplastic WT/L262Pγ strain were used for identification of the PAD1 and ESAG9 markers following differentiation of slender to stumpy forms, *in vivo*.

The isogenic WT/WTγ strain (simply referred to as WTγ) and two akinetoplastic clones (simply referred to as aAK) were injected into mice to enable differentiation from slender to

stumpy forms. These stumpy forms were further induced to differentiate to procyclic forms via the addition of 6 mM cis-aconitate (Czichos et al., 1986) and incubated at 27 °C.

The parental EATRO 1125 wild type strain and the isogenic wild type strain procyclic forms were grown *in vitro*. Prior to performing a Northern blot assay, ESAG9 and PAD1 riboprobes were prepared according to manufacturer's protocol (see Section 2.11.1) and run on 1% agarose gel to determine their sizes (Figure 3.1). The sizes between 400 and 1000 bp obtained were satisfactory to proceed to probe for PAD1 and ESAG9.

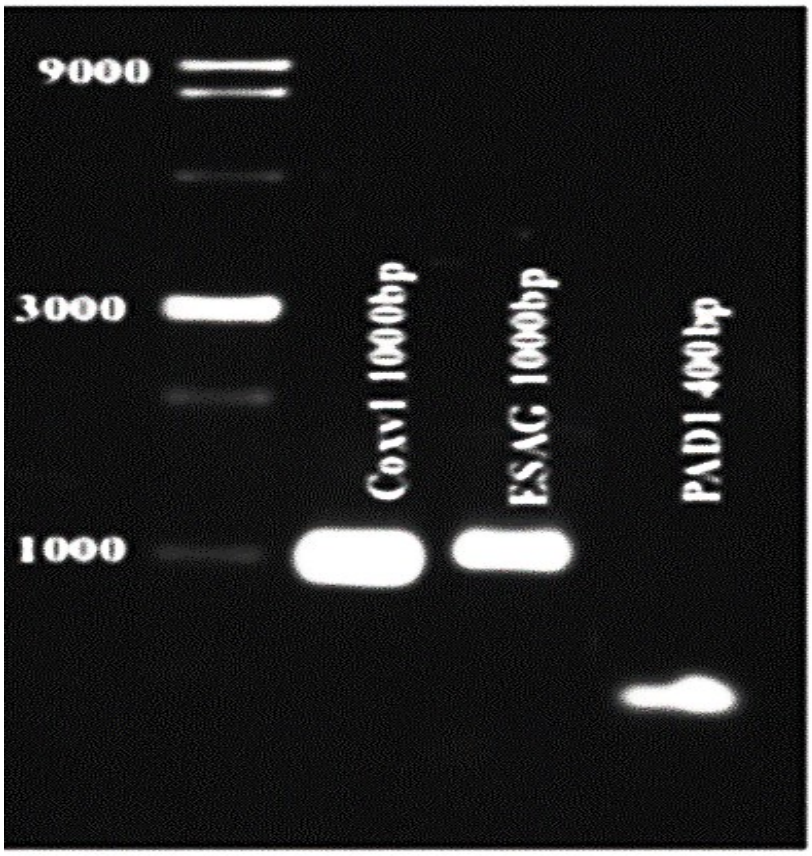

Figure 3.1 Determination of sizes of the *COX VI, ESAG9* and *PAD1* riboprobes using agarose gel electrophoresis. The molecular weight of the DNA ladder shown as 1000, 3000 and 9000 are in bp. The sizes of the *COX VI, ESAG9* and *PAD1* DNA bands are indicated on the agarose gel.

RNA that were extracted from the stumpy and slender forms of the two aAk, as well as the isogenic WTγ clone and the parental EATRO 1125 strain (WT) were used for Northern blot assay for identification of the presence of the PAD1 and ESAG9 markers. To generate stumpy or slender forms of *T. brucei*, MF1 mice were infected with the above-named cell lines via IP injection. Accurate measures of parasitaemia level and morphology during infection was recorded from wet blood smears for each cell line. Cells were harvested 4 days post infection (dpi), when morphologically slender cells dominated, and 7 dpi, when the population of cells were scored as being predominantly stumpy. RNA was also extracted from procyclic forms of the parental wild type strain (WT) and the isogenic wild type strain (WTγ). The procyclic RNA samples were extracted from cultured cells. The procyclics and slender cells were both used as negative controls, as these PCF samples were not expected to express the PAD1 and ESAG9 markers. Following Northern blotting, the membranes were first hybridized with the PAD1 riboprobe to detect the presence of PAD1 mRNA. Thereafter, the detection of ESAG9 mRNA using the ESAG9 riboprobe was also tested. As shown in Figure 3.2, there was increased expression of the PAD1 and ESAG9 mRNAs in the stumpy forms (SS) of the two aAk clones and the WTγ (SS) clone relative to the slender forms (SL) of the same clones. These observations supports recent findings demonstrating the differentiation of slender forms of *T. brucei* to stumpy forms in mice despite the absence of kDNA (Dewar et al., 2018) (Figure 3.2).

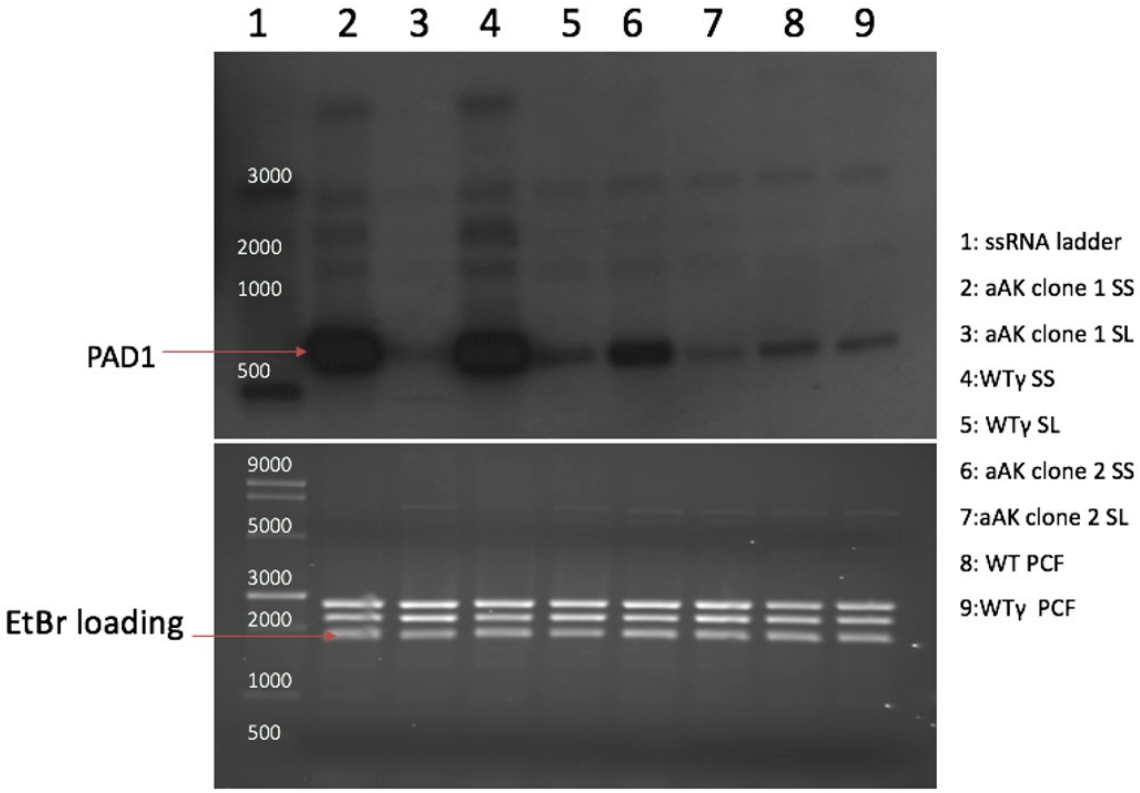
1 2 3 4 5 6 7 8 9
3000
2000
1000
500
PAD1
9000
5000
3000
2000
1000
500
EtBr loading
1: ssRNA ladder
2: aAK clone 1 SS
3: aAK clone 1 SL
4:WTγ SS
5: WTγ SL
6: aAK clone 2 SS
7:aAK clone 2 SL
8: WT PCF
9:WTγ PCF

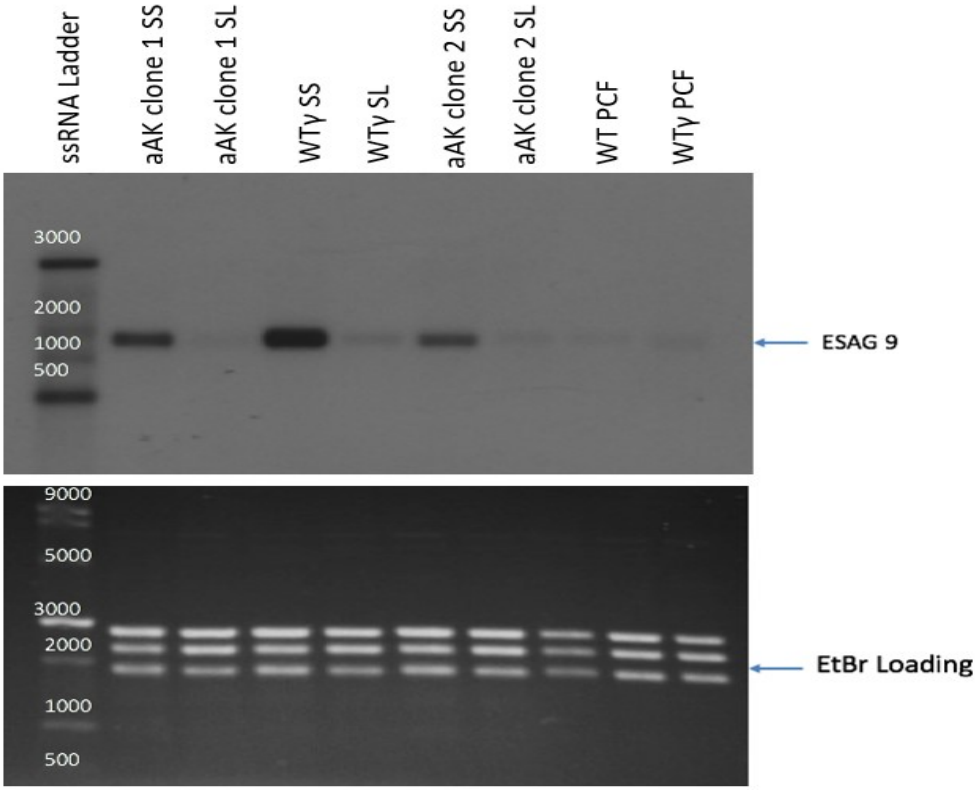

Figure 3.2. Detection of *PAD1* and *ESAG9* markers in stumpy forms of wild type and akinetoplastic cell lines of *T. brucei*. The *PAD1* and *ESAG9* riboprobes were used for the Northern blot assay. The *PAD1* Northern blot is shown as the two upper images and the *ESAG9* Northern blot is shown as the two lower images. *PAD1* Northern blot: Lanes 2, 4 and 6 represent stumpy form (SS) samples for aAk and WTγ clones while lanes 3, 5 and 7 represent slender form (SL) samples of these clones. Single-stranded RNA (ssRNA) ladder is in lane 1 while the wild type procyclic samples are in lanes 8 and 9. *ESAG9* Northern blot: Lane 1, 3 and 5 represent stumpy form samples for WTγ and aAK clones while lanes 2, 4 and 6 represent slender form samples of these cones. Lanes 7 and 8 represent the wild type procyclic samples.

3.3 Nuclearly-encoded cytochrome oxidase is upregulated in differentiated *T. brucei* cells

The RNA samples that were isolated from the two aAk, the WTγ clone and the parental EATRO 1125 strain (WT) were also used for determining the expression of cytochrome oxidase (COX VI) mRNA using the *COX VI* riboprobe (see Section 2.11.1). The main objective was to ascertain whether the absence of mitochondrial DNA in *T. brucei* affects the expression of nuclear-encoded genes such as the *COX VI* gene.

The data shown in Figure 3.3 indicate that there was higher expression of *COX VI* mRNA in the WTγ stumpy, procyclic forms (WT and WTγ) and aAK stumpy cell lines relative to the slender forms. The high expression of *COX VI* mRNA in the procyclic forms is expected, as previous study has shown that the *COX VI* mRNA and protein levels are enriched upon transformation of the bloodstream form of *T. brucei* to the insect form (Tasker et al., 2001).

Interestingly, the expression of *COX VI* mRNA in aAK clone 2 stumpy form was lower than that of aAK clone 1 and WTγ stumpy form. The low expression of *COX VI* mRNA in one of the aAk clones may be due to clonal variation, although this cell line was found to express high levels of ESAG9 and PAD1 mRNA during stumpy development (Figure 3.2).

The upregulation of *COX VI* expression have been reported in stumpy cells (Tasker et al., 2001). The authors found that during the differentiation of stumpy forms to procyclic forms in *T. brucei*, there is an initial upregulation of *COX VI* expression, which is later translated to proteins. The data shown in the present study indicates that the level of mRNA expression in the stumpy form of wild type strain was similar to the stumpy form of the aAK clone 1 cell line, which suggests that the absence of kDNA did not alter the expression of the nuclear-encoded *COX VI* gene.

This observation might correlate with data from Timms and colleagues (Timms et al., 2002), where it was found that knockdown of *COX VI* mRNA in differentiating parasites did not affect mRNA levels of mitochondrially-encoded constituents of the same enzyme complex during development to procyclic.

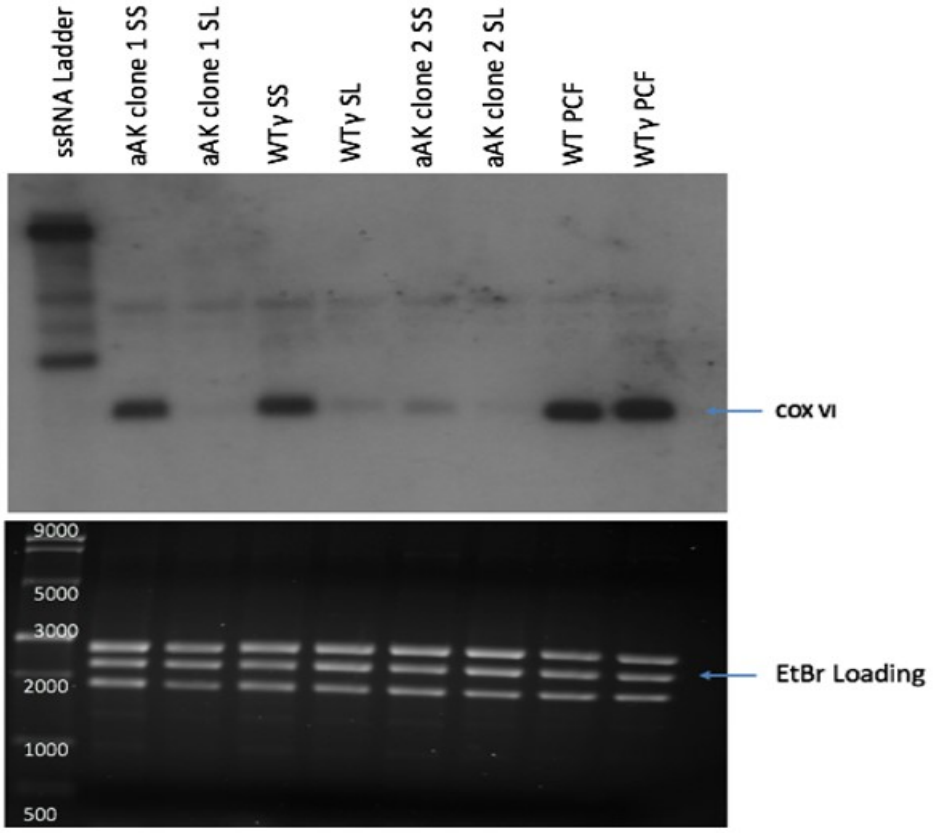

Figure 3.3 Detection of *COX VI* mRNA expression at the various stages of the life cycle of *T. brucei.* The *COX VI* riboprobe was used for the northern blot assay. The stumpy form samples for WTγ and aAK clones 1 and 2 are represented by lanes 1, 3 and 5. The slender form samples for WTγ and aAK clones 1 and 2 are represented by lanes 2, 4 and 6. The procyclic form samples are in lanes 7 and 8.

3.3.1 Akinetoplastic stumpy cells cannot differentiate into procyclic forms

To investigate the presence of the procyclic marker EP procyclin on the differentiated cell lines, a Western blot assay was performed using the EP procyclin antibody to identify the presence of the procyclic marker, EP procyclin, on akinetoplastic *T. brucei* cell lines following differentiation of stumpy forms. Stumpy forms of the *T. brucei* cells were harvested from infected mice, purified by DE52 chromatography and allowed to differentiate to procyclic (Section 2.1.4). The elongation factor 1 (EF1; Millipore, CA) was used as a loading control (Rosenberry et al., 1989).

It was observed that the akinetoplastic stumpy forms were unable to differentiate to late procyclic forms, as cell death was recorded approximately 48 hours after the initiation of differentiation. The data shown in Figure 3.4 indicate that only kDNA-containing procyclic forms (WT- and WTγ-differentiated procyclic forms) showed detectable protein band for EP procyclin on the Western blot. As was expected, the expression of EP procyclin was not detected for the bloodstream forms of *T. brucei*.

This observation has already been reported by Dr. Caroline Dewar (PhD thesis, 2015) and also supports previous published data (Timms et al., 2002). Collectively, these data provide evidence for the requirement of kDNA-encoded gene products in procyclic development. Moreover, the data indicates that the L262P mutation cannot compensate for the requirement of kDNA during differentiation of bloodstream forms of *T. brucei* to procyclic (except where a compensatory mutation has been introduced). The checkpoint is independent on regulation of the initial differentiation from slender to stumpy but is required for the establishment of procyclic differentiation (Timms et al., 2002).

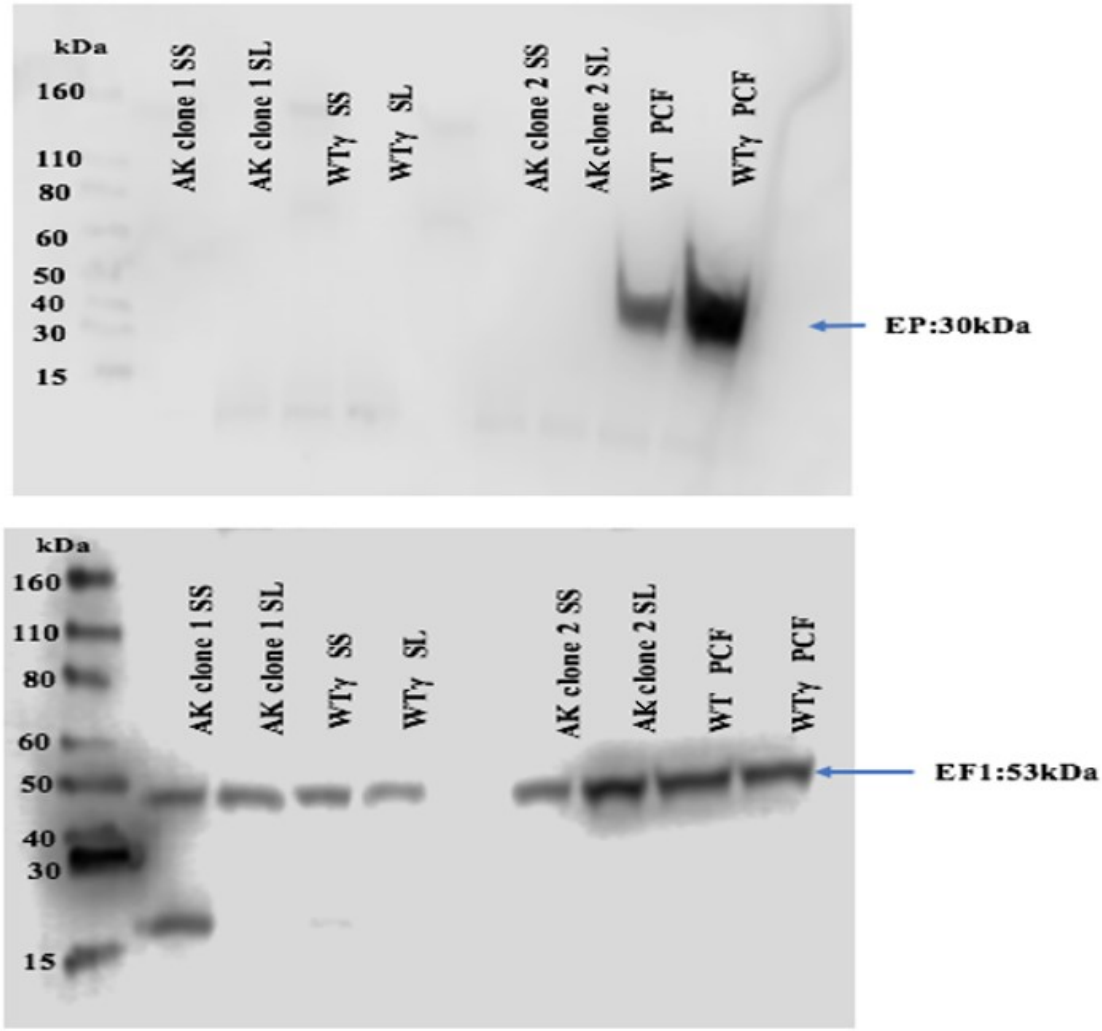

Figure 3.4 Detection of EP procyclin in the procyclic forms of *T. brucei.* Upper gel: Western blot detection of EP procyclin in wild type and akinetoplastic cell lines of *T. brucei*. Lower gel: Detection of elongation Factor 1 (EF1), which was used as a loading control. The EP procyclin protein runs at approximately 35kDa and the elongation factor 1 (EF1) loading control runs at approximately 53 kDa**.**

3.4 Validation of RNA samples prior to RNA-Seq analysis

As previously reported, akinetoplastic stumpy cells lack a membrane potential and have a reduced lifespan *in vitro* and in mice (Dewar et al., 2018). The loss of membrane potential might have led to the occurrence of programmed cell death, which could be attributed to the limited life span of stumpy cells (Duszenko et al., 2006). These observations raised the question on how stumpy forms generate mitochondrial ATP and Δψm, and whether the akinetoplastic cells also differ from WT at the gene level which may modulate gene expression during differentiation. The transcriptomics analysis that is described in this thesis was performed to provide insight into these unanswered questions. To compare the nuclear transcriptome of a wild type strain with an AK mutant, before and after differentiation from the slender to stumpy, mice were infected with two pleomorphic *T. brucei* EATRO 1125 (AnTat1.1 90:13) cell lines. One of the cell lines has one allele of the nuclear-encoded F_1F_O-ATPase subunit γ replaced with L262P mutation, WT/L262Pγ (kDNA^0) (AK). This AK cell line lost all mitochondrial DNA spontaneously. The other cell line is an isogenic control (WT/WTγ) (WTγ) whose L262Pγ allele was replaced by wild type (WT) ATPase subunit γ. Stumpy characteristics of each cell line were confirmed by indirect immunofluorescence staining for PAD1, a marker expressed on the cell surface of stumpy cells. PAD1 expression was seen in AK and WTγ stumpy cells (Figure 3.5). This provided further evidence that kDNA is not required for differentiation to stumpy (Dewar et al., 2018). The IFA results for PAD1 detection in the other biological replicates for AK and WTγ are shown in Appendix C.

Total RNA was purified from parasites during their biological progression from slender to stumpy forms. RNA was extracted from three mice for WTγ slender and stumpy, four individual samples for WT/L262Pγ AK stumpy and three samples for WT/L262Pγ AK slender and were analysed by RNA-seq. This allowed biological variability to be assessed and tested statistically. The integrity of the DNase-treated RNA was assessed using the Agilent RNA 6000 Nano chip on 2100 Agilent bioanalyser.

The expression of PAD1 in Figure 3.5 combined with morphological analysis, confirmed that highly enriched stumpy populations had been generated for each biological replicate.

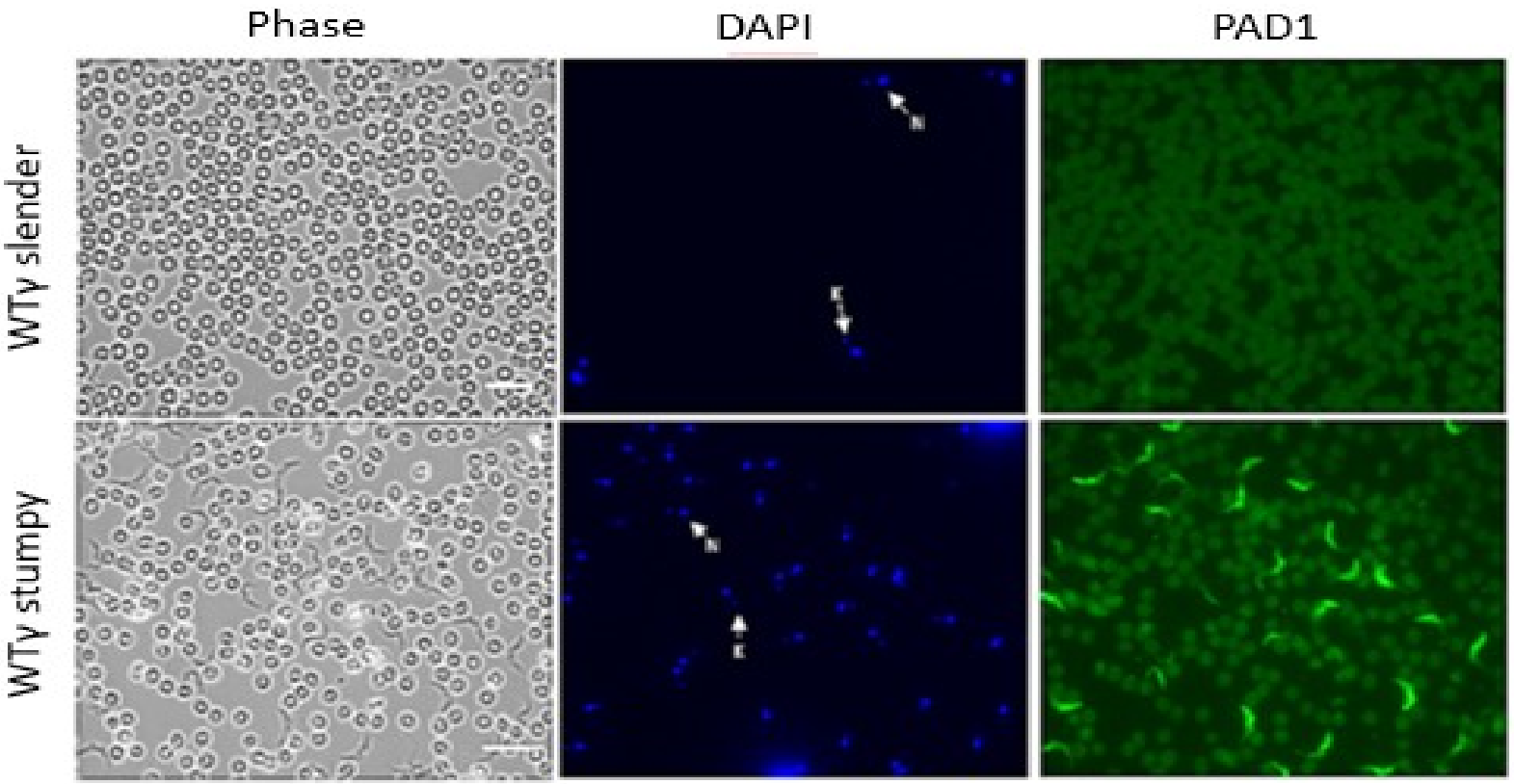
Phase
DAPI
PAD1
WTγ slender
WTγ stumpy

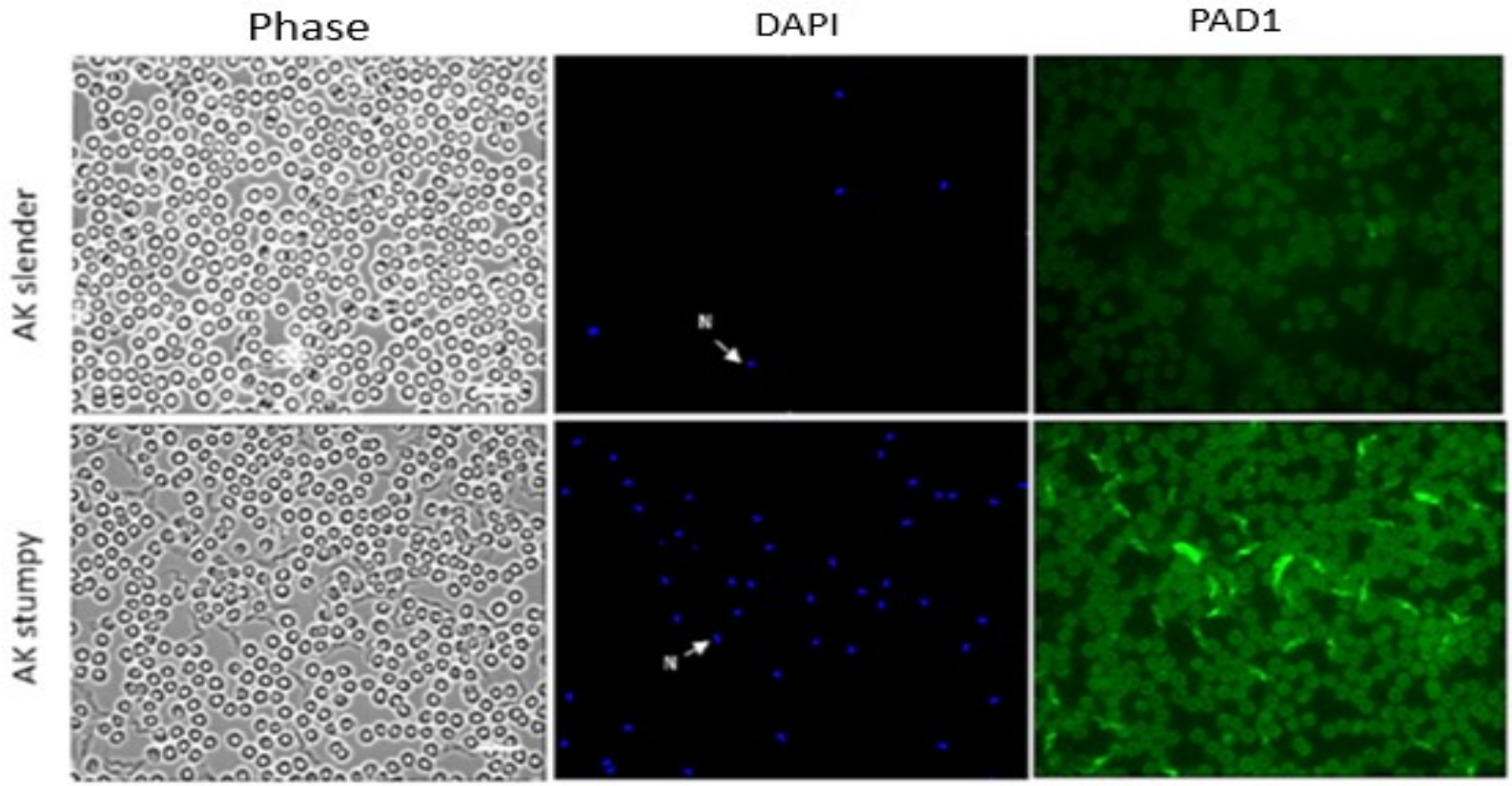

Figure 3.5 Immunofluorescence staining of PAD1 on stumpy forms of *T. brucei*. Both WTγ and AK expressed the PAD1 surface protein marker, labelled in green. DAPI staining (in blue) shows nucleus (N) and kinetoplast (K), which are indicated with a white arrow. Scale bar 5µm.

The minimal or no expression for PAD1, and the analysis of morphology also indicated that slender populations were obtained for the RNA-Seq analysis. Both stumpy and slender RNA samples form AK and WTγ showed satisfactory purity and integrity (Figure 3.6).

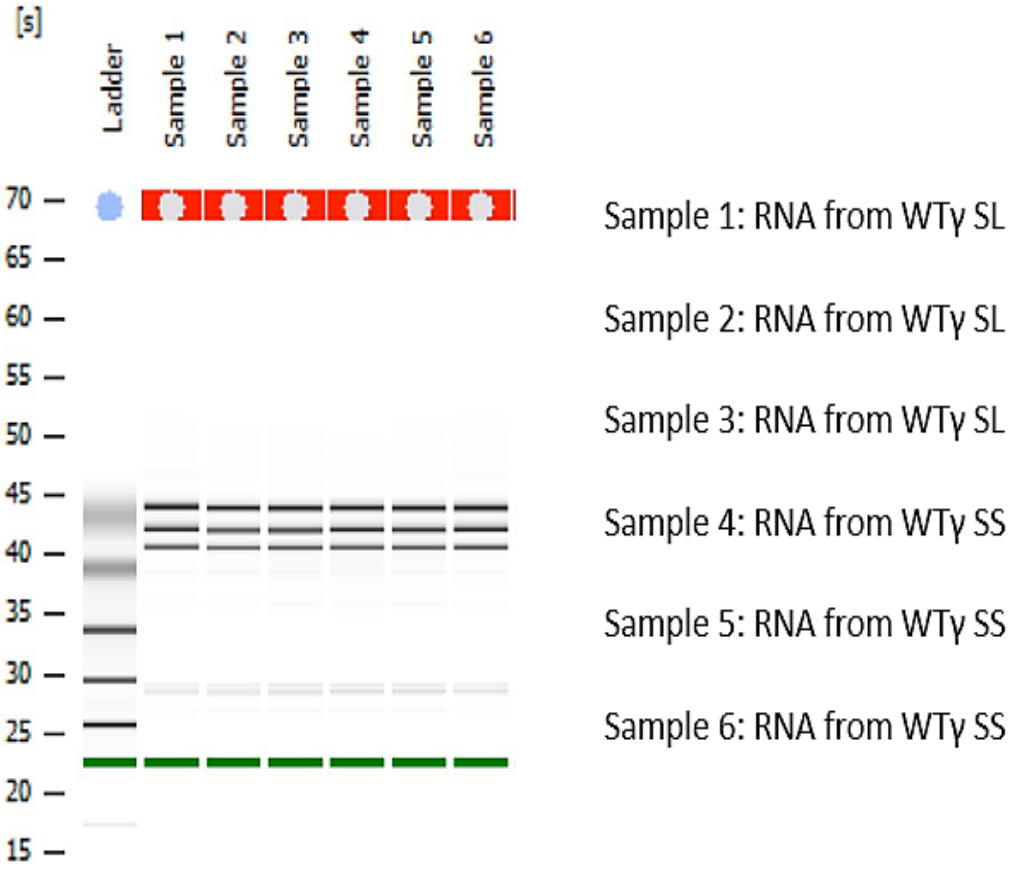

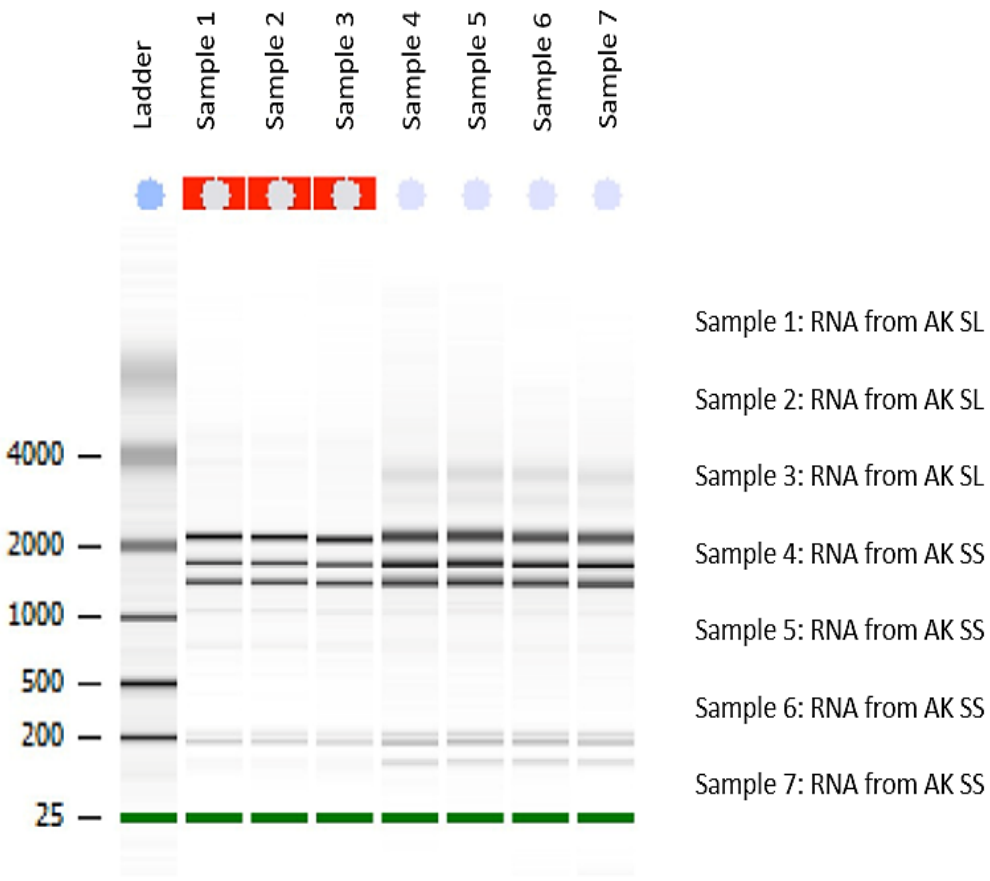

Figure 3.6 Assessing the purity and integrity of RNA samples prior to RNA-seq analysis. The upper gel image shows six samples: three RNA samples extracted from three mice infected with *T. brucei* parasites and harvested on day 4 when parasites were predominantly slender forms, and the remaining three RNA samples were extracted from three mice infected with *T. brucei* parasites harvested on day 7 post-infection with cell population being predominantly stumpy forms. The lower gel image shows integrity profile of RNA samples from three slender forms and four stumpy forms of Akinetoplastic cell lines.

3.5 Validation of transcriptome datasets

To validate dataset for analysis of mRNAs that are regulated during differentiation events, sequence reads of 100–125 bp were aligned to the *T. brucei* reference genome to reveal families of related genes. Requirement for concordant read pair mapping to more than one locus included and all discordant alignments were discarded. In addition, all reads mapped to more than one position on the *T. brucei* reference genome were discarded. Results were then normalised to the sample with the lowest number of alignments, counts converted to $\log_2$ and quantile normalised for linear model fitting purpose. A pairwise comparison of sample groups was performed on the normalised counts (See Section 2.14.1).

The counts were converted to $\log_2$, and the quantile was normalised for linear model fitting purposes. Alignments of sequence reads to the *T. brucei* reference genome were performed using bowtie 2. Data from Eleanor Silvester's thesis (2016) was used as a reference; she had previously performed a similar analysis using the slender and the stumpy forms of pleomorphic *T. brucei* EATRO 1125 cell line without any genetic manipulation.

For simplicity purposes, the reference samples would be referred to as REF SL or REF SS, whereas the samples generated from the present study would be designated as WTγ SL or WTγ SS for the isogenic control cell lines and AK SL and AK SS for the akinetoplastic cell lines. These six main groups of datasets (REF SL, REF SS, WTγ SL, WTγ SS, AK SL and AK SS) were used to generate 15 pairwise comparisons. A total of 19 samples were analysed (with assistance from Dr Alasdair Ivens, Director of Bioinformatics, Centre for Immunity, Infection and Evolution (CIIE) University of Edinburgh). All 19 samples passed the quality control analysis using FASTQC. A total of 15 multi-factor comparisons were performed using empirical Bayesian approaches; REF SL was compared to either REF SS or WTγ SS; WTγ SL was compared to AK SL; REF SS was compared to either WTγ SS or AK SS; and all other comparisons. For statistical robustness, only those samples with adjusted p-value < 0.05 were analysed.

To further find out if the genes expressed in the RNA datasets obtained have similar transcript profile clustering or are unrelated, Principal Component Analysis (PCA) was performed. This is a technique used to emphasize variation and bring out strong patterns in a dataset. There were six distinct groups of samples, generally behaving similarly with profiles within each sample being in concordance with each other. The PC1 represents the biggest variation in the datasets which clearly separates stumpy cells from slender forms with 35% proportion of variance. From the score plot, the PC2 shows separation between two similar datasets which shows less variation of 22% whiles the least variable was seen in PC3 with 9.5% variation (Figure 3.7).

The first three axes accounted for cumulative proportion of 35%, 57% and 67% of overall genetic variance in the six groups. The cumulative proportion for PC2 and PC3 are inverse of the proportion of variance. Both the two-dimension (2D) and three- dimension (3D) score plots convey the same information.

This analysis confirmed that genes expressed in either slender or stumpy forms of both the REF and the WTγ cell lines were similar (See Table 3.1 and 3.2). In addition to the PCA, the datasets were analysed for the expression profile of known transcripts predicted to exhibit differential regulation during the development from slender to stumpy forms. The WTγ datasets were compared to the reference dataset using stringent threshold parameters (adjusted p-value of < 0.05 for comparison and fold change ≥ 1)**.** Consistent with what was expected, the stumpy form cell lines expressed significantly more mRNA for PAD1 transcripts (Tb927.7.5930), a cell surface protein involved in regulating developmental processes (Dean et al., 2009) and *ESAG9* (Tb927.5.4620), a post transcriptional regulator of gene expression (Monk et al., 2013). The *PIP39* dephosphorylation protein was also enriched in stumpy forms.

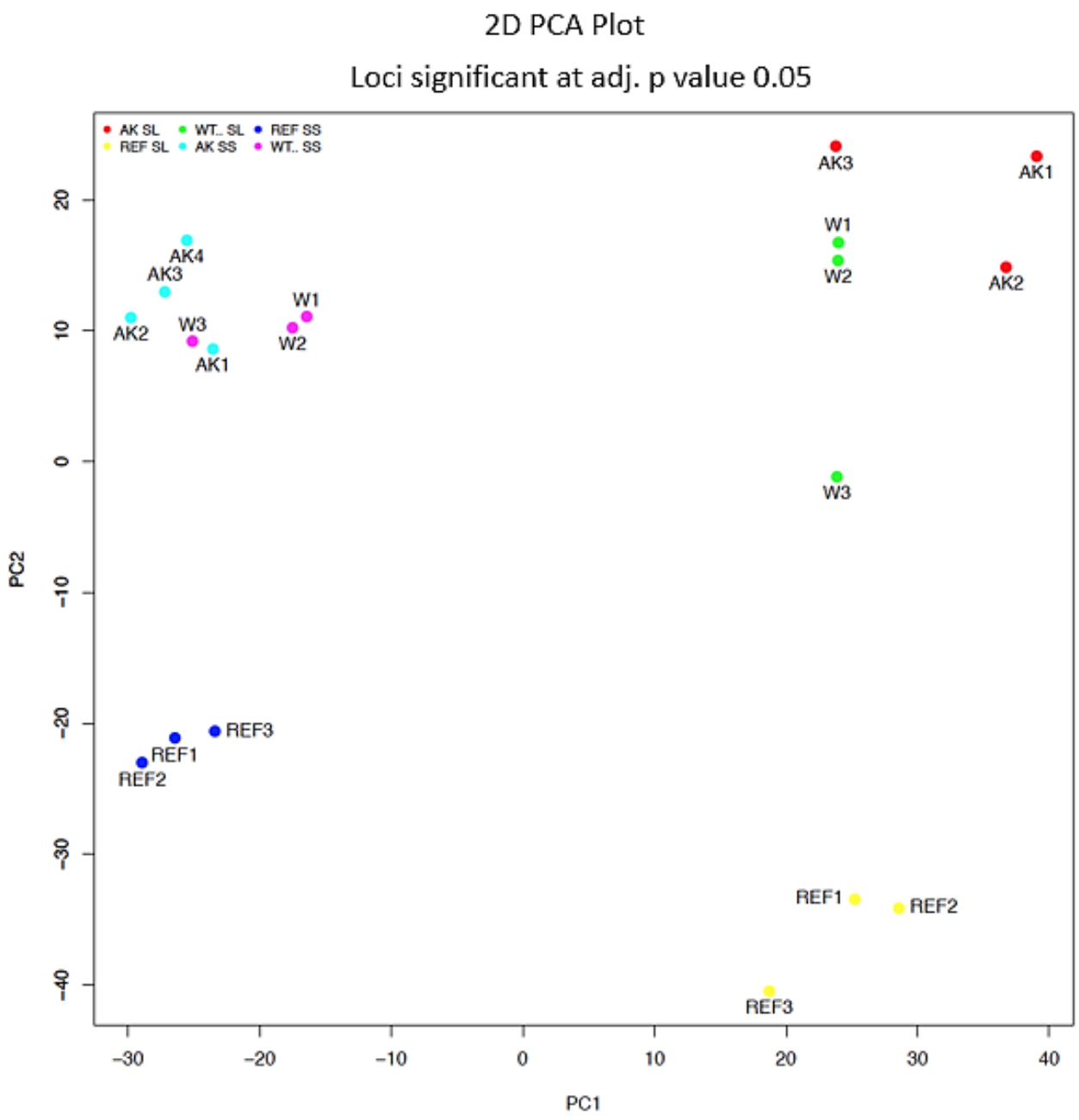
2D PCA Plot
Loci significant at adj. p value 0.05
AK SL
REF SL
WT.. SL
AK SS
REF SS
WT.. SS
AK3
AK1
W1
W2
AK2
AK4
AK3
W1
W3
AK2
W2
AK1
W3
REF3
REF1
REF2
REF1
REF2
REF3
PC2
PC1
20
10
0
−10
−20
−30
−40
−30
−20
−10
0
10
20
30
40

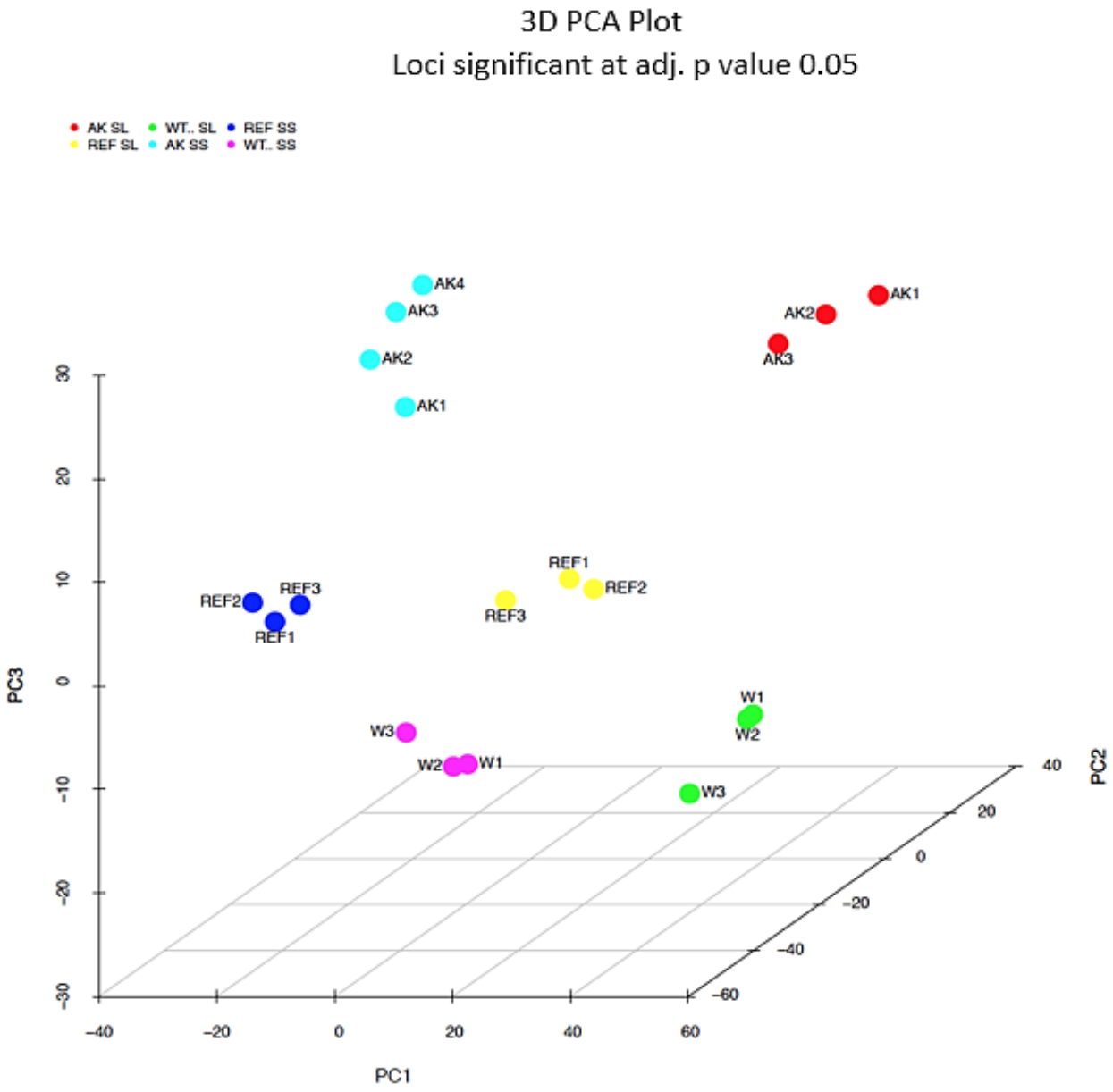

Figure 3.7 Principal component analysis (PCA) of stumpy and slender forms of WT and AK samples of *T. brucei.* REF SS is represented in blue, WTγ SS in pink. The points with similar colours represent the number of sample replicates used. REF SL (yellow), WTγ SL is shown in green. The numbers after each letter are indicative of the replicates used for the analysis. Both two-dimensional (upper image) and three-dimensional relationships for the 19 samples on PCA score plot show similar level of variation. The clustered datasets show relatedness.

The presence of abundant EP1 and GPEET procyclins was seen in stumpy cells. The procyclic form in the tsetse midgut has glycoprotein coat GPEET that is normally expressed 3 days after infection of the vector which is replaced by glycosylated EP procyclins by day 7 of infection (Acosta-Serrano et al., 2001; Vassella et al., 2001a, 2000). Also, among the upregulated transcripts in stumpy cells was Nek1/NIMA-related kinase which has a serine/threonine kinase activity. This kinase has been identified by (Nett et al., 2009), where they analysed cytosolic bloodstream form of *T. brucei* kinome and identified three members of the NEK kinase group out of 44 phosphorylated protein kinases. Purine nucleobase transporters has been reported to be encoded by multiple isogenes and their mRNAs are up-regulated in procyclics (Henriques et al., 2003).

The abundant expression of procyclin mRNAs in the stumpy form showed that these cells were pre-adapting for differentiation at the mRNA level as procyclins are the most abundant procyclic-specific transcripts and proteins (Roditi et al., 1998). Genes specifically elevated in stumpy forms are summarised in Table 3.1. The WTγ cells showed decreased expression of NEK1, Purine nucleoside transporter NT10, EP1 and GPEET when compared to the reference stumpy sample (REF). Though both REF and WTγ stumpy forms were morphologically similar, the difference in expression of stumpy specific stage transcript make the WTγ less stumpy compared to the REF.

Down regulated transcripts in stumpy cells are those known to have increased expression in slender forms. Transcription factor II Human (TFIIH, Tb927.1.1080) which is essential in trypanosome RNA maturation was decreased in stumpy cells (Lee et al., 2009). Likewise, the RNA-binding protein (RBP7) has been shown to be required for quorum sensing and promoting cell-cycle arrest when overexpressed (Mony et al., 2014) (see Table 3.2). The elevation of these transcripts in the REF stumpy compared to the WTγ stumpy cells may indicate that the REF SS cells were more enriched for stumpy forms than the WTγ samples. However, the histone transcript (Tb927.10.10580) and mRNAs for paraflagellar rod (PFR) and structural components of the cell (Tb927.8.1550) were decreased in the stumpy forms which supports similar findings.

The data showed that genes differentially expressed between slender or stumpy forms of WTγ were also differentially expressed in the REF samples, even though most of the expression differences were more pronounced in the REF datasets than WTγ. Likewise, the morphology of both cells showed stumpy shape when differentiated in mice (Figure 3.5).

Table 3.1 Selection of proteins showing greater than 1 fold differential change in WTγ and REF stumpy cell lines with p value of <0.05. The transcripts are denoted by (+) for increased or (-) for decreased. The fold change is shown as FC**.** Stumpy specific genes were more enriched in REF samples when compared with WTγ.

Gene ID	Description	REF SS vs REF SL FC	WTγ SS vs WTγ SL FC	WTγ SS vs REF SL FC	WTγ SS vs REF SS FC	Reference
Tb927.7.5930	Protein Associated with Differentiation (PAD1)	+1.74	+1.02	+1.79	+1.04	(Dean et al., 2009)
Tb927.5.4620	Expression site-associated gene (ESAG9)	+4.29	+1.58	+3.25	+1.18	(Monk et al., 2013)
Tb927.9.6100	TFIIF-stimulated CTD phosphatase	+2.00	+2.46	+2.30	+2.83	(Szoor et al., 2010)
Tb927.9.6090	PTP1-interacting protein	+1.96	+2.64	+2.14	+2.83	(Brenchley et al., 2007; Szoor et al., 2010)
Tb927.10.10260	EP1 procyclin	+10.56	+6.06	+1.64	-1.09	(Acosta-Serrano et al., 2001)
Tb927.6.510	Procyclic form specific polypeptide A	+1.29	+2.00	+4.92	-1.15	(Vassella et al., 2000)
Tb927.4.5390	Nek1/NIMA-related kinase A	+2.14	-1.21	+2.00	-1.28	(Nett et al., 2009)
Tb927.9.7470	Purine nucleoside transporter	+2.83	+1.64	+2.83	-2.46	(Sanchez et al., 2004)

Table 3.2 Downregulated genes in WTγ and REF stumpy cells. Both WTγ stumpy and REF stumpy cells showed decreased level of expression of transcripts known to be upregulated in slender forms when greater than 1-fold differential change was considered with p value of <0.05.

Gene ID	Description	REF SS vs REF SL FC	WTγ SS vs WTγ SL FC	WTγ SS vs REF SL FC	WTγ SS vs REF SS FC	Reference
Tb927.1.1080	TFIIH basal transcription factor subunit	-1.04	-1.23	-1.06	-1.36	(Lee et al., 2009)
Tb927.10.12100	RNA-binding protein	-1.93	-2.30	-1.09	-1.34	(Mony et al., 2014)
Tb927.10.10580	Histone	-4.59	-1.67	-2.14	-1.01	(Kabani et al., 2009)
Tb927.8.1550	Paraflagellar rod component	-2.00	-1.39	-1.53	-1.04	(Kabani et al., 2009)

3.6 Comparison of mRNA expression between WTγ and AK strains

The rationale was to test whether cells differentiating in either WTγ or REF background regulate similar genes expressed between REF slender and WTγ slender cells. The pairwise comparison dataset of REF slender relative to WTγ slender was analysed. Transcripts significantly regulated at adjusted p-value of < 0.05 with fold change greater than 2 gave 150 genes to be enriched in slender cells. The expression level of these transcripts is illustrated in a volcano plot (Figure 3.8).

A summary on gene list in Table 3.3 illustrates enriched transcripts in REF slender relative to WTγ slender showing 40 most enriched genes ordered by their relative fold change, superior to 2-fold change and p value of <0.05. Most of these upregulated genes were hypothetical proteins. Interestingly, RNA-binding protein, UBP1 (Tb927.11.500; 74-fold) which participates in RNA degradation and maintaining the integrity and stability of RNA in *T. cruzi* (Cassola et al., 2015) was identified. The remaining were transcripts encoding glycolytic enzymes or transporters for either glucose or hexose (Table 3.3), suggesting increased dependence on glucose as an energy source in the slender forms. The *THT1* hexose transporter is known to be highly expressed in slender forms (Bringaud and Baltz, 1993) and glyceraldehyde-3-phosphate dehydrogenase (Tb927.6.4300) both showing 2.1-fold increase in REF slender compared to WTγ slender. Likewise, histones (Tb927.5.4200, 3-fold increased) and paraflagellar rod (Tb927.3.4330, 2.5-fold) increased were observed to be enriched in REF slender sample. Histone and PFR has been reported to be enriched in slender cells of *T. brucei* (Kabani et al., 2009). This observation was in concordance with data of this study.

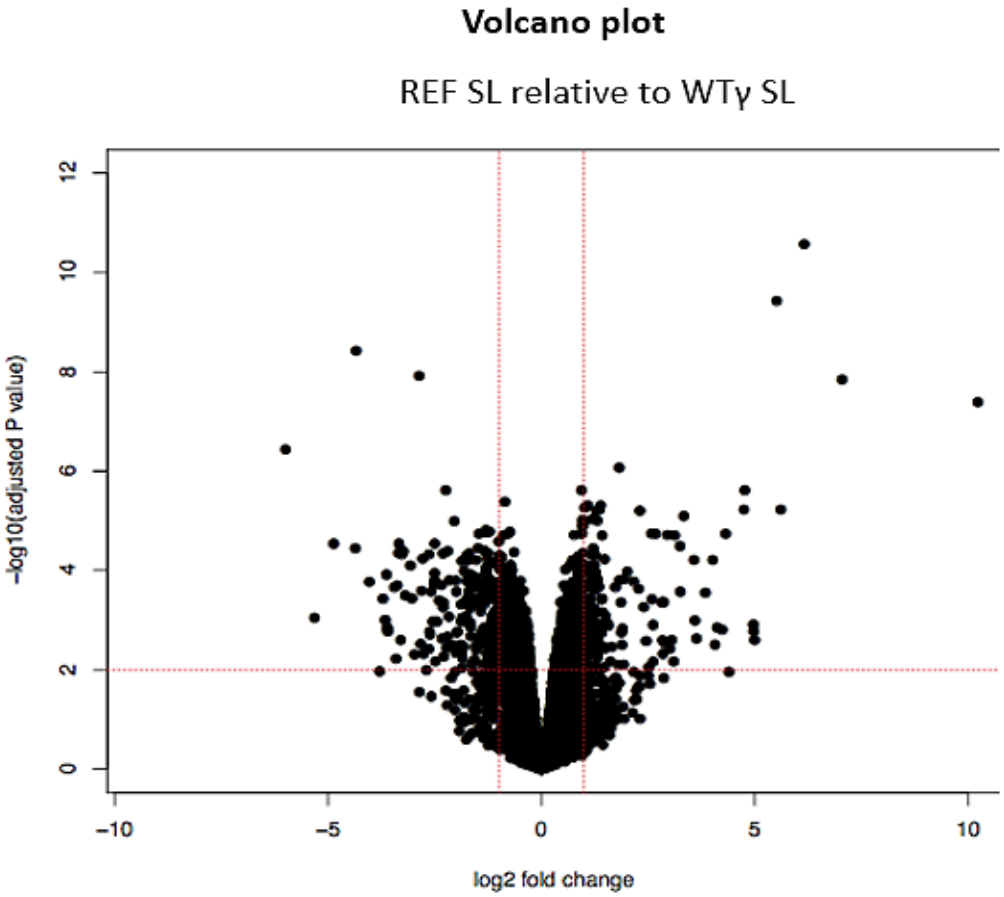

Figure 3.8 A volcano plot showing genes that are differentially expressed in REF slender (SL) cells versus WTγ slender forms. Positive values represent genes that were enriched in SL cells while the negative values signify down-regulated genes. The genes that clustered around zero were without any difference in expression. The Y-axis is the log $_{10}$ adjusted p value while the x-axis denotes the $\log_2$ fold change. The vertical red dotted line is the 2 FC cut off for genes considered as significant with p value of <0.05. on horizontal red line. The genes within the two vertical red dotted lines are coregulated and the ones that fall outside the lines are either upregulated for positive values or downregulated for negative values. Each dot in black represent a gene.

Table 3.3 Illustrates enriched transcripts in REF slender relative to WTγ slender. The list shows 40 most enriched genes ordered by their relative fold change, superior to 2-fold change and p value of <0.05. Most of these upregulated genes were hypothetical proteins.

Gene ID	Description	logFC	FC
Tb927.11.500	RNA-binding protein, UBP1	7	128
Tb927.11.130	expression site-associated gene 9 (ESAG9),	6.2	74
Tb927.11.110	expression site-associated gene 9 (ESAG9),	5.5	45
Tb927.9.380	expression site-associated gene 3 (ESAG3),	5	32
Tb927.6.5490	expression site-associated gene 3 (ESAG3),	5	32
Tb927.9.16880	expression site-associated gene 3 (ESAG3),	4.2	18
Tb927.11.20150	expression site-associated gene 3 (ESAG3),	4.1	17
Tb927.5.5230	expression site-associated gene (ESAG3),	4.1	17
Tb927.6.500	gene related to expression site-associated gene	3.3	10
Tb927.11.530	RNA-binding protein, putative	3.3	10
Tb927.6.470	gene related to expression site-associated gene	3.1	9
Tb927.5.4660	expression site-associated gene 3 (ESAG3),	3	8
Tb11.v5.0297	variant surface protein, putative	2.9	7
Tb927.3.250	expression site-associated gene 3 (ESAG3),	2.9	7
Tb927.1.20	expression site-associated gene 3 (ESAG3),	2.8	7
Tb11.15.0008	expression site-associated gene 3 (ESAG3),	2.8	7
Tb927.6.540	gene related to expression site-associated gene	2.7	6
Tb11.v5.0850	hypothetical protein conserved	2.6	6
Tb927.8.450	expression site-associated gene 3 (ESAG3),	2.6	6
Tb927.9.560	expression site-associated gene 3 (ESAG3),	2.5	6

Tb927.11.19800	hypothetical protein	2.5	6
Tb927.4.1910	hypothetical protein conserved	2.4	5
Tb927.9.16700	expression site-associated gene 3 (ESAG3),	2.3	5
Tb11.v5.0752	expression site-associated gene 3 (ESAG3)	2.2	5
Tb927.10.14540	hypothetical protein	2	4
Tb927.9.4080	hypothetical protein conserved	1.9	4
Tb927.11.6600	hypothetical protein conserved	1.9	4
Tb927.8.910	hypothetical protein conserved	1.9	4
Tb927.7.2420	glycogen synthase kinase-3 alpha, putative	1.8	3
Tb927.10.14550	ATP-dependent DEAD/H RNA helicase, putative	1.8	3
Tb927.10.5150	zinc finger protein family member, putative	1.8	3
Tb927.9.620	expression site-associated gene 3 (ESAG3),	1.8	3
Tb927.11.1880	histone H1, putative	1.7	3
Tb927.11.6890	DNA repair and recombination helicase protein	1.6	3
Tb927.11.14220	hypothetical protein conserved	1.6	3
Tb11.v5.0537	polyubiquitin, putative	1.5	3
Tb927.3.1910	hypothetical protein conserved	1.5	3
Tb927.5.4200	histone H4, putative	1.5	3

3.7 Evidence for retrograde signalling?

A three-way comparison using 3 groups of datasets comprising slender to stumpy differentiation in REF, WTγ and AK cells will be instrumental in ascertaining whether a correlation between the two WT datasets exists. Moreover, the comparison would provide relevant information as to whether any upregulated genes were unique to each dataset and thereby linked to the genetic background of each cell line. Following the comparison, it was observed that many transcripts were unique and not shared, however, PCA analysis in indicates overall relatedness of samples.

Of the four hundred and seventeen transcripts enriched in REF SL forms when compared to REF SS forms, 146 genes were uniquely expressed in REF slender. Examples of such genes included expression site-associated gene 3 (*ESAG3*) (Tb927.9.16880; 15-fold), flagellar protein PF16 (Tb927.1.2670; 3.2-fold), beta tubulin (Tb927.1.241; 4-fold) and histone H4 (Tb927.5.4220; 4-fold). The rest were glycosomal glycerol kinase (Tb927.9.12550; 2.8-fold) and enzymes involved in glycerol metabolism and known to be located in the glycosome (Hart et al., 1984), and procyclin-associated gene 2 (Tb11.v5.1027; 2-fold). All these transcripts that have been reported to be upregulated in slender forms. Approximately, two-third of the transcripts encoded hypothetical proteins. A summary of the unique and shared genes is illustrated in a 3-way Venn diagram in Figure 3.9.

Fifty-one distinct genes were unique to WTγ slender and the remaining genes were shared with both REF slender and AK slender. Consistent with what was expected, WTγ SL cells expressed the following elevated genes: RBP32 (Tb927.9.4560; 3 fold), adenosine transporter (Tb927.2.6220; 2.8 -fold) which is an amino acid transporter (*AAT6*) also involved in eflornithine uptake and that has been shown to be detected only in slender forms (Carter and Fairlamb, 1993; Sanchez et al., 2002), retrotransposon hot spot protein 7 (RHS7) (Tb927.7.2030; 2.5 fold), a purine nucleoside transporter (Tb927.6.220; 2.1 fold) which is detected in both bloodstream and procyclic life cycle stages (Sanchez et al., 2002), GPI inositol deacylase 2 (Tb927.3.2610; 2-fold) and expression site-associated gene 4 (*ESAG4*)

(Tb927.9.16010; 2 -fold). The remaining two-third of these transcripts were hypothetical proteins.

Finally, a total of 446 genes were up-regulated (≥2-fold change) in AK slender relative to AK stumpy. Out of these, 141 were unique to this dataset. The genes upregulated in AK SL included *ESAG3* (Tb927.3.460; 7-fold), procyclin-associated gene 5 (*PAG*5) protein (Tb927.10.10230; 3.7- fold), retrotransposon hot spot protein 3 (RHS3) (Tb927.4.280; 3.7-fold), BARP protein (Tb927.9.15550; 2.6-fold), flagellar protofilament ribbon protein (Tb927.8.4640; 2.5-fold), *TFIIF*-stimulated CTD phosphatase (Tb927.10.14270; 2.3 -fold) and paraflagellar rod (Tb927.10.8930; 2.3- fold).

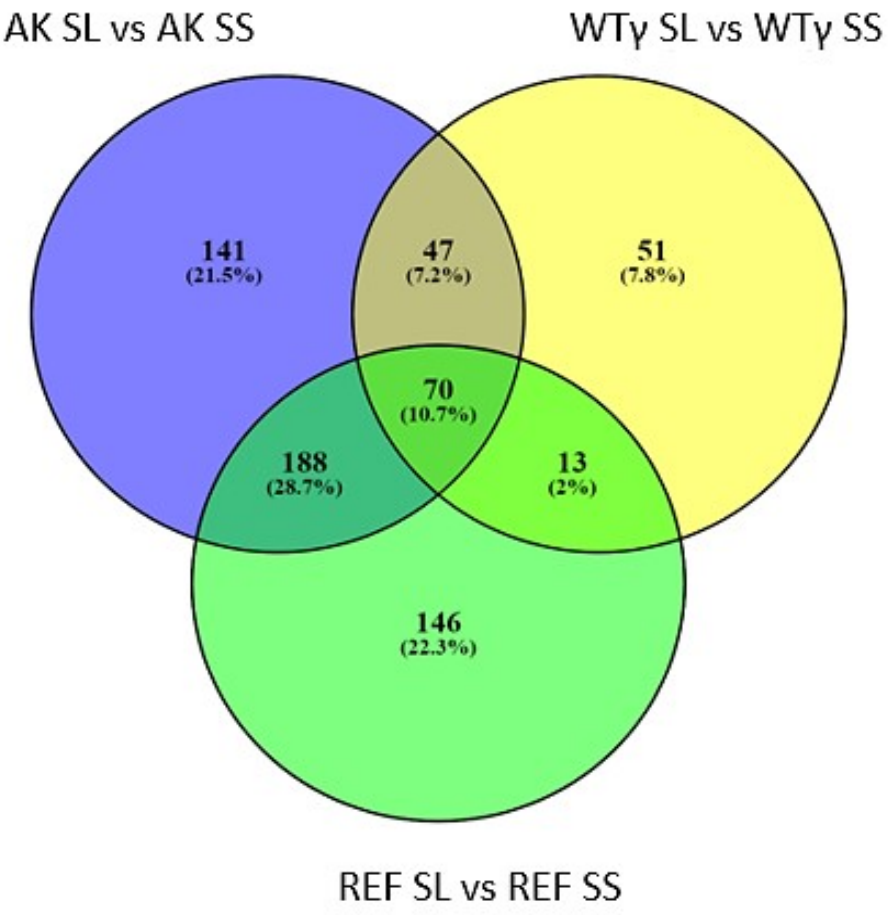

Figure 3.9 A 3-way Venn diagram illustrating distribution of unique and shared genes among slender AK, slender REF and slender WTγ RNA samples. The AK genes are shown in blue, WTγ in yellow and REF in green. The number of genes that are uniquely expressed as well as those shared among the three groups are shown in the Venn diagram. This Venn was created using Venny 2.1.0.

Surprisingly, only 70 genes were shared among the three datasets, accounting for 11% of the total transcripts upregulated in the three slender cell samples (Figure 3.9). Comparing the shared genes to the unique transcripts retained within the two WT datasets clearly showed a poor correlation between REF and WTγ cell lines. A list of the transcripts whose expression profiles were shared among the three datasets are shown in Table 3.4. The common genes that were significantly regulated among the three datasets include: ESAG transcripts (ESAG2, ESAG11), histone transcripts, mRNAs for structural components such as beta tubulin, which has also been reported (Kabani et al., 2009) and glucose and THTI hexose

transporters, which are in agreement with previous reports (Bringaud and Baltz, 1993; Geiger et al., 2011; Hug et al., 1993). A third of these transcripts represented hypothetical proteins.

Table 3.4: Significantly expressed trypanosome stage-regulated genes shared among slender AK, slender REF and slender WTγ. The table was generated when a three-way comparison of three different datasets comprising slender to stumpy differentiation in REF, WTγ and AK cells was performed to ascertain whether a correlation exist between REF and WTγ datasets.The genes listed in the table are genes enriched in slender forms. FC represents fold change of 2 and above with p value of <0.05.

Symbol	Description	LogFC	FC
Tb927.6.500	gene related to expression site-associated gene	3.8	13.9
Tb927.6.540	gene related to expression site-associated gene	3.7	13
Tb927.11.14840	chromosomal passenger protein	3.3	9.8
Tb927.10.10210	procyclin-associated gene 4 (*PAG*4) protein	2.5	5.7
Tb927.4.2740	hypothetical protein conserved	2.5	5.7
Tb927.7.610	mitochondrial DNA ligase homolog, *LIG* k-alpha	2.4	5.3
Tb927.8.2280	hypothetical protein conserved	2.4	5.3
Tb927.10.8440	glucose transporter 1B	2.3	4.9
Tb927.11.6550	*PUF* nine target 1	2.3	4.9
Tb927.11.890	hypothetical protein conserved	2.3	4.9
Tb927.9.1340	Nucleoporin	2.3	4.9
Tb11.v5.0308	*THT1* - hexose transporter, putative	2.2	4.6
Tb927.10.8460	glucose transporter, putative	2.2	4.6
Tb11.v5.0676	expression site-associated gene 2 (*ESAG2*)	2.1	4.3
Tb927.11.1510	leucine rich repeat protein, putative	2.1	4.3

Tb927.3.3270	ATP-dependent phosphofructokinase	2.1	4.3
Tb927.7.2830	histone H2A, putative	2	4
Tb11.v5.0531	fructose-bisphosphate aldolase, glycosomal,	1.9	3.7
Tb927.10.5620	fructose-bisphosphate aldolase, glycosomal	1.9	3.7
Tb927.3.2580	hypothetical protein conserved	1.9	3.7
Tb927.6.210	leucine-rich repeat protein 1 (*LRRP*1),	1.9	3.7
Tb927.3.2500	hypothetical protein	1.8	3.5
Tb927.7.2920	histone H2A, putative	1.8	3.5
Tb927.8.2270	hypothetical protein conserved	1.8	3.5
Tb927.8.5340	hypothetical protein	1.8	3.5
Tb927.8.6240	STOP axonemal protein	1.8	3.5
Tb11.v5.0307	*THT1* - hexose transporter, putative	1.7	3.2
Tb927.1.2050	hypothetical protein, unlikely	1.7	3.2
Tb927.1.3830	glucose-6-phosphate isomerase, glycosomal	1.7	3.2
Tb927.10.12820	hypothetical protein conserved	1.7	3.2
Tb927.10.14160	aquaporin 3, putative	1.7	3.2
Tb927.11.11980	corset-associated protein 15	1.7	3.2
Tb927.3.2530	expression site-associated gene 11 (*ESAG11*),	1.7	3.2
Tb927.9.15770	hypothetical protein conserved	1.7	3.2
Tb927.9.6290	AK1	1.7	3.2
Tb11.v5.0330	*THT1* - hexose transporter, putative	1.6	3
Tb927.10.13930	phosphatidic acid phosphatase, putative	1.6	3
Tb927.6.350	hypothetical protein conserved	1.6	3
Tb927.9.15740	hypothetical protein conserved	1.6	3

Tb927.9.7400	expression site-associated gene 11 (*ESAG11*)	1.6	3
Tb927.9.8190	hypothetical protein conserved	1.6	3
Tb11.01.6240	expression site-associated gene 2 (*ESAG2*)	1.5	2.8
Tb11.01.6241	expression site-associated gene (*ESAG*) protein,	1.5	2.8
Tb927.8.2070	hypothetical protein conserved	1.5	2.8
Tb927.8.2260	hypothetical protein conserved	1.5	2.8
Tb927.2.5660	adenylate kinase, putative	1.4	2.6
Tb927.3.2590	hypothetical protein	1.4	2.6
Tb927.6.3180	hypothetical protein conserved	1.3	2.5
Tb927.9.11580	glycosomal membrane protein	1.3	2.5
Tb11.v5.0668	protein disulphide isomerase	1.2	2.3

3.8 Differential gene expression in slender WTγ versus stumpy WTγ

To determine differences in gene expression between slender to stumpy specifically in the AK and WTγ cell line, I first compared genes differentially expressed between slender and stumpy cells in WTγ cells. Out of 2010 genes which were significantly differentially expressed (1001 up-regulated and 1009 down-regulated), 246 genes were identified as differentially regulated with a 2-fold increase between slender forms and stumpy forms with a p value < 0.05. The differential expressed genes are shown in the volcano plot (see Figure 3.10).

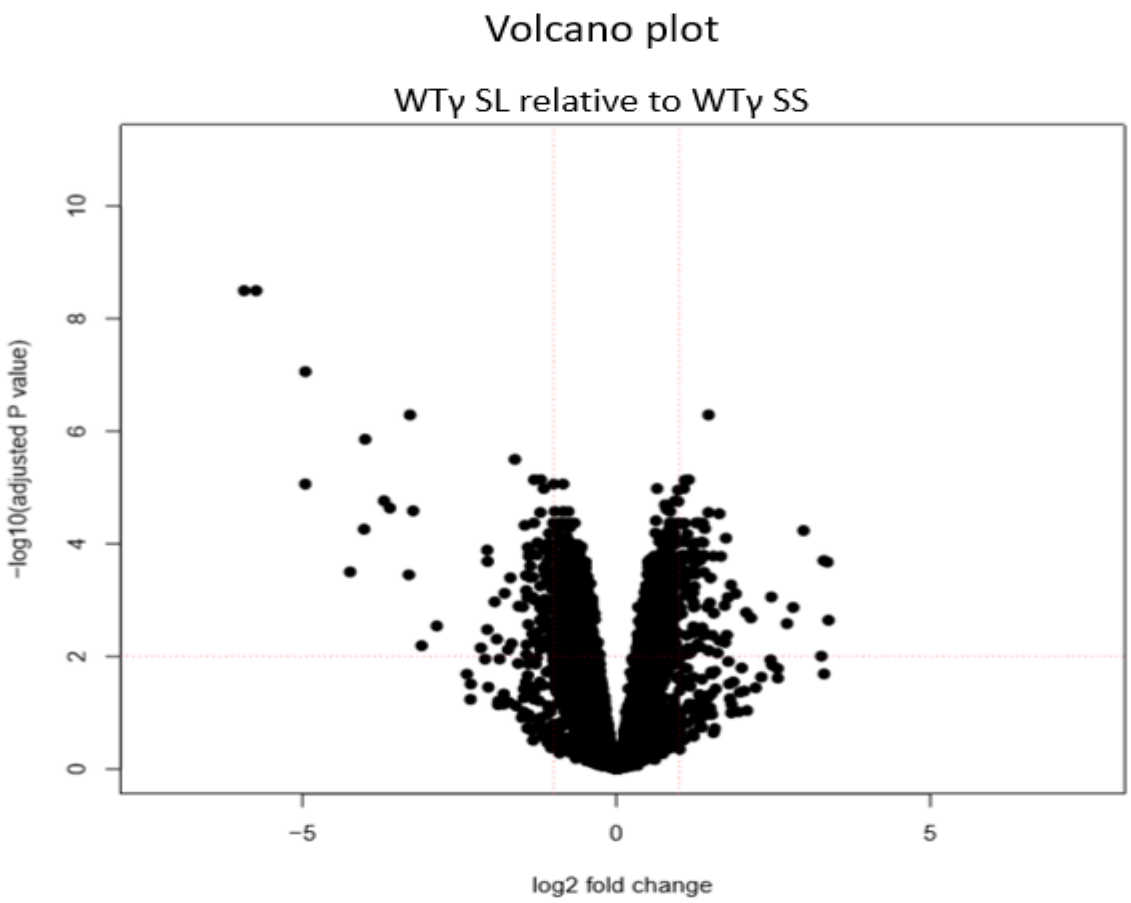

Figure 3.10 Volcano plot showing genes that were differentially expressed in WTγ slender cells relative to WTγ stumpy forms. The genes that grouped around zero were co-regulated. The Y-axis is the log $_{10}$ adjusted p value while the x-axis denotes the $\log_2$ fold change. The vertical red dotted line is the 2 FC cut off for genes considered as significant with p value of <0.05. on horizontal red line. The genes within the two vertical red dotted lines are coregulated and the ones that falls outside the lines are either upregulated for positive values or downregulated for negative values.

One-third of the 246 selected transcripts encoded predicted hypothetical proteins. The analysis also revealed that transcripts encoding glycosomal proteins, such as fructose-bisphosphate aldolase (Tb927.10.5620), were among the 246 selected genes. It has previously been reported that the expression of fructose-bisphosphate aldolase is at least six times higher in bloodstream trypanosomes compared to procyclic forms (Hug et al., 1993). Another study also demonstrated that the aldolase was decreased within 24 hours after differentiation to stumpy in *T. brucei* cells (2009) and this data confirmed the trend, with an upregulation of 3.7 FC in WTγ slender forms with respect to WTγ stumpy forms (Table 3.5) glycolytic enzymes such as glyceraldehyde-3-phosphate dehydrogenase

(Tb927.6.4280), which is known to be upregulated in slender and downregulated in stumpy forms (Queiroz et al., 2009), and pyruvate kinase (Tb927.10.14140) were both increased by 4.6-fold in WTγ slender (Table 3.5). The *PNT1* protein (Tb927.11.6550), which is required for kDNA maintenance, was also upregulated by 3-fold in WTγ slender compared to WTγ stumpy. I noticed as a trend that genes that were upregulated in WTγ slender were also upregulated in REF slender, but expression differences were more pronounced in the REF slender cells. A complete list of the genes is attached as electronic files.

Table 3.5 List of top 50 upregulated transcripts expressed in WTγ slender compared to WTγ stumpy with p value of <0.05 and a fold change of 2 and above.

Symbol	Description	logFC	FC
Tb927.5.4000	hypothetical protein	3.60	12.1
Tb927.10.7650	hypothetical protein	3.30	9.8
Tb927.10.7150	hypothetical protein	3.00	8.0
Tb927.1.2020	hypothetical protein	2.40	5.3
Tb927.9.13190	hypothetical protein, unlikely	2.40	5.3
Tb927.11.18280	*ESAG7* (expression site associated protein 7),	2.30	4.9
Tb927.10.14140	pyruvate kinase 1	2.20	4.6
Tb11.v5.0605	pyruvate kinase 1, putative	2.20	4.6
Tb927.6.4280	glyceraldehyde 3-phosphate dehydrogenase,	2.20	4.6
Tb927.6.4300	glyceraldehyde 3-phosphate dehydrogenase,	2.10	4.3
Tb927.1.3470	hypothetical protein,	2.10	4.3

Tb927.1.3330	hypothetical protein,	2.10	4.3
Tb927.11.9000	cation transporter, putative	2.00	4.0
Tb927.4.3280	expression site-associated gene 2 (*ESAG2*)	2.00	4.0
Tb11.v5.0531	fructose-bisphosphate aldolase, glycosomal,	1.90	3.7
Tb927.10.5620	fructose-bisphosphate aldolase, glycosomal	1.90	3.7
Tb927.9.7840	hypothetical protein,	1.90	3.7
Tb11.v5.0514	cation transporter, putative	1.90	3.7
Tb927.9.7950	hypothetical protein	1.90	3.7
Tb927.1.3720	hypothetical protein,	1.90	3.7
Tb927.8.5340	hypothetical protein	1.80	3.5
Tb927.2.1470	hypothetical protein conserved	1.80	3.5
Tb927.10.7170	hypothetical protein	1.80	3.5
Tb927.11.2400	hypothetical protein conserved	1.70	3.2
Tb927.10.8440	glucose transporter 1B	1.70	3.2
Tb927.11.9380	hypothetical protein	1.70	3.2
Tb11.v5.0307	*THT1* - hexose transporter, putative	1.70	3.2
Tb927.7.1960	retrotransposon hot spot protein 7 (RHS7),	1.70	3.2
Tb927.6.810	hypothetical protein	1.70	3.2
Tb927.4.3290	hypothetical protein conserved	1.70	3.2
Tb927.3.3430	hypothetical protein conserved	1.70	3.2
Tb927.11.14840	chromosomal passenger protein	1.60	3.0

Tb927.11.6550	*PUF* nine target 1	1.60	3.0
Tb927.9.4560	RBP32	1.60	3.0
Tb927.6.350	hypothetical protein conserved	1.60	3.0
Tb927.8.2280	hypothetical protein conserved	1.60	3.0
Tb927.1.2050	hypothetical protein,	1.60	3.0
Tb11.v5.0330	*THT1* - hexose transporter, putative	1.60	3.0
Tb927.7.2010	retrotransposon hot spot protein 7 (RHS7),	1.60	3.0
Tb927.10.10210	procyclin-associated gene 4 (*PAG*4) protein	1.60	3.0
Tb927.7.2020	retrotransposon hot spot protein 7 (*RHS*7),	1.60	3.0
Tb927.11.11990	hypothetical protein	1.60	3.0
Tb927.9.13160	hypothetical protein	1.60	3.0
Tb927.9.7860	hypothetical protein conserved	1.60	3.0
Tb927.9.4830	hypothetical protein	1.60	3.0
Tb927.6.210	leucine-rich repeat protein 1 (LRRP1),	1.60	3.0
Tb927.10.12820	hypothetical protein conserved	1.50	2.8
Tb927.7.610	mitochondrial DNA ligase homolog, *LIG k*-alpha	1.50	2.8
Tb927.11.11980	corset-associated protein 15	1.50	2.8
Tb927.3.5690	hypothetical protein conserved	1.50	2.8

I further compared the transcript levels of genes expressed within stumpy cells generated from AK and WTγ pleomorphic trypanosomes. Specifically, I examined whether differentiation to stumpy forms in an akinetoplastic background influences gene expression and whether any identified difference can be attributed to the absence of the kinetoplast. The same procedure of sorting significant genes with an adjusted p-value of <0.05 was used for this analysis. The data analysis revealed that 405 gene features were statistically significant, consisting of 234 genes with increased expression and 171 down-regulated genes in AK stumpy compared to WTγ stumpy. More stringent analysis revealed that 34 genes were differentially expressed (either upregulated or downregulated) with a fold change of 2 in AK stumpy samples (Table 3.6).

Table 3.6 List of expression transcripts in akinetoplasti (AK) stumpy cells .Genes were sorted by p value of < 0.05 and a fold change (FC) of 2 and above. The (+) are enrichment in AK stumpy whiles (-) indicates decreased expression. Stringent analysis revealed that 34 genes were differentially expressed (either upregulated or downregulated).

Symbol	Description	Log FC	FC
Tb927.11.500	RNA-binding protein, UBP1	+6.20	+73.5
Tb927.9.7950	hypothetical protein	+2.80	+7.0
Tb927.1.3770	hypothetical protein, unlikely	+1.70	+3.2
Tb927.8.200	UDP-Gal or UDP-GlcNAc-dependent	+1.60	+3.0
Tb927.9.11200	hypothetical protein	+1.60	+3.0
Tb927.9.3220	hypothetical protein	+1.50	+2.8
Tb927.10.8340	hypothetical protein	+1.40	+2.6
Tb927.2.5720	hypothetical protein	+1.40	+2.6
Tb927.11.17880	expression site-associated gene 9 (ESAG9)	+1.40	+2.6
Tb927.9.7340	expression site-associated gene 9 (ESAG9)	+1.20	+2.3
Tb927.1.910	hypothetical protein	+1.00	+2.0

Tb927.9.15980	nucleoside transporter	+1.00	+2.0
Tb927.10.6430	hypothetical protein	+1.00	+2.0
Tb927.11.14840	chromosomal passenger protein	-1.00	-2.0
Tb927.8.1640	MSP-B, putative	-1.00	-2.0
Tb927.8.1620	MSP-B, putative	-1.00	-2.0
Tb927.8.1630	MSP-B, putative	-1.00	-2.0
Tb927.11.3390	hypothetical protein	-1.00	-2.0
Tb927.9.7550	adenylosuccinate lyase, putative	-1.10	-2.1
Tb927.10.15060	hypothetical protein	-1.10	-2.1
Tb927.8.5340	hypothetical protein	-1.20	-2.3
Tb927.7.130	expression site-associated gene 3 (ESAG3)	-1.30	-2.5
Tb927.11.7820	endonuclease/exonuclease/phosphatase	-1.40	-2.6
Tb927.6.510	procyclic form specific polypeptide A-alpha	-1.40	-2.6
Tb927.6.480	procyclic form specific polypeptide A-beta	-1.50	-2.8
Tb927.9.4160	hypothetical protein	-1.60	-3.0
Tb927.9.4180	hypothetical protein	-1.70	-3.2
Tb927.9.15970	hypothetical protein	-1.70	-3.2
Tb927.6.520	procyclic form specific polypeptide A-beta	-1.70	-3.2
Tb927.8.480	phosphatidic acid phosphatase protein	-2.10	-4.3
Tb927.10.10250	EP2 procyclin	-2.20	-4.6
Tb927.9.16070	hypothetical protein	-3.60	-12.1
Tb927.3.290	expression site-associated gene 3 (ESAG3)	-4.40	-21.1
Tb927.5.5340	expression site-associated gene (ESAG3)	-5.30	-39.4

Genes that were highly expressed in AK stumpy relative to WTγ stumpy samples included a predicted RNA-binding protein, UBP1 (Tb927.11.500; 74-fold) which participates in RNA degradation and maintenance of the integrity and stability of RNA in *T. cruzi* (Cassola et al., 2015), and a UDP-GlcNAc dependent-protein (Tb927.8.200 3-fold increase). Another transcript which was enriched and was consistent with cells being quiescent was the expression site-associated gene 9 (*ESAG9*) (Tb927.9.7340; 2.3-fold). This observation is in agreement with data from a previous study indicating that the gene is upregulated in stumpy forms (Monk et al., 2013). A third of the remaining transcripts were hypothetical proteins. A summary of these transcripts is shown in the volcano plot (Figure 3.11).

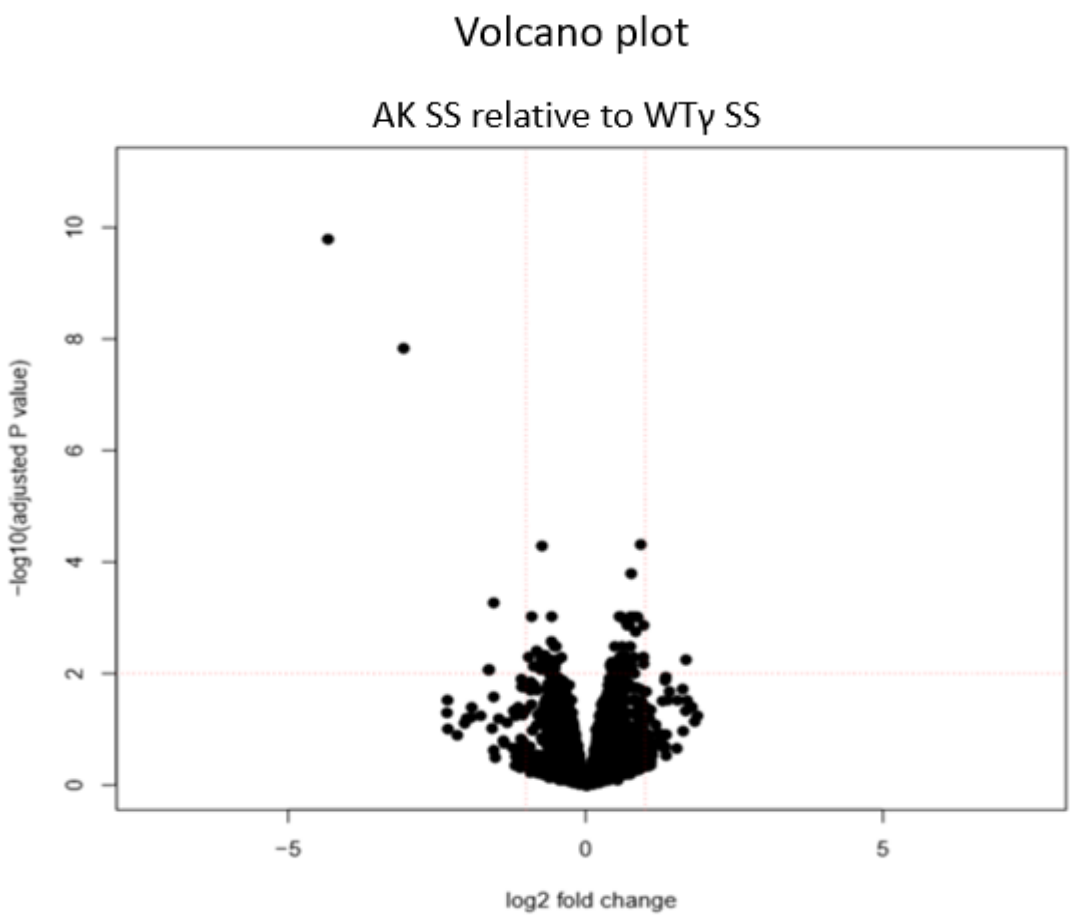

Figure 3.11 Volcano plot representing 405 genes that were either upregulated or downregulated in stumpy AK cells. Positive values signify upregulated genes while negative values represent downregulated genes in AK SS. The genes that grouped around zero were co-regulated. The Y-axis is the $\log_{10}$ adjusted p value while the axis denotes the $\log_2$ fold change. The vertical red dotted line is the 2 FC cut off for genes considered as significant with p value of <0.05 (Horizontal red line). The genes within the two vertical red dotted lines are coregulated and the ones that fall outside the lines are either upregulated for positive values or downregulated eg. ESAG3 genes with negative values.

Further analysis investigated if there were differences in transcript expression between AK stumpy in REF stumpy cells and WTγ stumpy cells. To achieve this objective, the abundance of AK stumpy transcripts was compared to the WTγ and REF stumpy datasets. One hundred and seventy-five unique genes were statistically differentially expressed in AK when compared to the reference cell line and 22 unique genes were found when compared to WTγ cells**.** However, comparing the common differences between two datasets revealed 13 genes to be regulated and shared among the two datasets Figure 3.12.

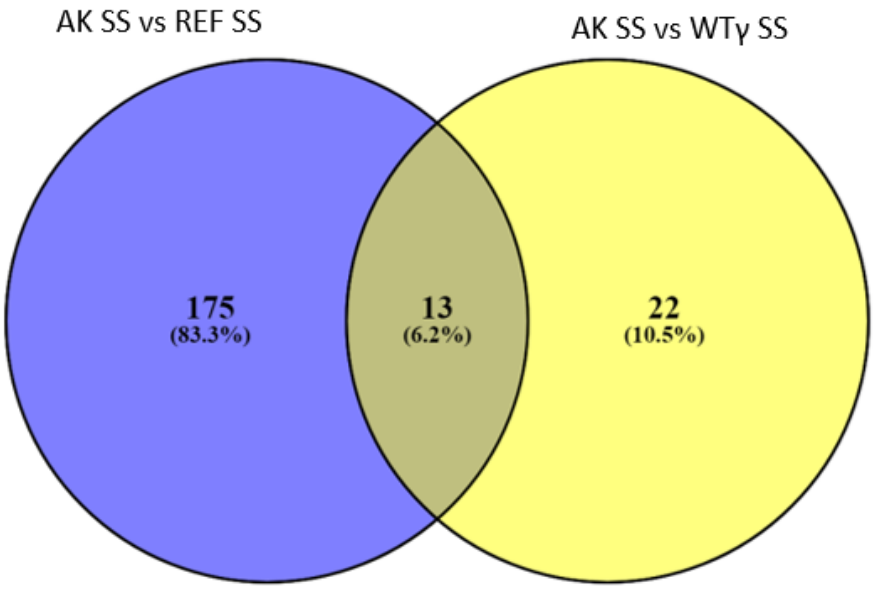

Figure 3.12 Venn diagram showing robust gene expression in stumpy cells. The number of genes expressed in AK SS and REF SS cells are shown in blue whereas those expressed in AK SS and in WTγ SS cells shown in yellow. The 13 genes that are common to both are shown in light brown. The unique genes for both datasets are indicated,22 genes represented AK stumpy in WTγ cell lines and 175 genes for AK stumpy in reference cells. The diagram was created as described (Cai et al., 2013).

The analysis from two independent biological replicates (REF and WTγ) showed genes that were uniquely expressed to each dataset. Examples from the 22 genes expressed only in the AK stumpy cells versus the WTγ stumpy cells were RNA-binding protein, *UBP1* (Tb927.11.500 74-fold increase), *ESAG9* (Tb927.11.17880, 2.6-fold increase), nucleoside transporter 1 (Tb927.9.15980, 2-fold increase) and hypothetical protein (Tb927.9.7950, 7-fold increase, Tb927.2.5720, 2.6-fold increase and Tb927.1.910, 2-fold increase).

Among the 13 genes were *UDP-Gal* or *UDP-GlcNAc*-dependent (Tb927.8.200), hypothetical proteins (Tb927.10.8340 and, Tb927.10.6430), *ESAG9* (Tb927.9.7340), which is expressed in stumpy cells (Monk et al., 2013), *GPEET2* procyclin precursor (Tb927.6.510) and *EP2* procyclin (Tb927.10.10250), which is upregulated in stumpy form (Matthews and Gull, 1998). These transcripts were more pronounced in REF stumpy cells compared to that of WTγ stumpy. This suggests that the WTγ cells were less stumpy than those used to produce the REF stumpy RNA samples and thus not expressing transcripts to the same level. However, the expression of *EP3*-2 procyclin (Tb927.6.520) was enriched in AK stumpy generated from WTγ cells. These transcripts are summarized in Table 3.7.

Table3.7 A list of genes with increased mRNA levels in stumpy cells of *T. brucei*. The list shows enrichment or downregulation of genes in AK stumpy cells compared to either WTγ or REF stumpy cells. The genes were sorted by p value of < 0.05 and a fold change (FC) of 2 and above.

		AK SS vs WTγ SS		AK SS vs REF SS	
Gene ID	**Description**	**logFC**	**FC**	**logFC**	**FC**
Tb927.1.3770	hypothetical protein, unlikely	1.70	3.2	2.20	4.6
Tb927.8.200	*UDP-Gal* or *UDP-GlcNAc*-dependent	1.60	3.0	1.60	3.0
Tb927.9.11200	hypothetical protein, unlikely	1.60	3.0	1.20	2.3
Tb927.9.3220	hypothetical protein, unlikely	1.50	2.8	1.90	3.7
Tb927.10.8340	hypothetical protein	1.40	2.6	2.10	4.3
Tb927.9.7340	expression site-associated gene 9 (*ESAG9*)	1.20	2.3	1.20	2.3
Tb927.10.6430	hypothetical protein	1.00	2.0	1.30	2.5

Tb927.9.7550	adenyl succinate lyase, putative	-1.10	-2.1	-1.40	-2.6	
Tb927.11.7820	endonuclease/exonuclease/phosphatase,	-1.40	-2.6	-1.70	-3.2	
Tb927.6.510	procyclic form specific polypeptide A	-1.40	-2.6	-1.60	-3.0	
Tb927.6.480	procyclic form specific polypeptide A	-1.50	-2.8	-1.50	-2.8	
Tb927.6.520	procyclic form specific polypeptide A	-1.70	-3.2	-1.50	-2.8	
Tb927.10.10250	EP2 procyclin	-2.20	-4.6	-2.30	-4.9	

There were likewise genes that were uniquely expressed in AK cells generated in a WT background. The number of regulated mRNAs that were found was higher than that found to be expressed in the WTγ cells. A total of 175 transcripts were differentially expressed between the AK stumpy and REF stumpy dataset. Among the differential expression transcripts were expression site-associated gene 3 (*ESAG3*) (Tb927.9.16260, 3-fold increase), hypothetical protein (Tb927.9.9930, 2.4-fold increase), SLACS reverse transcriptase (Tb927.9.14660, 2.2-fold increase) and two-thirds of the transcripts were hypothetical proteins. Surprisingly, *UBP1* was also upregulated in AK stumpy cells compared with WTγ cell, as well as being upregulated in AK slender when compared to WTγ slender. Studies has shown that UBP1 depletion in bloodstream form by RNAi was simultaneous with UBP2. Moreover, UBP1 was undetectable by Western blotting in several cell lines (Hartmann et al., 2007). One possible explanation of UBP1 in AK samples could be a retrograde response which generates upregulation of *UBP1* in both the AK slender and stumpy cell lines. However, the difference in *UBP1* expression was only detected in WTγ and not REF cells, suggestion that that the culturing and genetic manipulation of WTγ may have led to the loss of *UBP1* rather than a retrograde response caused by loss of the kinetoplast.

3.9 Validation of RNA-Seq data for differentially expressed genes

Data obtained from this study has shed light on the genes that are enriched in stumpy forms or commonly shared in *T. brucei* cells differentiating from slender to stumpy forms. Particularly intriguing is the presence of *UBP1* both significantly upregulated in AK slender (56-fold) and AK stumpy (74-fold) when compared with the same life stages in WTγ cell line.

The upregulation of this gene in both AK slender and AK stumpy cells was suggestive of retrograde signalling existing in *T. brucei* as this gene is expressed in the AK cells and not the WTγ cells. To confirm this, gene expression profile, complementary DNA (cDNA) was prepared from slender and stumpy RNA samples of AK and WTγ and quantitative reverse transcriptase PCR (qRT-PCR) performed (Section 2.10).

Figure 3.13 shows *UBP1* expression was pronounced in only the AK samples, contrasting with the low expression seen in WTγ cells. *GPI8* was used as constitutively expressed housekeeping gene to normalise the samples.

Qualitative investigation of *UBP1* revealed that its elevated expression in AK samples was consistent with the RNA-Seq data.

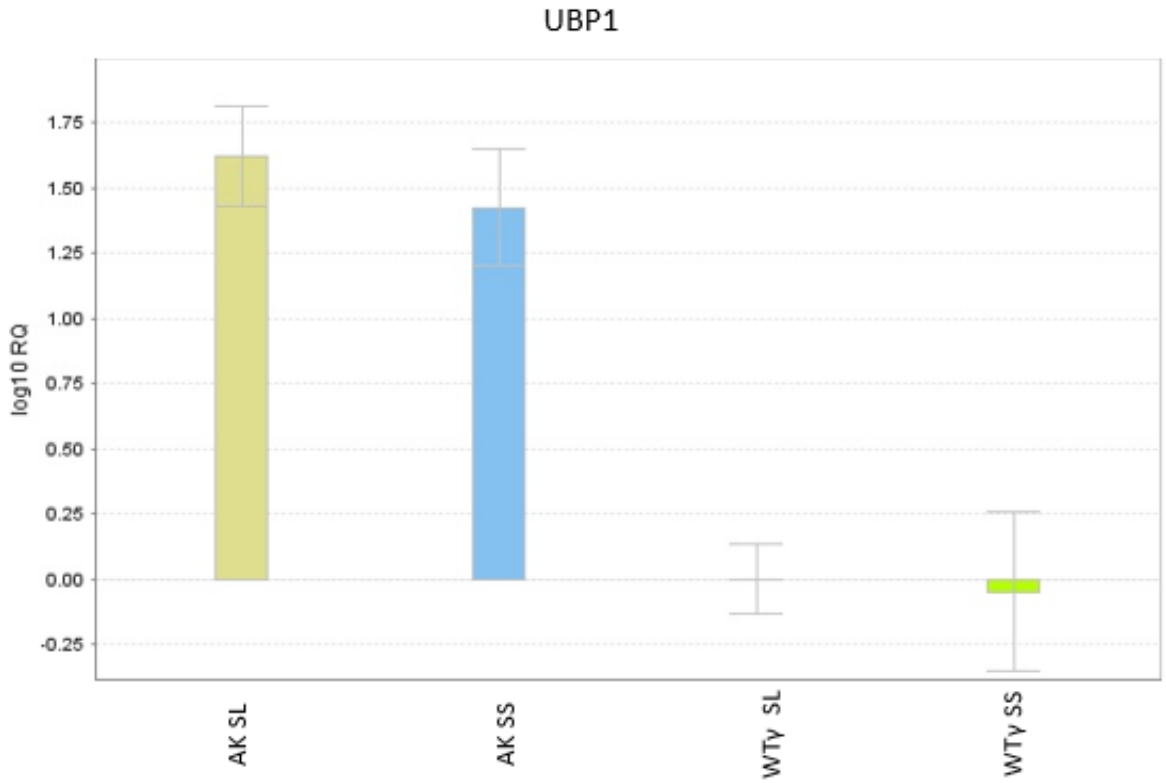

Figure 3.13 Gene expression analysis by qRT-PCR for AK and WTγ samples. The Expression of UBP1 was enriched in both AK slender and AK stumpy forms, shown in yellow and blue respectively. Both slender and stumpy forms of WTγ have no detectable UBP1 expression. The expression of UBP1 in the other cell lines was normalized using WTγ SL as reference sample. The Y axis represents the $\log_{10}$ relative quantification values reflecting the fold change and the X-axis is the individual samples investigated.

I further investigated this gene in monomorphic cell lines incapable of differentiating to stumpy and procyclic. The monomorphic cells used were previously listed in Table 2.1 of Chapter 2. In this analysis, the *UBP1* mRNA was still highly expressed in the AK cell line, but this was at level similar to that seen in the monomorphic cell lines (Figure 3.14). Next, the mutated and acriflavine treated monomorphic cell lines were used to test if *UBP1* was highly expressed in them as seen in pleomorphic AK cells.

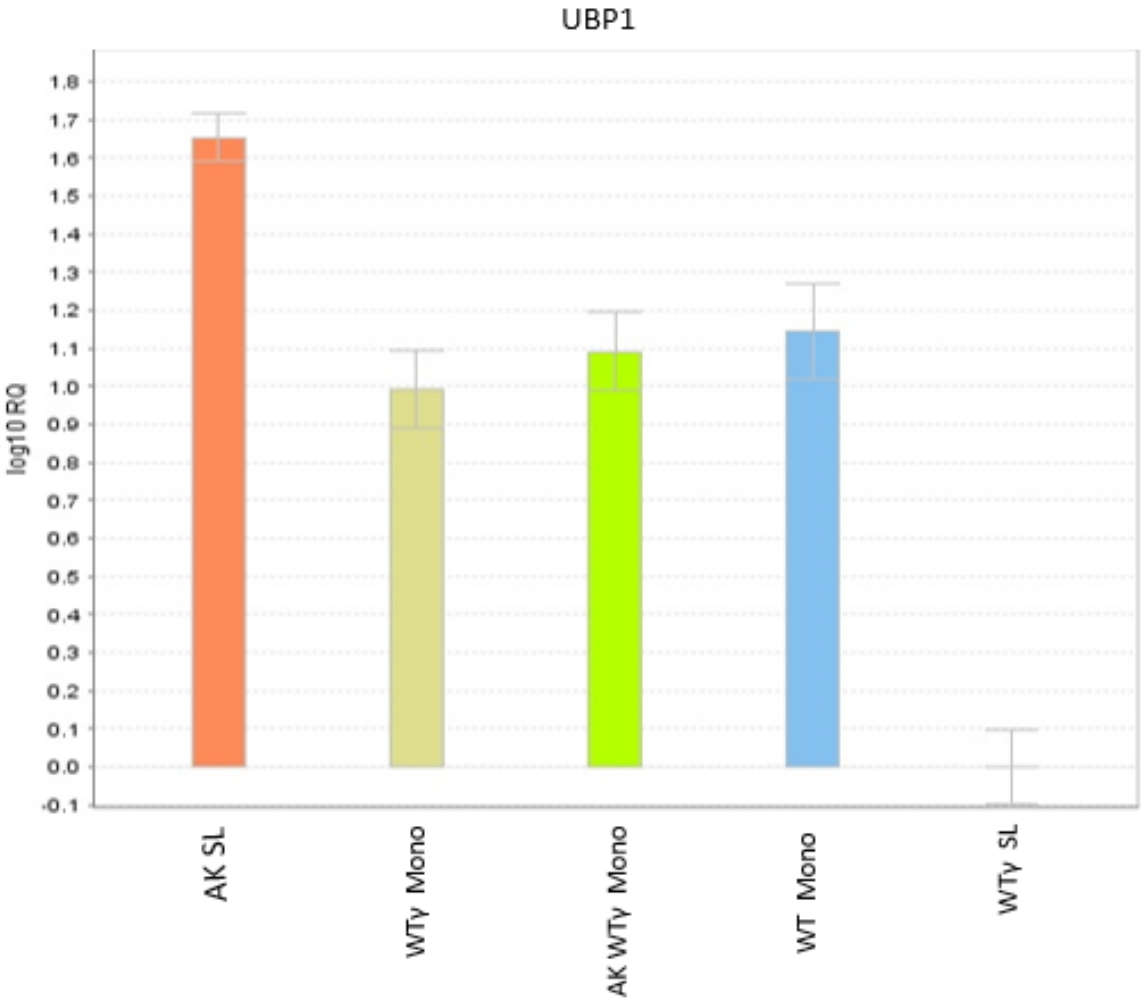

Figure 3.14 Comparison of UBP1 expression in pleomorphic and monomorphic AK and WTγ cell lines. UBP1 was highly expressed in pleomorphic AK SL with no significant change between monomorphic AK and WTγ cells. Expression levels of UBP1 in the other cell lines were normalized using WTγ SL as reference sample The Y axis represents the $\log_{10}$ relative quantification values reflecting the fold change and the X-axis is the individual samples investigated.

In *T. brucei*, there are approximately 70 different proteins having at least one RNA Recognition Motif (RRM) of which some are essential for normal growth in at least one life-cycle stage (Alsford et al., 2011; Wurst et al., 2009). *UBP1* and *UBP2*, are known to be similar proteins with a single RRM domain (Hartmann et al., 2007) and both are recognised by the same antibody, generated against the *T. cruzi* protein but also able to recognise *T. brucei* UBP1 and UBP2 (Hartmann et al., 2007). It was important therefore to determine if the elevate UBP1 signal observed was caused by UBP1, UBP2 or both genes.

Firstly, I did a BLAST search to align both *UBP1* and *UBP2* from *T. brucei* to identify conserved regions, allowing the design of primers outside to specifically target *UBP2.* Primers specific for *UBP2* were designed within the red regions for specificity (Figure 3.15). Using these primers revealed that the *UBP2* signal generated by qRT-PCR did not correspond to the *UBP1* data. Instead, analysis of the expression profile of UBP2 transcripts revealed there was low level expression of the gene across all the cell lines, including AK slender cells which expressed high levels of *UBP1* when compared to the WTγ slender cells (Figure 3.16).

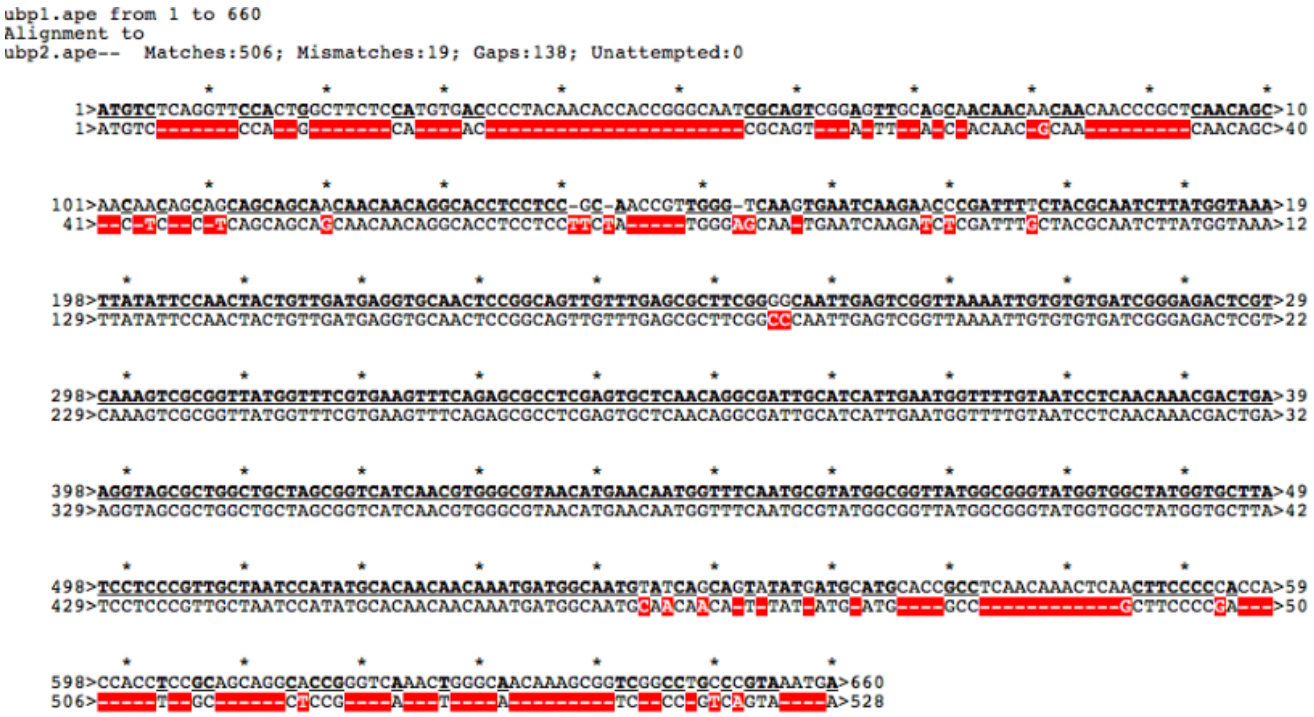

Figure 3.15 A BLAST result of aligned UBP1 and UBP2 coding sequence. The conserved region for both UBP1 and 2 are shown in black whereas the red highlighted region is unique to UBP2.

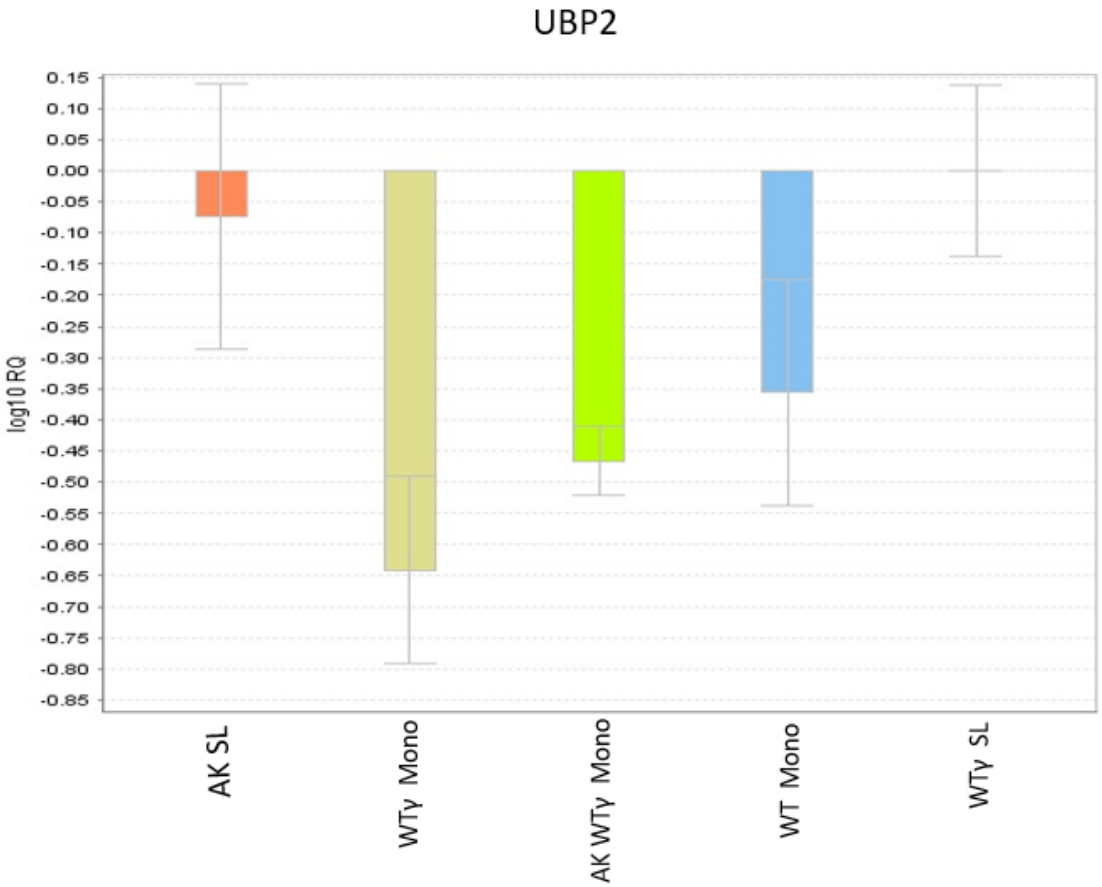

Figure 3.16 UBP2 expression in pleomorphic and monomorphic AK and WT cell lines. The UBP2 expression was downregulated in both pleomorphic and monomorphic cell lines regardless of the presence of the kinetoplast. The Y axis represents the $\log_{10}$ relative quantification values and the X-axis is the individual samples investigated. The expression levels of UBP2 in the other cell lines were normalized using WTγ SL as reference sample.

After getting these results, I performed a similar analysis to probe for *UBP1* expression levels using the parental cell lines from which the AK clone was generated, to test if the *UBP1* levels were similar there. The cell lines used were the parental pleomorphic cell line *T. brucei* EATRO 1125 AnTat 1.1 90:13 (REF), the isogenic control line (WT/WTγ) (WTγ), the same parental cell line with the L262P mutation with intact KDNA (WT/L262Pγ kDNA^{+}) or devoid of kinetoplast (WT/L262Pγ (kDNA^{0}). The results revealed *UBP1* to be downregulated in all the parental cell lines with or without kDNA (Figure 3.17).

The upregulation of *UBP1* was in AK slender and AK stumpy in WTγ cells but not in the REF slender or stumpy samples (Figure 3.13). This suggested that UBP1 is at unusually low level in WTγ cell lines comparted to all other lines tested, including the AK cells, and thus the high expression of UBP1 in AK cells was not due to retrograde signalling. The loss of UBP1 expression may have resulted from passaging processes and other manipulations of the WTγ line.

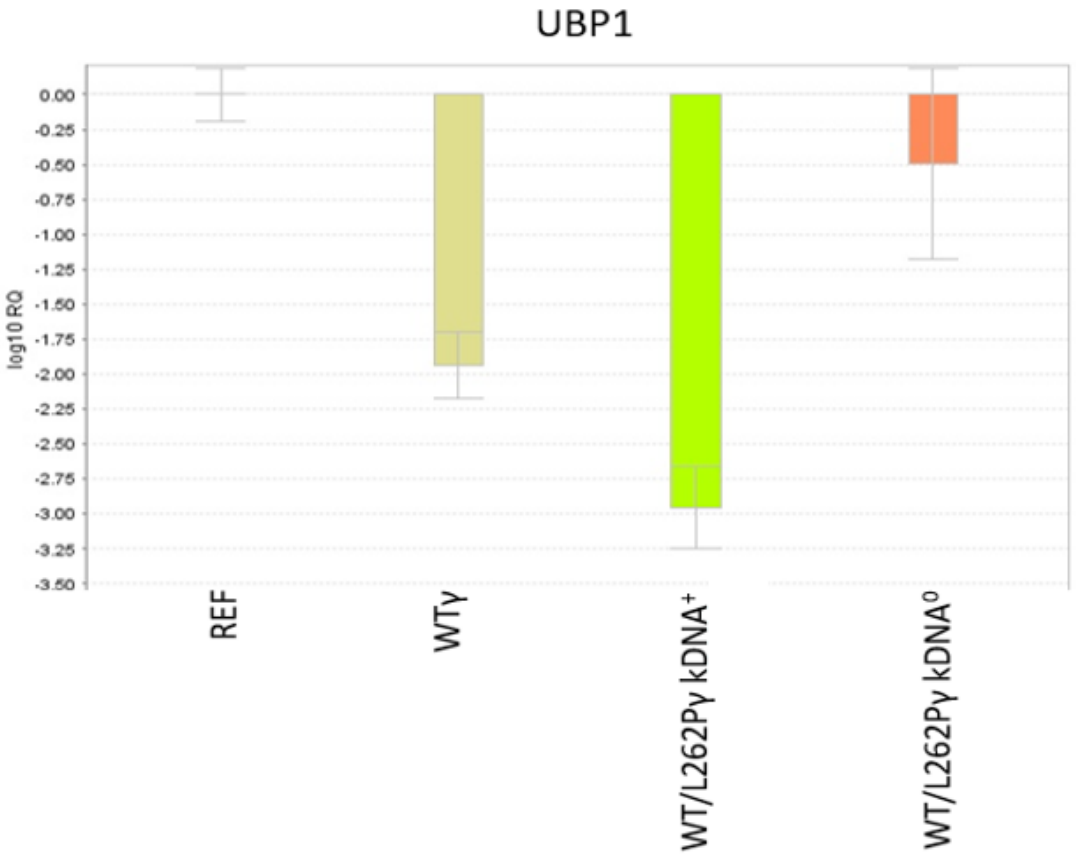

Figure 3.17 qRT-PCR result for UBP1 expression in bloodstream form pleomorphic *T. brucei* EATRO 1125 cell lines. The expression of UBP1 was downregulated across all cells. The Y- axis represents the $\log_{10}$ relative quantification values and the X-axis is the individual samples investigated. Expression levels of UBP1 in all cell lines were normalized using REF as reference sample.

3.10 *UBP1* protein expression in *T. brucei*

To analyse the expression of *TbUBP1* protein, I performed a western blot and probed the membrane with a *TcUBP1* polyclonal antibody. This antibody was raised against recombinant *TcUBP1* as an immunogen (D'Orso and Frasch, 2001). The use of the *T. cruzi* antibody is possible against *T. brucei* extracts, because the UBP1 and 2 sequences are well conserved between the species. The samples analysed were AK slender and AK stumpy cells, WTγ slender and WTγ stumpy cells, and samples from two parental cell lines—*T. brucei* EATRO 1125 (AnTat1.1 90:13) (REF1), and *T. brucei* EATRO 1125 (AnTat1.1) (REF2). EATRO 1125.

As controls for antibody specificity, samples from *TbUBP*1/2 RNAi bloodstream and procyclic cell lines were used, since RNAi induction in these cell lines would result in decreased expression of both proteins in procyclic forms of the parasite and an absence of *UBP1* in bloodstream form (Hartmann et al., 2007). The cell lysates were denatured using SDS-gel electrophoresis and blotted (see Section 2.12), prior to detection using polyclonal antiserum to *TcUBP1*. The result is shown in Figure 3.18, with the predicted molecular weights of *TbUBP2* to be 19.5 kDa and that of *TbUBP*1 to be 24.3 kDa. As expected, the antibody recognized both *UBP1* and *UBP2,* generating a corresponding double band for both. In addition to the expected bands are non-specific bands that run at 50 kDa UBP2 was expressed in the AK slender, AK stumpy as well as WTγ slender and stumpy but not *UBP1* (Figure 3.18, upper blot). The two pleomorphic *T. brucei* EATRO 1125 however showed both *UBP1* and *UBP2* expression. As expected, the RNAi bloodstream samples showed reduced expression of the protein upon induction. The procyclic protein samples neither showed reduction upon the induction of RNAi. These findings support to the data obtained by Hartmann et al. (2007) where they showed an absence of *UBP1* in bloodstream form cell lines even though they express *UBP2,* except for *T. brucei* EATRO 1125 AnTat 1.1 and *T. brucei* 247 strains which expressed both *UBP1* and *UBP2.*

In contrast, procyclic *T. brucei* EATRO 1125 AnTat1.1, *T. brucei* 247, *T. brucei* TREU927/4 and *T. brucei* 427 strains all expressed both *UBP1* and *UBP2.* (Hartmann et al., 2007). The expression of *UBP2* was much more pronounced in both AK slender and WTγ slender than their stumpy counterparts. The data suggests that *UBP1* proteins are not expressed in bloodstream form *T. brucei*.

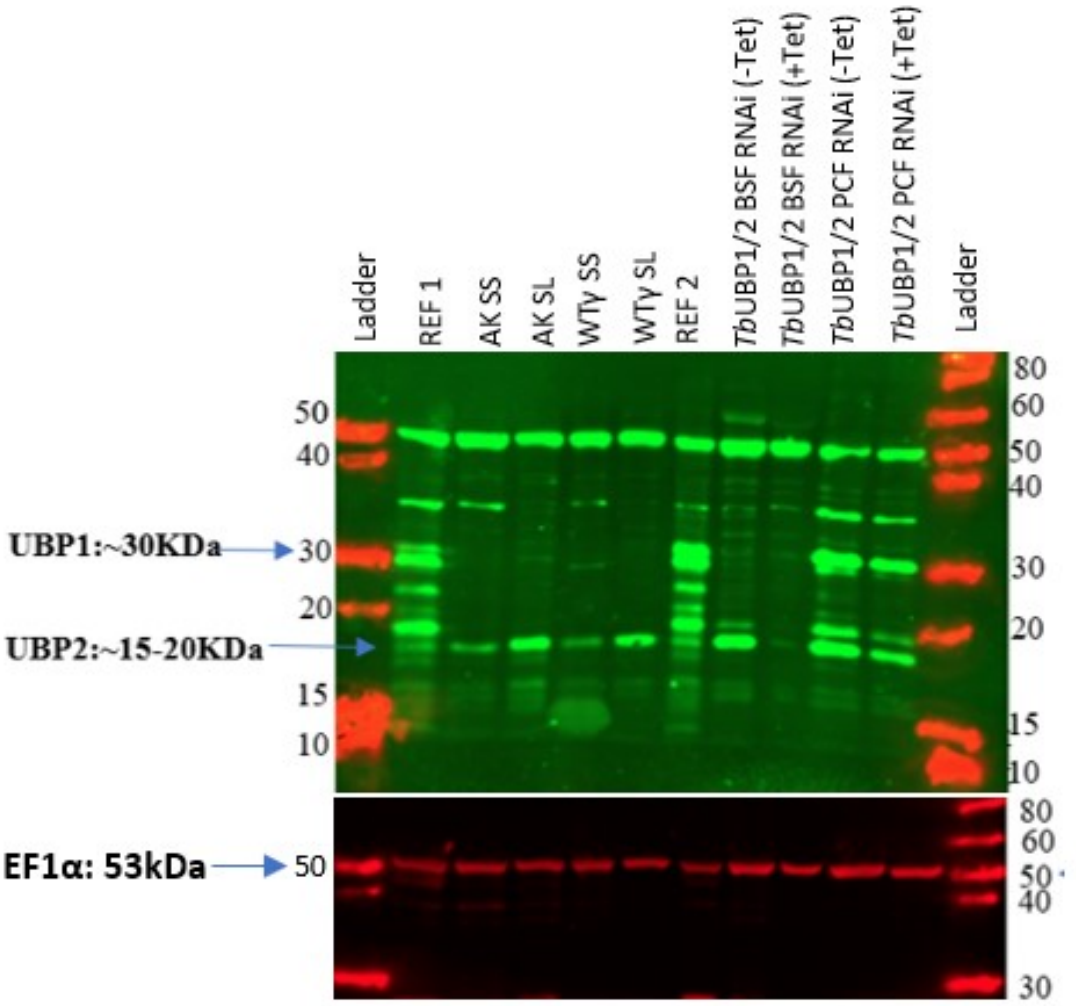

Figure 3.18 TbUBP1/2 protein expression in *T. brucei.* Western blot using extracts of different trypanosome strains and the anti-*TcUBP1* antibody. Upper gel detects *UBP1* and 2 in 2 x 10^6 cells/ml for each named cell line. Images were developed with Odyssey CLx imaging system. The positions of molecular mass markers are indicated with expected sizes for *UBP1* (30 kDA) and *UBP2* (~20 kDa) in the upper blot and EF1 (53 kDa) shown in the lower blot. The lower gel shows *EF1*, used as a loading control.

3.10.1 Validation of differential gene expression in akinetoplastic cell lines by qRT-PCR

As documented earlier, the elevated transcript level of *UBP1* in AK slender and AK stumpy cells was suggestive of retrograde signalling occurring in *T. brucei.* However, hypothesis was found to be incorrect, with instead *UBP1* being lost in WTγ cells and not because of the absence of kinetoplast causing upregulation of this transcript as a compensatory response. Beyond *UBP1*, however, akinetoplastic cells have shown the upregulation of certain other transcripts that were statistically significantly more expressed in both AK slender and AK stumpy forms in comparison to WTγ slender and WTγ stumpy cells. Among these genes were *PNT1*, a cysteine peptidase (Tb927.11.6550 1.7-fold increase in AK slender important for kDNA maintenance (Grewal et al., 2016). *PNT1* is regulated during the cell cycle where it mostly peaks at S-phase (Archer et al., 2009). Studies have shown over-expression of *PNT1* to be associated with kinetoplast-related defects, such as the presence of mislocated kinetoplasts (Archer et al., 2009). Since this gene is known for kinetoplast maintenance, its potential upregulation in akinetoplastic cells compared to WTγ was of interest to pursue. For example, the absence of kDNA in the akinetoplastic cells could possibly convey the loss of kDNA information from the mitochondrion to the nucleus to elicit the upregulation of this gene to compensate for the loss. In addition to *PNT1*, two hypothetical proteins (Tb927.10.8340, 2.6 -fold increase and Tb927.10.6430, 2-fold increase) also showed differences in expression between AK stumpy and WTγ stumpy. These hypothetical proteins, unfortunately, have no data on their cellular localisation, structural analysis and functional prediction. Nonetheless, I analysed these transcripts by qRT-PCR to experimentally confirm the expression profile of these three genes. The results obtained by qRT-PCR reproduced the higher expression of *PNT1* in AK slender as compared to WTγ slender as seen by RNA-Seq (Figure 3.19).

Thus, the expression in AK slender was higher than in WTγ slender with p value of 0.016 (*) even though the difference was not as pronounced as found by the RNA-Seq data. In contrast, the expression in AK slender relative to AK stumpy gave a p value of <0.0001 (****),

whereas the expression of WTγ slender cells versus WTγ stumpy cells showed downregulation of *PNT1* in stumpy forms with p value <0.0001 (****), this being consistent with the RNA-Seq data.

I further analysed the expression of *PNT1* at the protein level, using slender and stumpy samples as well as two *PNT1* RNAi knock down samples. As expected, the RNAi samples showed reduced expression of the protein upon induction but there was little or no difference between slender and stumpy cells despite the differences seen at the RNA level earlier. The expression of *PNT1* at the protein level also varied across different cell lines (Figure 3.20).

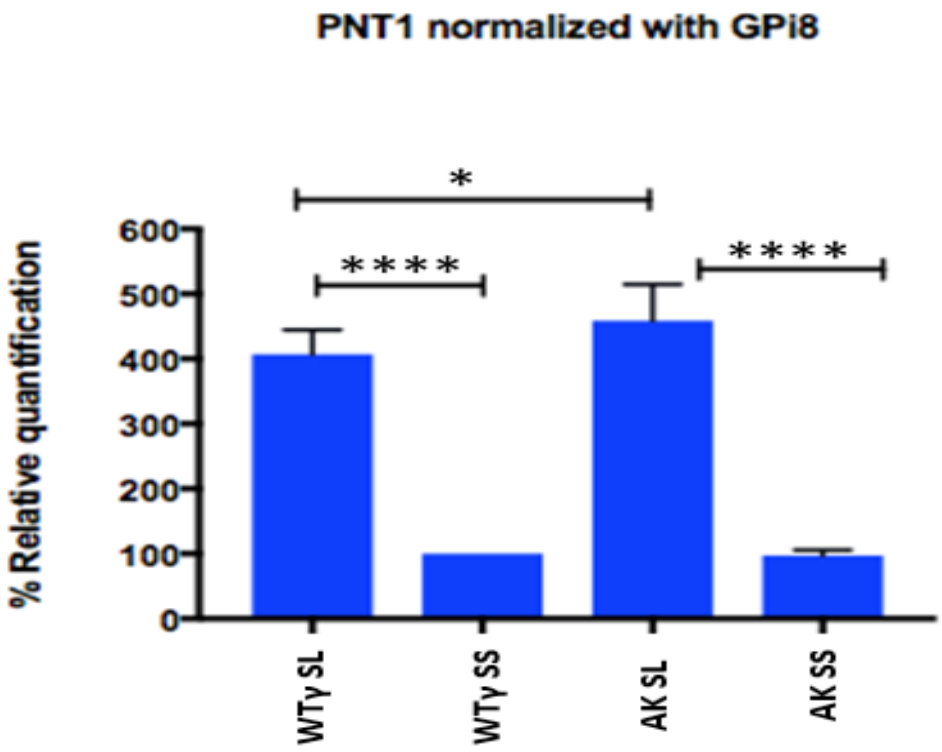

Figure 3.19. Detection of *PNT1* in slender and stumpy *T. brucei* by qRT-PCR assay. The expression of PNT1 is lower in SS forms with respect to SL forms. The Y axis represents the % relative quantification values and the X-axis is the individual samples investigated. Asterisks indicate level of statistical significance between the compared cells. The expression levels of *PNT1* was first normalised with *GPI8* and then all samples normalized using WTγ SS as reference sample.

I further analysed the expression of PNT1 at the protein level, using slender and stumpy samples as well as two PNT1 RNAi knock down samples. As expected, the RNAi samples showed reduced expression of the protein upon induction but there was little or no difference between slender and stumpy cells despite the differences seen at the RNA level earlier. The expression of PNT1 at the protein level also varied across different cell lines (Figure 3.20).

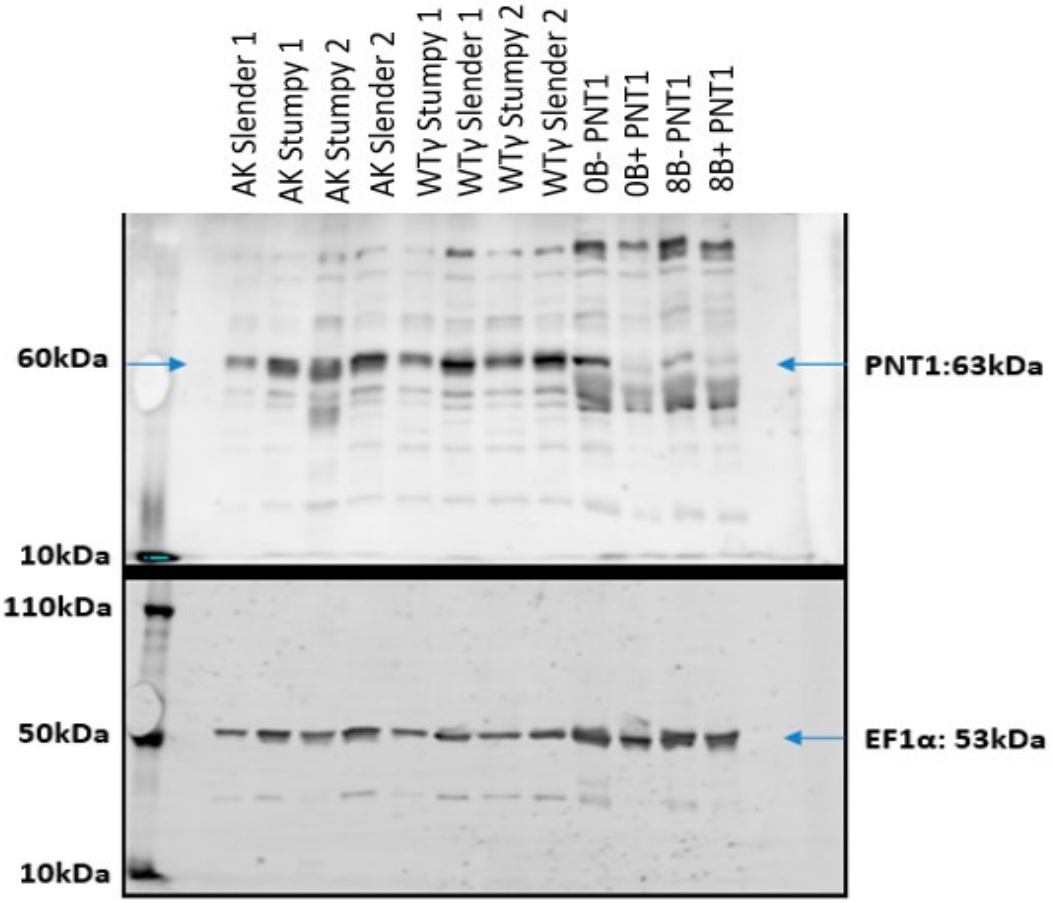

Figure 3.20 Western blot of *PNT1* expresison. The position of the *PNT1* bands corresponds to 60kDa for each sample. Lanes were loaded with $2x10^6$ cells/ml for each SL or SS cells for the first eight wells and the last 4 wells to the right are the RNAi control samples. The Upper panel was probed with *PNT1* and same blot was used for an EF1 loading control (lower panel).

3.10.2 Validation of hypothetical proteins (Tb927.10.6430 and Tb927.10.8340)

Strongly regulated genes in AK stumpy relative to WTγ stumpy included hypothetical proteins Tb 927.10.6430 and Tb927.10.8340. A BLAST search gave no useful information on these genes, and no orthologs are reported for these genes. Also, there was not any information on any interPro domains, cellular location, functional prediction nor proteomic profile. Nonetheless, I performed qRT-PCR on these uncharacterised transcripts to determine the validity of the RNA-Seq data. My results showed that cDNAs generated by RT-PCR reproduced the highly expressed transcripts revealed in the RNA-Seq data (Figure 3.21 and Figure 3.22).

Thus, the expression of Tb927.10.8340 in AK stumpy relative to WTγ stumpy was-2-fold upregulated with p value of < 0.006 (**). In contrast, the gene was 7.3-fold decreased in AK slender when compared to AK stumpy with p value of <0.0001 (****). Similarly, this gene in WTγ slender was 6-fold decreased in comparison with WTγ slender with p value of <0.0001 (****). There was no significant difference in Tb927.10.8340 expression between the AK slender and WTγ slender which gave p value of 0.479 as shown in Figure 3.21.

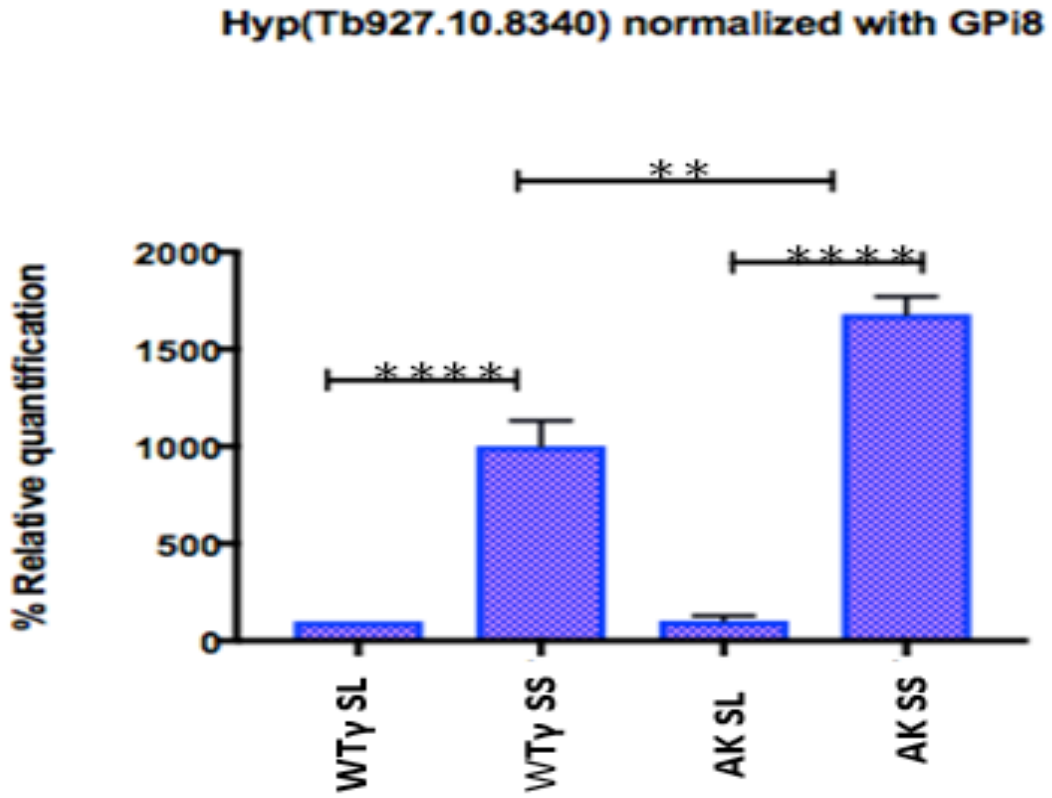

Figure 3.21 Experimental validation of the transcripts for uncharacterised hypothetical proteins in *T. brucei*. Relative quantification expressed in percentage on the Y-axis for Tb927.10.8340. The asterisk reflects the magnitude of significant difference between each paired comparison. The expression was downregulated in SL forms compared to SS forms. The Y axis represents the percentage relative quantification values and the X-axis is the samples investigated. The expression levels of the hypothetical gene were first normalised with *GPI8* and then all samples normalised using WTγ SL as reference sample.

The hypothetical gene Tb927.10.6430 expression was upregulated in AK stumpy compared to WTγ stumpy by 2.6- fold with p value of 0.042 (*). By comparison with AK slender, the transcript was 6.9-fold decreased in AK slender forms relative to AK stumpy with p value of <0.0001 (****).

WTγ slender levels of Tb927.10.6430 were 5.7-fold downregulated when compared to WTγ stumpy with p value of <0.0001 (****). There was no significant difference in the expression of Tb927.10.6430 in both AK slender and WTγ slender with p value of 0.117 (Figure 3.22).

The intriguing observation of the three genes mentioned earlier to be upregulated in AK slender and stumpy relative to WTγ cells is suggestive of retrograde response influencing gene expression and other cellular activities in the absence of mitochondrion.

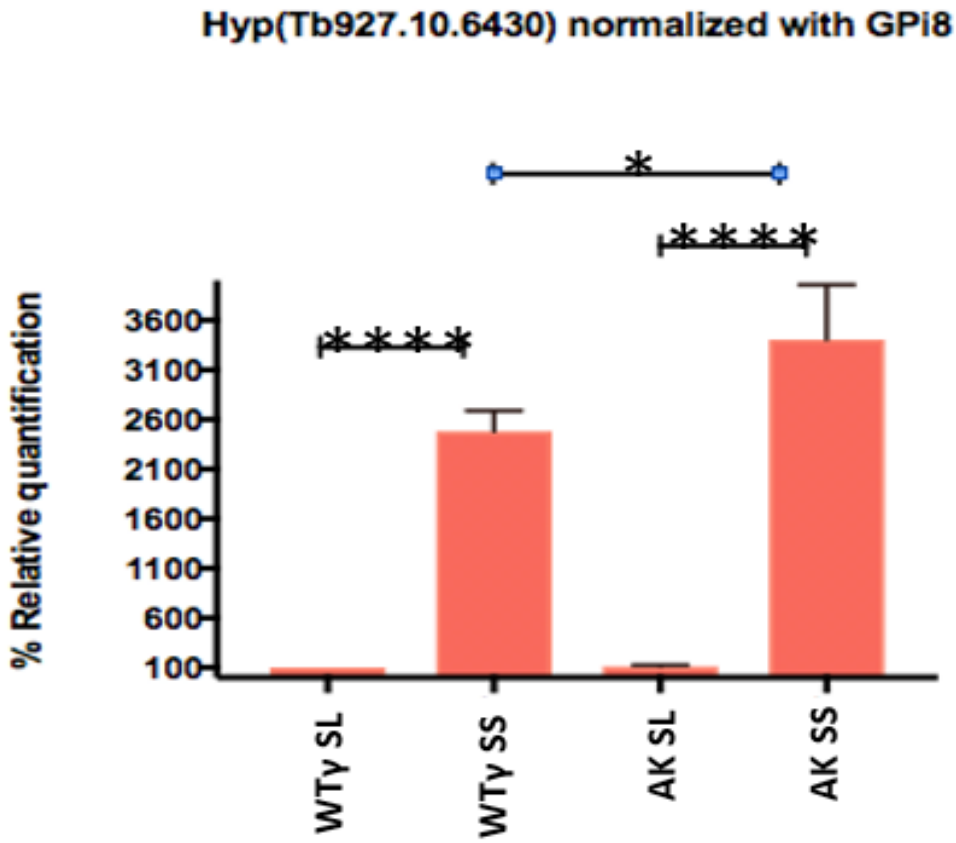

Figure 3.22 Estimation of Tb927.10.6430 mRNA abundance by qRT-PCR. AK SS shows increased expression of the transcript relative to WTγ SS and decreased levels of the transcript in SL cells. The relative abundance of transcript expressed as a percentage is plotted on the Y axis and X-axis shows the SL and SS cells investigated. The expression levels of the hypothetical gene were first normalised with *GPI8* and then all samples normalised using WTγ SL as reference sample.

3.11 Discussion

3.11.1 Nuclear gene expression is not affected by absence of kinetoplast in *T. brucei* stumpy forms

Differentiation of African trypanosomes involves developmental regulation of mitochondrial activity which requires regulation of the nuclear genome and the kinetoplast. Thus, the mechanisms that control the nuclear and mitochondrial genomes are vital to understanding the control of metabolic development. Successful progression through the life cycle stages of *T. brucei* involves modulation of gene expression, as well as immunological, metabolic and morphological changes (discussed in Section 1.2.6). As previously reported, the developmental regulation of mitochondrial activity requires coordination between the nucleus and kinetoplast (Schneider, 2001). Hence this study used the nuclearly encoded subunit of cytochrome oxidase *COX VI*, which has been extensively studied (Matthews and Gull, 1998), to investigate whether absence of the kinetoplast influences the regulation of nuclear gene expression. Data obtained from this study showed that the absence of kinetoplast did not influence nuclear expression of *COX VI* mRNA.

Although similar studies have examined the regulation of nuclear and mitochondrial components of the cytochrome oxidase complex during differentiation between bloodstream form and procyclic form, they were unable to establish clonal lines of dyskinetoplastid bloodstream form either by acriflavine treatment or RNA interference ablation of mitochondrial topoisomerase II. However, an akinetoplastic cell line used to investigate communication between the nucleus and kinetoplast during differentiation between slender and stumpy showed that transition to stumpy forms was independent of the presence of the mitochondrial genome (Dewar et al., 2018). Indeed, PAD1 staining (Dean et al., 2009) and the increased expression of the *ESAG9* differentiation marker (Monk et al., 2013), in akinetoplastic cell lines, confirmed this observation in the present study.

However, the akinetoplastic stumpy cells described by Dewar et al., (2018) lacked membrane potential and had a reduced lifespan *in vitro* and *in vivo.* These cells showed delayed peak in parasitaemia with rapid decline in parasitaemia after reaching peak density.

The authors showed that akinetoplastic stumpy cells died quicker than WT stumpy cells with intact kinetoplast (Dewar et al., 2018). Stumpy forms can utilise both glucose and α-ketoglutarate as carbon sources for mitochondrial substrate phosphorylation *in vitro* (Bienen et al., 1993)**.**

As reported previously (Timms et al., 2002), *COX VI* mRNA depletion had no effect on morphological development to stumpy forms, indicating no requirement for an intact cytochrome oxidase complex during early differentiation events. Moreover, analysis of the relative transcript levels of the kinetoplast-encoded components of the *COX* complex demonstrated that these were independent of the level of nuclear encoded *COX VI* (Timms et al., 2002). In the present study, the expression profile of *COX VI* in slender, stumpy and procyclic forms confirmed that stumpy and procyclic forms express higher amount of *COX VI* mRNA relative to slender cells. This observation corroborates a study which showed that the abundance of *COX VI* mRNA is stage-regulated and more abundant in procyclic (Tasker et al., 2001). Coordination between the nucleus and mitochondrial genome has been studied in organisms such as yeast, mammals and plants (Kleine and Leister, 2016).

However, yeast cells with defects in the mitochondrial genome (rho mutants) showed altered transcription of class I and II RNA of nuclear genes because these strains had lost the ability to carry out mitochondrial protein synthesis, and thus lacked most of the mitochondrial transcripts found in respiratory competent cells (Parikh et al., 1987). The class I transcription has been shown to be conserved in *T. brucei,* which utilizes RNA pol I for both rRNA synthesis and transcription of the major surface antigens, procyclin and VSG (Schimanski et al., 2004). Likewise, the mitochondrial unfolded protein response (UPR^{mt}), conveys information on the functional status of the mitochondrion to the nucleus, thereby modulating expression of nuclear genes (Kleine and Leister, 2016; Knorre et al., 2016; Qureshi et al., 2017). The unfolded protein response (UPR) is induced when the quality control machinery of the cell is overloaded with unfolded proteins. The mitochondrial ABC transporter HAF-1 modulates the nuclear accumulation transcription factor ATFS-1, a key regulator of the UPR^{mt}. ATFS is a basic-leucine zipper (bZip) transcription factor, which translocates to the mitochondrion and is degraded by mitochondrial protease in the absence

of oxidative stress (Nargund et al., 2012). Under physiological conditions, ATFS-1 localises in the mitochondrion for degradation by proteases. However, in the presence of mitochondrial dysfunction, ATFS-1 accumulates in the nucleus to restore mitochondrial function by the induction of mitochondrial proteases and ROS detoxifying genes as well as metabolic regulators to compensate for the defect (Nargund et al., 2012). Trypanosomes lack conventional transcription regulation, and thus, lack most of the UPR machinery present in other eukaryotes (Michaeli, 2015).

In summary, this study was unable to establish that the absence of mitochondrial genome elicits response from nucleus to compensate for the defect, as reported in yeast.

3.11.2 Effect of differentiation on abundance of transcripts.

Regulation of gene expression throughout the cell cycle has been addressed in several organisms like bacteria, budding yeast, mouse, trypanosomes and human cells (Chávez et al., 2017), both at the level of individual genes as well as in a genome-wide manner. Many of the regulated mRNAs described so far have known functions, and/or had previously shown preferential expression in either slender, stumpy or procyclic forms. Thus, this study also compared global changes in the transcriptomes of WTγ and AK *T. brucei* during differentiation from slender to stumpy. The goal was to have a comprehensive view of the potential effects of mitochondrial dysfunction on nuclear gene expression in these parasites. Expression of known stage-regulated genes were detected during analysis of the data obtained from the present study, thereby validating of the dataset. A novelty, however, was the downregulation of some hypothetical proteins in WTγ, which were much less expressed in AK cells compared to WTγ. RNA-Seq was performed on biological replicates of slender and stumpy samples from akinetoplastic and wild type cells.

This is the first datasets for akinetoplastic slender and stumpy bloodstream forms compared to wild type slender and stumpy forms. The UDP-Gal is annotated as pseudogene on TriTrypDB and mentioned to have a UDP-glycosyltransferase activity. This gene is a cell surface protein. The phylogeny of UDP-dependent glycosyltransferases (UGTs) confirms that

they represent a considerable parasite-specific innovation, which has differentiated independently in the distinct trypanosomatid lineages (Silva Pereira and Jackson, 2018). Thus, future work is recommended to investigate the upregulation of this gene in AK stumpy cells. The hypothetical proteins enriched in stumpy AK cells have no available data on their cellular localisation, structure and functional prediction.

This study suggests that the absence of the mitochondrial genome has an unexpectedly less dramatic effect on the levels of nuclearly-encoded mRNA in bloodstream forms (slender and stumpy) of *T. brucei*. It can be postulated that the difference in gene expression is due to stress response.

In addition to these comparisons, I examined slender AK cells differentiating to stumpy forms, to identify common or enriched genes between slender and stumpy forms in the AK cells. Genes identified were mostly annotated as 'pseudogene', or 'hypothetical unlikely'. Among these were transcripts encoding glycolytic enzymes and the *THT1* hexose transporter (Tb11.v5.0307, 5.3-fold increase). The *THT1*-encoded transport system for glucose is life-cycle stage dependent with bloodstream expressing 40-fold more *THT1* than *THT2* which is detectable in procyclic (Bringaud and Baltz, 1993). Other differentially expressed genes included DNA ligase *LIG k* alpha (Tb927.7.610, 9.2-fold increase) and *PNT1* (Tb927.11.6550 5.7-fold), a cysteine peptidase required for kDNA maintenance (Grewal et al., 2016), which was more highly expressed in AK slender forms than in WTγ slender. Studies that have depleted *PNT1* by RNAi in the bloodstream form *T. brucei* have shown this gene to be essential both *in vitro* culture and *in vivo,* with the induced cells being enriched for accumulated cells without a kinetoplast, confirming the role of *PNT1* in kDNA maintenance. (Grewal et al., 2016).

To focus on identification of differences in gene expression in cells differentiating from slender to stumpy, the genes implicated in glycolytic process have also been reported in different species of trypanosomes. In *T. cruzi*, histones have been reported to be enriched in blood form (Chávez et al., 2017). Likewise, ESAG3 and enzymes involves in glycolysis such as glyceraldehyde 3 phosphate have been reported to be enriched in blood form of *T. theleri* (Kelly et al., 2017). Proteomic analysis of *T. vivax* showed upregulation of beta tubulin,

histones, fructose bisphosphate, aldolase and glyceraldehyde 3 phosphate in bloodstream form relative to epimastigote and metacyclic stages. The upregulation of similar scripts has been reported in the RNA-Seq dataset.

Further to the transcripts expressed in slender and stumpy cells, the study also compared transcript levels of genes expressed in the stumpy forms generated from different genetic backgrounds. As expected, Tb*PIP39*, dihydrolipoyl dehydrogenase and *EP1* procyclin were detected, thereby confirming differentiation of the stumpy forms of the AK cell line. Surprisingly, *UBP1* was also upregulated in AK stumpy cells compared with WTγ cell, as well as being upregulated in AK slender when compared to WTγ slender. A possible explanation for the difference in UBP1 expression detected in WTγ and not REF cells, may be due to culturing and genetic manipulation of WTγ, rather than a retrograde response caused by loss of the kinetoplast.

Undoubtedly, the data obtained in this Chapter has provided insights on the possible occurrence of a retrograde response, even though the transcriptomic studies suggest that the absence of the mitochondrial genome has a limited effect on the levels of nuclearly encoded mRNAs in bloodstream form of *T. brucei*.

3.11.3 qRT-PCR validation of differentially expressed genes corroborated transcript profile

After validating the observed dynamic mRNA changes during differentiation from slender to stumpy forms, transcripts that were enriched in akinetoplastic cells were validated by qRT-PCR. The genes validated were *PNT1* and two hypothetical proteins (Tb927.10.8340 and Tb927.10.6430) which showed differences in expression between AK stumpy and WTγ stumpy. The results obtained by qRT-PCR reproduced the higher expression of *PNT1* in AK slender as compared to WTγ slender as seen by RNA-Seq (Figure 3.19.) Consistent with observation, the two hypothetical proteins were highly expressed in AK stumpy cell relative to WTγ stumpy form (Figure 3.21 and Figure 3.22). All together, these data support the hypothesis that the absence of kinetoplast influence gene expression.

3.12 Outlook

In this chapter, data obtained from this study demonstrated that the absence of kinetoplast had minimal effect on gene expression. Even though enriched transcripts were obtained for stumpy akinetoplast cell, the study was unable to perform in-depth investigation of the hypothetical proteins and the UDP-Gal protein. Hopefully, future analysis of these proteins will discover the biological function of these genes. A possible approach is to either knockdown or overexpress these proteins to ascertain their effect on the parasite. The minimal difference in mRNA expression in akinetoplastic and wild type stumpy cells could be because of the few numbers of sample replicate used for this study. A previous study which was conducted to ascertain how many biological replicates are needed to ensure valid biological interpretation of RNA -seq data or which statistical tools are best for analysing the data suggested that at least 6 biological replicates are required to enable identification of significantly and differentially expressed genes for all fold changes (Schurch et al., 2016). This data suggests a repeat of transcriptome comparison between akinetoplastic procyclic and wild type at early differentiation time point as akinetoplastic cells cannot establish late procyclic. This may give a bigger picture of gene expression during stumpy and procyclic differentiation.

4 Assessing the effects of mitochondrial dysfunction on differentiation of bloodstream *T. brucei*

4.1 Background and rationale

The mitochondrion plays important roles in the life cycle of *T*. *brucei*, with its activity changing across the various stages of the parasite's life cycle (Priest and Hajduk, 1994). Complex I (NADH:ubiquinone oxidoreductase) is the primary electron entry point in the mitochondrial electron transport chain which pumps proton into the mitochondrial inner membrane to produce ATP (Hirst, 2005). In addition to its role of being a coenzyme used in electron transport chain, NADH is also involved in generating acetyl-CoA which enters the citric acid cycle (Figure 4.1). As bloodstream form of the parasites in adipose tissue showed upregulation in the beta-oxidation pathway (Trindade et al., 2016), it is likely that there is increase demand for NADH dehydrogenase activity to generate energy.

RNAi knockdown of three core subunits of complex I (*NUBM, NUKM, NUEM*) revealed no growth defect in procyclic forms, *in vitro*, neither was there an effect on Δψm (Verner et al., 2). However, these cell lines had a 20% reduction of total mitochondrial NADH oxidation activity. A recent study which used knockout of two core subunits of complex I (*NUBM* and NUKM) has suggested that complex I may be implicated in energy transduction in akinetoplastic stumpy cells, thereby resulting in shorter life span (Dewar et al., 2018). There are no reports on the life span of stumpy cells in other hosts; the effect of parasite distribution on the life span of stumpy cells in different tissues is also unknown (Trindade et al., 2016). An alternative NADH dehydrogenase with rotenone-insensitive NADH oxidation activity in trypanosomatids has also been reported. It has been hypothesized that NDH2 may

facilitate rapid growth of procyclic forms when the activity of complex I limits growth and allows NAD+ regeneration for other mitochondrial dehydrogenases (Fang and Beattie, 2003).

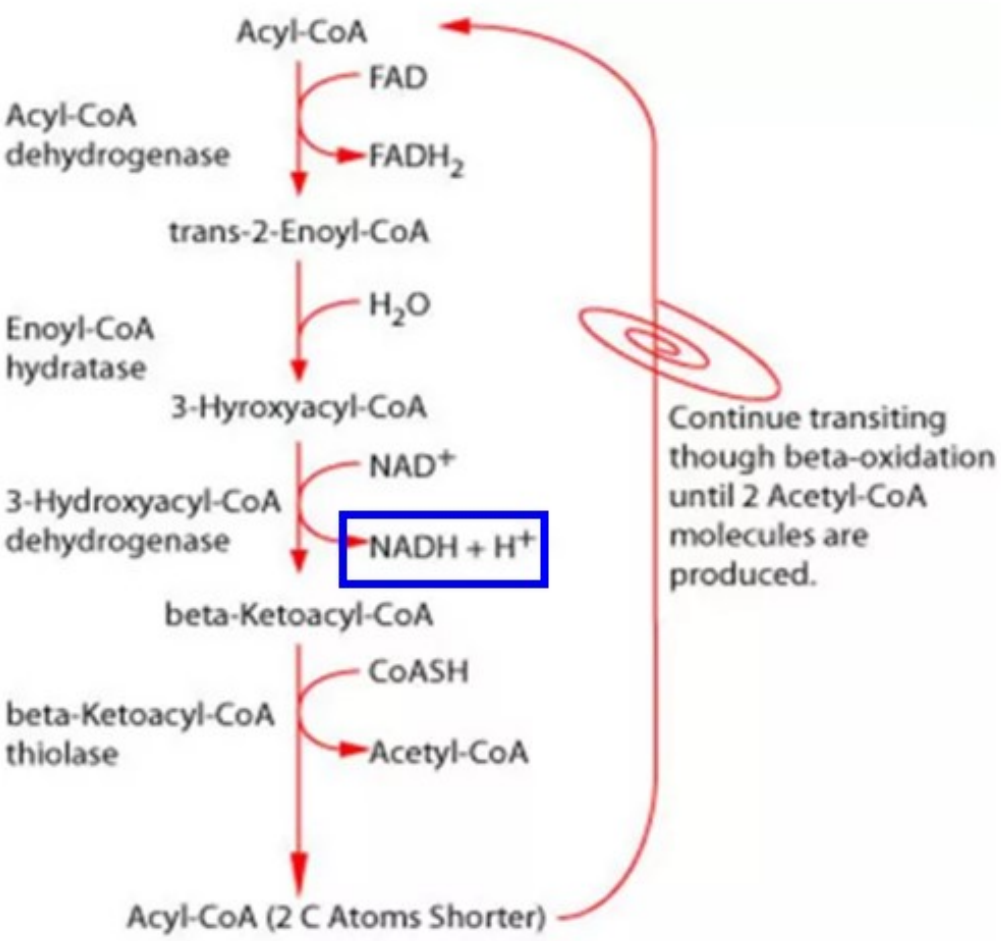

Figure 4.1 The beta oxidation metabolic pathway. The oxidation reaction occurs on the β carbon of an acyl-CoA molecule and breaks the fatty acid chain into two α and three β carbon atoms. The reaction generates $FADH_2$, NADH and acyl CoA. The acyl CoA dehydrogenase removes two hydrogen from the α and β carbon atoms. Enoyl-CoA hydratase catalyses the second step, which is hydration of the fatty acid. Hydroxyacyl-CoA dehydrogenase removes the hydrogen in the hydroxyl group to produce NADH + and ketoacyl-CoA thiolase catalyses the thiolytic cleavage. The NADH and FADH2 molecules produced by both fatty acid β-oxidation and the TCA cycle are used by the electron transport chain to produce ATP. The NADH molecule produced by this metabolic pathway is indicated in blue square. The image is adapted from (Chhabra, 2015).

However, *T. brucei* NDH2 has been suggested to be oriented towards the intermembrane space and hence, is unable to compensate for the loss of complex I; oxygen consumption was detected when NADH was applied externally to digitonin-permeabilised procyclic cells (Verner et al., 2013). The lack of permeability of mitochondrial membrane to NADH suggest that NDH2 is situated within the mitochondrial membrane and is oriented towards the cytosol. If this is correct, it would be highly questionable whether NDH2 is capable of compensating for loss of complex I activity. Studies have shown that depletion of NDH2 by RNAi knockdown affects parasite growth and decreases $\Delta\psi m$ in procyclic forms (Verner et al., 2013). Assessing the effects of mitochondrial dysfunction on nuclear gene expression (discussed in Chapter 3 of this thesis) has been followed up by investigating the effect of absence of kDNA on temporal and spatial differentiation of bloodstream form of *T. brucei*. Attempts to generate complex I null mutants and akinetoplastic cell lines are two different means of assessing the effect of mitochondrial dysfunction. Recent work has shown adipose tissue as a third major reservoir for *T. brucei*, aside the colonisation of blood in early infection and later crossing the blood-brain barrier (BBB) in mammalian hosts (Trindade et al., 2016). These parasites also reside in the lymphatic system, interstitial spaces of organs, choroid plexuses and meninges of the brain (Kennedy, 2013). Studies describing tropism of the skin have also shown that *T. brucei* is found near the subcutaneous adipocytes (Caljon et al., 2016; Capewell et al., 2016). Previous studies have showed that parasites from adipose, heart, and brain tissues can re-invade the bloodstream to establish new infection (Trindade et al., 2016).

The adipose tissue form (ATF) of *T. brucei* differs from the bloodstream form and the procyclic form because the ATF utilise fatty acids as an external carbon source, which would be in contrast to usage of glucose and proline as major carbon sources by bloodstream and procyclic forms, respectively (Szöör et al., 2014). These predictions were suggested by transcriptomic analysis, where upregulated genes in ATF included putative fatty acid β-oxidation enzymes such as carnitine-acyltransferases, which is responsible for mitochondrial import of fatty acids (Trindade et al., 2016). Consistent with active fatty acid β-oxidation in

the mitochondrion of ATFs, the same study also reported that these parasites were able to utilize exogenous myristate and formed β-oxidation intermediates. The beta oxidation may require increase demand for NADH, which may be the role of complex I, eventually generating energy for ATF of the parasite.

4.1.1 Hypotheses

The Vassella research group has reported that HMI-9-based medium containing methylcellulose allowed several pleomorphic *T. b. brucei* strains to proliferate without growth arrest (Vassella et al., 2001b). Growth-arrested populations can also be established by culturing slender forms of *T. brucei* in methylcellulose medium without dilution for 48 hours to allow accumulation of SIF and subsequent stumpy formation (Zimmermann et al., 2017). This technique was used in the present study for differentiation of complex I null mutants and the WT EATRO to stumpy forms, *in vitro.* This chapter investigated the following hypotheses:

1. Complex I play an important role in stumpy forms and/or in cells residing in adipose tissue.
2. Complex I may be required for viability of *T. brucei* stumpy cells.

4.2 Results

4.2.1 Complex I null mutant in bloodstream form trypanosome.

To generate functional cI null mutants in pleomorphic *T. brucei*, EATRO 1125 strain AnTat 1.1 cells (Engstler and Boshart, 2004) were grown in HMI-9 medium containing 1.1% (w/v) methylcellulose, supplemented with 20% (v/v) foetal calf serum (FCS) and 5% serum plus (Section 2.1.2). As targets for generating functional cI null mutants, core subunits NUBM and NUKM were chosen. NUBM and NUKM are found within the hydrophilic part of the cIα subcomplex and forms part of the four-core complex I nuclearly encoded proteins. The flavoprotein NUBM is the first protein to receive electrons from NADH, whereas the iron-sulphur cluster protein NUKM is the last protein in the redox chain to pass electrons to

ubiquinone. The homologous recombination strategy chosen to generate blood form cell lines lacking the *NUBM* or *NUKM* genes is depicted in Figure 4.2 and follows a general approach originally described by Wirtz et al. (1999). Approximately 500 bp of the 5' and 3' intergenic regions from NUKM and NUBM were amplified using the primers listed in Appendix A. These sequences were then inserted upstream and downstream, respectively, of cassettes encoding either T7 RNA polymerase (T7RNAP) and neomycin resistance (NEO) genes (pTbNUBM-KO1 and pTbNUKM-KO1, to replace the first allele) or Tet repressor (TETR) and hygromycin resistance (HYG) genes (pTbNUBM-KO2 and pTbNUKM-KO2, to replace the second allele). Single knock out (SKO^{NEO}) cell lines were generated with pTbNUBM-KO1 and pTbNUKM-KO1 and used to generate double knockout (DKO) null mutants (Δnubm::NEO/Δnubm::HYG and Δnukm::NEO/Δnukm::HYG) by replacing the second allele with pTbNUBM-KO2 and pTbNUKM-KO2 (Figure 4.2). Hence, the DKO null mutants were resistant to both NEO and HYG. This study used published constructs described by Surve et al.(2012). Also, conditional knockout (CKO) cell lines for NUBM and NUKM used in this study were kind gift from Sachin Surve (Seattle Biomedical Research Institute, Seattle, Washington, USA). These were cell lines generated in the study conducted by Surve et al. (2012).

After transfection and selection (See Section 2.1.2), the resulting blood form lines were analyzed by PCR (testing for correct integration of the knockout constructs and absence of the coding sequence). The locations of primers used for the confirmation of KO cells are shown in Figure 4.3 C and D. For confirmation of correct 5' end integration of constructs, forward primers (Primer 1) were used that corresponded to 5' intergenic regions upstream of the sequences used to generate the KO constructs; reverse primers (Primer 2) corresponded to sequence within the T7RNAP gene. Likewise, correct 3' end integration was tested with PCR primers that corresponded to a region within the NEO gene (Primer 3) and to 3' intergenic regions downstream of the ones used to generate the KO constructs (Primer 4).

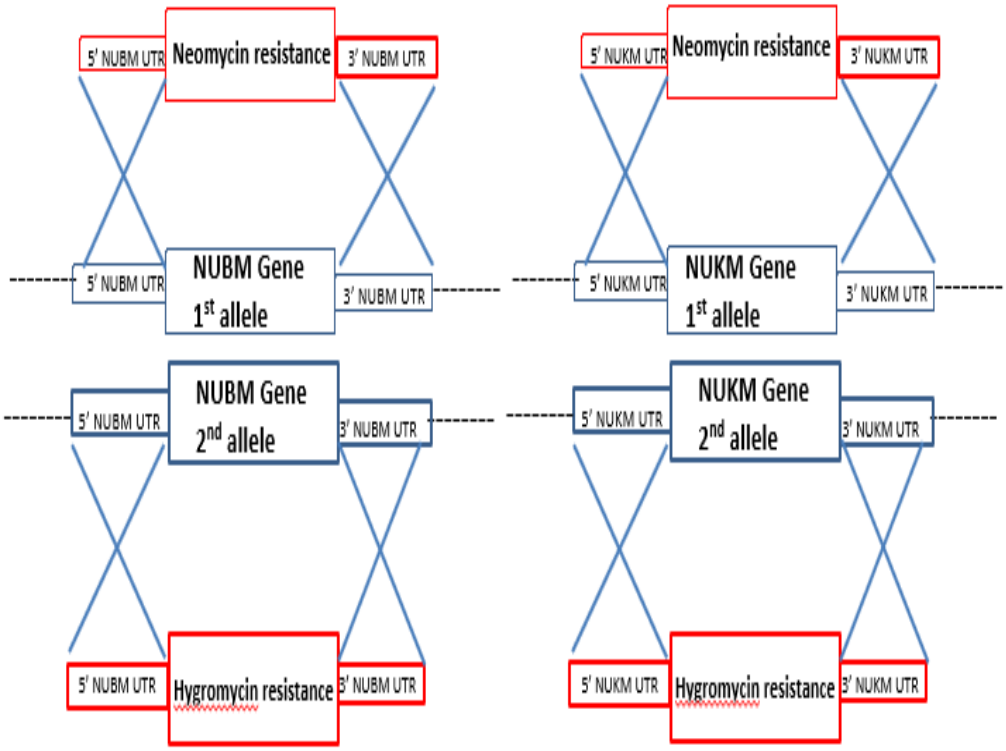

Figure 4.2 Deletion of complex I subunits. Schematic illustration of NUBM and NUKM loci and constructs used for gene deletion by homologous recombination. Each construct contains 3' and 5' intergenic regions from either the NUBM or NUKM gene and an antibiotic-resistance gene (Surve et al., 2012). The first alleles of both NUKM and NUBM were replaced by a G418/neomycin resistance (NEO), while the second allele was replaced by hygromycin resistance (HYG) cassette. Knockout constructs were generated as described by (Ochatt et al., 1999).

A 980-bp fragment from the F_1F_O-ATPase subunit γ was amplified to control for presence of gDNA in each sample. For detection of correct integration of the construct into the EATRO 1125 AnTat 1.1 genome, primers were designed to target 3' and 5' intergenic regions and within T7RNAP and TETR genes *of* constructs. Correct integration of the construct to replace one *NUBM* allele would be expected to yield band sizes of 1120 bp and 1200 bp for 5' and 3' end integrations, respectively (A). Analysis of a putative *nukm* SKO cell line by PCR gave the results shown in Figure 4.3 B.

To this end, the putative SKO clones were transfected with the constructs containing the NEO and T7 RNAP (for PCR confirmation) cassette, flanked by *NUBM* or *NUKM* upstream and downstream regions (Figure 4.2 C and D). The location of annealing primers is indicated for checking correct integration of construct.

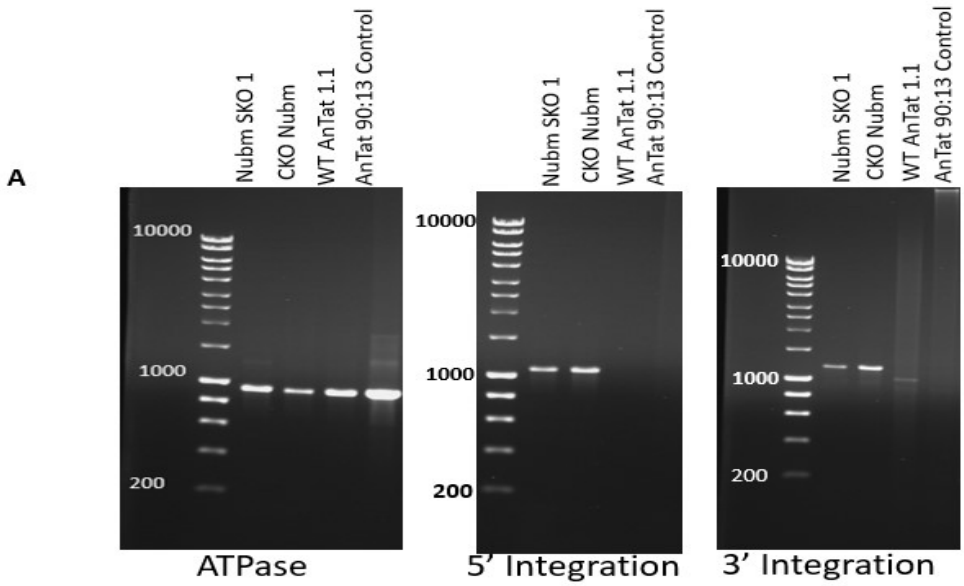

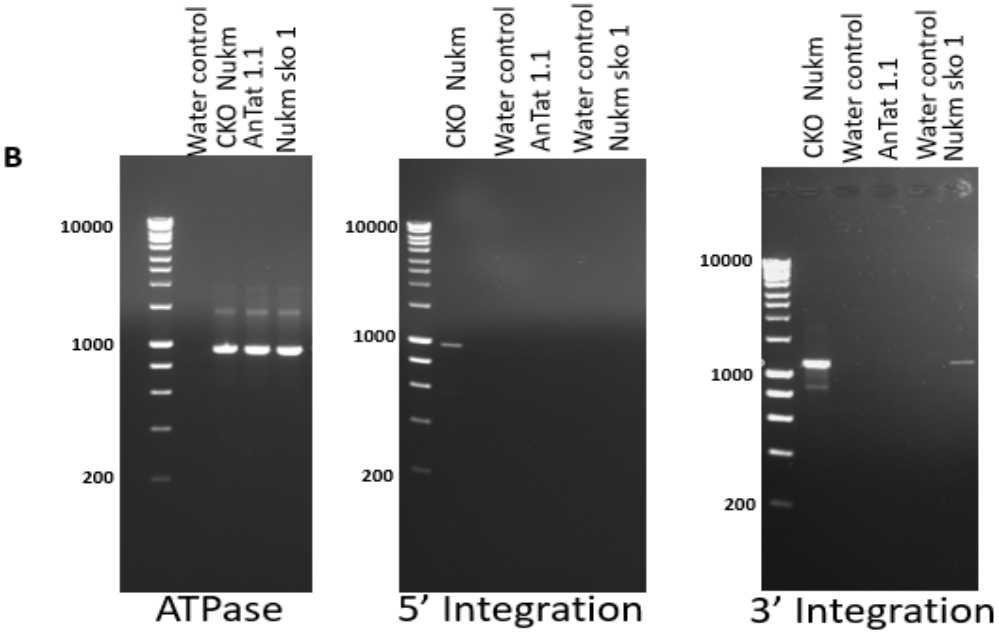

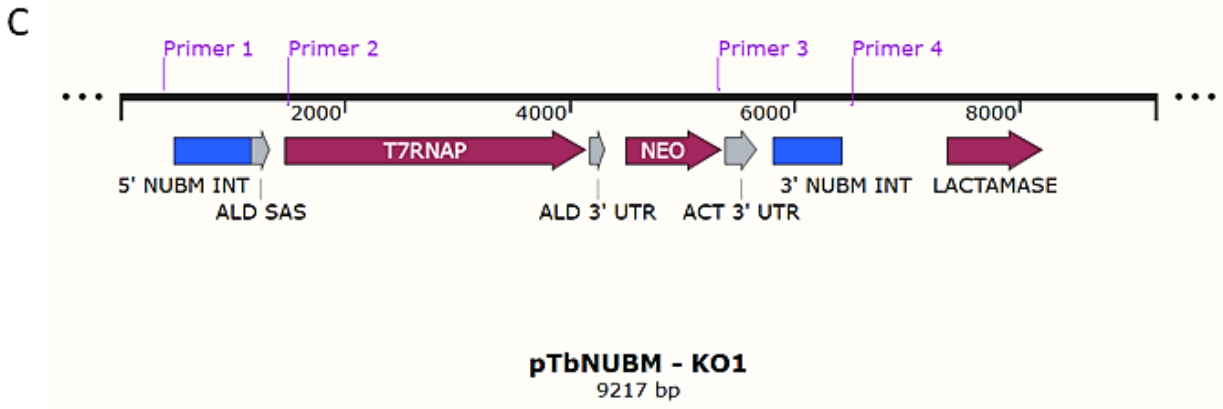

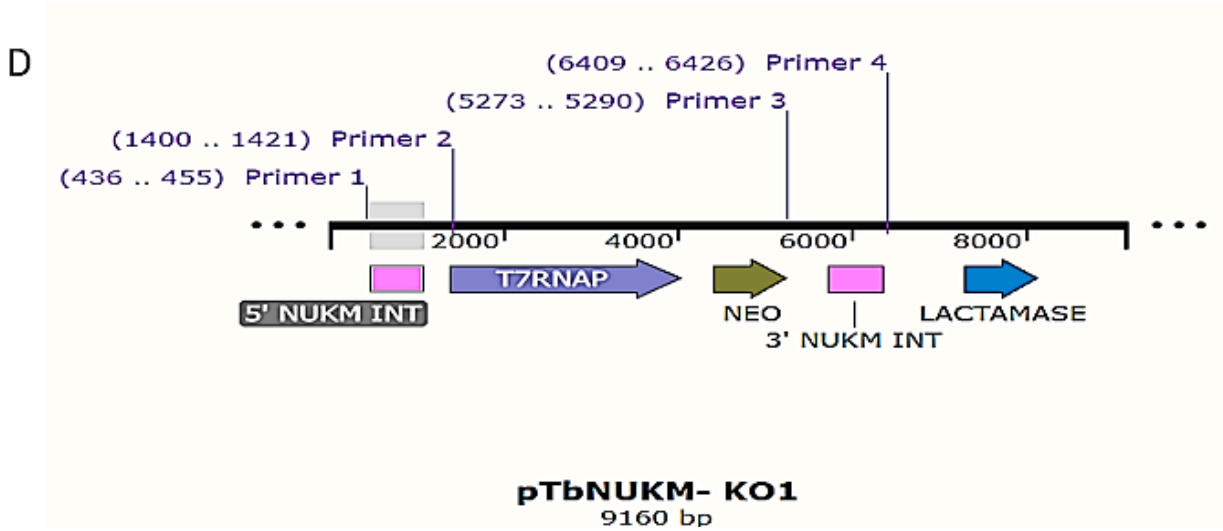

Figure 4.3 Assessment of correct replacement of one *NUBM* allele (panel A) or *NUKM* allele (panel B) with the *NEO* and T7 RNA pol cassette. Primers were designed and used to test integration of the pTbNUBM-KO1 and pTbNUKM-KO1 constructs into the EATRO 1125 AnTat 1.1 strain to generate *NUBM* (A) and *NUKM* (B) SKO cell lines, respectively. The images show the amplification products for each cell line after agarose gel electrophoresis. The ATPase γ subunit was amplified to confirm presence of gDNA in the samples. (A) DNA band sizes of 1120 bp and 1200 bp indicate correct 5' and 3' end integration, respectively, of the construct into the *NUBM* locus. (B) DNA band sizes expected for correct integration of construct were 971 bp and 1154 bp which corresponded to 5'and 3' end integration. (C) Location of primers for amplifying 5' and 3' integration of construct on NUBM locus. (D) A linear map showing primer annealing sites on the NUKM locus to detect correct integration of plasmid.

For NUBM, seven G418/hygromycin resistant clones were selected and analysed in a duplex PCR for the NUBM and ATPase subunit γ coding sequence (CDS). Assessment of deletion of NUBM alleles in the seven selected clones was done by PCR. The parental WT AnTaT 1.1 strain was used as control. The expected sizes for the NUBM and ATPase subunit γ amplification products were 1488 bp and 980bp, respectively. Clone A and B were transfectants with NUBM CDS still present after second round attempt to generate NUBM double knockout clones. The remaining five DKO clones (1-5) had the NUBM gene succesfully deleted. The parental WT cell line served as positive control, where the expected fragment size of 1488 bp was amplified (Figure 4.4). However, only two clones were able to grow continuously in the presence of both drugs in the medium.

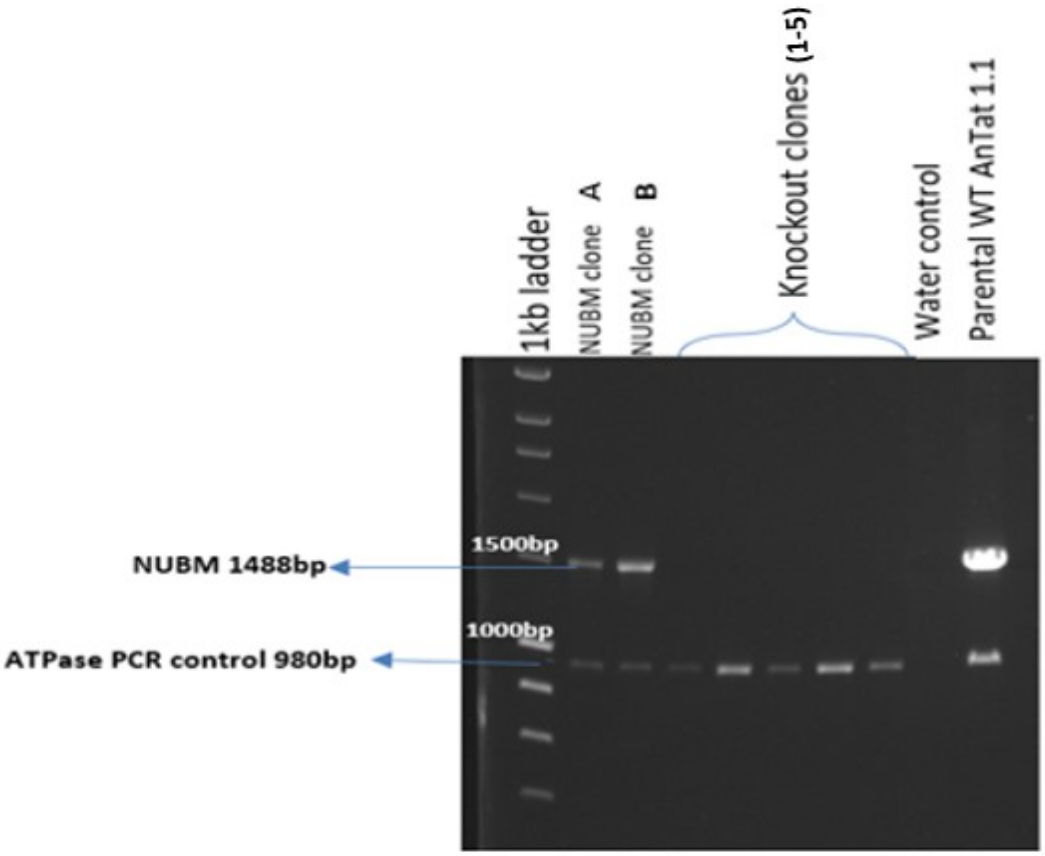

Figure 4.4 Assessment of deletion of *NUBM* alleles in the seven selected clones by PCR. The parental WT AnTaT 1.1 strain was used as control. The expected sizes for the NUBM and ATPase subunit γ amplification products were 1488 bp and 980bp, respectively. Clone A and B were transfectants with NUBM CDS still present after second round attempt to generate NUBM double knockout clones. The remaining five DKO clones (1-5) had the NUBM gene succesfully deleted. The parental WT cell line served as positive control, where the expected fragment size of 1488 bp was amplified. The water control confirmed absence of T. brucei DNA contamination in the PCR master mixture. The 1-kb DNA ladder was used to extrapolate the sizes of the PCR products.

For *NUKM*, fourteen clones were resistant to G418/hygromycin drugs. Successful deletion of both alleles was assessed by a PCR reaction specific for the CDS of *NUKM*, carried out as duplex PCR by simultaneous amplification of the F_1F_O-ATPase subunit γ gene as positive

control (as described in Section 2.4.1). All fourteen antibiotic resistant clones for *NUKM* could be confirmed for absence of gene (Figure 4.5).

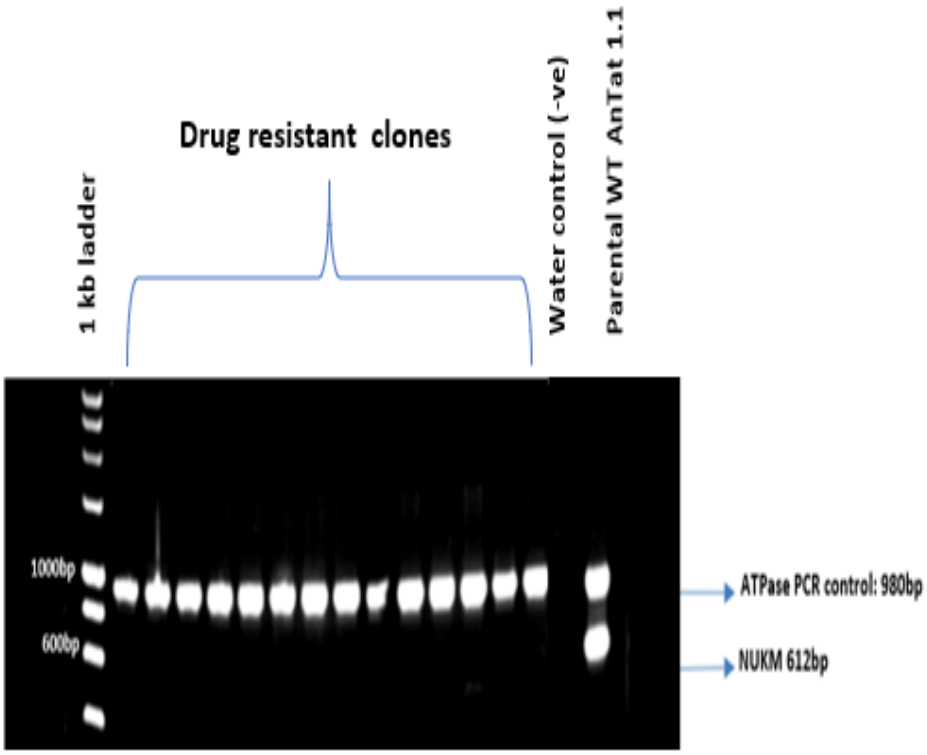

Figure 4.5 Confirmation of deletion of both *NUKM* genes by PCR. *NUKM* CDS-specific primers were used to enable confirmation of the presence or absence of the gene in the parental and antibiotic resistantclones, respectively. All 14 clones analysed showed successful deletion of both *NUKM* alleles. The parental cell line showed the expected size of 612 bp for the *NUKM* amplicon. The ATPase subunit γ gene was used as positive control in the same reaction. The water control which served as negative showed no amplicon, indicating the absence of contamination of the PCR master mixture.

4.2.2 Southern blot analysis confirmed complex I double knockout clones

Following PCR analysis, Southern blot analysis was performed to validate the absence of either the *NUBM* or *NUKM* gene in the selected clones. The presence of PstI endonuclease sites upstream and downstream of the *NUKM* gene was expected to result in the presence

of a ~ 3.0 kb fragment in PstI-digested genomic DNA that can be detected by Southern analysis using a probe to the *NUKM* CDS (top map of Figure 4.6).

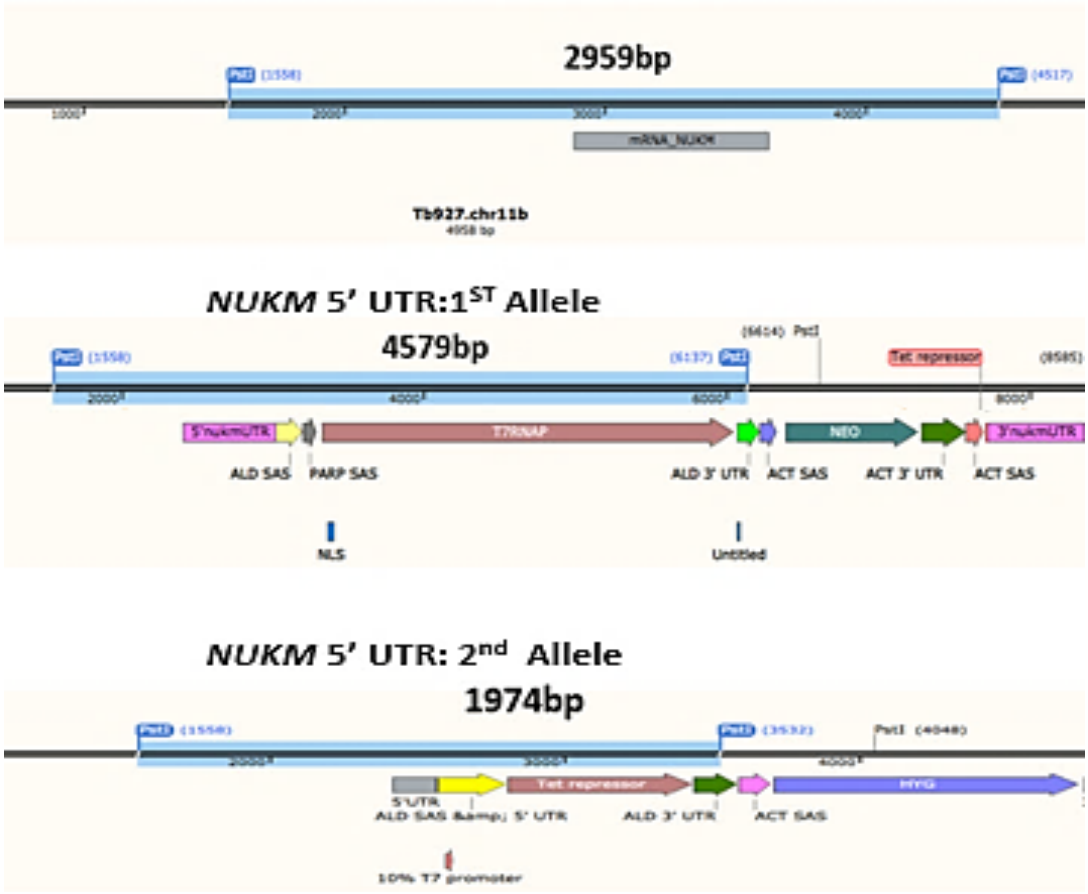

Figure 4.6 A Schematic representation of the NUKM locus on chromosome 11 of the *T. b. brucei* TREU927 genome, before and after integration of KO constructs. The PstI fragment detected by the *NUKM* 5'-UTR probe (and, in case of the WT, by the CDS probe) is highlighted in blue. A DNA band size of 2959 bp is expected for the WT *NUKM* locus. Successful replacement with the *T7RNAP*/*NEO* and *TETR*/*HYG* cassettes in the DKO clones is expected to result in detection of *PstI* DNA fragments of 4579 bp and 1974 bp with the same probe. The *NUKM* 5' and 3' intergenic region is highlighted in pink and grey on the middle and bottom maps, respectively. Abbreviations: ALD- Aldolase, ACT- Actin, NLS- Nuclear localization signals , PARP- procyclic acidic repetitive protein, SAS- splice acceptor site and HYG- Hygromycin.

Hybridising a blot of *PstI*-digested genomic DNA with the *NUKM* CDS probe showed the ~3.0 kbp band that indicates presence of the gene only in the WT AnTat 1.1 control cell line; this

band was absent in the putative DKO clones, but, surprisingly, also in the SKO and CKO cell lines (Figure 4.7, left panel). The absence of NUKM gene in the SKO cell could be that the remaining DNA sequence of NUKM is below detection level with this technique. The detection of *NUKM* in WT with two alleles showed weak signal. The CKO cell may not have the gene present in the genome even outside the rDNA locus. For presence of both 5' UTR in the SKO could be a possible contamination of SKO DNA by the other samples. When probed with the 5'-UTR probe, DKO and CKO cell lines showed band sizes of ~2 kbp and ~4.5 kbp, consistent with correct integration of both constructs (Figure 4.7, right panel). Again, the SKO cell line showed the same result as the DKO cell lines, which was unexpected. The WT AnTat1.1 parent cell line showed once again only the expected ~3.0 kbp band. Altogether, the Southern analysis further validated the deletion of both alleles of the *NUKM* gene in the four clones investigated.

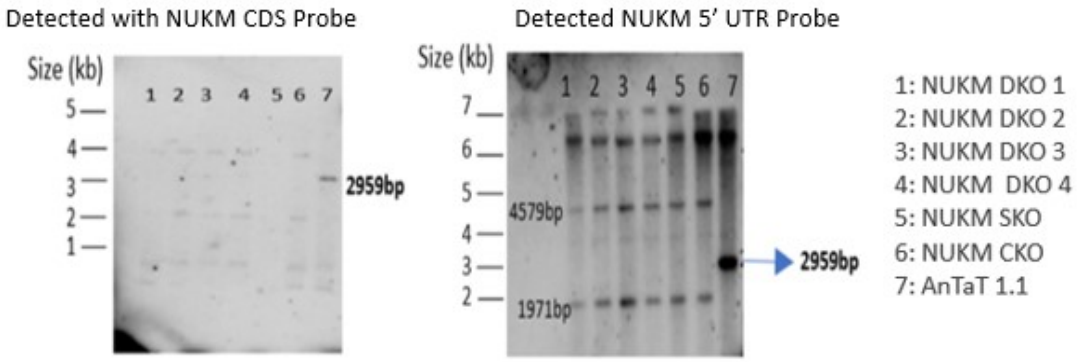

Figure 4.7 Assessment of deletion of *NUKM* alleles in four clones by Southern analysis. Southern blot analysis of PstI-digested genomic DNA (1 µg) from Δnukm::NEO/Δnukm::HYG (DKO *NUKM*) (4 clones) Δ*nukm*/*NUKM* (SKO); inducible *NUKM* cell line (CKO *NUKM*) and wild-type trypanosomes (AnTat 1.1) and using a probe against the CDS (left panel with each number corresponding to samples investigated) and 5'-UTR (right panel) of *NUKM*. The size (kb) migration of marker DNAs are indicated. Blot hybridised with *NUKM* gene probe gave ~3.0 kbp for presence of gene in the wild type AnTaT 1.1 control cell line and absent in the DKO clones in left panel. DKO cell lines show sizes for both construct integration when probed with 5' *NUKM* UTR DNA probe (1971 bp and 4579 bp) on the right blot. Same size of ~3.0 kbp was obtained for WT when probed with 5' *NUKM* UTR DNA probe. The top DNA bands of about 6.5 kb on the right blot in all cells shows nonspecific hybridization.

Similarly, putative *NUBM* DKO mutants were subjected to Southern analysis using a probe for the *NUBM* 5'-UTR (results with a CDS probe were of poor quality, data not shown). Probing *PstI*-digested genomic WT *T. brucei* DNA with was predicted to result in a 5.1 kbp band (Figure 4.8, top map), whereas ~4.4 kbp and ~2.3 kbp bands were expected for DKO clones (Figure 4.8, middle and bottom maps).

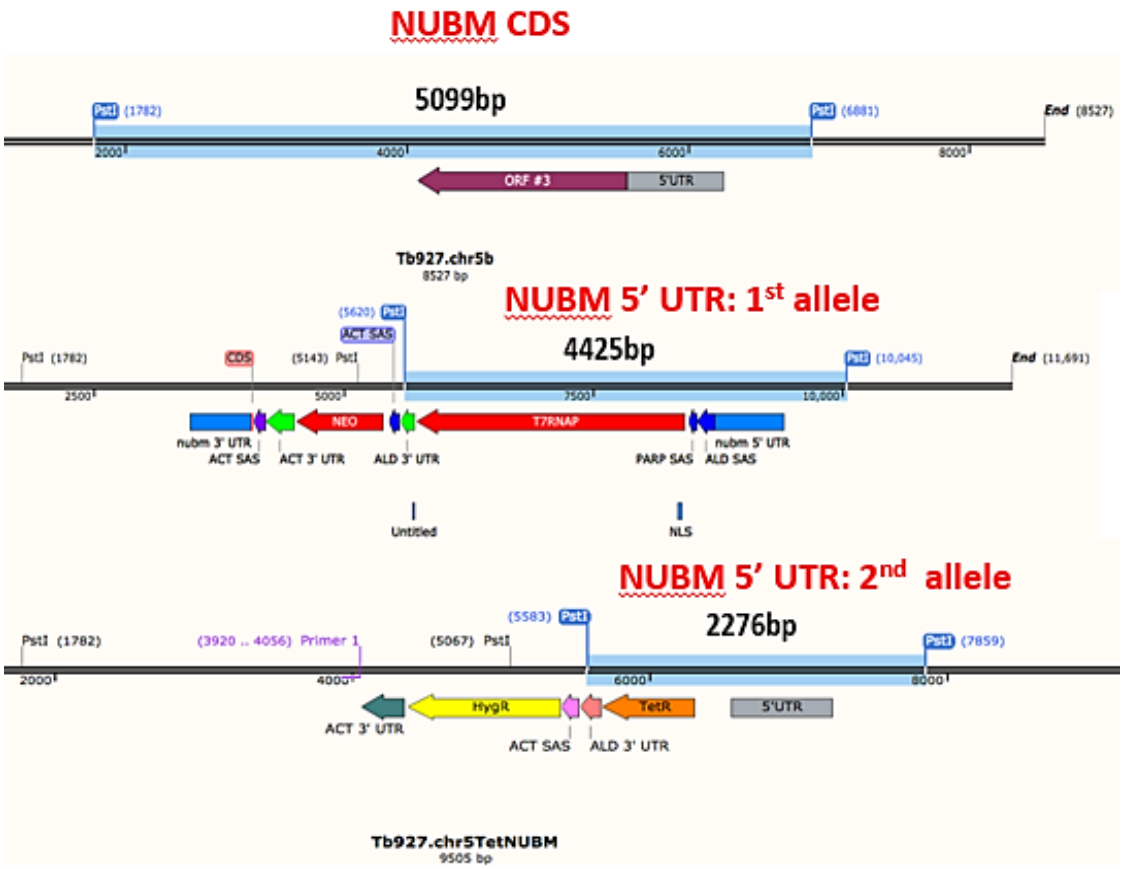

Figure 4.8 A schematic representation of the *NUBM* locus on chromosome 5 of the *T. b. brucei* TREU927 genome, before and after integration of KO constructs. The *PstI* fragment detected by the *NUBM* 5'-UTR probe (and, in case of the WT, by the CDS probe) is highlighted in blue. A DNA band size of 5099 bp is expected for the WT *NUBM* locus. Successful replacement with the *T7RNAP*/*NEO* and *TETR*/*HYG* cassettes in the DKO clones is expected to result in detection of two *PstI* DNA fragments (4425 bp and 2276 bp) with the same probe. The NUKM 5' and 3' intergenic region is highlighted in blue and gray/green on the middle and bottom maps, respectively. Abbreviations:: ALD- Aldolase, ACT- Actin, NLS- Nuclear localization signals , PARP- procyclic acidic repetitive protein, SAS- splice acceptor siteTetR- Tretracycline repressor gene, NEO-neomycin, HYGR- Hygromycin resistance.

Only *PstI*-digested genomic DNA of the WT AnTat 1.1 strain gave a DNA band size of ~5 kb when probed with the *NUBM* 5'-UTR (Figure 4.9). For the DKO cell lines, DNA bands of ~ 4.4 kb and ~ 2.3 kb confirmed successful replacement of the *NUBM* alleles with the *T7RNAP*/*NEO* and *TETR*/*HYG* cassettes (Figure 4.9). The blot also showed DNA bands between 2 kb and 4 kb, as well as below 1 kb, some of which were present in all cell lines, suggesting non-specific hybridisation. Overall, the Southern analysis confirmed the Δ*nubm* genotype of two putative DKO clones tested.

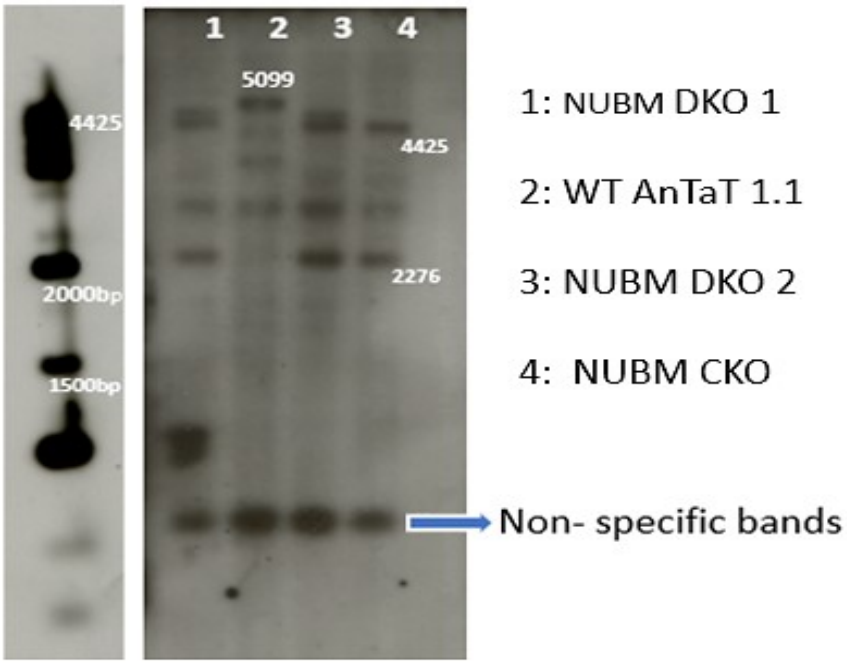

Figure 4.9 Detection of deletion of both alleles of the *NUBM* gene using Southern blotting. Genomic DNA was digested with the PstI enzyme. Specific probes were used for hybridization under the same conditions used initially for the detection of NUKM. Two DKO of NUBM clones (Δnubm::NEO/Δnubm::HYG, Lanes 1 and 3), WT control EATRO 1125 AnTat 1.1 (Lane 2), CKO NUBM (ΔnubmI::NEO/Δnubm::HYG, Lane 4) cell lines. Non-specific bands are shown on the blot between 2kb and 4kb and well as below 1kb, albeit, all expected band sizes were detected for NUBM CDS (5099 bp) in WT and 4425 bp for 5' UTR target region when replaced with pTbKO1 construct. The 2276 bp is fragment size probed with 5' UTR to test integration of pTbKO2 construct.

4.2.3 Stumpy cells generated in methylcellulose

The ability of *NUKM* and *NUBM* null mutants to differentiate, as well as the parental cell line, in methylcellulose was investigated. Prior to the start of this study, I cultivated EATRO 1125 strain AnTat1.1 in HMI-9 based medium supplemented with 20% (v/v) foetal calf serum, 5% serum plus, and 1.1% (w/v) methylcellulose as described (Vassella et al., 2001b). The pleomorphic cell line was used because they possess the ability to undergo full developmental stages and hence was suitable for analyses of trypanosome differentiation (M. Engstler and Boshart, 2004; Fenn and Matthews, 2007). This cell line was a kind gift from Professor Markus Engstler laboratory (Department of Cell and Developmental Biology, Biocenter, University of Würzburg, Germany). To generate density-induced stumpy parasites, slender cells at a seeding density of 5 x 10^5 cells/ml were left in culture without dilution for 48 hours. This procedure allowed the build-up of SIF and led to stumpy formation (Zimmermann et al., 2017). After 48 hours incubation at 37 °C, a pH change was observed via detection of an orange-yellowish colour. Cell death was also detected in a sub-population of cells for both WT and null mutant, even though majority of the cells were viable. Microscopic examination of culture revealed cell crenation, and debris. These observations suggested that timing of the experiment was critical because when cells were incubated beyond 48 hours, most of the cells, if not all, became inviable. A total of two clones were differentiated for *NUBM* mutant lines and fourteen clones for *NUKM* mutant cells. The differentiated stumpy forms showed the characteristic morphological change from long slender shape to short stumpy, and expressed the protein associated with differentiation (PAD1 surface marker; Figure 4.10 (Dean et al., 2009), which was detected by immunofluorescence (Section 2.5.1).

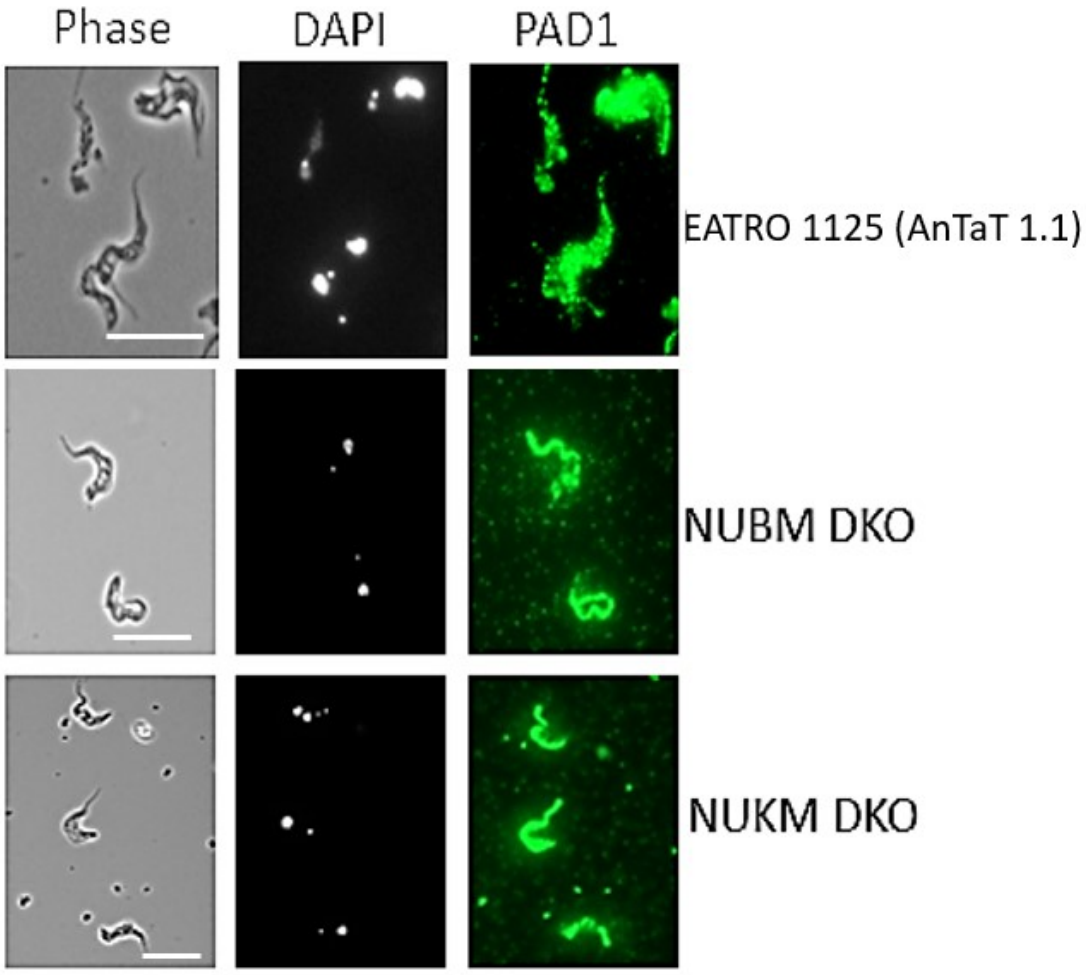

Figure 4.10 Expression of PAD1 by methylcellulose differentiated stumpy cells of *T. brucei*. The analyses were conducted with methylcellulose-induced stumpy cells for WT AnTat 1.1, *NUKM* DKO clone 1, and *NUBM* DKO clone 1 lines. Stumpy formation was initiated after slender cells were seeded at a density of 5x 10^5 cells/ml and left undiluted in HMI-9 medium with 1.1% (w/v) methylcellulose supplemented with 20% (v/v) foetal calf serum (FCS) and 5% serum plus for 48 hours. The differentiated stumpy cells were then harvested by diluting the viscous medium (1:4 dilution) with trypanosome diluting buffer (TDB), spun down to discard supernatant and spread remaining cells on microscopic slides for air drying. The WT and mutant stumpy trypanosome cells displayed a homogenous cytoplasmic PAD1 signal (green) as revealed by immunofluorescence. Nuclear (N) and mitochondrial DNA (K) were stained with DAPI (white). The phase image shows stumpy morphology of the differentiated cells. Scale bar is 10 µm on phase contrast image.

4.2.4 Complex I null mutant cells can differentiate to procyclic forms

The development of stumpy cells to procyclic forms is accompanied by replacement of cell surface VSG with EP-procyclin coat (a form of procyclin rich in glutamate and proline repeats) (Matthews and Gull, 1994b). To investigate whether cI null mutants cells were able to differentiate to procyclic forms, they were exposed to cis-aconitate and a temperature shift to 27 °C (Section 2.1.4) (Rolin et al., 1998). To monitor differentiation, expression of EP procyclin protein, a marker of differentiation (Acosta-Serrano et al., 2001), was analysed by immunoblotting with a EP antibody. *In vitro* differentiated trypanosomes show procyclin coat is gained after 2 hours, after replacing the VSG coat (Matthews, 1999). This is the reason for testing this protein in the differentiated cell lines. As shown in Figure 4.11, both WT and null mutant procyclic cells were able to express EP procyclin. Expression of EP in the single knockout cell line was not abundant in comparison to the null mutants. EF1 was used as a loading control as well as normalisation of the expression levels in each sample.

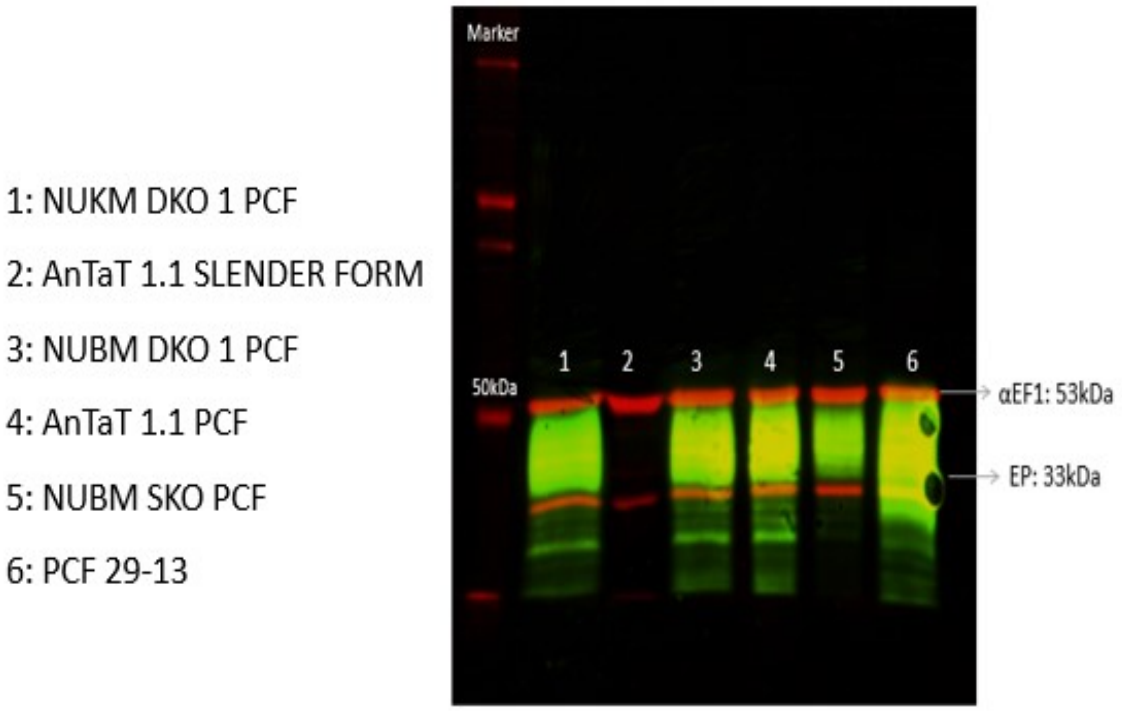

Figure 4.11 Expression of stage-specific marker by differentiating trypanosomes. Methylcellulose-induced stumpy trypanosomes were exposed to cis-aconitate to facilitate differentiation into procyclic forms. Aliquots of procyclic differentiated cells of WT EATRO 1125 (AnTaT 1.1 strain), DKO, SKO were analysed by SDS-PAGE and immunoblotting 72 hours post induction of differentiation by adding cis-aconitate and placing cultures at 27 °C. Undifferentiated BSF was used as negative control and PF strain 29-13 as positive control. All cell lines expressed EP procyclin except the BSF slender sample. The 33-kDa EP protein is shown in green and the 53-kDa elongation factor (EF-1α) (Grewal et al., 2016), which was used as a loading control, is shown in red. As a negative control, bloodtream form that do not express the EP procyclin was used.

4.2.5 Growth analyses of complex I null procyclic *T. brucei* mutants

This study has shown the ability to generate and propagate *NUBM* DKO and *NUKM* DKO cell lines in HMI-9 supplemented with 1.1% methylcellulose and induce stumpy formation in these cell lines. To generate the null mutant in EATRO AnTat 1.1, the cells were cultivated in medium described in Section 2.1.3. After transfection, selected clones were able to grow in normal HMI-9 without the methylcellulose. Unfortunately, comparative growth analysis of WT and *NUBM* DKO versus *NUKM* DKO in HMI-9 medium was not performed.

The *in vitro* differentiation to procyclic form was generated as described (Section 2.1.4). *NUBM* DKO procyclic cells and the differentiated parental EATRO 1125 AnTat1.1 procyclic cells were grown in SDM-79 medium for two weeks before performing the growth analyses. One WT AnTat 1.1 and two distinct clones of the *nukm* null mutant procyclic cells were investigated. Each cell line had two replicates of cell culture. In SDM-79 medium, *NUBM* DKO cells grew marginally slower compared to WT when cultured under the same conditions for two weeks (Figure 4.12). The generation time for WT AnTat 1.1 was 10.5 hrs and that of *NUBM* clone 1 and 2 was 14.04 and 19.4 hrs respectively. Hence, the data shown Figure 4.12 represent the growth analyses of only WT and *NUBM* procyclic *in vitro*. The results show growth defect in *NUBM* procyclic cells when compared to the parental cell line WT AnTaT 1.1 procyclic. Thus, the absence of *NUBM* gene retards growth with the evident phenotype.

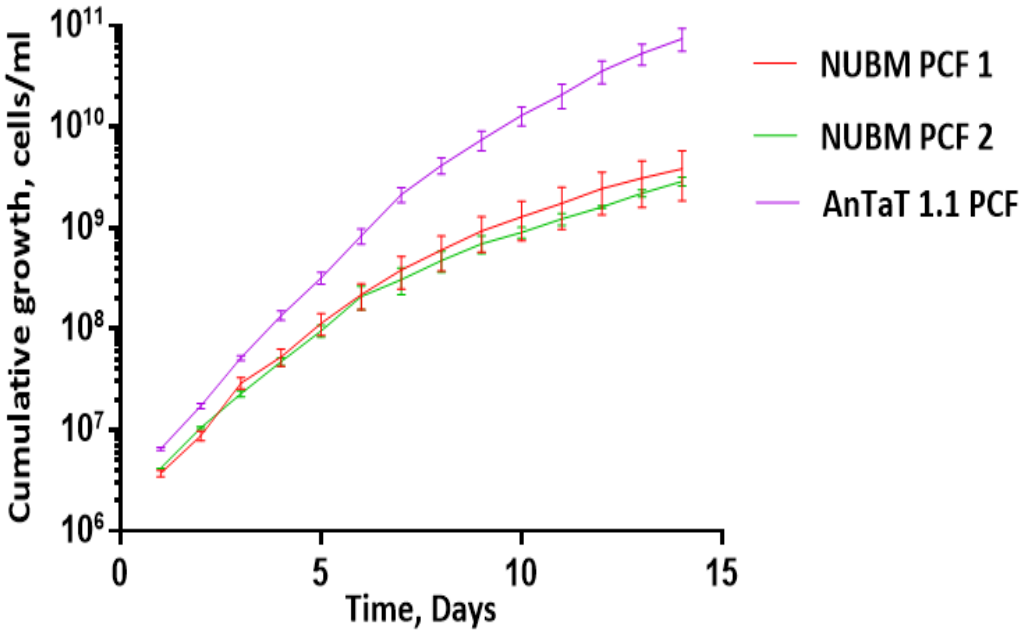

Figure 4.12 Growth analysis of complex I mutant procyclic form upon triggering differentiation with cis-aconitate. Growth analyses of WT and NUBM mutant procyclic clone 1 and 2 cultivated in vitro, are shown. Both WT and null mutant PCF were maintained at 2 x 10^6 daily after each cell count. Parasite densities were measured daily and then passaged by adjusting density to 2 × 10^6 cells/ml in fresh medium. The population growth was then calculated as cell density multiplied by the cumulative dilution factors. The cumulative growth curves after normalization for dilution at each subculture of WT and cI null mutant NUBM differentiated PCF cells were determined over a period of two weeks in SDM-79. WT is shown in lilac, NUBM PCF clone 1 and 2 in orange and green, respectively.

4.2.6 Virulence of *NUBM* and *NUKM* DKO parasites in mice

To test the ability of the *NUBM* and *NUKM* DKO cell lines to differentiate into stumpy cells in mice, three different treatments were administered to three different groups of 10-week old male MF1 mice. These mice were infected intraperitoneally with 2000 cells of EATRO 1125 AnTat 1.1 cell line or *NUBM* DKO clone 1 and 2 or *NUKM* DKO clone 1 and 2.

These cells were resuspended in HMI-9 prior to mice inoculation. The parasitaemia and survival of these mice were monitored daily until day 6. Mice infected with WT parasites and *NUBM* or *NUKM* DKO cells reached parasitaemia of 10^8 and > 10^8 /ml of blood respectively (Figure 4.13), for which only 30% and 20% respectively of the parasite population

differentiated to stumpy forms. Pleomorphic cells differentiate in a density-dependent manner from the proliferative slender form, through an intermediate stage, to the non-proliferative then to fly-infective stumpy stage form (MacGregor et al., 2013).

These stumpy forms are visible between day 4–6 post infection with parasitaemia plateaus at about day 5–7 post infection with >80% cell population exhibiting morphological stumpy forms (MacGregor et al., 2013), but that was not the case of these cell lines. The hyperparasitaemia observed in DKO clones resulted in the death of one out of the two *NUKM* DKO clone 1 infected mice. Collectively, the hyperparasitaemia observed in mice infected with either WT or DKO *T. brucei* suggest that these trypanosomes have lost pleomorphism.

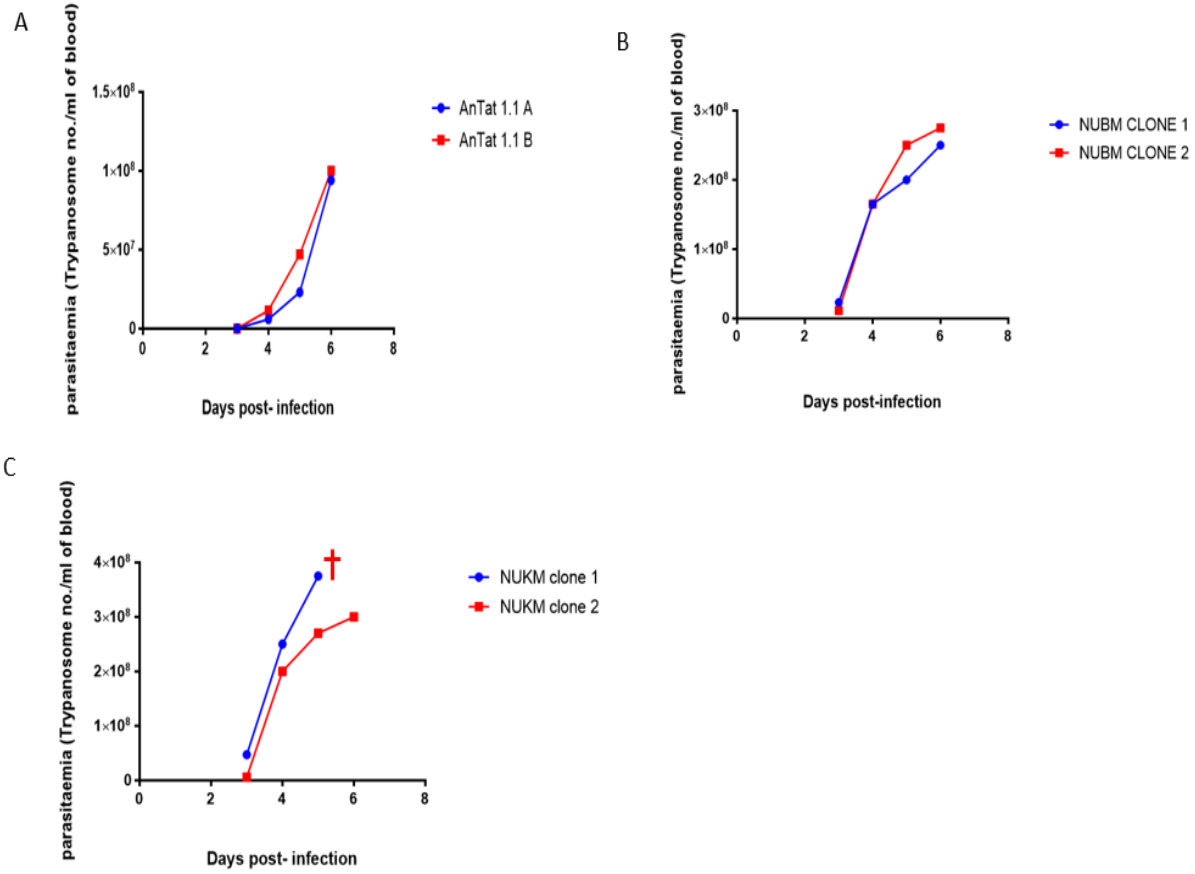

Figure 4.13 Parasitaemia profile of *T. brucei* infection. WT and *NUBM* and NUKM cells were used to inoculate 10 weeks MFI male mice with 2 × 10^3 trypanosomes. Parasite levels were monitored from day 3 till day 6 post-infection. Two mice were used per each clone of cell line. By day 6. WT (A) parasitaemia had reached 1x 10^8, whiles *NUBM* (B) and *NUKM* (C) cells showed uncontrollable growth of ~3 x 10^8 and ~4 x 10^8 parasites/ ml of blood respectively. The Y-axis is $\log_{10}$ parasite count per ml of blood and X-axis is number of days post-infection. One mouse infected with *NUKM* clone 1 died on day 6-post infection.

4.2.7 Confirmation of pleomorphic trypanosome strain EATRO 1125 AnTat1.1

The cell line obtained from Professor Markus Engstler's laboratory in Würzburg only showed 30% stumpy cells after 6 days post-infection to differentiate to stumpy forms. Pleomorphism is the ability of *T. brucei* slender forms to differentiate to stumpy forms with >80% of cell population in a mouse model. To generate new cI null mutant in a pleomorphic *T. brucei* background, different batches of stabilates of EATRO 1125 AnTat1.1 were obtained from the same laboratory, which originated from the Matthews laboratory (University of Edinburgh, United Kingdom). These batches of samples were validated to confirm that they were true pleomorphic cell lines. The data shown in Figure 4.14 demonstrate that these cell lines differentiated to stumpy forms in mice on day 6 post-infection and expressed PAD1 (Dean et al., 2009) when analysed by immunoblotting. Analysis of cell morphology also revealed that cells were stumpy-shaped when differentiated in mice (Figure 4.14) and this compares with the cell shape reported previously (Matthews et al., 2015).

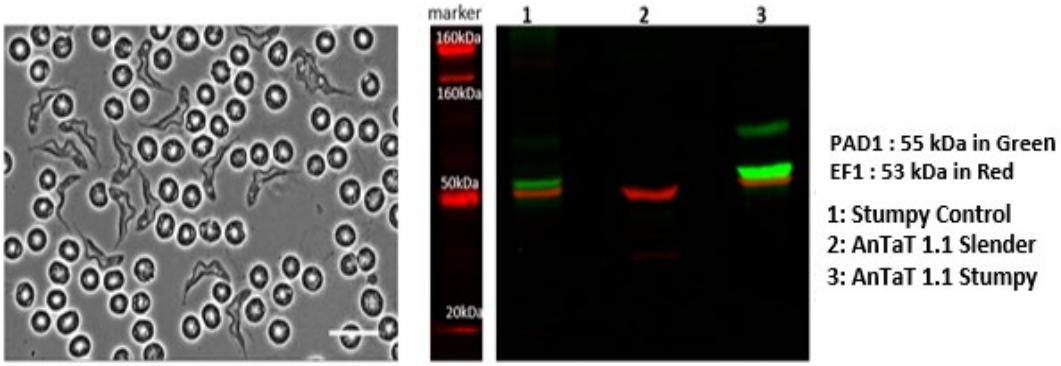

Figure 4.14 Confirmation of pleomorphic *T. brucei* cell line. EATRO 1125 serodeme AnTat1.1 differentiated to stumpy morphology as shown in the brightfield microscopy picture (left panel). Blood was harvested, and lysates from purified trypanosomes were fractionated by SDS-PAGE and analysed by immunoblotting (right panel) with antibodies against PAD1 (green signal) and EF-1α as loading control (red signal). For each sample, 2 x10^6 cells were loaded. Two control cell lines (stumpy control and AnTat1.1 BSF) were run alongside the sample of interest. The negative control, AnTat1.1 BSF (lane 2) showed no expression for PAD1, whereas the positive AnTat1.1 stumpy cell lines (lane 1 and 3) expressed PAD1. EF1 was used as a loading control. Western Images were developed with Odyssey CLx imaging system.

4.2.8 Generation of complex I null mutant in pleomorphic *T. brucei*

Having confirmed that the new batch of EATRO 1125 AnTat1.1 efficiently differentiates into stumpy cells during a mouse infection, these cells were used in a new attempt to generate *NUKM* null mutants in a truly pleomorphic background. In parallel, it was attempted to establish *NUKM* null mutants in the EATRO 1125 AnTat1.1 90:13 cell line, a well-established model for differentiation studies as it is particularly amenable to the generation of transgenic cell lines (MacGregor et al., 2013). The slender AnTat1.1 parasite was cultured in HMI-9 medium. The slender AnTat1.1 parasite was cultured in HMI-9 medium as described in Section 2.1.3. The medium used for culturing the slender forms of EATRO 1125 (AnTat1.1 90:13) cells is also described in Section 2.1.1.

These trypanosome cultures were kept at densities below 5 x 10^5 cells/ml to prevent cells from differentiating to the stumpy stage. The plasmids used to attempt deletion of both alleles of *NUKM* in EATRO 1125 AnTat1.1 have been described in Section 4.21 and by Surve et al (2012) and are listed in Table 2.2. In two separate attempts of transfection with pTbNUBM-KO1 and pTbNUKM-KO1, 74 putative *NUBM* SKO and 63 *NUKM* SKO clones were generated. Analysis of 15 transfectants each for *NUBM* and *NUKM* by PCR gave no amplicon and thus integration of construct to delete gene was unsuccessful. A summary of the transfections that were performed, the type of cell line used, the number of selected clones from each round of transfection and the validation method for the selected clones are shown in Table 4.1.

Table 4.1 Summary of cell line, plasmid and validation method used to confirm transfectants

GENETIC BACKGROUND	PLASMID USED	GENE KNOCKOUT	SKO/ DKO	CLONES OBTAINED	VALIDATING METHOD	OUTCOME
AnTat 1.1	pTbNUBM-KO1 (pLew 13)	NUBM	SKO	74	PCR	Tested 15, none gave an amplicon. ATPase synthase γ was amplified
AnTat 1.1	pTbNUKM-KO1 (pLew 13)	NUKM	SKO	63	PCR	Tested 15, none gave an amplicon. ATPase synthase γ was amplified

The selectable marker genes in plasmids pTbNUKM-KO1 (G418 resistance) and pTbNUKM-KO2 (hygromycin resistance) are already present in cell line EATRO 1125 AnTat1.1 90:13. Two synthetic constructs were designed because the AnTat 1.1 90:13 has neomycin and hygromycin to maintain the expression of T7-polymerase and the tetracycline repressor. These selectable markers and genes are also present in two existing constructs (pTbNUKM-KO1 and pTbNUKM-KO2).

Consequently, the two synthetic constructs (containing blasticidin and phleomycin resistance genes as selectable markers) were used in attempt to delete the *NUKM* gene. The constructs were designed such that one had the distal end of *NUKM* UTRs and the other had the proximal end closer to the coding sequence of the *NUKM* gene (Appendix B). Here, ~300 nucleotide targeting sequences were used to provide greater recombination frequency, and thus an efficient transfection (Merritt and Stuart, 2013).

Successful integration of both constructs would result in deletion of both alleles of the *NUKM* gene. Three independent transfections with construct pEX-K4-NUKM-1 gave 25 putative SKO clones that grew stably in blasticidin (Table 4.2). The gDNA was of sufficient concentration and quality when quantified with Nanodrop ND-1000. Attempts to validate

clones by PCR for integration of pEX-K4 NUKM-1 revealed that, two samples had 5' integration with one additionally showing integration at 3'end (Figure 4.15). The 5' and 3' replacement by pEX-K4 plasmid expected size is 2459 bp, whiles the 5' end integration fragment size is 1519 bp and that of 3' end integration is 1186 bp. As shown on the linear map and confirmed by PCR (Figure 4.15).

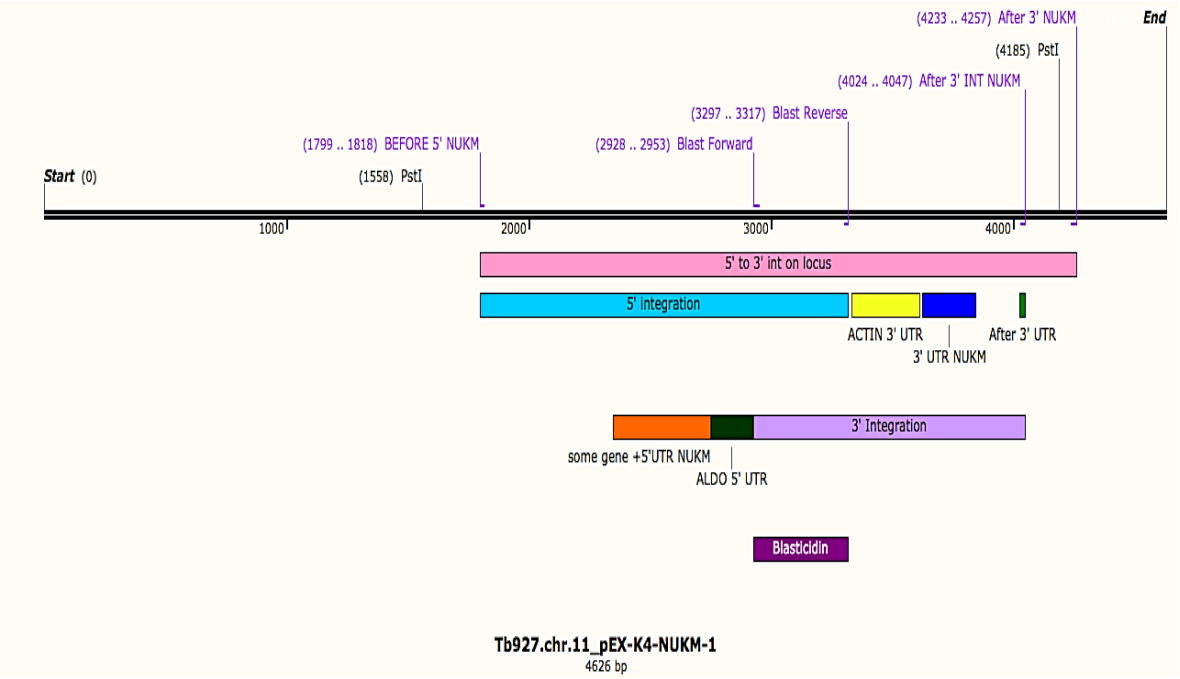

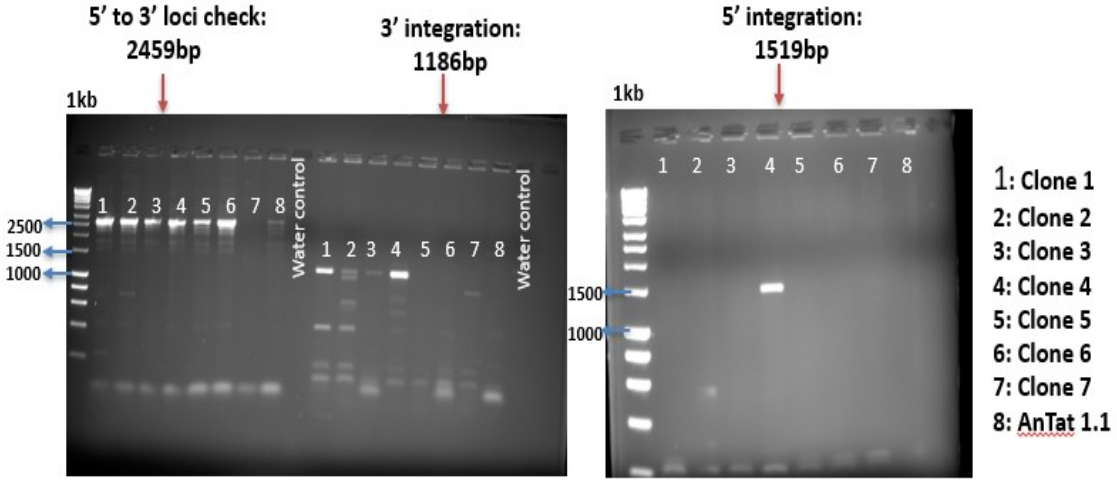

Figure 4.15 Confirmation of correct integration of construct by PCR and gel electrophoresis. Primers were designed to amplify the NUKM 5' and 3' UTR loci in WT (control) and to confirm the integration of construct with either 5' end or 3' end of NUKM in SKO lines. The parental cell line showed no amplicon, as expected for construct integration but the 2459 bp size was expected to serve as control for the 5' to 3' ends of the UTR loci on the EATRO 1125 genome. Two clones (1 and 4) showed successful integration of 3' end in one allele of the NUKM gene. Clone 4 then gave the correct size of 1519 bp for 5' end integration of the construct. The water control showed no amplicon, indicating the absence of contamination of the PCR master mixture.

Mouse infections showed that neither of these two SKO clones were able to efficiently differentiate into stumpy forms in mice (data not shown). This suggests that the attempt to delete cI subunit hinders differentiation ability of pleomorphic cell line. The other clones either gave no amplicon with PCR or incorrect sizes from what was expected for correct integration (data not shown). Attempts to delete the second allele of *NUKM* in this *NUKM* SKO clone with plasmid pEX-K4-NUKM-2 were unsuccessful (Table 4.2). Efforts to start *NUKM* gene deletion in the parental cell line with plasmid pEX-K4-NUKM-2 resulted in sixty viable clones, 19 clones tested for absence of the *NUKM* gene by PCR analysis gave inconclusive results (Table 4.2). Thus, all efforts to generate *NUBM* or *NUKM* null mutants in parasites that are competent for efficient stumpy differentiation in mice have been unsuccessful. A summary of cell line used, the number of selected clones and validation methods is presented in Table 4.2.

Table 4.2 A detailed information on transfection and validation methods

GENETIC BACKGROUND	PLASMID USED	GENE KNOCKOUT	SKO/ DKO	CLONES OBTAINED	VALIDATING METHOD	OUTCOME
AnTat 1.1 90:13	pEX-K4 NUKM-1	NUKM	SKO	7. Only 5 survived in 5 µg/ml blasticidin	PCR	Wrong sizes for 3' & 5' UTR NUKM integration
AnTat 1.1 90:13	pEX-K4 NUKM-2	NUKM	SKO	0		
AnTat 1.1 90:13	pEX-K4 NUKM-2	NUKM	SKO	0		
AnTat 1.1 90:13	pEX-K4 NUKM-2	NUKM	SKO	12. Only 5 survived in 0.5 µg/ml phleomycin	PCR	No amplicon for integration. ATPase synthase γ gave amplicon
AnTat 1.1 90:13	pEX-K4 NUKM-1	NUKM	SKO	20. Only 15 survived in 5 µg/ml blasticidin	PCR	Six clones gave band sizes close to size of 5' to 3' NUKM UTR integration. Two out of the six gave correct 3' & 5' NUKM UTR integration of construct
AnTat 1.1 90:13	pEX-K4 NUKM- 1	NUKM	SKO	0	PCR	
NUKM SKO Clone 1	pEX-K4 NUKM-2	NUKM	DKO	0		

NUKM SKO Clone 1	pEX-K4 NUKM-2	NUKM	DKO	60	PCR	Tested 19 out of 60 for presence of NUKM gene; all were positive.
NUKM SKO Clone 2	pEX-K4 NUKM-2	NUKM	DKO	0		
NUKM SKO Clone 3	pEX-K4 NUKM-2	NUKM	DKO	0		

4.2.9 The *T. brucei NUKM* null mutant shows decreased fitness in fat

As described before (Section 4.2.6) the *T. brucei* EATRO 1125 AnTat1.1 cell line (Würzburg strain) and *NUBM* or *NUKM* null mutant cell lines derived from it did not efficiently differentiate into stumpy forms *in vivo* at peak parasitaemia (i.e. after six days post infection), although individual cells exhibited morphological characteristics of short stumpy forms and also expressed PAD1, a stumpy marker (see Figure 4.10). All cell lines were virulent in mice with hyperparasitaemia. Thus, parasite grew faster with change in parasite density with time in infections such that the parasite level exceeded $>10^8$ trypanosomes/ml which overwhelmed the host.

The absence of cI subunit *NUBM* or *NUKM* in *T. brucei* bloodstream form may render the knockout (KO) cells incapable of activating complex I of the respiratory chain for the parasites to survive in adipose tissue. This was done because it has been published that the adipose tissue is a niche for *T. brucei*, and these adipose tissue forms are capable of replicating within the fat (Trindade et al., 2016). The rationale here was to use null mutant to test if complex I is required for survival in adipose tissue. Because these KO cells were unable to fully differentiate in mice (Section 4.2.6), only first peak of parasitaemia was considered and tested. This is in contrast to what was done in the study conducted by Trindade et al (2016), where parasitaemia was monitored until day 28 post-infection. The AnTat1.1 WT parental and *NUBM* and *NUKM* null mutant cells were used to inoculate three groups (one with WT, one with *NUBM* and one with *NUKM*) of 10-weeks old female C57BL/6J mice and monitored levels of parasitaemia in various tissues, including the ability of these parasites to invade the AT. Parasitaemia profile observed in WT reached first peak by day 5

post-infection and drop on day 6 even though it could not differentiate into stumpy form. The parasitaemia pattern with this same cell line gave a different profile when infection was done in MF1 mice strain. As shown in Figure 4.13, parasitaemia was 10^8 trypanosomes/ml by day 6 post-infection and mice had to be euthanised.

The KO clones parasitaemia depicted that of monomorphic cell line where there was rapid parasite growth by day 5 post-infection with >3 x 10^8 parasites/ ml of blood and continued increasing in parasite number without differentiating to stumpy forms (Figure 4.16). The hyperparasitaemia observed for these cell lines is the consequence of their inability to differentiate to stumpy, as shown in Section 4.2.6. *NUKM* KO cells were most virulent among the three cell lines as mice infected by these cell lines started dying by day 6 post-infection.

This study was done in collaboration with the Figueiredo laboratory in Lisbon, some of the animal experiments were carried out by that laboratory by the help of Tiago Rebelo who helped in generating some of the data in this section.

Both WT and DKO cells peaked on day 5 but parasitaemia level reduced on day 6 for WT infection. Having established the parasitaemia profile of these cell lines, organs harvested on day 6 post-infection from WT and *NUBM* infected mice were used for qPCR analysis. However, a new infection was set up for WT and *NUKM* and organs of infected mice with these cell lines were harvested on day 5 post-infection to assess the ability of these null mutant and parental cell line parasites to invade other tissues and organs apart from blood. After perfusing mice with PBS with heparin, various organs were harvested. The perfusion was done to remove all traces of blood from the organs to allow only observation of resident parasites. DNA was extracted from the samples, and parasite density quantification in the heart, liver, kidney and gonadal adipose tissue (AT) was performed by measuring parasite DNA by quantitative PCR (qPCR).

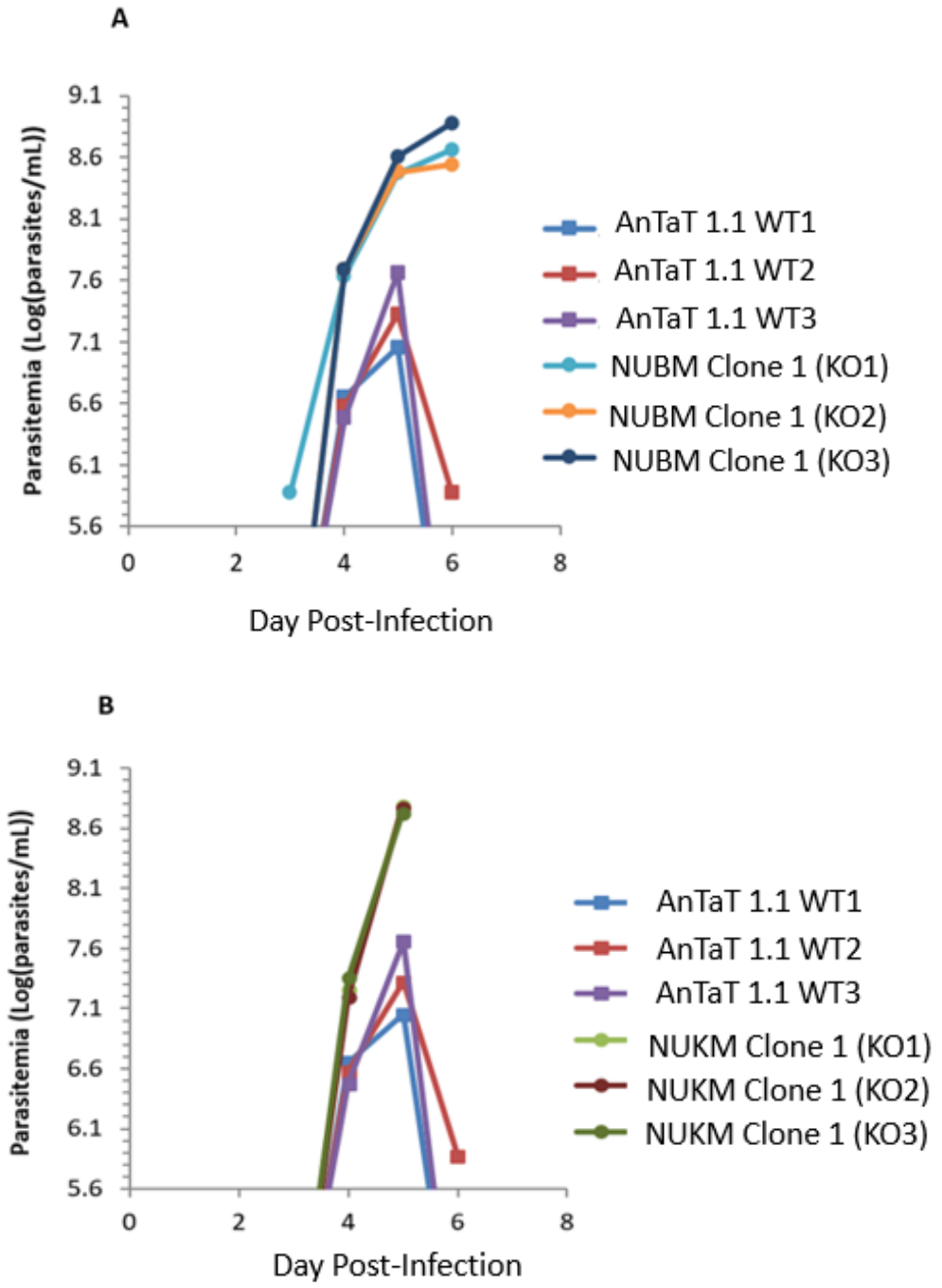

Figure 4.16 Growth of WT and *NUBM* or *NUKM* null mutant cell lines of *T. brucei* in immunocompetent C57BL/6J mice. Data presents individual infections (3 replicates) with the same WT cell line or DKO clone1.or NUBM clone 1. Panel A shows infection with *NUBM* and B show *NUKM* infection. The WT data are the same both panel A and B The parasitaemia in blood was fixed in formaldehyde solution and cells counted using Neubauer haemocytometer.

These organs were chosen because Trindade and colleagues showed an increase in parasite load in most of these organs by immunohistochemical staining (Trindade et al., 2016). High parasite density was observed in the heart, liver and kidney, respectively, with statistical significance of differences indicated by asterisks: * $p \leq 0.05$ and ** $p \leq 0.01$ p values s in the organs infected with *NUBM* KO cells compared to the WT cell infected organs (Figure 4.17), where parasitaemia in blood had dropped on the day of organ harvest. In contrast, there was no significant difference in the total parasite numbers in the gonadal AT of both WT and *NUBM* KO cells. The density of parasites per milligram of organ or tissue was calculated as a ratio of parasite gDNA versus mouse gDNA in each tissue. This was done by weighing the tissue and used calibration curve to translate qPCR signal into numbers of parasite.

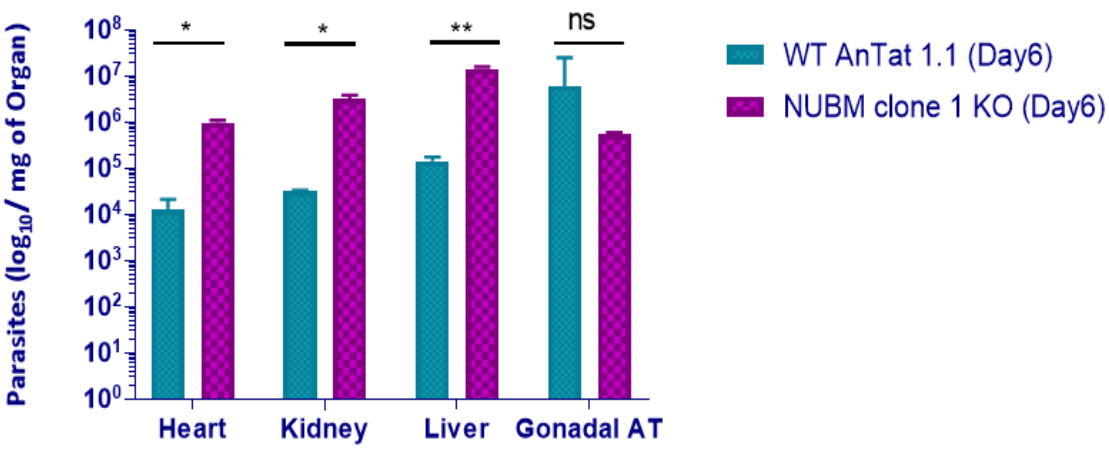

Figure 4.17 Quantification of WT and *NUBM* DKO parasite density of different organs in mice. Parasite loads in organs of C57BL/6J mice were quantified by qPCR targeting trypanosome 18S rRNA genes (converted to parasite numbers using a calibration curve) and are given as parasites (log_{10}) per mg of organ. Shown are average values from three mice per cell line, and three technical qPCR replicates per sample (n = 9) Error bars are standard error of the mean (SEM). The *NUBM* parasite load was significantly more than the one observed with WT parasite in heart with p-value of 0.01 (*). *NUBM* parasite load was higher than WT in the kidney and liver (* = p value of 0.027, ** = p value of 0.009). There was no significant difference between WT and *NUBM* parasite load in the gonadal adipose tissue.

Similarly, the parasite load in the heart, kidney and liver of mice infected with *NUKM* DKO parasites were higher compared to those infected with the WT (Figure 4.18), with statistical significance of differences indicated by asterisks: * $p \leq 0.05$ but not as high as levels observed in *NUBM* DKO samples. The *NUKM* DKO cells showed ~10-fold more parasites in heart, liver and kidney when compared to those infected with the WT cells. Interestingly, in striking contrast to what was observed for blood, heart, kidney and liver, the total parasite numbers measured in the gonadal AT was ~4-fold lower for *NUKM* DKO cells compared to WT cells (Figure 4.18). The parasite density was calculated as mentioned earlier.

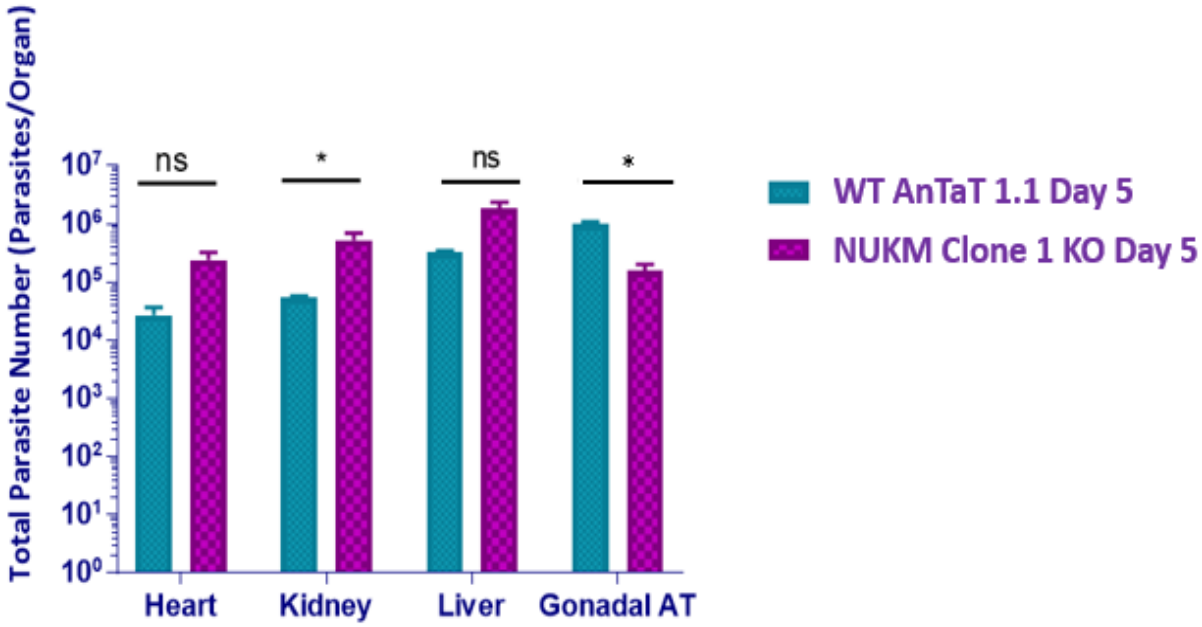

Figure 4.18 Quantification of parasite density of different organs in mice infected with either WT or *NUKM* KO cells. Parasite loads in organs of C57BL/6J mice were quantified by qPCR targeting trypanosome 18S rRNA genes (converted to parasite numbers using a calibration curve) and are given as parasites (log_{10}) per mg of organ. Shown are average values from three mice per cell line, and three technical qPCR replicates per sample (n = 9). Error bars are standard error of the mean (SEM). The *NUKM* parasite load was significantly more than the one observed with WT parasite in kidney with p-value of 0.012 (*). There was no significant difference in heart and liver infected with either WT or *NUKM* lines. *NUKM* parasite load was however, lower than WT in the gonadal AT (* = p value of 0.025).

This interesting observation of the difference in parasite numbers in gonadal AT relative to other tissues when *NUKM* DKO / *NUBM* DKO parasites were compared to WT appeared to support the hypothesis that cI activity may be important for efficient invasion of or survival in AT. It was surprising, however, that this phenotype was much more pronounced for *NUKM* null mutants than for *NUMB* null mutants, because both *NUBM* and *NUKM* are core subunits of complex cI and essential for electron transfer. Nonetheless, these observations prompted further testing to investigate if cI activity may be important for parasites to adapt to the AT environment.

4.2.10 Generation of *NUKM* add-back cell line

The increased parasite load in blood and organs by KO cells compared to WT cells could presumably be because of direct consequence of hyperparasitemia due to lack of stumpy differentiation. The gonadal AT did not show a similar increase in parasite load when *NUBM* DKO cells were compared with WT and was even lower in the gonadal AT of mice infected with *NUKM* DKO cells. WT parasites behaved differently in the Lisbon experiments compared to that conducted in Edinburgh. The parasite increased over the period of time (Figure 4.13), contrast to what was observed in Figure 4.16. The phenotype with *NUKM* null mutants was stronger, so I focused on these mutants for further analysis to test the hypothesis that cI may be important for metabolism in AT. If the hypothesis is correct, introducing a functional WT *NUKM* allele into the *NUKM* double knockout (DKO) mutant should restore the virulence. In order to generate such a cell line, the coding sequence of *NUKM* was cloned into the HindIII and BamHI sites of pHD1344tub. The NUKM gene was cloned into the pHD1344tub plasmid (Carnes et al., 2012), for ectopic constitutive *NUKM* expression from the tubulin locus.

The add-back construct was sequenced to confirm the *NUKM* insert, and this construct was used to transfect *NUKM* DKO clone 1. After selection of puromycin resistant parasites, 10 clones were analysed by PCR to test for the presence of *NUKM*. All 10 clones gave the correct

size of 612 bp for the *NUKM* gene fragment (Figure 4.19). WT AnTat1.1 cell and the *NUKM* DKO cell line served as positive and negative PCR controls, respectively.

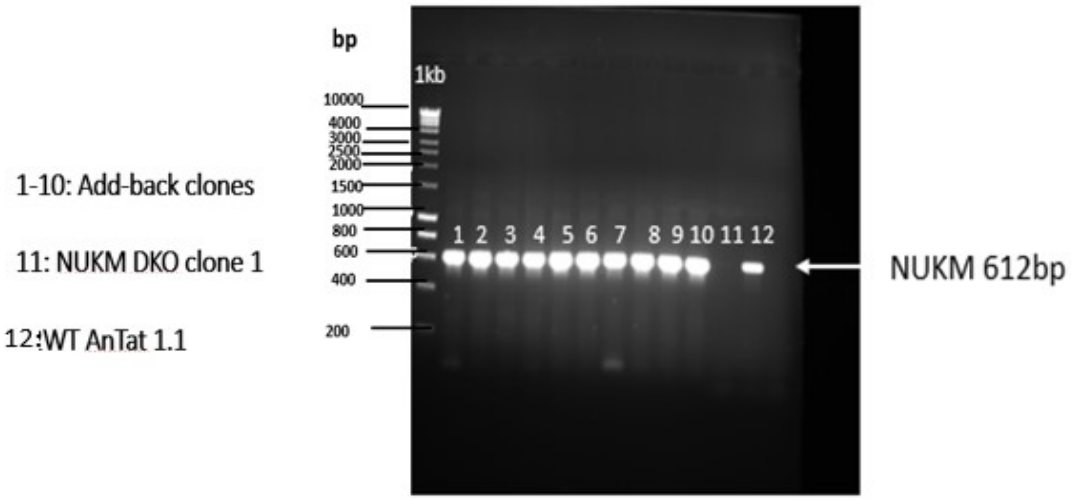

Figure 4.19 PCR confirmation of *NUKM* add-back cell lines. Ten clones selected were tested for successful introduction of the *NUKM* gene into *NUKM* DKO clone 1. DNA extracted from *NUKM* DKO cells and from AnTat1.1 WT cells was used as negative and positive control, respectively. The 1-kb ladder was used and expected size of *NUKM* gene is 612 bp.

To confirm expression of the ectopic allele, levels of *NUKM* mRNA were assessed by qRT-PCR analysis in two of the add-back clones. EATRO 1125 strains AnTat1.1 and AnTat1.1 90:13 and the parental *NUKM* DKO cell line were used as controls. As shown in Figure 4.20, *NUKM* mRNA expression in the add-back cell lines was ~10-fold higher in both add-back clones compared to the WT cell. This is presumably because the *NUKM* gene in the pHD1344-tub plasmid features a 3' UTR from actin, a constitutively expressed housekeeping gene, and because that construct recombines into the stably transcribed β tubulin locus. As expected, expression in *NUKM* DKO clone 1 was at background levels.

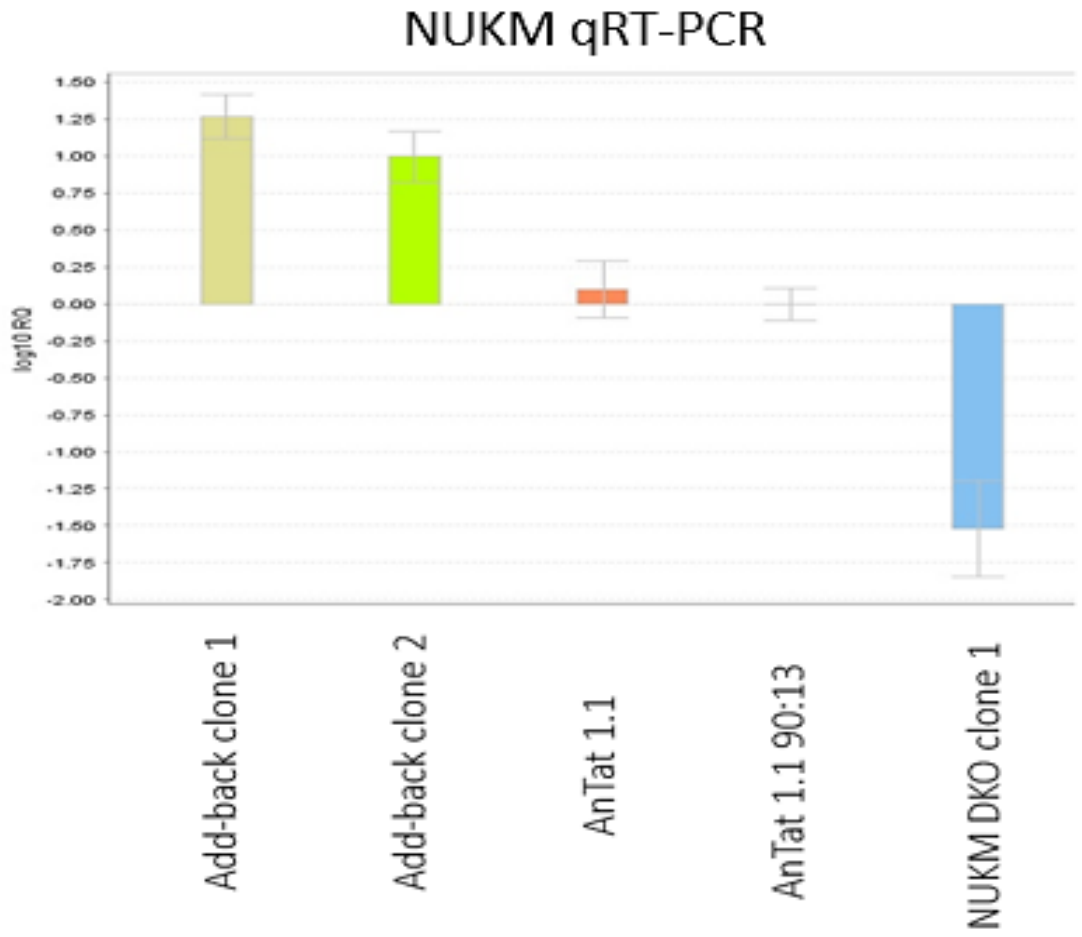

Figure 4.20. Quantitative RT-PCR with *T. brucei* cDNA for detection of NUKM. On the Y-axis is $\log_{10}$ relative quantification (RQ) plotted against the samples investigated. Three biological replicates each of sample were analysed. The levels of the NUKM mRNA were normalised with GPI8, and then all samples were normalised against WT AnTaT 1.1 90:13 as reference sample. The NUKM clone 1 was used as a negative control. Each sample was three technical replicates and -R control was included.

4.2.11 *NUKM* add-back does not restore a WT phenotype

To test whether *NUKM* add-back cell lines can rescue the hyperparasitemia, eight-week-old female C57BL/6J mice were inoculated with WT cells, two *NUKM* add-back cell lines and two *NUKM* DKO cell lines (clone 1 and clone 2 (Table 4.3). Five mice were infected per cell line.

Table 4.3. Summary of cell lines used for monitoring level of parasitaemia and mice survival following transfection.

Cell line	Number of mice	Sacrifice at day 5	Follow Survival/Parasitaemia
EATRO AnTat 1.1	5	3	2
NUKM KO Clone 1	5	3	2
NUKM KO Clone 2	5	3	2
Add-back NUKM KO Clone 1	5	3	2
Add-back NUKM KO Clone 2	5	3	2

Blood parasitaemia was assessed daily from day three post-infection. Three mice from each group were sacrificed on day five post-infection as previous experiment with KO cells were analysed on day 5 post-infection to enable comparison with previous data. Mice were perfused, and the various organs harvested, while blood parasitaemia continued to be monitored for the other two mice in each group (Figure 4.21). WT AnTat1.1 showed a normal pattern of blood parasitaemia, peaking at day six and dropping afterwards. The two different clones for both *NUKM* DKO and *NUKM* add-back were more virulent and showed hyperparasitemia. Mice infected with *NUKM* DKO cells had to be sacrificed or died between day five and day seven post-infection. *NUKM* add-back clone 1 infected mice died between day six and day seven post-infection (Figure 4.21). *NUKM* add-back clone 2 infected mice had no detectable parasites as of day five post-infection. This clone was eliminated from parasite number quantifications in the organs. However, from day 6 post-infection, mice presented with hyperparasitemia and had to be sacrificed or died.

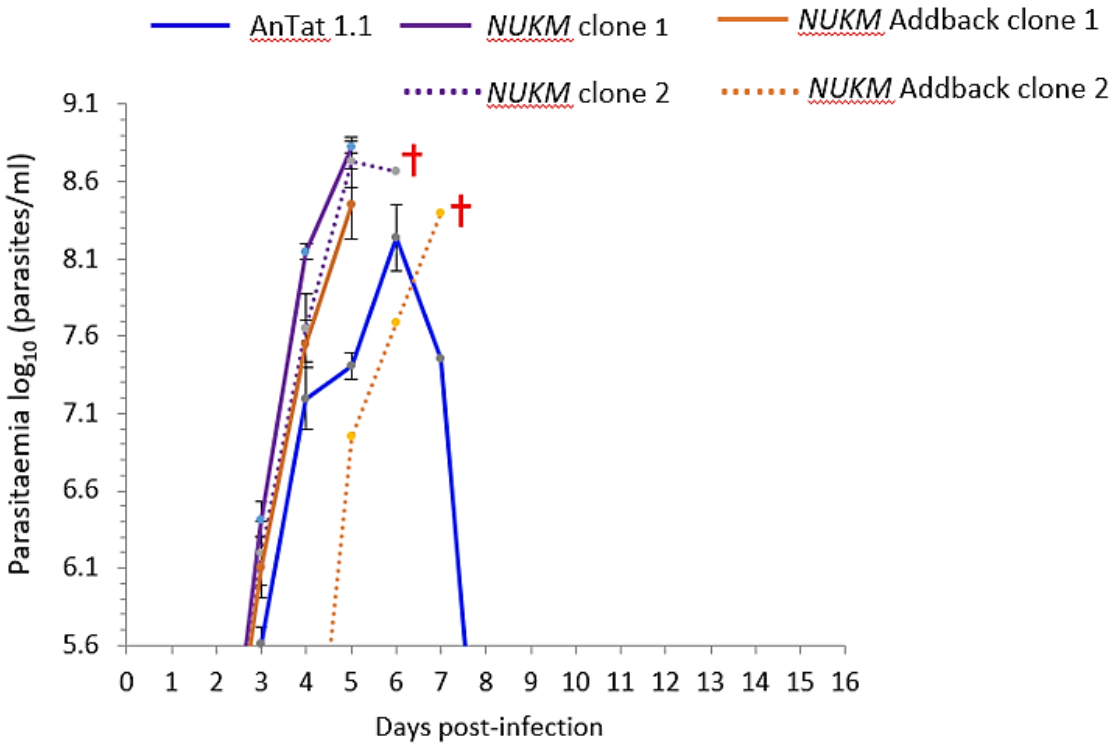

Figure 4.21. Blood parasitaemia profile of WT, NUKM DKO and NUKM add-back cell lines. The WT EATRO 1125 AnTat1.1 cell line, two NUKM DKO cell lines and two NUKM add-back cell lines were used to infect five mice each and parasite load in blood was monitored over time. WT is shown in blue, NUKM DKO clones 1 and 2 are shown in solid purple and dash lines respectively, and NUKM add-back clones 1 and 2 in solid orange and dash, respectively. The Y-axis shows the $\log_{10}$ of blood parasitaemia /ml and the X-axis represents the number of days post-infection. Three mice for each cell line were sacrificed on day 5 for parasite quantification in organs. In the two remaining mice from each group, blood parasitaemia continued to be monitored until mice had to be sacrificed because they showed signs of suffering. Despite best efforts, some mice died.

For the organ samples from day 5, parasite quantification was performed by qPCR targeting trypanosome 18S DNA from heart, kidney and gonadal AT, as previously. Unpaired t test followed by post analysis test using ANOVA showed that AnTat 1.1 had high parasite load in AT when compared the NUKM clone 1, 2 and add-back clone 10 with a p value of 0.0049 (**). The two *NUKM* DKO lines showed higher parasite numbers in heart (**= p value of 0.004). There was no significant difference in parasite density in kidney infected with either WT, NUKM clone 1, 2 or add-back clone 1 cell line. A post hoc test was performed to know which of the data points accounted for the significant difference found in the ANOVA. The

multiple comparison done on the kidney data showed no significant difference between WT in comparison with NUKM KO clones 1 and 2 nor Addback clone 1. The significant value indicated for heart was generated from WT comparison with NUKM clone 1 and 2. Finally, the significant difference obtained for gonadal AT was from WT in comparison with NUKM clone 1, clone 2 and Addback clone 1 as shown in Table 4.4. The *NUKM* add-back clone 1 showed a similar phenotype as the *NUKM* DKO clones (Figure 4.22).

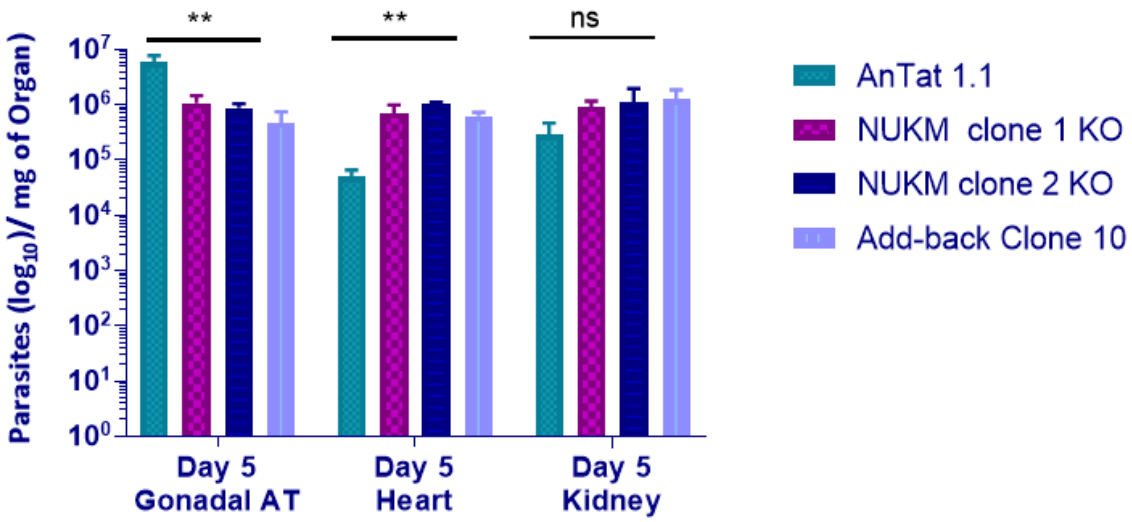

Figure 4.22. Parasite density in organs determined by qPCR. Mice were infected with WT, NUKM DKO or NUKM add-back cell lines. Parasite loads in organs of C57BL/6J mice on day 5 post-infection were quantified by qPCR targeting trypanosome 18S rRNA genes (converted to parasite numbers using a calibration curve) and are given as parasites (log_{10}) per mg of organ. Shown are average values from three mice per cell line, and three technical qPCR replicates per sample (n = 9). Error bars are standard error of the mean (SEM). Statistical significance of differences is indicated by asterisks: ** $p \leq 0.01$.

Table 4.4 A detailed information of the post hoc pairwise comparison indicating samples that accounted for significant difference found with ANOVA as illustrated in figure 4.22

Turkey's multiple comparison test

Multiple Comparison	Mean Difference	Adjusted P Value	Summary
Kidney AnTaT 1.1 vs Kidney NUKM KO 1	-606667	0.8465	ns
Kidney AnTaT 1.1 vs Kidney NUKM KO 2	-1183333	0.4362	ns
Kidney AnTaT 1.1 vs Kidney Addback 1	-1092667	0.4989	ns
Kidney NUKM KO 1 vs Kidney NUKM KO 2	-576667	0.8643	ns
Kidney NUKM KO 1 vs Kidney Addback 1	-486000	0.912	ns
Kidney NUKM KO 2 vs Kidney Addback 1	90667	0.9993	ns
Heart AnTaT 1.1 vs Heart NUKM KO 1	-738533	0.022	.
Heart AnTaT 1.1 vs Heart NUKM KO 2	-996533	0.004	..
Heart AnTaT 1.1 vs Heart Addback 1	-590867	0.0632	ns
Heart NUKM KO 1 vs Heart NUKM KO 2	-258000	0.5734	ns
Heart NUKM KO 1 vs Heart Addback 1	147667	0.8705	ns
Heart NUKM KO2 vs Heart Addback 1	405667	0.2364	ns
Gonadal AT AnTaT 1.1 vs Gonadal AT NUKM KO 1	5246000	0.0049	..
Gonadal AT AnTaT 1.1 vs Gonadal AT NUKM KO 2	5510333	0.0036	..
Gonadal AT AnTaT 1.1 vs Gonadal AT Addback 1	5851000	0.0025	..
Gonadal AT NUKM KO 1 vs Gonadal AT NUKM KO 2	264333	0.9941	ns
Gonadal AT NUKM KO 1 vs Gonadal AT Addback 1	605000	0.938	ns
Gonadal AT NUKM KO 2 vs Gonadal AT Addback 1	340667	0.9876	ns

A number of different scenarios could explain this finding. One possibility is that the phenotype observed for the *NUKM* DKO clones was unrelated to loss of *NUKM* (e.g. a random genetic change in the stumpy differentiation pathway resulting in monomorphism). Finally, the phenotype could be caused by *NUKM* deficiency, but *NUKM* expression levels in the add-back cell line might be inappropriate (for example, the qRT-PCR analysis suggested overexpression, see Figure 4.20).

4.2.12 Chronic infection in mice infected with Akinetoplastic and isogenic control cell lines

Previous studies done in Prof. Achim Schnaufer's research laboratory using mouse model infected with akinetoplastic (AK) cell line showed that the AK line pleomorphic cell line EATRO 1125 (AnTat1.1 90:13) with L262P mutation in the nuclear-encoded F_1 subunit γ permitted survival of slender bloodstream forms lacking kDNA. Nevertheless, the absence of mtDNA in these parasites causes an alteration in mitochondrial metabolism and a reduced life span (Dewar et al., 2018). The WT used here is the same parental cell line with wild type version (WTγ) introduced to generate an isogenic control (WT/WTγ). This is called WTγ for simplicity sake. To test whether cI is needed by the AK cells for longevity, AK and WTγ infected mice were subjected to chronic infection in mice. This will enable comparison of AK cells to WTγ to know whether the AK can exhibit cyclical waves of parasitaemia. The AK pleomorphic cell line under investigation has one allele of the nuclear-encoded F_1F_O-ATPase subunit γ replaced with an L262P mutation. The AK cells were generated by acriflavine treatment (Dean et al., 2013) (aAK) or spontaneously lost the kinetoplast without acriflavine treatment (AK). The survival of mice was monitored for 57 days. Female C57BL/6J mice were each inoculated with either WTγ or AK cell lines. By the 7th day following inoculation, WTγ started showing detectable parasitaemia contrary to early normal parasitaemia wave seen on day 3 post- infection in mice infected with AK cells. However, the peak was lower and cleared quickly compared to that usually observed for the AnTat 90:13 strain (Data not shown). Moreover, fluctuating parasitaemia of 10^6 to 10^7parasites/mL were detected for AK infected mice and 10^7 to 10^8 parasites/mL were also detected for WTγ infected mice, by day 12 post-infection. By day 20, parasite levels dropped to 10^5 to 10^6 parasites/mL for two of the AK infected mice while the third mice had undetectable parasitaemia. WTγ infected mice also had parasitaemia level fluctuating between 10^6 to 10^7 by day 20 post infection (Data not shown).

One out of the three mouse in the AK group died by day 30 post-infection while all the three mice in the WT group were still alive at that time. Interestingly, the remaining mice in the AK and WTγ groups demonstrated restored rates of survival until day 57 post-infection.

The parasitaemia profile observed in C57BL/6J mice by Dr Luisa Figueiredo's co-workers in Lisbon did not correlate with the observations from our study using the same cell lines. Detailed comparison between these cell lines have been conducted (Dewar et al., 2018). In their report, they showed that WTγ cell line had parasitaemia earlier (day 3) than AK cell line (day 4) and parasites declined quickly (by day 7 post- infection) than WTγ (parasitaemia dropped between day 7 and 8 post-infection). However, at peak parasitaemia, populations of both cell lines showed 80–90% stumpy cells (Dewar et al., 2018). The following factors may account for the difference and fluctuations in parasitaemia profile of C57BL/6J mice infected with either AK or WTγ cells. Firstly, the mice strain used in Lisbon is C57BL/6J and sex is female whereas the one I use in Edinburgh is MFI males. The second contributing factor could be the difference in culture medium; there is high possibility that the AK and WTγ cells have adapted to the MFI mice strain, hence further investigations with these two cell lines were carried out using the MFI mice strain.

4.2.13 *T. brucei* akinetoplastic parasite showed preference in adipose tissue when compared to other organs

The mouse infections with *NUBM* DKO and *NUKM* DKO parasites presented above (see Figure 4.17 and Figure 4.18) showed that parasitaemia in AT was similar or even lower compared to the WT control, a noteworthy contrast to the substantially higher parasite load in blood and other organs tested. Insertion of an ectopic *NUKM* gene into the *NUKM* DKO cell line did not restore the WT phenotype (see Figure 4.22), hence evidence for a potential role of cI in tropism for, or proliferation in, AT, remained inconclusive.

To obtain further experimental evidence for or against a role of in AT parasites, the AK *T. brucei* EATRO 1125 AnTat1.1 cell line expressing L262Pγ that had spontaneously lost the mitochondrial genome (Dean et al., 2013), and thus lacked all eight mitochondrially-encoded cI subunits, was used. These subunits are critical for cI function, and analysis of an AK *T. b. evansi* cell line had in fact suggested absence of cI in the absence of kDNA (Surve et al., 2012). It was therefore expected that a reduced relative parasitaemia in AT should be observed for the AK cells if cI was important in AT parasites. To test this prediction, 10-week old female MF1 mice were inoculated with either the AK *T. brucei* L262γ cell line or the otherwise isogenic cell line expressing WTγ (see Section 2.1.1). The level of parasitaemia in blood was monitored daily, and parasite load in various organs was determined by quantifying trypanosome gDNA at 7 days post-infection. The organs were harvested on day 7 post-infection due to the infection dynamics of these cell lines and parasite load in various organs was determined by quantifying trypanosome gDNA (mentioned in Section 4.2.12). The blood had a 10-fold higher parasite density in WTγ cells relative to AK L262Pγ cells on day 7 post-infection (Figure 4.23), presumably reflecting the observation that the AK cells typically show a slower rise in parasitaemia (Dewar et al., 2018).

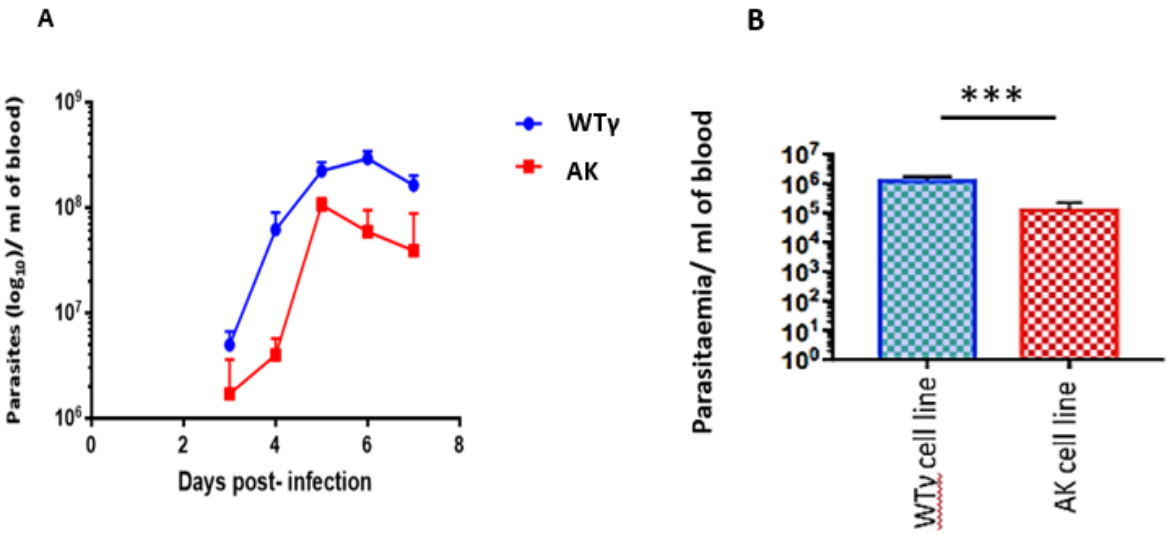

Figure 4.23 Parasitaemia level in blood of WTγ and AK L262Pγ infected mice. (A) Parasitaemia during mouse infections with WT and AK cells was measured over time. Mice were infected at day 0, with three mice infected per cell line. Error bars are standard error of the mean (SEM). Tail snips were performed every daily from day 3 post- and cell counts were estimated from blood smears. (B). Parasitaemia was determined by isolating DNA from infected mouse blood on 7 dpi and performed qPCR targeting trypanosome 18S rRNA genes.The 18S qPCR signal was converted to parasite density using a calibration curve. Shown are average values from three mice per cell line, and three technical qPCR replicates per sample (n = 9). Error bars are standard error of the mean (SEM). The WT parasite load was higher than AK parasite in blood.(*** = p value of 0.0002).

The parasite densities in solid organs were also quantified on day 7 post-infection (Figure 4.24). The data show that, with the notable exception of the gonadal AT, parasite load was lower in organs from mice infected with AK *T. brucei* relative to the control*:* heart, liver and kidney from infections with AK parasites had a 2-to 5-fold lower parasite loads compared to the control. This probably reflected the lower parasitaemia in blood.

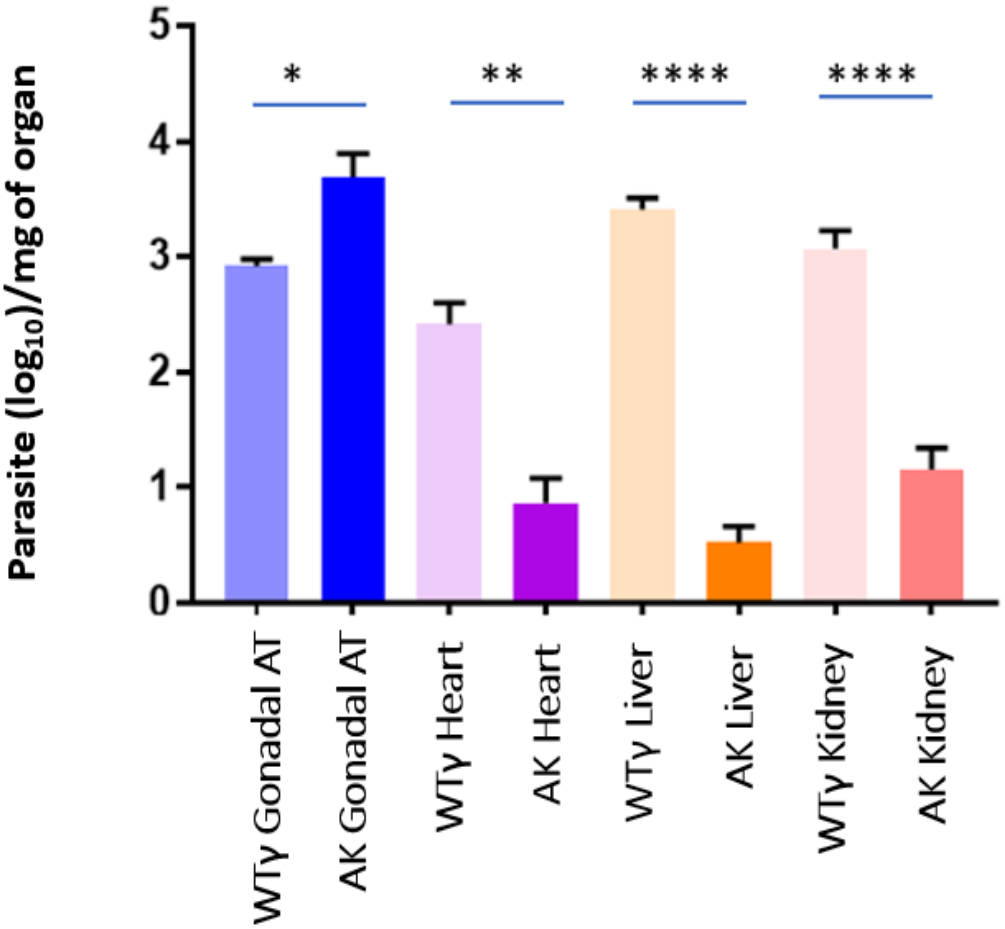

Figure 4.24 Parasite density quantification in organs from mice infected with AK and control parasites at day 7 post-infection (experiment 1). Parasite loads in gonadal AT, heart, liver and kidney of MF1 mice were quantified by qPCR targeting trypanosome 18S rRNA genes (converted to parasite numbers using a calibration curve) and are given as parasites (log_{10}) per mg of organ**.** Shown are average values from three mice per cell line, and three technical qPCR replicates per sample (n = 9). Error bars are standard error of the mean (SEM). Three biological replicates were run, and each sample had three technical replicates. The AK parasite load was significantly more important than the one observed with WTγ parasite in AT with p-value of 0.0189 (*). WTγ parasite load was higher than AK in the heart, kidney and liver (**** = p value of <0.0001, ** = p value of 0.0019).

To validate the high number of AK parasites in AT relative to WTγ, the previous experiment was repeated using different AK and WT control cell lines, also published by Dewar et al. (2018). In this case, kDNA deletion from the *T. brucei* EATRO 1125 AnTat1.1 L262Pγ cell line had been achieved by acriflavine treatment (indicated by the 'aAK' designation below). As a control, different clone of the EATRO 1125 AnTat1.1 WTγ cell line was used. Each of these two cell lines was inoculated into two 10-week old female MF1 mice. As before, blood

parasitaemia was monitored daily, and mice were sacrificed at day 7 post-infection for parasite quantification in heart, liver, kidney and AT. The organs were harvested on day 7 post-infection due to the infection dynamics of these cell lines mentioned in Section 4.2.12. Tail snips were performed daily from day 3 post infection till day 7 and cell counts were estimated from blood smears using Rapid Matching method. Parasitaemia profile for both WT and aAK shown in Figure 4.25 A. Quantification of parasite load in organs gave a similar picture as before (Figure 4.25 B). Parasite loads of aAK parasites in liver and kidney were significantly lower compared to the WT control, but significantly higher in AT. A difference to the first experiment was that parasite load in heart tissues was also slightly increased for AK parasites.

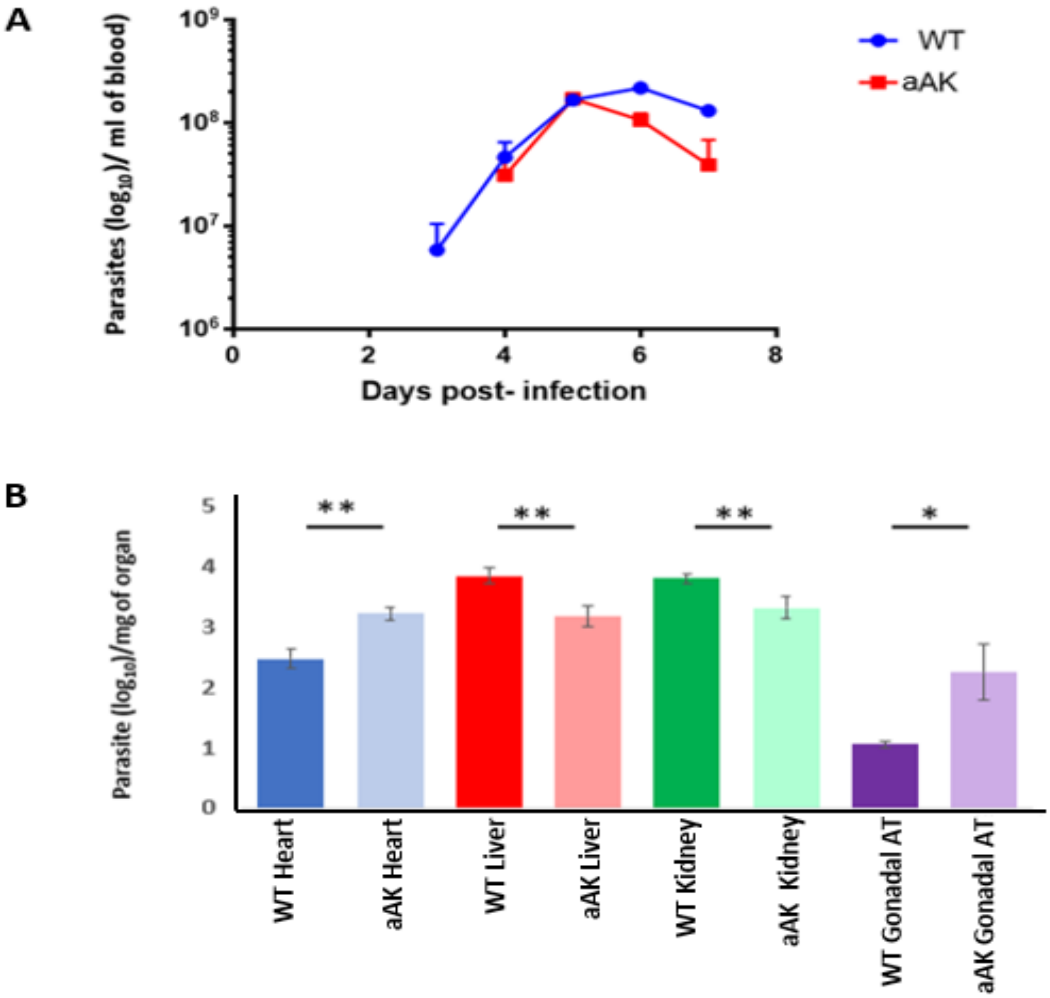

Figure 4.25 Parasite density quantification in blood and organs from mice infected with AK and control parasites (experiment 2). (A) Parasitaemia during mouse infections with WT and AK cells was measured over time. Mice were infected at day 0, with three mice infected per cell line. Error bars are standard error of the mean (SEM). Tail snips were performed every daily from day 3 post- and cell counts were estimated from blood smears. (B) Parasite loads in gonadal AT heart, liver and kidney of MF1 mice were quantified by qPCR targeting trypanosome 18S rRNA genes (converted to parasite numbers using a calibration curve) and are given as parasites (log_{10}) per mg of organ**.** Shown are average values from three mice per cell line, and three technical qPCR replicates per sample (n = 9). Error bars are standard error of the mean (SEM). The WT parasite load was significantly more than the one observed with aAK parasite in liver and kidney with p-value of 0.002 (**). The aAK parasite load was higher than WT in the heart and gonadal (** = p value of 0.004, and * = p value of 0.023) respectively.

The results show that akinetoplastic cells have a niche in adipose tissue. The results obtained with *NUBM* mutant infection showed increased parasite levels in solid organs when compared to WT infected organs. However, there was no significant difference observed in

adipose tissue infected with either WT or *NUBM*. In contrast to infection done with *NUKM* cell line, the gonadal adipose tissue had low *NUKM* parasite when compared to WT. Interestingly, when similar infection was done using akinetoplastic cell line, the parasites showed preference to gonadal adipose tissue than the other organs. The aAK parasites were able to differentiate like the WT in both in blood and in adipose tissue (Figure 4.26). On day 4 post- infection, blood smear was taken to get a control of slender forms of both cell lines. On day 7 post-infection, blood and fat were collected, and parasites isolated. The presence of slender and stumpy parasites is shown by phase contrast image and DAPI stained images show presence and absence of kinetoplast (Figure 4.26)**.**

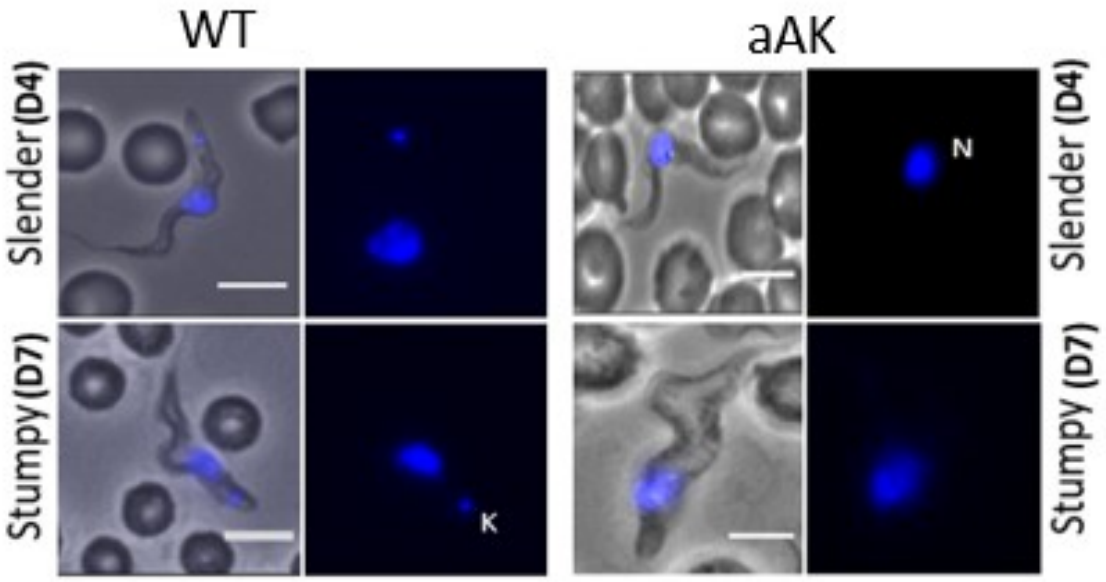

Figure 4.26 Micrographs showing parasite differentiation in blood. Images are representative of all three mice infected with either WT or aAK cells. Phase contrast DAPI images are shown. Scale bar, 5 µm is indicated on phase contrast image.

Data obtained from Figure 4.24 and Figure 4.25 showed high number of AK cells in AT when quantified by qPCR. Here, WT and aAK parasites harvested from AT on day 7 were examined for differentiated stumpy forms. Both WT and aAK cells differentiated in AT (Figure 4.27).

However, difference in experiments with *NUKM/NUBM* null mutants and that of data generated using akinetoplastic cell line, does not support an important role of cI in AT.

.

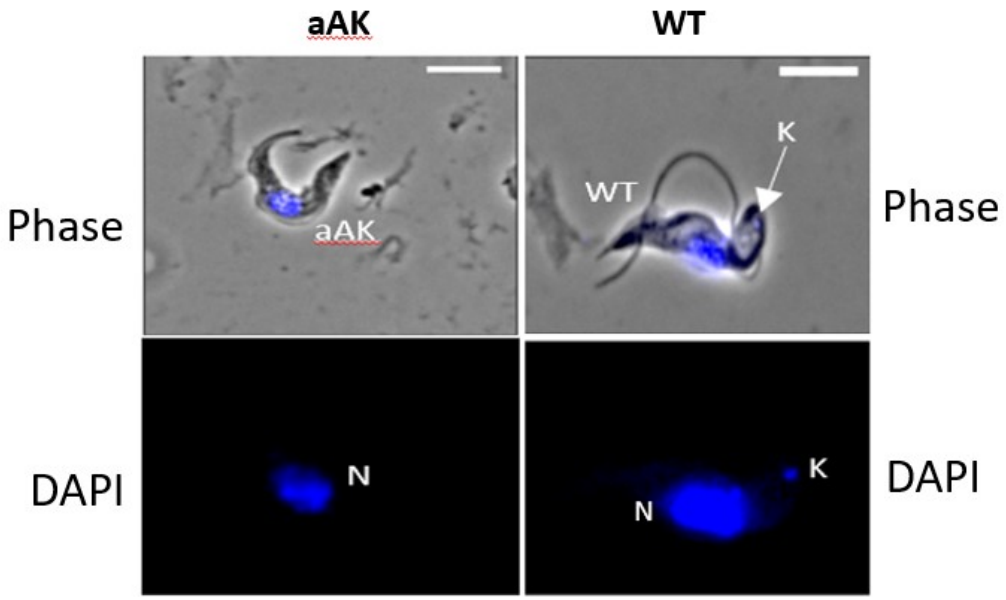

Figure 4.27. Micrographs showing presence of stumpy forms in adipose tissue. Representative images of parasites isolated on day 7 post-infection from gonadal AT from mice infected with aAK *T. brucei* (left) and WT control parasites (right). Absence or presence of kDNA was assessed by DAPI staining. Upper images show merged phase contrast and DAPI staining, and bottom images show DAPI staining alone. Scale bar, 5µm indicated on phase contrast image**.**

4.2.14 *T. brucei* akinetoplastic cell showed preference for adipose tissue

Because aAK parasite levels were higher than WT in AT in independent infections, a co-infection of WT and aAK was carried out to investigate the apparent relative preference of AK *T. brucei* for AT more directly. Already, this akinetoplastic cell line has shown to proliferate and differentiate in blood and AT (see Figure 4.26 and Figure 4.27) respectively. Three mice were inoculated with 2000 trypanosomes for both WT and aAK cells and blood

parasitaemia and morphology were monitored from day 3 post-infection. Blood smears were taken daily from day 3 to day 6 post-infection and parasitaemia was judged by eye, based on the Rapid Matching method (Herbert and Lumsden, 1976). On day 6, parasitaemia had reached 5 x 10^8 cells/ml (Figure 4.28) which was higher as compared to average parasitaemia levels of the three mice with parasite count of 1.89 x 10^8 cells/ml and 9.4 x 10^7 cells/ml observed on day 7 post-infection for WT and aAK *T. brucei*, respectively, in the single infection experiments (see Figure 4.25).

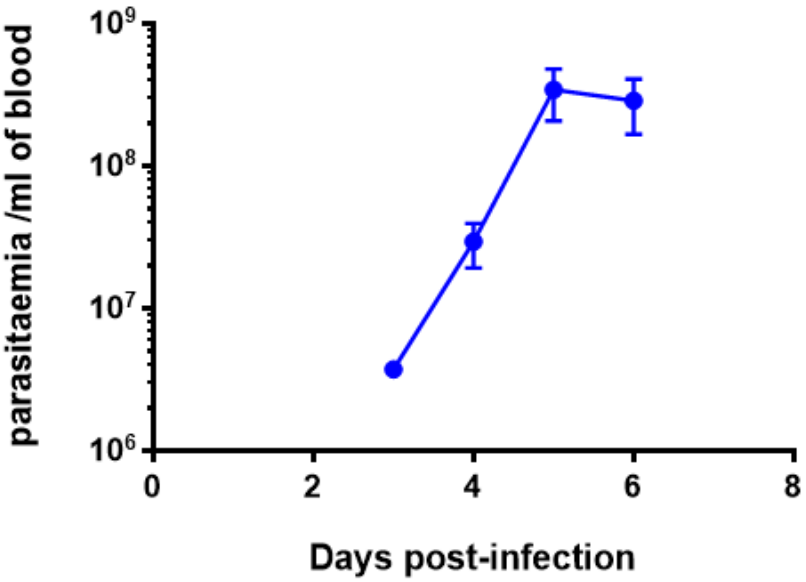

Figure 4.28 Parasiteamia in mice infected with WT and akinetoplastic *T. brucei* cell lines. Mice were infected at day 0, with both WT and akinetoplastic cell line and parasite numbers monitored from day 3 post-infcetion till day 6. Three mice were inoculated in this experiment. Error bars are standard error of the mean (SEM). Tail snips were performed day 3 to day 6 post infection and cell counts were estimated from blood smears.

At day 6, mice were sacrificed, and AT parasites collected and fixed for microscopy. From the blood smears, it was observed that WT parasites came up earlier than aAK parasites, with peaks at day 6 vs. day 5 post-infection. The morphology of selected parasites is indicated (Figure 4.29). DAPI staining showed that, as of 3 dpi, only WT cells with kinetoplast

were seen (Figures 4.29 and 4.30). The aAK parasite (without kinetoplast) were observed from 4 dpi. This observation is comparable to earlier experiments with the other akinetoplastic cell line that lost kDNA without treatment. In both experiments, the akinetoplastic cell lines showed delayed rise in parasitaemia but rapidly decreased and cleared once peak density had been reached. Similar infection dynamics have been observed between WT and akinetoplastic cells (Dewar et al., 2018).

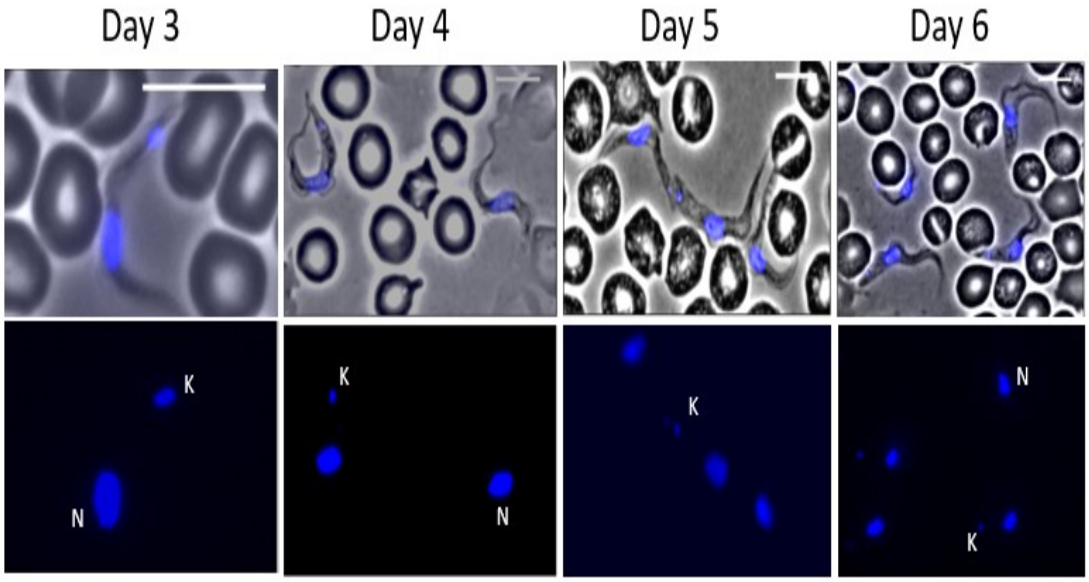

Figure 4.29 Micrographs showing differentiation of WT and aAK cells from slender to stumpy in blood from a co-infected mouse. The images are morphology of selected parasites WT and aAK cells were inoculated into mice, and blood smears were taken daily after day 3 post-infection until day 6. Exclusively slender cells were observed on days 3 and 4, with differentiation starting on day 5 and stumpy forms being observed on day 6 post-infection. Upper panels = merged phase contrast and DAPI images. Lower panels = DAPI stained image alone. Scale bar, 5µm. shown in phase contrast images.

As shown in Figure 4.29, differentiation from slender to stumpy was observed in blood from day 5 post infection with WT and aAK cell line. WT parasites were first seen on day 3 post-infection followed by aAK parasites on day 4 post-infection. Parasitaemia increased over the period of infection with WT cell lines dominating in the coinfection. The scoring was based

on DAPI stain of fixed smeared blood to differentiate AT (without kDNA) from WT (with kDNA). Parasite differentiation during infection was assessed by determining manually proportions of stumpy, intermediate, and slender cells on days 3-6 post-infection for blood and on day 6 only (the day mice were sacrificed) for AT. Differentiation was assessed based solely on morphology, as for this experiment it was not possible to use PAD1 staining (Dean et al., 2009) to confirm stumpy forms due to technical problems. The changes in parasite morphology observed for both blood and AT compartments were similar for AK and WT control *T. brucei*, and comparable to what has been described (Trindade et al., 2016).

The average percentage counts for stumpy, intermediate and slender form parasites in blood on day 6 were 80%, 7% an11%, respectively, for WT cells, and 77%, 11% and 10%, respectively, for aAK. In AT, percentages of stumpy, intermediate and slender of were 20%, 15% and 65%, respectively, for WT, and 15%, 10% and 75%, respectively, for aAK parasites (Figure 4.27) shows a representative micrograph image. The percentage count in blood and adipose tissue for the three infected mice used in the coinfection is summarised in Table 4.5.

Table 4.5 A summary of percentage score for stumpy, intermediate and slender forms of *T. brucei* in blood and adipose tissue on day 7 post infection. Infected with three replicate samples of either WT or aAK cells and parasite count monitored from day 3 post-infection.

% WT in Blood

Life cycle stages	M1	M2	M3	Mean Count	Standard Deviation
Stumpy forms	85	80	75	80	4.1
Intermediate	5	10	10	8.3	2.4
Slender forms	10	10	13	10.7	1.4

% WT in Adipose Tissue

Life cycle stages	M1	M2	M3	Mean Count	Standard Deviation
Stumpy forms	25	20	22	22	2.05
Intermediate	15	20	12	16	3.3
Slender forms	65	60	66	62	2.8

% AK in Blood

Life cycle stages	M1	M2	M3	Mean Count	Standard Deviation
Stumpy forms	75	82	75	77.3	3.3
Intermediate	15	8	15	11	2.9
Slender forms	10	10	10	11.7	2.4

% AK in Adipose Tissue

Life cycle stages	M1	M2	M3	Mean Count	Standard Deviation
Stumpy forms	15	18	15	16	1.4
Intermediate	10	14	15	13	2.2
Slender forms	75	68	70	71	2.9

Thus, on day 6, AT parasites contained a lower percentage of stumpy forms than blood, similar to what has been described in other studies for skin and gonadal AT (Capewell et al., 2016; Trindade et al., 2016). Parasitaemia in blood for WT cells increased much earlier, and to higher numbers, than for aAK cells (Figure 4.30).

Figure 4.31 shows stumpy forms of WT and aAK in coinfection experiment. The morphology of stumpy cells in adipose tissue corresponding to the morphology of stumpy forms found in blood (see Figure 4.29). However, the relative distribution of these parasites differs from blood. Parasitaemia in AT was judged by eye, based on the Rapid Matching method (Herbert and Lumsden, 1976) and, thus, parasite score count was done to score for each cell line. Figure 4.32 shows the percentage scores for either WT or aAK parasites in AT.

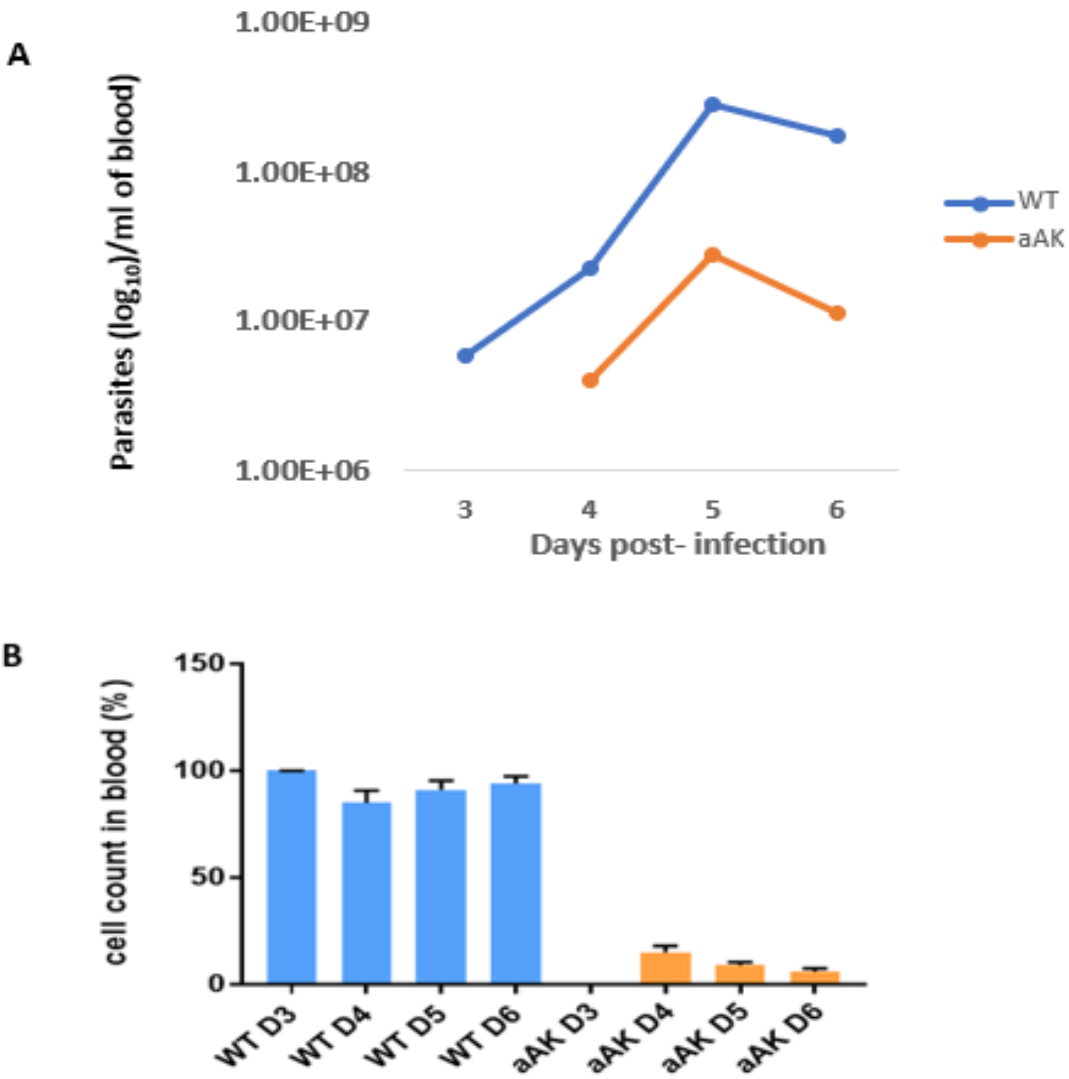

Figure 4.30 Blood parasitaemia profile of WT and aAK *T. brucei* cell lines in a coinfection experiment in mice. Mice were inoculated via IP injection with WT and aAK *T. brucei* cells and parasites collected from day 3 post infection till day 6. (A) Tail snips were performed from day 3 post-infection and cell counts estimated from blood smears. WT parasites was seen in mice by day 3 post-infection whiles aAK parasitaemia was seen from day 4 post-infection. (B) Parasites were counted by semi-quantitative scoring (Capewell et al., 2016) on the entire blood smear, and relative numbers of WT and aAK parasites are given for each day. The values represented are the means of the percentage of the cell population on day 3 to 6 of infection for WT and aAK. WT cells are in blue and aAK in orange.

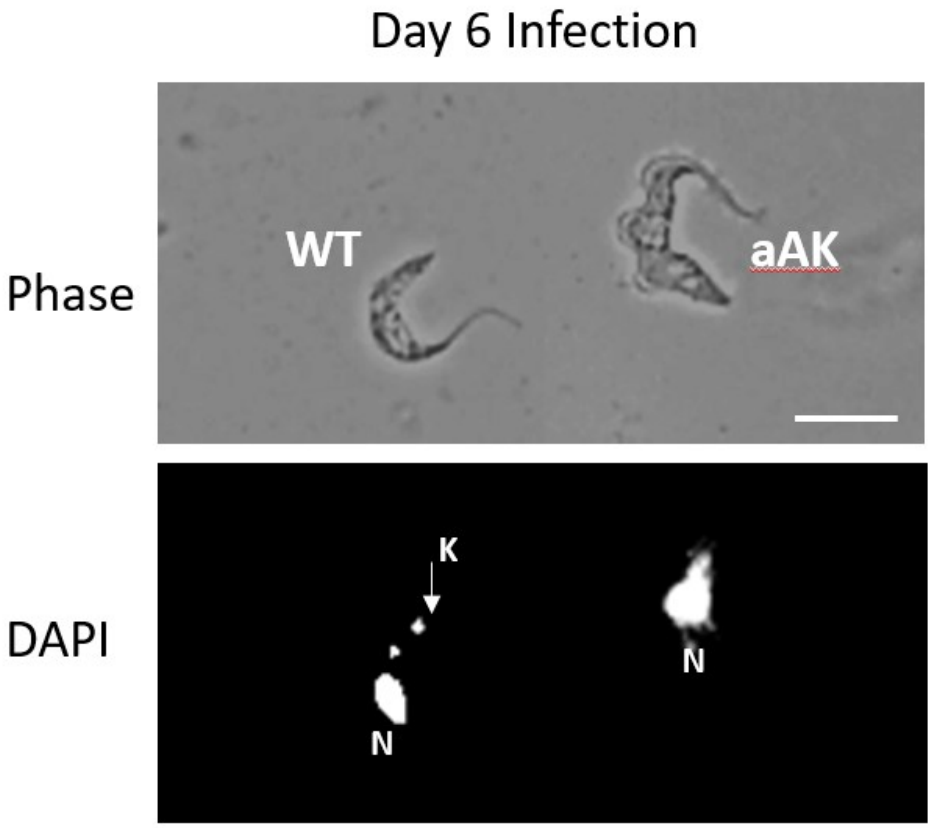

Figure 4.31 AnTat1.1 90:13 cells with and without kDNA are able to differentiate to the stumpy form in AT. Both WT and aAK cells were used to inoculate mice in a coinfection experiment, and AT parasites were harvested after mice were sacrificed on day 6 post-infection. AT parasites were fixed, and micrographs taken for phase contrast (top) and DAPI images (bottom). Arrows indicate an aAK parasite without kDNA and a WT parasite with kDNA in the DAPI stained image. Scale bar, 5 µm.

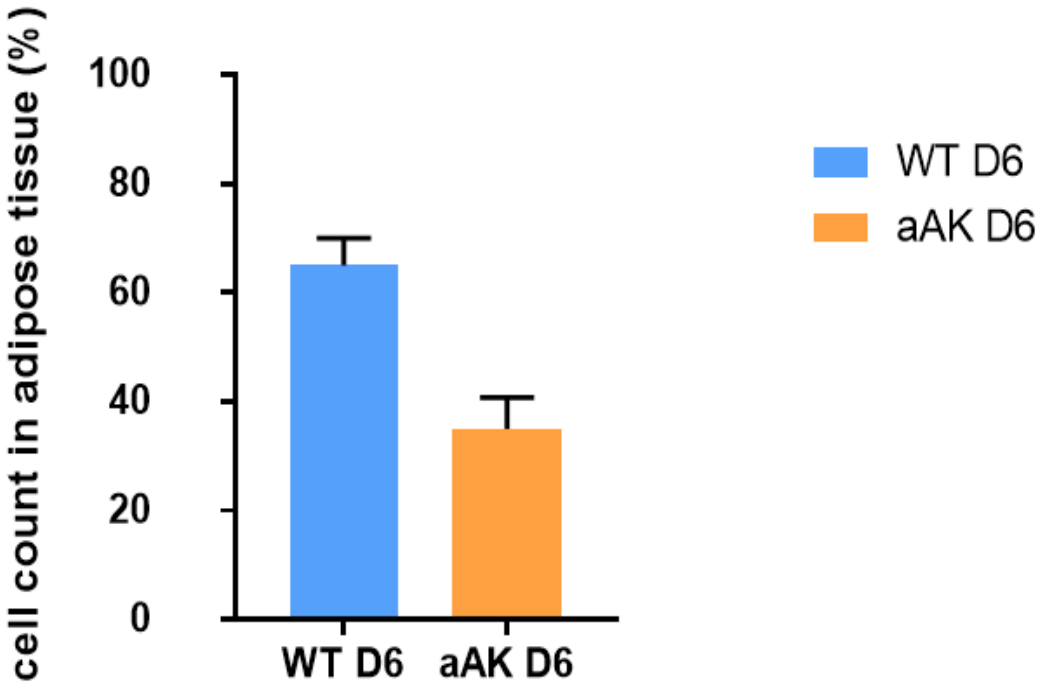

Figure 4.32 Relative levels of parasitaemia of WT and aAK *T. brucei* cells in AT of co-infected mice. Both WT and aAK cells were used to inoculate 10-week-old female MF1 mice in a coinfection experiment. AT parasites were harvested after mice were sacrificed on day 6 post infection, fixed, and DAPI stained micrographs used to count relative numbers of WT and AK parasites. The parasite count was assessed by semi-quantitative scoring. The values represented are the means of the percentage from the three infected mice. The scoring was performed blinded and independently for consistency and accuracy and also to prevent bias. Morphology was scored by three individuals, Gloria Amegatcher, Dr Mathieu Cayla and Dr Julie Wallis.

4.3 Discussion

4.3.1 *T. brucei* cI mutants and akinetoplastic cells infiltrated solid organs and adipose tissue

Organisms such as viruses (e.g. HIV) (Damouche et al., 2015), parasites (*T. brucei*) (Capewell et al., 2016; Trindade et al., 2016) and bacteria (*Mycobacterium tuberculosis*) (Neyrolles et al., 2006) have been reported to reside in adipose tissue (AT). *T. brucei* accumulates in blood, solid organs, CNS, adipose tissue and skin, and it has been recently shown that the parasites also accumulate in testis, infiltrates inflammatory cell and cause severe tissue damage which triggers strong immune response (Carvalho et al., 2018). RNA Seq analysis has shown *T. brucei* adipose tissue form parasites (ATF) to upregulate genes that encode enoyl-CoA hydratase and 3-ketoacyl-CoA thiolase which forms part of the β-oxidation cycle (Trindade et al., 2016). Additionally, acyl-CoA synthases and carnitine-acyltransferases were also upregulated (Trindade et al., 2016). This catabolic pathway produces NADH and would be expected to put more demand on systems for NADH oxidation, such as cI. Thus, we hypothesise that cI is important for efficient energy production in AT. However, this hypothesis can only be tested with cI mutants in a pleomorphic background. Unfortunately, mutants generated in this study did not differentiate in mice, so experiments performed could only look at the first peak of parasitaemia. To test this hypothesis, mice were infected with *T. brucei* parasites that are null for *NUKM* and *NUBM,* subunits expected to be critical for cI activity (Zhu et al., 2016) Here, data reported in this chapter show that *T. brucei NUBM* and *NUKM* null mutant were both found in AT during the first peak of parasitaemia. Even though both mutants were virulent, with evident hyperparasitaemia in blood and other organs, *NUBM* mutant showed no significant difference in AT parasitaemia when compared to WT cells. Interestingly, the NUKM showed less parasitaemia in AT when compared to the WT. The reasons for difference in preference for AT between the two main core subunits of cI was unknown.

The NUBM parasitaemia in AT was less than what was observed for blood and other organs which supported the decision to focus on *NUKM* mutants with stronger phenotype (Figure 4.18). A rescue experiment with an *NUKM* add-back cell line gave the same phenotype as

the *NUKM* null mutant lines, with high parasite numbers in solid organs and less in AT when compared to a control cell line (Figure 4.22). Trypanosomes have been described previously in organs such as liver, spleen, AT, kidney and heart (Kennedy, 2004; Trindade et al., 2016). However, there is no investigation on survival nor invasion of *T. brucei* parasites that are null for *NUKM* and *NUBM* subunits in these organs. In summary, the data show that *NUKM* null mutant can survive in AT and solid organs such as heart, liver and kidney.

4.3.2 *T. brucei* akinetoplastic cells show relative increase in AT over blood

Another hypothesis of this study is to test whether cI is required for full viability of stumpy cells. Could this be a consequence of upregulation of NADH producing activities in stumpy form mitochondria? The hypothesis is supported by the observation of a shorter lifespan of akinetoplastic stumpy cells observed by Dewar et al. (2018), and that inhibiting cV (another activity that depend on kDNA-encoded genes) pharmacologically did not reduce the lifespan (cIII and cIV are not expressed, so are unlikely to be responsible). Addressing this question would have required the generation of cI deficient mutants in a pleomorphic background, which was not achieved. Nonetheless, these cell lines were used to inoculate mice to test whether they can infect adipose tissue and differentiate to stumpy forms. In separate infections, the parasite load of AK cells was typically lower in blood and solid organs but higher in gonadal AT, compared to control parasites (Figure 4.24; Figure 4.25). A co-infection experiment showed WT parasites accumulating in both blood and AT during the first peak of parasitaemia, whereas AK parasites came up on day 4 post infection and dropped by day 6. The smaller number of parasites could be a competitive situation where the AK forms were losing out or were not as viable as WT. However, it was intriguing to note that the AK cell line had a relative preference for AT, with a shift from 6% of parasites in the blood being AK, to 35% in AT (Figure 4.32).

The relative accumulation of the AK cells in AT could be due to several reasons: AT serves as a protective environment to evade immune response. This is supported by recent studies where they saw no parasites in the lumen of intact epididymal ducts or seminiferous tubules of the testis, thus avoiding immune site (Carvalho et al., 2018). Another reason could be that

parasite differentiation may be delayed and the affinity for fatty tissue could be upregulating other mitochondrial NADH dehydrogenase activities, such as NDH2.

To investigate whether AK cells differentiate to stumpy forms in AT, mice were co-infected with AK and WT cells and parasitaemia and differentiation was monitored. Cells were harvested on day 6 post-infection due to increased number of parasites present in mice. However, most of the cells in the blood had differentiated to stumpy forms. Although the results obtained here showed about a fourth of number of stumpy found in blood, the morphology and percentage number of stumpy in these null mutant are similar to what has been reported (Trindade et al., 2016). The parasites in blood expressed high levels of GFP (86%) and that in fat was around 21% GFP positive. (Trindade et al., 2016). These stumpy percentages are like what was in this study, where stumpy forms found in blood was 80% on the average for WT and 75% for mutant cell line and around 18% for what was observed in AT. In summary, data obtained in this chapter present evidence that AK trypanosomes have a relative preference for AT and can differentiate into the transmission competent stumpy stage trypanosome. However, to understand the apparently preferential tropism of AK *T. brucei* parasites for AT, further studies are necessary to elucidate the mechanisms these parasites use to adapt in adipose tissue during *T. brucei* infection.

This study is the first to investigate the ability of *T. brucei* cells that are complex I deficient, either due to specific deletions of nuclear genes or due to akinetoplastidy, to reside in AT and to differentiate from the dividing slender trypanosomes to non-dividing stumpy forms in AT. Additionally, these parasites have shown to infect other solid organs.

Even though the hypothesis that cI is important in AT could not be tested due to inability to generate cI null mutant in pleomorphic background, the ability of these cell lines to reside and differentiate in AT was established.

The AK parasite showed relative increase in AT over blood when compared to WT. It is possible that these parasites are evading the immune response from the blood. This observation may be of biological relevance. *T. equiperdum,* is sexually transmitted and cause wasting disease in equines, (Desquesnes et al., 2013). It is possible that the parasites hide in the gonadal adipose tissue and male reproductive organs to contribute to the wasting seen in infected animals and transmission. The wasting may result from breakdown of fat to produce glucose to maintain glucose level for metabolism in the new environment. Here, one could speculate that these ATF parasites possess specific receptor required for crossing barriers between blood and other tight control checks to evade evading immune response and reside in other compartments. Another question to be addressed is to find out whether these parasites are evenly spread across the adipocytes or have compartmentalised niche in stromal vascular fraction (SVF) of cells. The SVF includes preadipocytes, endothelial cells, adipose tissue macrophages and fibroblasts. This will help scientist to know more about transmission of these disease and also for accurate diagnostic techniques.

Another outstanding question to be addressed is whether these ATF parasites contribute to poor drug response during treatment as the parasites are covered in the fat and resist drug action in infected organisms which affect drug distribution. This will help with the design of liposoluble compound hits to improve the poor bioavailability of drugs used to treat trypanosomiasis. Indeed, this study has shown that parasites were relatively abundant in AT compared to blood. But this raises further questions: are the parasite evading immune response and stay in AT for survival? Possibly hiding from drug action? Does residence in gonadal AT imply a potentially higher likelihood of sexual transmission? Where does the parasite have to reside in order to be sexually transmissible? Thus, the transmission dynamics of these parasites needs to be studied in detail.

4.3.3 Complex I is not important in bloodstream form *T. brucei* cells

The existence and functionality of cI in *T. brucei* have been debated (Duarte and Tomás, 2014; Opperdoes and Michels, 2008; Surve et al., 2012, 2017; Verner et al., 2011).

Recent research suggests that cI contributes around 20% of the specific NADH dehydrogenase (i.e. NADH:ubiquinone oxidoreductase) activity in procyclic *T. brucei*, even though cI seems not to be essential (Verner et al., 2011). However, BF null mutants of cI subunits showed normal growth both *in vitro* and *in vivo* (Surve et al., 2012, 2017). Here, it was not possible to test the hypothesis that cI has a role to play in stumpy forms of *T. brucei* due to unavailability of null mutants in a truly pleomorphic background.

The hypothesis is supported by the observation of a shorter lifespan of akinetoplastic stumpy cells observed by Dewar et al., (2018). Knockout of two catalytic subunits (*NUBM* and *NUKM*) of cI, using the same constructs described by Surve et al., (2012), was confirmed by PCR. Unfortunately, I was unable to generate cI null mutant as the *T. brucei* null *NUBM* and *NUKM subunits* of cI was not able to differentiate *in vivo*. The EATRO AnTat 1.1 cell line has been used to study slender to stumpy differentiation (Dejung et al., 2016; Naguleswaran et al., 2018).

However, the parental cell line and the DKO cell lines (knockout of NUBM and NUKM) were unable to differentiate in mice. Since this study was unable to generate a cI null mutant, a possible approach to consider is the use of CRISPR Cas9 targeted gene method. The gene disruption of *NUBM* or *NUKM* could be achieved by using Cas9-based approach in pleomorphic *T. brucei* to generate cI null mutants. This approach of using inducible cas9 and guide RNAs is efficient, less time consuming and null mutant clones can be generated in a single transfection without selectable markers (Rico et al., 2018).

The data presented in this thesis confirmed that the EATRO 1125 AnTat1.1 strain with *NUBM* and *NUKM* knockouts differentiated to stumpy forms *in vitro* in methylcellulose and expressed PAD1. My data also showed that these methylcellulose differentiated stumpy underwent further differentiation to generate procyclic, which expressed EP, a differentiation marker of late stage procyclic (Acosta-Serrano et al., 2001). Similarly, the use

of methylcellulose to generate stumpy cells *in vitro* has been confirmed (Naguleswaran et al., 2018). Their study validated the use of cultured bloodstream as a substitute for animal-derived parasites using RNA-Seq analysis performed on biological replicates of culture-derived bloodstream form and early and late procyclic of *T. brucei*. Their datasets expression profiles confirmed that genes known to be stage-regulated in the animal and insect hosts were also regulated in culture derived cells.

As shown in Figure 4.11, *NUBM* and *NUKM* null mutant stumpy-like cells generated *in vitro* and induced for differentiation to PF revealed high expression of EP. Analysis of the growth profiles demonstrated that procyclic null mutants grew slightly slower compared with the parental control cell line. Under the same conditions, the WT cells differentiated to PF continued to grow robustly, whereas growth was slower in procyclic *NUBM* null mutants. The two independent *NUBM* null mutant procyclic clones showed similar growth profiles during the adaptation period.

Ultimately, the growth profiles indicate that the absence of cI activity in the *NUBM* null mutant affected growth in the procyclic stage. A second attempt to generate *NUBM* and *NUKM* null mutants used another pleomorphic cell line (Markus Engstler and Boshart, 2004) that was confirmed to efficiently differentiate into stumpy forms in mice. Unfortunately, only SKO cells could be generated in the time permitted for this project, and these cells had lost pleomorphism.

In MF1 mice, all cell lines (null mutants and parental) were largely monomorphic and virulent, precluding the study of any potential effects on differentiation efficiency or stumpy longevity. Since mutants did not differentiate in mice, the first peak of parasitaemia was considered in experiment with *NUBM* and *NUKM* mutant lines, which posed limitation to this study. One possible explanation could be that the maintenance of pleomorphism renders the deletion of the cI impossible. Thus, cI is essential in pleomorphic cells and probably for stumpy forms. This work shows that knockout *NUBM* and *NUKM* genes in the parental cell line was not fully pleomorphic in mice. However, these DKO cells were capable of differentiating to stumpy forms in methylcellulose. Finally, *NUBM* null mutant differentiated procyclic exhibited a slower growth than WT procyclic. Further work is

suggested to ascertain a functional role for cI in this null mutant cell. These could include biochemical and metabolic analyses to support the phenotypic growth defect that was observed.

4.4 Outlook

This study is the first to investigate the effects of mitochondrial dysfunction on nuclear gene expression. The transcriptome of wild type and akinetoplastic cell lines of *T. brucei* changes during differentiation from slender to stumpy forms was investigated. Transcripts enriched in slender and stumpy stage forms were identified. A novelty, however, was the downregulation of some hypothetical proteins in WTγ, which were much less expressed in AK cells compared to WTγ. The RNA-Seq result suggests that the absence of the mitochondrial genome has a limited effect on the levels of nuclearly encoded messenger RNA needed to make proteins in bloodstream stage of *T. brucei.* A future work on RNA-Seq analysis of transcriptome comparison between akinetoplastic procyclic and WT *T. brucei* within the first few hours after inducing differentiation will provide more information on possible changes in gene expression between stumpy and procyclic forms of these cells. Since akinetoplastic procyclic forms are not viable (Caroline's thesis), one can only check cells within 48 hr of differentiation.

This study is the first to investigate the ability of *T. brucei* cI deficient cells - obtained either through deletion of specific nuclearly encoded core cI genes or via loss of kDNA to reside and differentiate from the dividing slender trypanosomes to non-dividing stumpy forms in AT. Additionally, these parasites have been shown to infect other solid organs. Though the AK cell lines have shown affinity for fatty tissue, this experiment must be repeated as the available data is not enough to make a conclusion. It would be ideal to confirm whether the preference for fat is a common feature of this cell line and other *Trypanosoma species*. The *NUBM* and *NUKM* mutants however did not show any preference for AT. In C57 mice, differences with regard to monomorphism/pleomorphism were observed between

NUBM/NUKM mutants and parental cell line. The infection profile with the parental cell line followed progressive waves of parasitaemia (MacGregor et al., 2011).

The *NUBM* and *NUKM* mutants however were virulent with hyperparasitaemia. The hypervirulent nature of these mutants may be due to the mutation caused by deleting these subunits of cI. Here, one could speculate that these ATF parasites possess specific receptor required for crossing barriers between blood and other tight control checks to evade evading immune response and reside in other compartments. It is necessary to investigate in depth the selective advantage of these parasites to reside in adipose tissue as this tropism may contribute to treatment failure in infected organisms, since the drugs of choice for trypanosomiasis are not liposoluble.

Inevitably, this work leads on to questions that remain about the role of cI in the metabolism of ATF trypanosomes and as to whether it is important for longevity in AK cells of *T. brucei*. The data generated in this study does not support the hypothesis that cI is important for metabolism in AT. Thus, the phenotype observed in *NUBM* and *NUKM* mutant cells is not attributed to lack of complex I. In regard to the relative abundance of AK parasites in AT, a number of questions arose from this study. Does residence in gonadal AT imply a potentially higher likelihood of sexual transmission? Where does the parasite have to reside in order to be sexually transmissible? Could this influence the design of liposoluble drugs in the future?

One of the main questions is why the lack of kDNA lead to preferential tropism which is different from WT? A metabolomics analysis of the AK and WT will give some answers to this question. Is it also possible that these ATF parasites are easily eliminated in blood and therefore are protected in the adipose tissue? A possible approach to investigate this further is by comparing the immune response upon infection in each tissue by FACS using antibodies against different cell types and /or by immune-histology.

5 Appendices

5.1 Appendix A: List of primers in material and methods

Table 5.1 Primers used in this study

PRIMER NAME	SEQUENCE
qPCR GPI8_FWD	5' CGAAGCGCATTTGGATAGC 3'
qPCR GPI8_REV	5' AGCGCGTGATGACAGTGAAG 3'
COX6 FWD	5' GAAGCGTGCTCTAGGACATT 3'
COX6 REV	5' CCCTTGCGGTTTGTCTTTAC 3'
qPCR UBP1 FWD	5' GGGTCAAGTGAATCAAGAACCC 3'
qPCR UBP1 REV	5' CCGAAGCGCTCAAACAACTG 3'
qPCR UBP2 FWD	5' CAACAACATTATATGATG 3'
qPCR UBP2 REV	5' TTACTGACGGGATATCGGA 3'
NUKM qPCR FWD	5' ATTGCAGTATGCACAAATGACTTT 3'
NUKM qPCR REV	5' ACAATACCAAAACGATCCAAATC 3'
ADDBACK NUKM FWD	5' TTCACAAGCTTATGCTTCGTCGCA 3'
ADDBACK NUKM REV	5' TGGGCAGGATCCATCTCGAACAGAA 3'
ESAG9 FWD	5' GATCAGAGAGGGTTGGAATCTG 3'
ESAG9 REV	5' CTGTGGCATGATCTCCTGAA 3'
NUBM FWD	5' AGCTTATGCTCCGGCGTGTGGGTTTTCTTT 3'
NUBM REV	5' CGTTCCAATTCCGCACGATCTTTCCGTCC 3'
NUKM FWD	5' ATGCAAGCTTATGCTTCGTCGCACGTCG 3'
NUKM REV	5' GCATGGATCCATCTCGAACAGAATACTTTTG 3'
NUBM 5’ FWD	5' ATAGCGGCCGCGTTTTGTTGTGCGGGACGAA 3'
NUBM 5’ REV	5' ATAACGCGTCTCGAGCTACACACAAGGTTCAATTTGA 3'
NUBM 3’ FWD	5' ATATCTAGAATTTAAATGGTGGTGGTGTAGTATTGAA 3'
NUBM 3’ REV	5' ATAAGGCCTGCGGCCGCCGGAAGTCAGCGTTAAGTTA 3'
NUKM 5’ FWD	5' ATAGCGGCCGCCGGCATTTCTTCGAGGCAGT 3'
NUKM 5’ REV	5' ATAACGCGTCTCGAGTGCAAACTATTTATCTATCCTCTTC 3'
NUKM 3’ FWD	5' ATATCTAGAATTTAAATGAATCATGGTACAATAGGAGTTTCT 3'
NUKM 3’ REV	5' ATAAGGCCTGCGGCCGCGTTGCGACCGTTACGTTTGA 3'
M13 FWD	5' GTAAAACGACGGCCAGT 3'
M13 REV	5' CAGGAAACAGCTATGAC 3'
PHD1344 FWD	5' TTCACCCTCATGTTCCGTCG 3'
PHD1344 REV	5' GAGTTCTTGCAGCTCGGTGA 3'
PLASMID INSERT 5' end NUKM DISTAL	5' GAATACATATTTGTTATTGATTTA 3'
PLASMID INSERT 3' end NUKM DISTAL	5' CTACTTGCAGTTAAGAAATAAATG 3'

PAD1 FWD	5' GACCAAAGGAACCTTCTTCCT 3'
PAD1 REV	5' CACTGGCTCCCCTAAGCT 3'
ATP synthase FWD	5' CGGCGGCCGCATGTCAGGTAAACTTCGTCTTTACAAAG 3'
ATP synthase REV	5' ATAGGATCCCTACTTGGTTACTGCCCCTTCCCAG 3'
qPCR PNT1 FWD	5' CACCGCGGGAAACACATAAT 3'
qPCR PNT1 REV	5' AACGACACGGTGGAATAGGT 3'
qPCR HYP 6430 FWD	5' TGGAAGTTGGAGCCGTTAGT 3'
qPCR HYP 6430 REV	5' ATTTGTCCACGCAAGAACCC 3'
qPCR HYP 8340 FWD	5' TCATTCTTCCCGAGATGCGA 3'
qPCR HYP 8340 REV	5' TCCTTCCTTCCTTCCCTTGG 3'
TRYPS 18S FWD	5’ ACGGAATGGCACCACAAGAC 3’
TRYPS 18S REV	5’ GTCCGTTGACGGAATCAACC 3’
5' INT NUBM	5' CCCGAGCTAACGCAGCAGAT 3'
PLASMID T7RNAP NUBM	5' TTCGTTCTTAGCGATGTTAATC 3'
3' INT NUBM	5' AGAACGCGGCTACAATTAAT 3'
PLASMID NEO NUBM	5' CGCAGCGCATCGCCTTCTAT 3'
5' INT NUKM	5' CTCGTCACGGCCGCTACCTG 3'
PLASMID T7RNAP NUKM	5' TTCGTTCTTAGCGATGTTAATC 3'
3' INT. NUKM	5' CATACACATACGATTTAG 3'
PLASMID NEO. NUKM	5' GAGTTCTTCTGAGCGGGA 3'

5.2 Appendix B: Plasmids used in this study

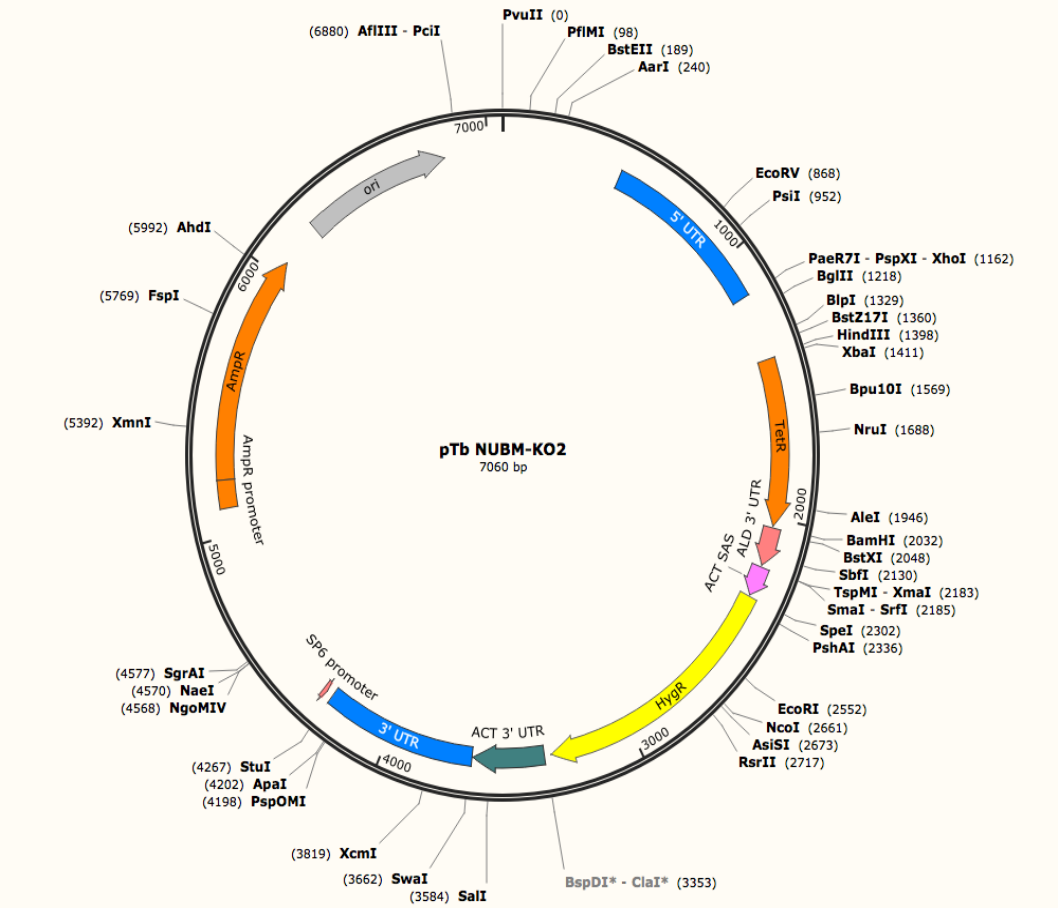

Figure 5.1 A plasmid map showing pLew90 with ampicillin as bacterial resistance with hygromycin selectable marker. Tet repressor is driven by 10% T7 promoter with target locus of tubulin. This plasmid served as the backbone to generate the knockout construct lacking cI subunit.

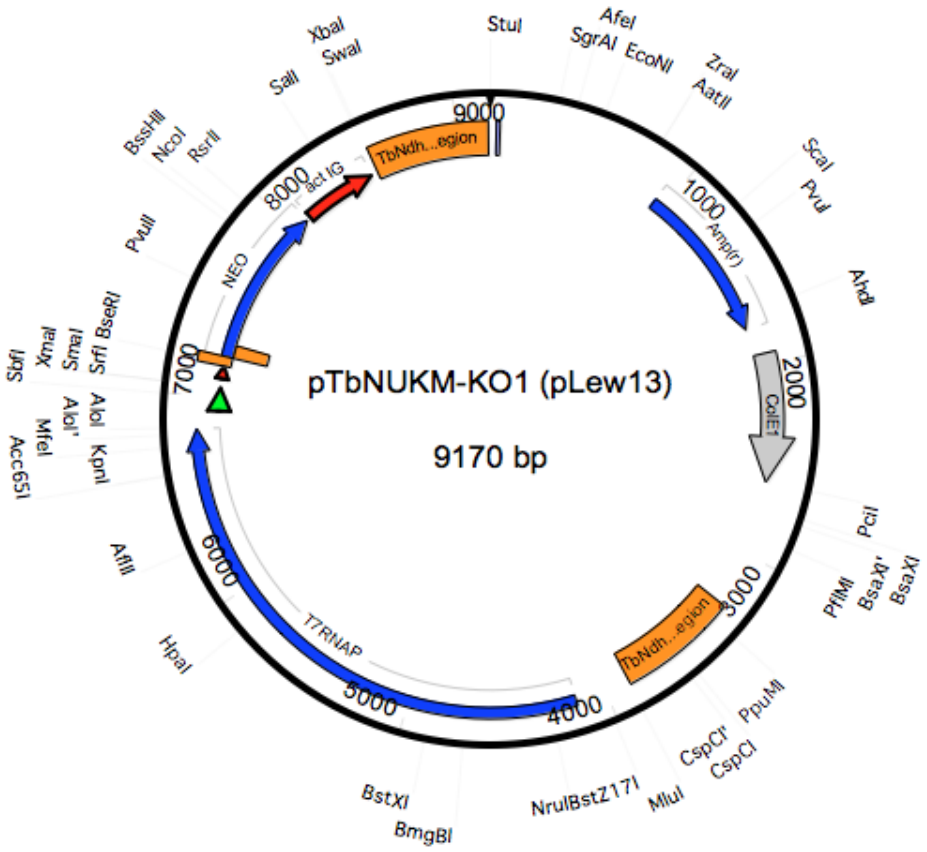

Figure 5.2 The pLew13 vector with T7 RNA polymerase and neomycin gene. The bacterial resistance is ampicillin and the target locus is tubulin. This plasmid served as the backbone to generate the knockout construct lacking cI subunits.

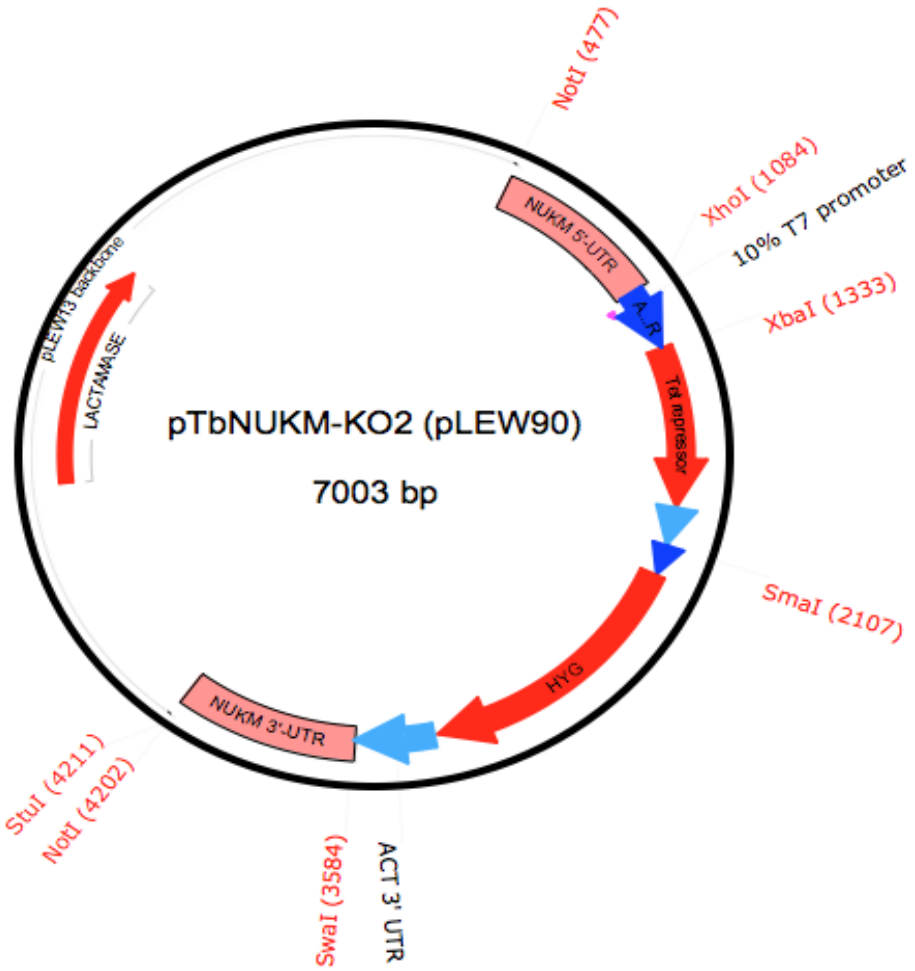

Figure 5.3 The plasmid map of pLew90 with ampicillin as bacterial resistance with hygromycin selectable marker. Tet repressor is driven by 10% T7 promoter with target locus of tubulin. This plasmid served as the backbone to generate the knockout construct lacking cI subunits.

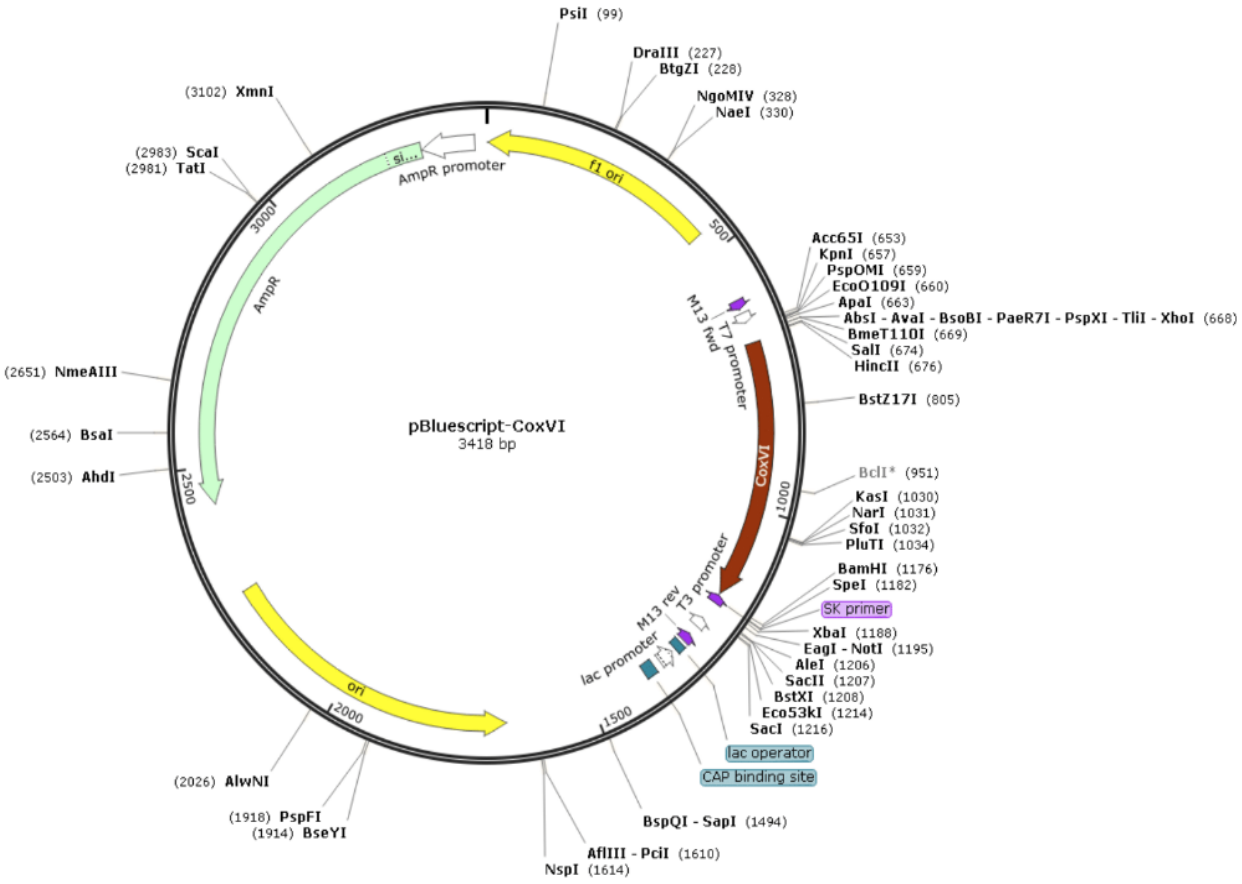

Figure 5.4 This is a pBluescript sk+ plasmid with *COXVI* coding sequence. The CDS was inserted within the multiple cloning site flanked by M13 forward and reverse primers. The PCR product of *COXVI* was then used to riboprobe for Northern Blot analysis.

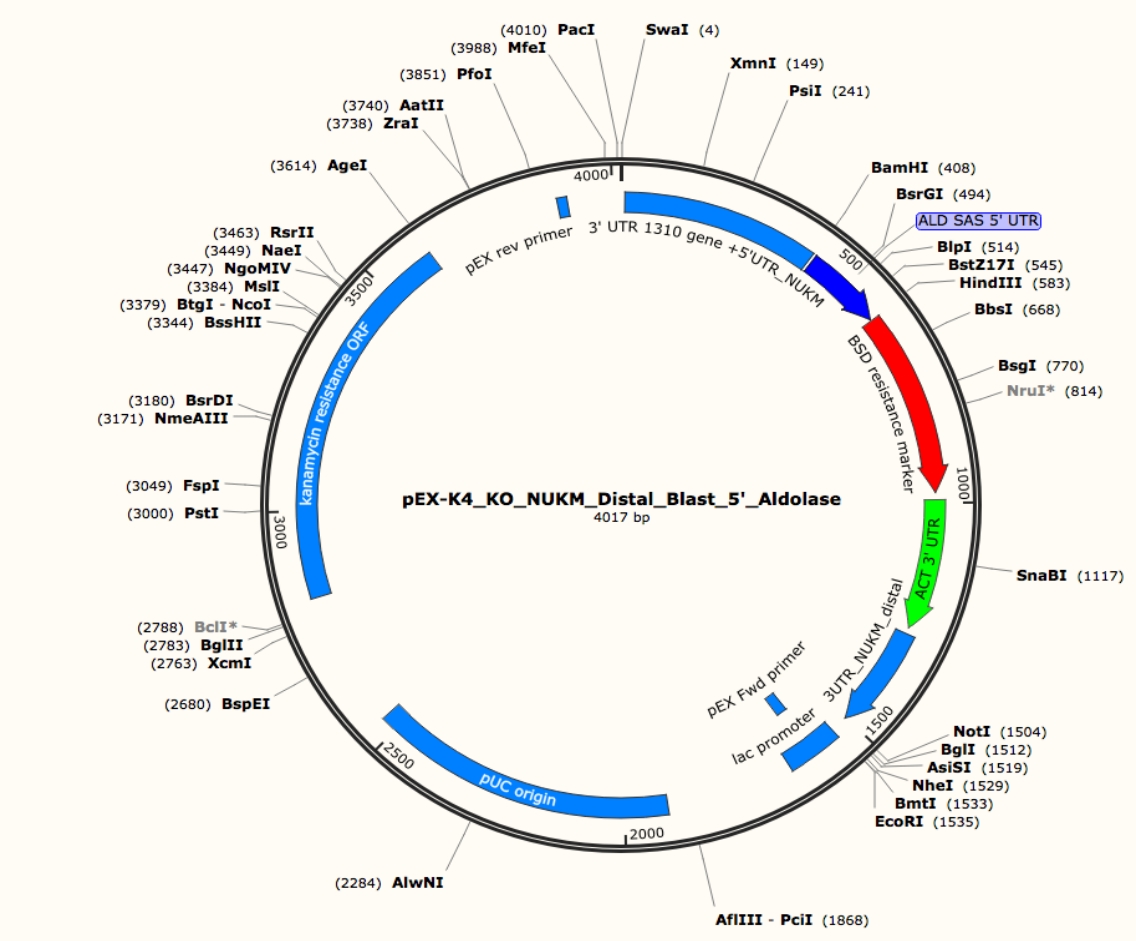

Figure 5.5 This pEX-K4 is a synthetic plasmid used for deleting complex I subunit, NUKM in *T. brucei* cell line. The selectable marker is kanamycin**.** The 5' and 3' UTR of NUKM selected were distant from the gene. The designed insert was cloned into the multiple cloning site.

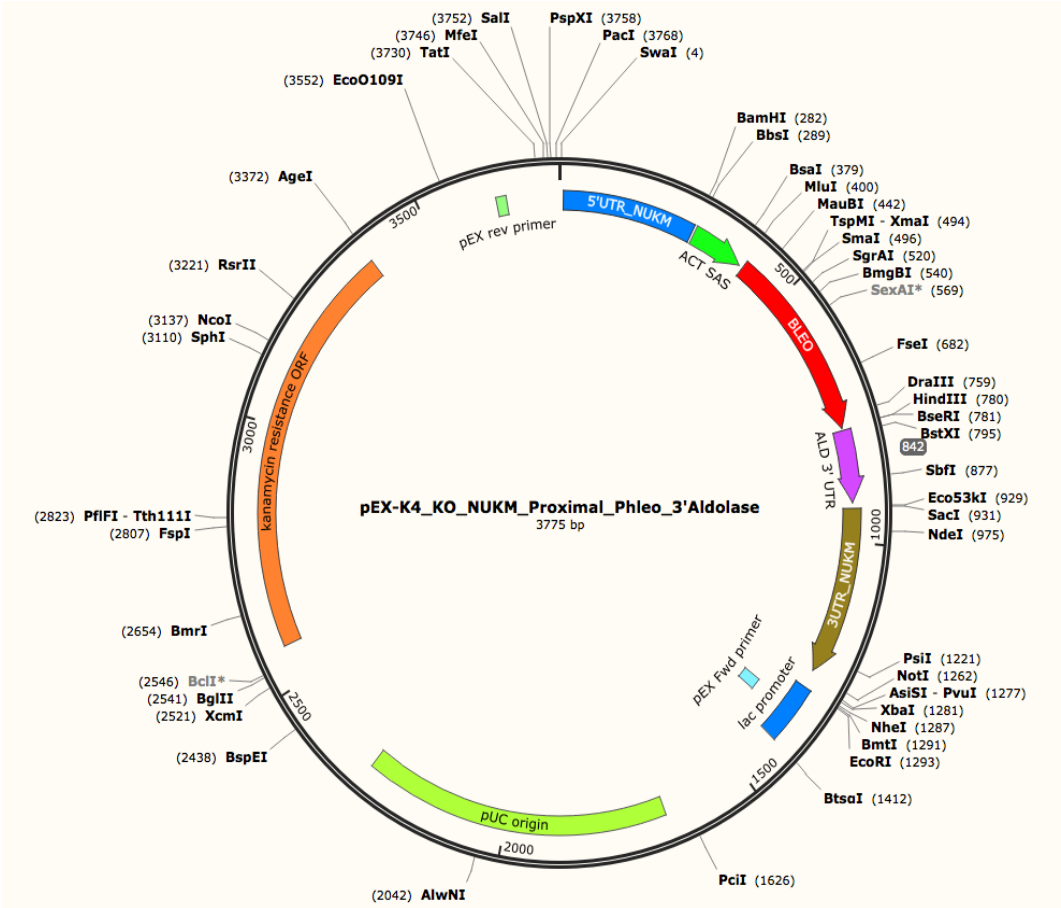

Figure 5.6 The pEX-K4 is a synthetic plasmid used for deleting complex I subunit, *NUKM* in *T. brucei* cell line. The selectable marker is kanamycin. The 5' and 3' UTR of *NUKM* selected were close to the coding sequence of the gene. The designed insert was cloned into the multiple cloning site.

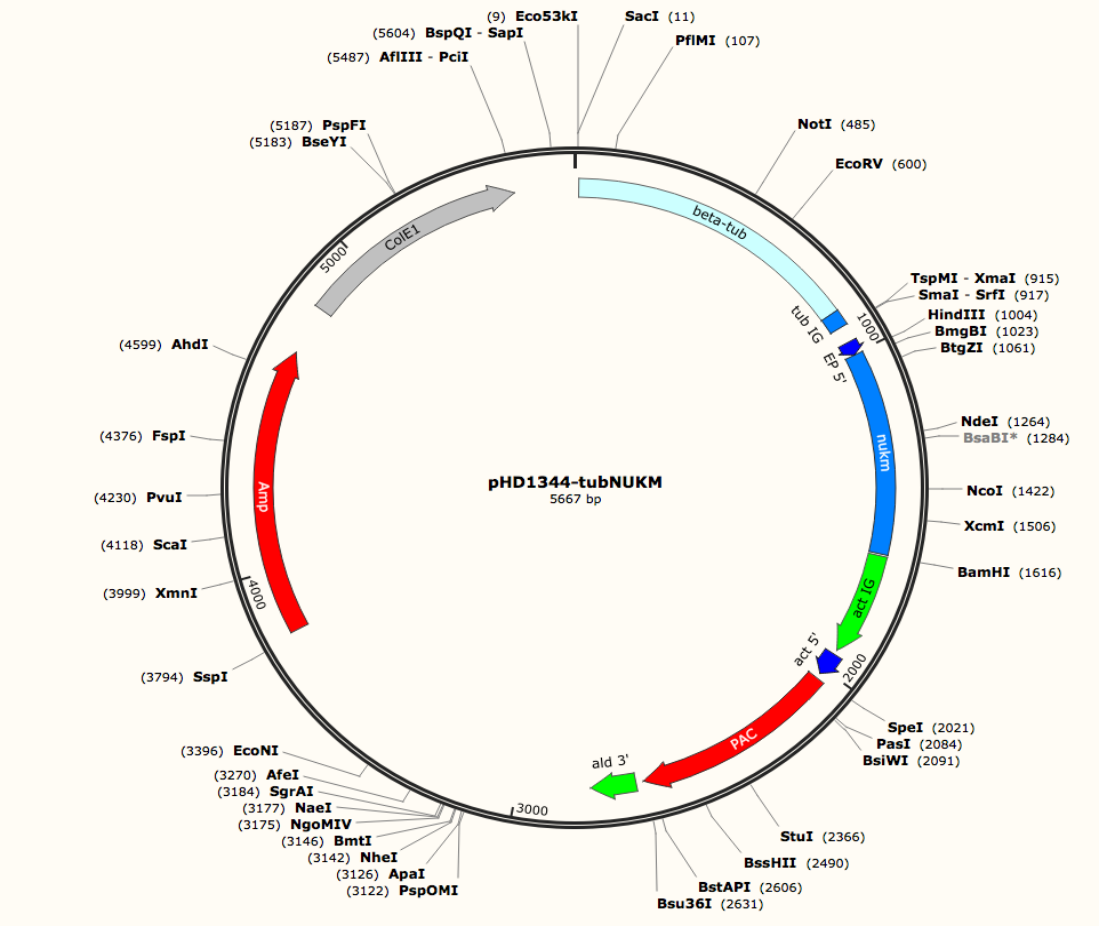

Figure 5.7 A pHD1344 plasmid with NUKM coding sequence replacing the CAT reporter gene. The PCR product NUKM was cloned into pHD1344 plasmid with puromycin resistance (PAC) selectable marker and allowed for constitutive expression from the β-tubulin locus.

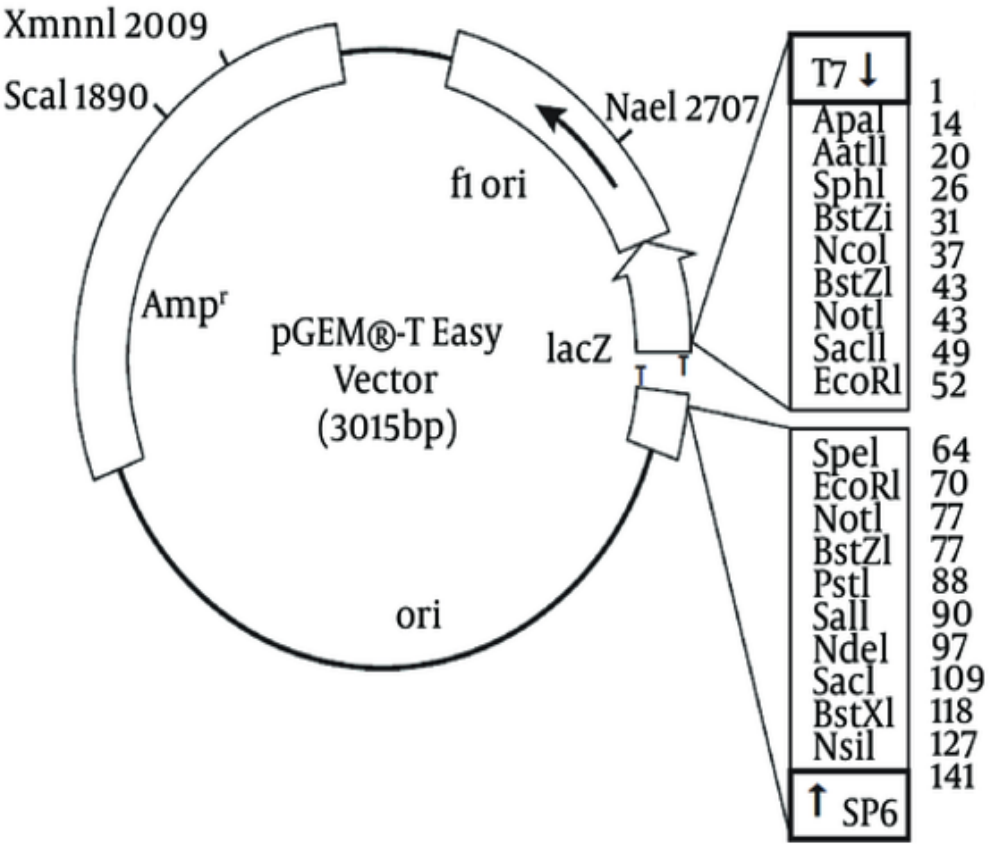

F**igure 5.7 The pGEM®-T Easy Vector Systems was used to cloning.** PCR products into multiple cloning site (MCS) and transformed cells were selected and used for subsequent experiments.

5.3 Appendix C: Immunofluorescence staining for PAD1 detection in *T. brucei* bloodstream forms

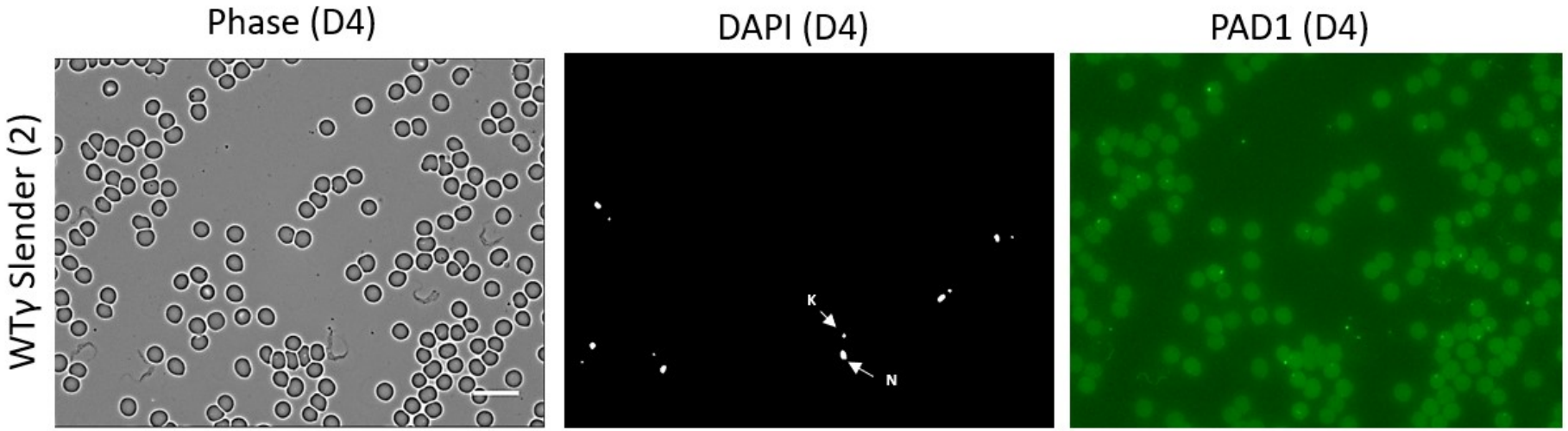

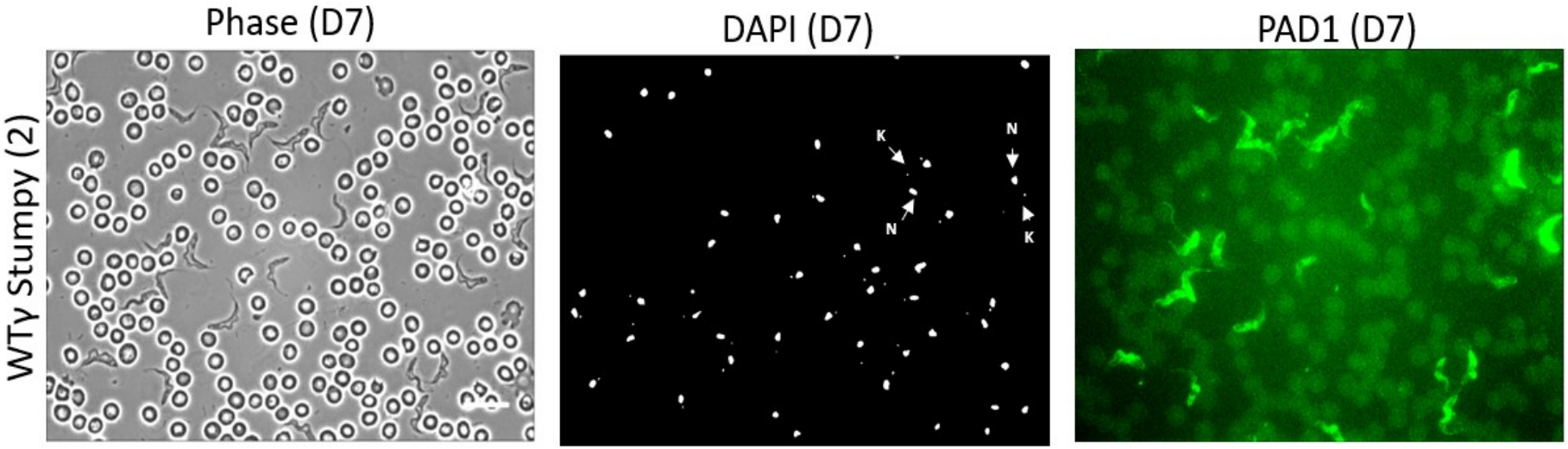
Phase (D7)
DAPI (D7)
PAD1 (D7)
WTγ Stumpy (2)
K
N
N
K

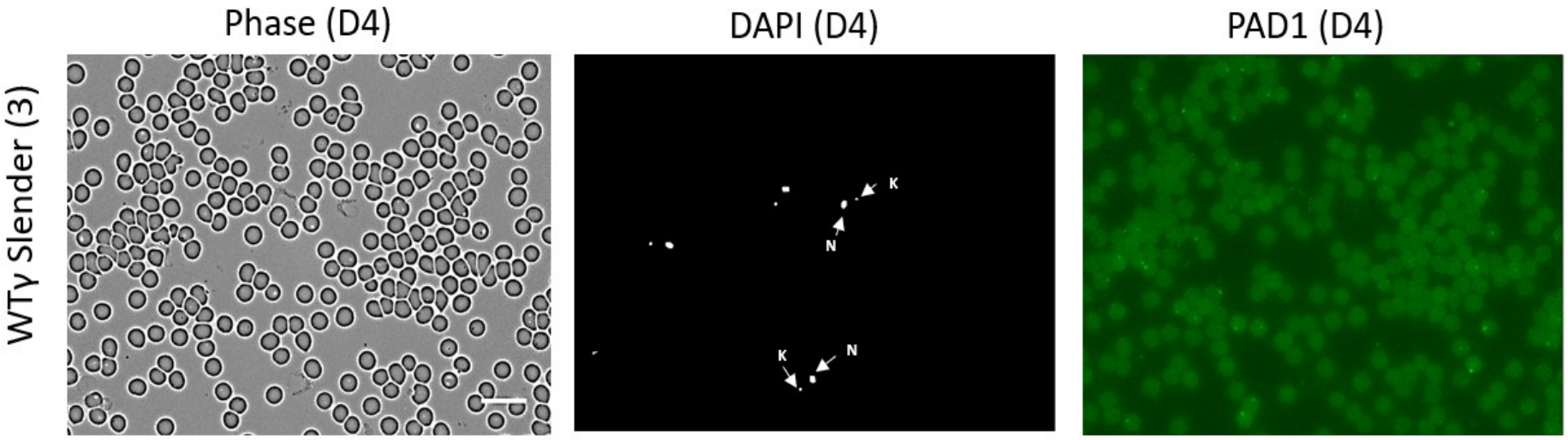
Phase (D4)
DAPI (D4)
PAD1 (D4)
WTγ Slender (3)
K
N
K
N

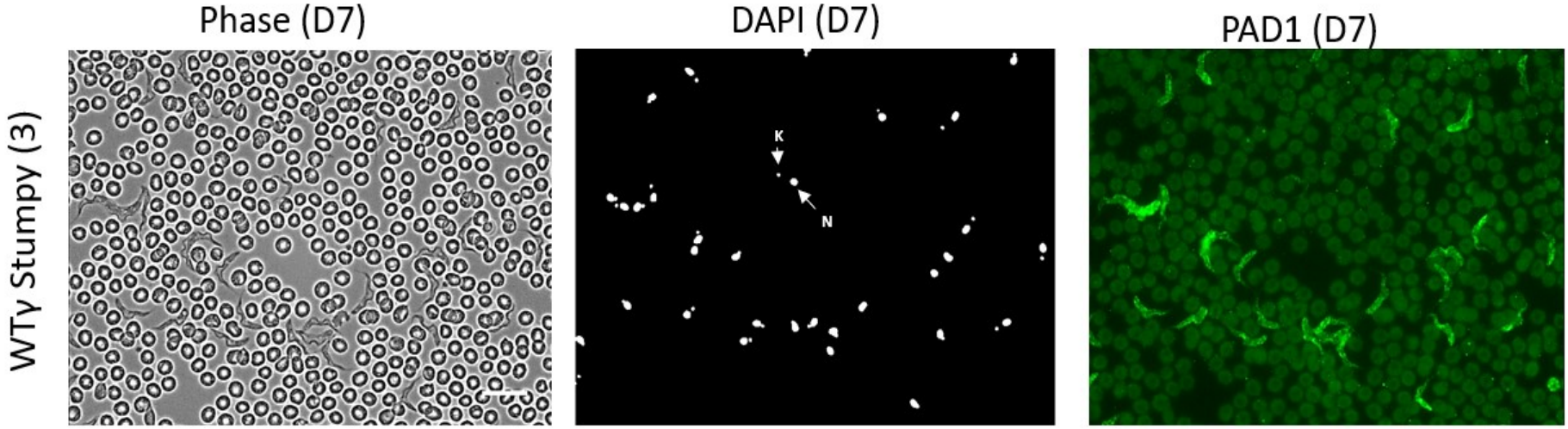
Phase (D7)
DAPI (D7)
PAD1 (D7)
WTγ Stumpy (3)
K
N

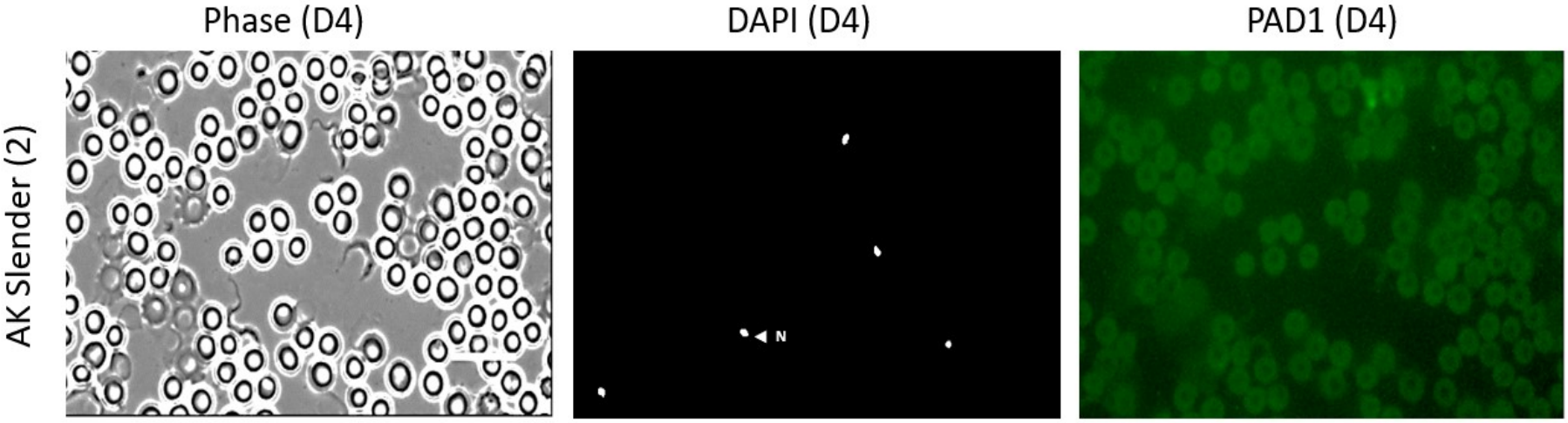
Phase (D4)
DAPI (D4)
PAD1 (D4)
AK Slender (2)
N

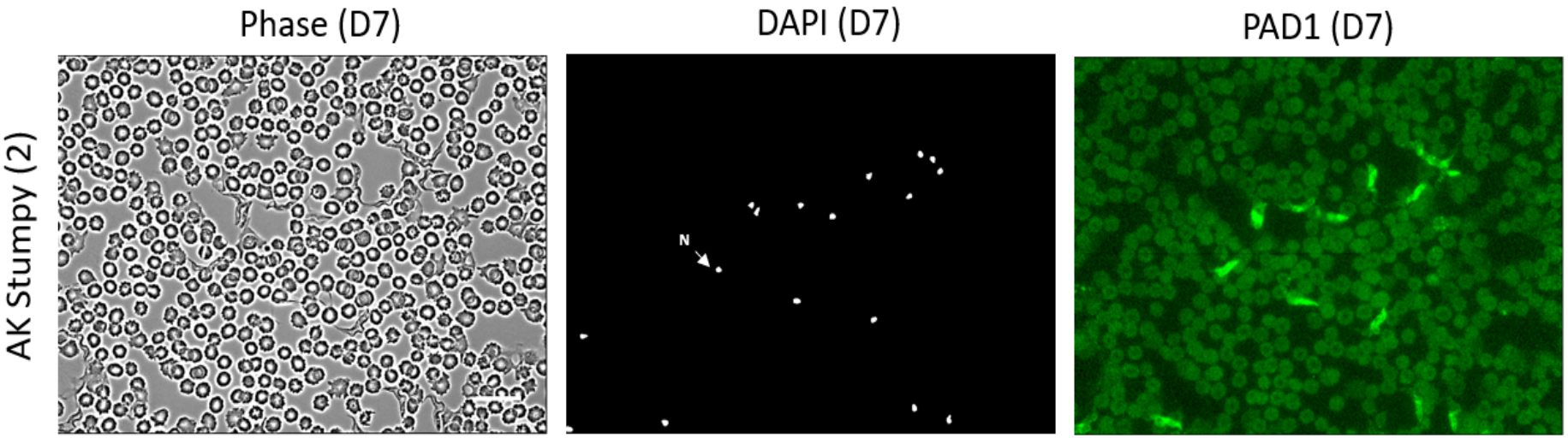
Phase (D7)
DAPI (D7)
PAD1 (D7)
AK Stumpy (2)
N

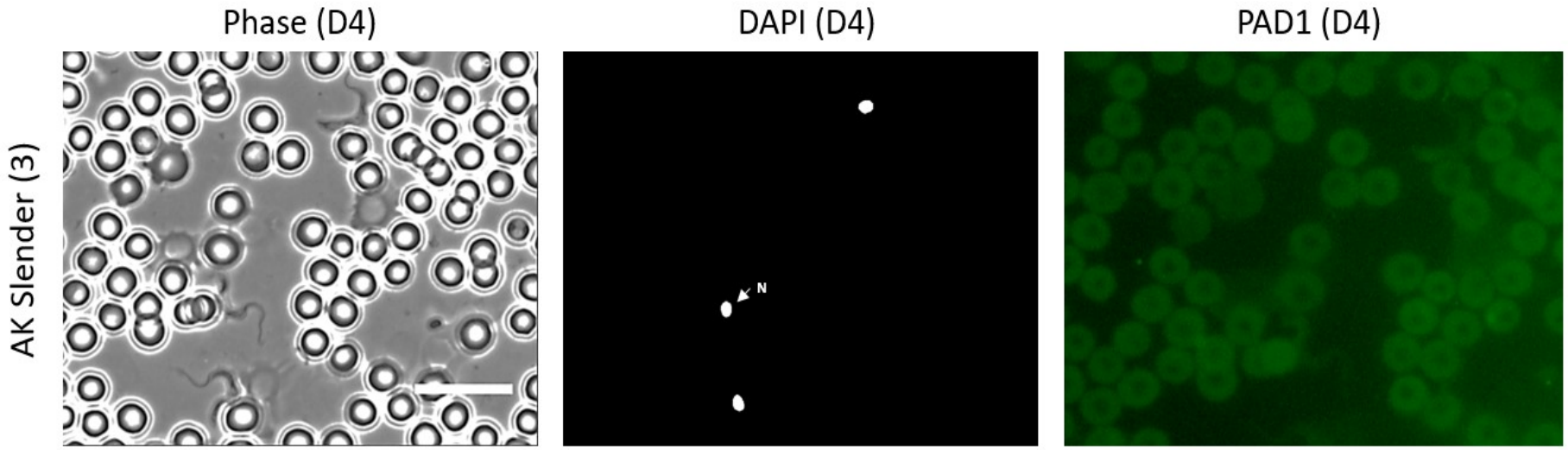
Phase (D4)
DAPI (D4)
PAD1 (D4)
AK Slender (3)
N

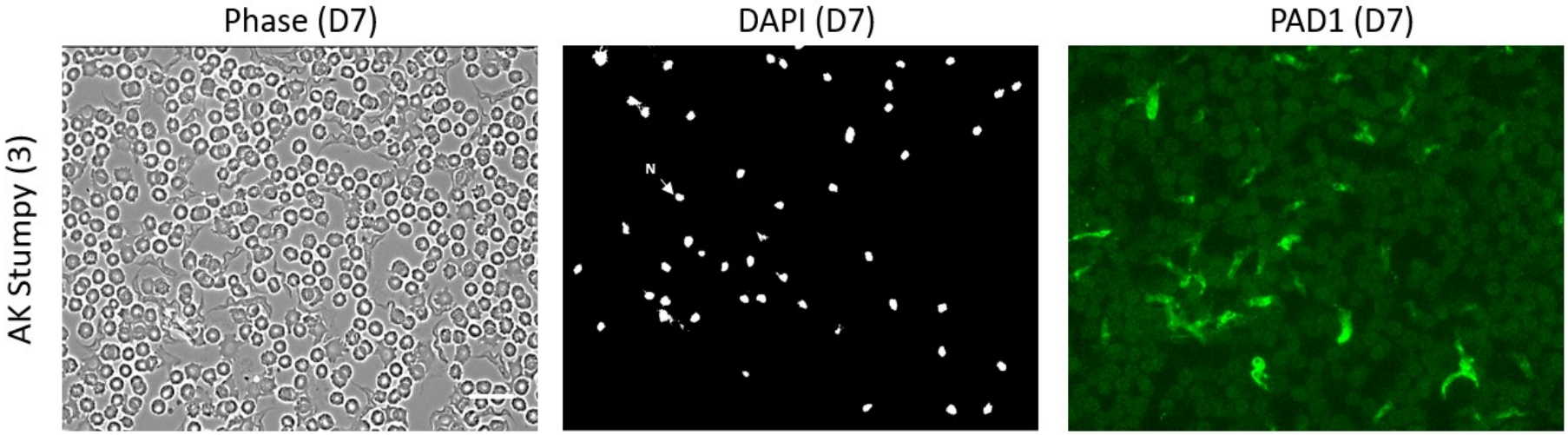
Phase (D7)
DAPI (D7)
PAD1 (D7)
AK Stumpy (3)
N

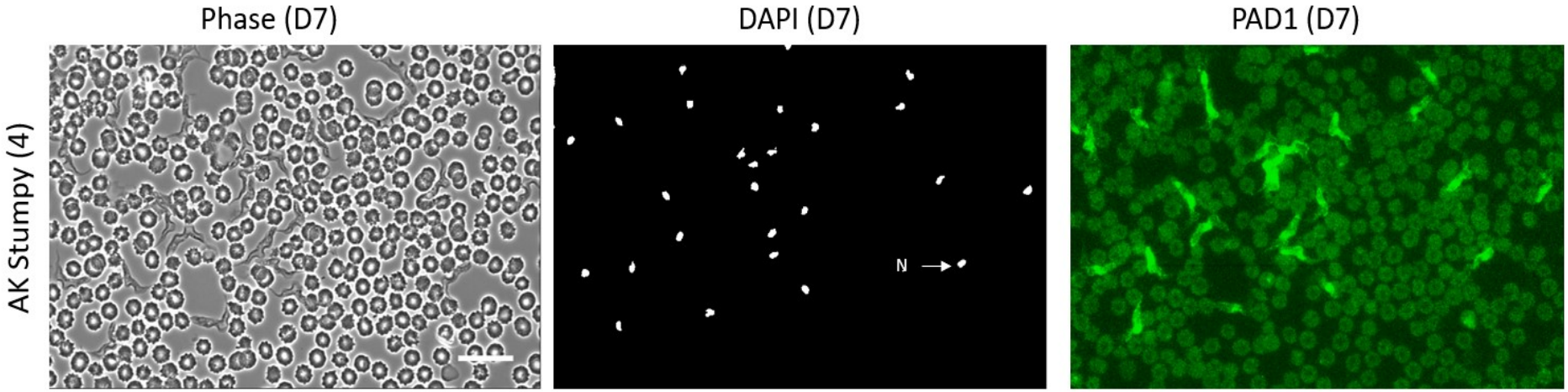

Figure 5.8 Immunoflourescence images for PAD1 staining in *T. brucei* bloodstream forms. These are the biological replicate samples used in the RNA-Seq analysis. Four replicate samples for stumpy AK, three for slender AK, Three each for WTγ stumpy and slender samples. Slender samples harvested from mice on day 4 post-infection whiles stumpy cells harvested on day 7 post-infection**.**

6 References

Abdi, R.D., Agga, G.E., Aregawi, W.G., Bekana, M., Van Leeuwen, T., Delespaux, V., Duchateau, L., 2017. A systematic review and meta-analysis of trypanosome prevalence in tsetse flies. BMC Veterinary Research 13, 100. https://doi.org/10.1186/s12917-017-1012-9

Absalon, S., Kohl, L., Branche, C., Blisnick, T., Toutirais, G., Rusconi, F., Cosson, J., Bonhivers, M., Robinson, D., Bastin, P., 2007. Basal body positioning is controlled by flagellum formation in *Trypanosoma brucei.* PloS one 2, e437. https://doi.org/10.1371/journal.pone.0000437

Acestor, N., Zikova, A., Dalley, R.A., Anupama, A., Panigrahi, A.K., Stuart, K.D., 2011. *Trypanosoma brucei* mitochondrial respiratome: composition and organization in procyclic form. Molecular & cellular proteomics : MCP 10, M110.006908. https://doi.org/10.1074/mcp.M110.006908

Acosta-Serrano, A., Vassella, E., Liniger, M., Renggli, C.K., Brun, R., Roditi, I., Englund, P.T., 2001. The surface coat of procyclic *Trypanosoma brucei*: Programmed expression and proteolytic cleavage of procyclin in the tsetse fly. PNAS 98, 1513–1518. https://doi.org/10.1073/pnas.98.4.1513

Aksoy, S., Buscher, P., Lehane, M., Solano, P., van den Abbeele, J., 2017. Human African trypanosomiasis control: Achievements and challenges. Plos Neglect Trop D 11. https://doi.org/10.1371/journal.pntd.0005454

Aksoy, S., Gibson, W.C., Lehane, M.J., 2003. Interactions between tsetse and trypanosomes with implications for the control of trypanosomiasis. Advances in parasitology 53, 1–83.

Albert, M., Wardrop, N.A., Atkinson, P.M., Torr, S.J., Welburn, S.C., 2015. Tsetse fly (G. f. fuscipes) distribution in the Lake Victoria basin of Uganda. PLoS Negl Trop Dis 9, e0003705. https://doi.org/10.1371/journal.pntd.0003705

Alsford, S., Eckert, S., Baker, N., Glover, L., Sanchez-Flores, A., Leung, K.F., Turner, D.J., Field, M.C., Berriman, M., Horn, D., 2012. High-throughput decoding of antitrypanosomal drug efficacy and resistance. Nature 482, 232–6. https://doi.org/10.1038/nature10771

Alsford, S., Field, M.C., Horn, D., 2013. Receptor-mediated endocytosis for drug delivery in African trypanosomes: fulfilling Paul Ehrlich's vision of chemotherapy. Trends in parasitology 29, 207–12. https://doi.org/10.1016/j.pt.2013.03.004

Alsford, S., Turner, D.J., Obado, S.O., Sanchez-Flores, A., Glover, L., Berriman, M., Hertz-Fowler, C., Horn, D., 2011. High-throughput phenotyping using parallel sequencing of RNA interference targets in the African trypanosome. Genome Res. 21, 915–924. https://doi.org/10.1101/gr.115089.110

Amano, T., Hisabori, T., Muneyuki, E., Yoshida, M., 1996. Catalytic activities of alpha3beta3gamma complexes of F1-ATPase with 1, 2, or 3 incompetent catalytic sites. J. Biol. Chem. 271, 18128–18133.

Amiguet-Vercher, A., Perez-Morga, D., Pays, A., Poelvoorde, P., Van Xong, H., Tebabi, P., Vanhamme, L., Pays, E., 2004. Loss of the mono-allelic control of the VSG expression sites during the development of *Trypanosoma brucei* in the bloodstream. Molecular microbiology 51, 1577–88.

Anene, B.M., Chime, A.B., Jibike, G.I., Anika, S.M., 1991. Prevalence of Trypanosomiasis in Zebu Cattle at Obudu Ranch - a Tsetse-Free Zone in Nigeria. Prev Vet Med 10, 257–260. https://doi.org/10.1016/0167-5877(91)90011-P

Aphasizhev, R., Suematsu, T., Zhang, L., Aphasizheva, I., 2016. Constructive edge of uridylation-induced RNA degradation. RNA Biol 13, 1078–1083. https://doi.org/10.1080/15476286.2016.1229736

Archer, S.K., Luu, V.-D., Queiroz, R.A. de, Brems, S., Clayton, C., 2009. *Trypanosoma brucei* PUF9 Regulates mRNAs for Proteins Involved in Replicative Processes over the Cell Cycle. PLOS Pathogens 5, e1000565. https://doi.org/10.1371/journal.ppat.1000565

Ashcroft, M.T., 1960. A comparison between a syringe-passaged and a tsetse-fly-transmitted line of a strain of *Trypanosoma rhodesiense*. Ann Trop Med Parasitol 54, 44–53.

Auty, H., Torr, S.J., Michoel, T., Jayaraman, S., Morrison, L.J., 2015. Cattle trypanosomosis: the diversity of trypanosomes and implications for disease epidemiology and control. Rev. - Off. Int. Epizoot. 34, 587–598.

Bakker, B.M., Krauth-Siegel, R.L., Clayton, C., Matthews, K., Girolami, M., Westerhoff, H.V., Michels, P.A.M., Breitling, R., Barrett, M.P., 2011. THE SILICON TRYPANOSOME. National Academies Press (US).

Barry, J.D., Graham, S.V., Fotheringham, M., Graham, V.S., Kobryn, K., Wymer, B., 1998. VSG gene control and infectivity strategy of metacyclic stage *Trypanosoma brucei.* Molecular and biochemical parasitology 91, 93–105.

Bates, P.A., Robertson, C.D., Tetley, L., Coombs, G.H., 1992. Axenic cultivation and characterization of Leishmania mexicana amastigote-like forms. Parasitology 105 (Pt 2), 193–202.

Berens, R.L., Krug, E.C., Marr, J.J., 1995. 6 - Purine and Pyrimidine Metabolism, in: Biochemistry and Molecular Biology of Parasites. Academic Press, San Diego, pp. 89–117. https://doi.org/10.1016/B978-012473345-9/50007-6

Berriman, M., Ghedin, E., Hertz-Fowler, C., Blandin, G., Renauld, H., Bartholomeu, D.C., Lennard, N.J., Caler, E., Hamlin, N.E., Haas, B., Böhme, U., Hannick, L., Aslett, M.A., Shallom, J., Marcello, L., Hou, L., Wickstead, B., Alsmark, U.C.M., Arrowsmith, C., Atkin, R.J., Barron, A.J., Bringaud, F., Brooks, K., Carrington, M., Cherevach, I., Chillingworth, T.-J., Churcher, C., Clark, L.N., Corton, C.H., Cronin, A., Davies, R.M., Doggett, J., Djikeng, A., Feldblyum, T., Field, M.C., Fraser, A., Goodhead, I., Hance, Z., Harper, D., Harris, B.R., Hauser, H., Hostetler, J., Ivens, A., Jagels, K., Johnson, D., Johnson, J., Jones, K., Kerhornou, A.X., Koo, H., Larke, N., Landfear, S., Larkin, C., Leech, V., Line, A., Lord, A., Macleod, A., Mooney, P.J., Moule, S., Martin, D.M.A., Morgan, G.W., Mungall, K., Norbertczak, H., Ormond, D., Pai, G., Peacock, C.S., Peterson, J., Quail, M.A., Rabbinowitsch, E., Rajandream, M.-A., Reitter, C., Salzberg, S.L., Sanders, M., Schobel, S., Sharp, S., Simmonds, M., Simpson, A.J., Tallon, L., Turner, C.M.R., Tait, A., Tivey, A.R., Van Aken, S., Walker, D., Wanless, D., Wang, S., White, B., White, O., Whitehead, S., Woodward, J., Wortman, J., Adams, M.D., Embley, T.M., Gull, K., Ullu, E., Barry, J.D., Fairlamb, A.H., Opperdoes, F., Barrell, B.G., Donelson, J.E., Hall, N., Fraser, C.M., Melville, S.E., El-Sayed, N.M., 2005. The genome of the African *T*rypanosome *Trypanosoma brucei.* Science 309, 416–422. https://doi.org/10.1126/science.1112642

Besteiro, S., Barrett, M.P., Riviere, L., Bringaud, F., 2005. Energy generation in insect stages of *Trypanosoma brucei*: metabolism in flux. Trends in parasitology 21, 185–91. https://doi.org/10.1016/j.pt.2005.02.008

Bienen, E.J., Maturi, R.K., Pollakis, G., Clarkson, A.B., 1993. Non-cytochrome mediated mitochondrial ATP production in bloodstream form *Trypanosoma brucei brucei*. Eur. J. Biochem. 216, 75–80.

Bienen, E.J., Saric, M., Pollakis, G., Grady, R.W., Clarkson, A.B., 1991. Mitochondrial development in *Trypanosoma brucei brucei* transitional bloodstream forms. Mol. Biochem. Parasitol. 45, 185–192.

Blum, J., Nkunku, S., Burri, C., 2001. Clinical description of encephalopathic syndromes and risk factors for their occurrence and outcome during melarsoprol treatment of human African trypanosomiasis. Trop Med Int Health 6, 390–400. https://doi.org/10.1046/j.1365-3156.2001.00710.x

Bochud-Allemann, N., Schneider, A., 2002. Mitochondrial substrate level phosphorylation is essential for growth of procyclic *Trypanosoma brucei.* J. Biol. Chem. 277, 32849–32854. https://doi.org/10.1074/jbc.M205776200

Bonnet, J., Boudot, C., Courtioux, B., 2015. Overview of the Diagnostic Methods Used in the Field for Human African Trypanosomiasis: What Could Change in the Next Years? Biomed Res Int 2015, 583262. https://doi.org/10.1155/2015/583262

Borst, P., 1972. Mitochondrial nucleic acids. Annu Rev Biochem 41, 333–76. https://doi.org/10.1146/annurev.bi.41.070172.002001

Bouyer, J., Seck, M.T., Sall, B., Ndiaye, E.Y., Guerrini, L., Vreysen, M.J.B., 2010. Stratified Entomological Sampling in Preparation for an Area-Wide Integrated Pest Management Program: The Example of Glossina palpalis gambiensis (Diptera: Glossinidae) in the Niayes of Senegal. J Med Entomol 47, 543–552.

Breidbach, T., Ngazoa, E., Steverding, D., 2002. *Trypanosoma brucei*: in vitro slender-to-stumpy differentiation of culture-adapted, monomorphic bloodstream forms. Experimental parasitology 101, 223–30.

Briggs, L.J., McKean, P.G., Baines, A., Moreira-Leite, F., Davidge, J., Vaughan, S., Gull, K., 2004. The flagella connector of *Trypanosoma brucei*: an unusual mobile transmembrane junction. J Cell Sci 117, 1641–51. https://doi.org/10.1242/jcs.00995

Bringaud, F., Baltz, T., 1993. Differential regulation of two distinct families of glucose transporter genes in *Trypanosoma brucei*. Mol Cell Biol 13, 1146–1154.

Bringaud, F., Riviere, L., Coustou, V., 2006. Energy metabolism of trypanosomatids: adaptation to available carbon sources. Molecular and biochemical parasitology 149, 1–9. https://doi.org/10.1016/j.molbiopara.2006.03.017

Brun, R., Schonenberger, M., 1981. Stimulating effect of citrate and cis-Aconitate on the transformation of *Trypanosoma brucei* bloodstream forms to procyclic forms in vitro. Zeitschrift fur Parasitenkunde (Berlin, Germany) 66, 17–24.

Burri, C., Blum, J., 1996. A case of reactive encephalopathy after treatment with suramin of first stage sleeping sickness. Trop Med Int Health 1, A36–A37.

Butow, R.A., Avadhani, N.G., 2004. Mitochondrial signaling: the retrograde response. Molecular cell 14, 1–15.

Cai, H., Chen, H., Yi, T., Daimon, C.M., Boyle, J.P., Peers, C., Maudsley, S., Martin, B., 2013. VennPlex–A Novel Venn Diagram Program for Comparing and Visualizing Datasets with Differentially Regulated Datapoints. PLoS One 8. https://doi.org/10.1371/journal.pone.0053388

Caljon, G., Van Reet, N., De Trez, C., Vermeersch, M., Pérez-Morga, D., Van Den Abbeele, J., 2016. The Dermis as a Delivery Site of *Trypanosoma brucei* for Tsetse Flies. PLoS Pathog. 12, e1005744. https://doi.org/10.1371/journal.ppat.1005744

Callejas, S., Leech, V., Reitter, C., Melville, S., 2006. Hemizygous subtelomeres of an African trypanosome chromosome may account for over 75% of chromosome length. Genome research 16, 1109–18. https://doi.org/10.1101/gr.5147406

Capewell, P., Cren-Travaille, C., Marchesi, F., Johnston, P., Clucas, C., Benson, R.A., Gorman, T.A., Calvo-Alvarez, E., Crouzols, A., Jouvion, G., Jamonneau, V., Weir, W., Stevenson, M.L., O'Neill, K., Cooper, A., Swar, N.R.K., Bucheton, B., Ngoyi, D.M., Garside, P., Rotureau, B., MacLeod, A., 2016. The skin is a significant but overlooked anatomical reservoir for vector-borne African trypanosomes. Elife 5. https://doi.org/10.7554/eLife.17716

Carneiro, C.M., Sánchez-Montalvá, A., Corrêa-Oliveira, R., Sales Junior, P.A., Fonseca Murta, S.M., Salvador, F., Molina, I., 2017. Experimental and Clinical Treatment of Chagas Disease: A Review. The American Journal of Tropical Medicine and Hygiene 97, 1289–1303. https://doi.org/10.4269/ajtmh.16-0761

Carnes, J., Schnaufer, A., McDermott, S.M., Domingo, G., Proff, R., Steinberg, A.G., Kurtz, I., Stuart, K., 2012. Mutational analysis of *Trypanosoma brucei* editosome proteins KREPB4 and KREPB5 reveals domains critical for function. RNA 18, 1897–1909. https://doi.org/10.1261/rna.035048.112

Carnes, J., Stuart, K.D., 2007. Uridine insertion/deletion editing activities. Meth. Enzymol. 424, 25–54. https://doi.org/10.1016/S0076-6879(07)24002-9

Carter, N.S., Fairlamb, A.H., 1993. Arsenical-resistant trypanosomes lack an unusual adenosine transporter. Nature 361, 173–176. https://doi.org/10.1038/361173a0

Carvalho, T., Trindade, S., Pimenta, S., Santos, A.B., Rijo-Ferreira, F., Figueiredo, L.M., 2018. *Trypanosoma brucei* triggers a marked immune response in male reproductive organs. PLOS Neglected Tropical Diseases 12, e0006690. https://doi.org/10.1371/journal.pntd.0006690

Cassola, A., Romaniuk, M.A., Primrose, D., Cervini, G., D'Orso, I., Frasch, A.C., 2015. Association of UBP1 to ribonucleoprotein complexes is regulated by interaction with the trypanosome ortholog of the human multifunctional P32 protein. Mol. Microbiol. 97, 1079–1096. https://doi.org/10.1111/mmi.13090

Cassola, A., Romaniuk, M.A., Primrose, D., Cervini, G., D'Orso, I., Frasch, A.C., n.d. Association of UBP1 to ribonucleoprotein complexes is regulated by interaction with the trypanosome ortholog of the human multifunctional P32 protein. Molecular Microbiology 97, 1079–1096. https://doi.org/10.1111/mmi.13090

Cazzulo, J.J., 1992. Aerobic fermentation of glucose by trypanosomatids. FASEB journal : official publication of the Federation of American Societies for Experimental Biology 6, 3153–61.

Cermáková, P., Verner, Z., Man, P., Lukes, J., Horváth, A., 2007. Characterization of the NADH:ubiquinone oxidoreductase (complex I) in the trypanosomatid *Phytomonas serpens* (Kinetoplastida). FEBS J. 274, 3150–3158. https://doi.org/10.1111/j.1742-4658.2007.05847.x

Chacinska, A., Koehler, C.M., Milenkovic, D., Lithgow, T., Pfanner, N., 2009. Importing mitochondrial proteins: machineries and mechanisms. Cell 138, 628–44. https://doi.org/10.1016/j.cell.2009.08.005

Chappuis, F., Loutan, L., Simarro, P., Lejon, V., Buscher, P., 2005. Options for field diagnosis of human african trypanosomiasis. Clin Microbiol Rev 18, 133–46. https://doi.org/10.1128/CMR.18.1.133-146.2005

Chaudhuri, M., Sharan, R., Hill, G.C., 2002. Trypanosome Alternative Oxidase is Regulated Post-transcriptionally at the Level of RNA Stability. The Journal of Eukaryotic Microbiology 49, 263–269. https://doi.org/10.1111/j.1550-7408.2002.tb00367.x

Chávez, S., Eastman, G., Smircich, P., Becco, L.L., Oliveira-Rizzo, C., Fort, R., Potenza, M., Garat, B., Sotelo-Silveira, J.R., Duhagon, M.A., 2017. Transcriptome-wide analysis of the *Trypanosoma cruzi* proliferative cycle identifies the periodically expressed mRNAs and

their multiple levels of control. PLoS One 12. https://doi.org/10.1371/journal.pone.0188441

Checchi, F., Chappuis, F., Karunakara, U., Priotto, G., Chandramohan, D., 2011. Accuracy of five algorithms to diagnose gambiense human African trypanosomiasis. PLoS Negl Trop Dis 5, e1233. https://doi.org/10.1371/journal.pntd.0001233

Chhabra, D.N., 2015. Impaired beta oxidation of fatty acids [WWW Document]. Biochemistry for Medics - Lecture Notes. URL http://www.namrata.co/impaired-beta-oxidation-of-fatty-acids/ (accessed 8.28.18).

Chitanga, S., Marcotty, T., Namangala, B., Van den Bossche, P., Van Den Abbeele, J., Delespaux, V., 2011. High prevalence of drug resistance in animal trypanosomes without a history of drug exposure. PLoS Negl Trop Dis 5, e1454. https://doi.org/10.1371/journal.pntd.0001454

Clayton, A.M., Guler, J.L., Povelones, M.L., Gluenz, E., Gull, K., Smith, T.K., Jensen, R.E., Englund, P.T., 2011. Depletion of mitochondrial acyl carrier protein in bloodstream-form *Trypanosoma brucei* causes a kinetoplast segregation defect. Eukaryotic cell 10, 286–92. https://doi.org/10.1128/ec.00290-10

Clayton, C., 2013. The regulation of trypanosome gene expression by RNA-binding proteins. PLoS Pathog 9, e1003680. https://doi.org/10.1371/journal.ppat.1003680

Clayton, C., Shapira, M., 2007. Post-transcriptional regulation of gene expression in trypanosomes and leishmanias. Mol. Biochem. Parasitol. 156, 93–101. https://doi.org/10.1016/j.molbiopara.2007.07.007

Clayton, C.E., 2016. Gene expression in Kinetoplastids. Current opinion in microbiology 32, 46–51. https://doi.org/10.1016/j.mib.2016.04.018

Cordeiro, C.D., Saiardi, A., Docampo, R., 2017. The inositol pyrophosphate synthesis pathway in *Trypanosoma brucei* is linked to polyphosphate synthesis in acidocalcisomes. Mol. Microbiol. 106, 319–333. https://doi.org/10.1111/mmi.13766

Coulaud, J., Caquet, R., Froli, G., Saimot, G., Pasticier, A., Payet, M., 1975. Severe Renal and Pancreatic Involvement during Treatment of African Trypanosomiasis with Pentamidine. Ann Med Interne 126, 665–669.

Coustou, V., Biran, M., Breton, M., Guegan, F., Rivière, L., Plazolles, N., Nolan, D., Barrett, M.P., Franconi, J.-M., Bringaud, F., 2008. Glucose-induced remodeling of intermediary and

energy metabolism in procyclic Trypanosoma brucei. J. Biol. Chem. 283, 16342–16354. https://doi.org/10.1074/jbc.M709592200

Creek, D.J., Mazet, M., Achcar, F., Anderson, J., Kim, D.H., Kamour, R., Morand, P., Millerioux, Y., Biran, M., Kerkhoven, E.J., Chokkathukalam, A., Weidt, S.K., Burgess, K.E., Breitling, R., Watson, D.G., Bringaud, F., Barrett, M.P., 2015. Probing the metabolic network in bloodstream-form *Trypanosoma brucei* using untargeted metabolomics with stable isotope labelled glucose. PLoS pathogens 11, e1004689. https://doi.org/10.1371/journal.ppat.1004689

Cross, G.A., Wirtz, L.E., Navarro, M., 1998. Regulation of vsg expression site transcription and switching in Trypanosoma brucei. Molecular and biochemical parasitology 91, 77–91.

Crozier, T.W.M., Tinti, M., Wheeler, R.J., Ly, T., Ferguson, M.A.J., Lamond, A.I., 2018. Proteomic Analysis of the Cell Cycle of Procylic Form *Trypanosoma brucei*. Mol Cell Proteomics 17, 1184–1195. https://doi.org/10.1074/mcp.RA118.000650

Cuisance, D., Politzar, H., Merot, P., Tamboura, I., 1984. [Release of irradiated males in the integrated campaign against Glossina in the Sideradougou pastoral area (Burkina Faso)]. Rev Elev Med Vet Pays Trop 37, 449–67.

Czichos, J., Nonnengaesser, C., Overath, P., 1986. *Trypanosoma brucei*: cis-aconitate and temperature reduction as triggers of synchronous transformation of bloodstream to procyclic trypomastigotes in vitro. Experimental parasitology 62, 283–91.

Damouche, A., Lazure, T., Avettand-Fènoël, V., Huot, N., Dejucq-Rainsford, N., Satie, A.-P., Mélard, A., David, L., Gommet, C., Ghosn, J., Noel, N., Pourcher, G., Martinez, V., Benoist, S., Béréziat, V., Cosma, A., Favier, B., Vaslin, B., Rouzioux, C., Capeau, J., Müller-Trutwin, M., Dereuddre-Bosquet, N., Grand, R.L., Lambotte, O., Bourgeois, C., 2015. Adipose Tissue Is a Neglected Viral Reservoir and an Inflammatory Site during Chronic HIV and SIV Infection. PLOS Pathogens 11, e1005153. https://doi.org/10.1371/journal.ppat.1005153

Daniels, J.-P., Gull, K., Wickstead, B., 2010. Cell Biology of the Trypanosome Genome. Microbiol Mol Biol Rev 74, 552–569. https://doi.org/10.1128/MMBR.00024-10

Dean, S., Gould, M.K., Dewar, C.E., Schnaufer, A.C., 2013. Single point mutations in ATP synthase compensate for mitochondrial genome loss in trypanosomes. Proceedings of the National Academy of Sciences of the United States of America 110, 14741–6. https://doi.org/10.1073/pnas.1305404110

Dean, S., Marchetti, R., Kirk, K., Matthews, K.R., 2009. A surface transporter family conveys the trypanosome differentiation signal. Nature 459, 213–7. https://doi.org/10.1038/nature07997

Dejung, M., Subota, I., Bucerius, F., Dindar, G., Freiwald, A., Engstler, M., Boshart, M., Butter, F., Janzen, C.J., 2016. Quantitative Proteomics Uncovers Novel Factors Involved in Developmental Differentiation of *Trypanosoma brucei*., Quantitative Proteomics Uncovers Novel Factors Involved in Developmental Differentiation of Trypanosoma brucei. PLoS Pathog 12, 12, e1005439–e1005439. https://doi.org/10.1371/journal.ppat.1005439, 10.1371/journal.ppat.1005439

Delespaux, V., de Koning, H.P., 2007. Drugs and drug resistance in African trypanosomiasis. Drug resistance updates : reviews and commentaries in antimicrobial and anticancer chemotherapy 10, 30–50. https://doi.org/10.1016/j.drup.2007.02.004

Delespaux, V., Geerts, S., Brandt, J., Elyn, R., Eisler, M.C., 2002. Monitoring the correct use of isometamidium by farmers and veterinary assistants in Eastern Province of Zambia using the isometamidium-ELISA. Veterinary parasitology 110, 117–22.

Delespaux, V., Geysen, D., Van den Bossche, P., Geerts, S., 2008. Molecular tools for the rapid detection of drug resistance in animal trypanosomes. Trends Parasitol 24, 236–242. https://doi.org/10.1016/j.pt.2008.02.006

Desquesnes, M., Holzmuller, P., Lai, D.H., Dargantes, A., Lun, Z.R., Jittaplapong, S., 2013. *Trypanosoma evansi* and surra: a review and perspectives on origin, history, distribution, taxonomy, morphology, hosts, and pathogenic effects. BioMed research international 2013, 194176. https://doi.org/10.1155/2013/194176

Desy, S., Mani, J., Harsman, A., Käser, S., Schneider, A., 2016. TbLOK1/ATOM19 is a novel subunit of the noncanonical mitochondrial outer membrane protein translocase of *Trypanosoma brucei*. Mol. Microbiol. 102, 520–529. https://doi.org/10.1111/mmi.13476

Dewar, C.E., MacGregor, P., Cooper, S., Gould, M.K., Matthews, K.R., Savill, N.J., Schnaufer, A., 2018. Mitochondrial DNA is critical for longevity and metabolism of transmission stage *Trypanosoma brucei*. PLOS Pathogens 14, e1007195. https://doi.org/10.1371/journal.ppat.1007195

Dolan, R.B., Okech, G., Alushula, H., Mutugi, M., Stevenson, P., Sayer, P.D., Njogu, A.R., 1990. Homidium bromide as a chemoprophylactic for cattle trypanosomiasis in Kenya. Acta Trop 47, 137–44.

D'Orso, I., Frasch, A.C., 2001. TcUBP-1, a developmentally regulated U-rich RNA-binding protein involved in selective mRNA destabilization in trypanosomes. J. Biol. Chem. 276, 34801–34809. https://doi.org/10.1074/jbc.M102120200

Duarte, M., Tomás, A.M., 2014. The mitochondrial complex I of trypanosomatids - an overview of current knowledge. J Bioenerg Biomembr 46, 299–311. https://doi.org/10.1007/s10863-014-9556-x

Duszenko, M., Figarella, K., Macleod, E.T., Welburn, S.C., 2006. Death of a trypanosome: a selfish altruism. Trends Parasitol. 22, 536–542. https://doi.org/10.1016/j.pt.2006.08.010

Dyer, N.A., Rose, C., Ejeh, N.O., Acosta-Serrano, A., 2013. Flying tryps: survival and maturation of trypanosomes in tsetse flies. Trends in parasitology 29, 188–96. https://doi.org/10.1016/j.pt.2013.02.003

Elledge, S.J., 1996. Cell cycle checkpoints: preventing an identity crisis. Science 274, 1664–72.

Engstler, M., Boshart, M., 2004. Cold shock and regulation of surface protein trafficking convey sensitization to inducers of stage differentiation in *Trypanosoma brucei*, in: Genes Dev. pp. 2798–811. https://doi.org/10.1101/gad.323404

Engstler, Markus, Boshart, M., 2004. Cold shock and regulation of surface protein trafficking convey sensitization to inducers of stage differentiation in *Trypanosoma brucei*. Genes & Development 18, 2798–2811. https://doi.org/10.1101/gad.323404

Engstler, M., Pfohl, T., Herminghaus, S., Boshart, M., Wiegertjes, G., Heddergott, N., Overath, P., 2007. Hydrodynamic flow-mediated protein sorting on the cell surface of trypanosomes. Cell 131, 505–15. https://doi.org/10.1016/j.cell.2007.08.046

Esterhuizen, J., Rayaisse, J.B., Tirados, I., Mpiana, S., Solano, P., Vale, G.A., Lehane, M.J., Torr, S.J., 2011. Improving the cost-effectiveness of visual devices for the control of riverine tsetse flies, the major vectors of human African trypanosomiasis. PLoS Negl Trop Dis 5, e1257. https://doi.org/10.1371/journal.pntd.0001257

Fairlamb, A.H., Gow, N.A.R., Matthews, K.R., Waters, A.P., 2016. Drug resistance in eukaryotic microorganisms. Nat Microbiol 1, 16092. https://doi.org/10.1038/nmicrobiol.2016.92

Fairlamb, A.H., Patterson, S., 2018. Current and Future Prospects of Nitro-compounds as Drugs for Trypanosomiasis and Leishmaniasis. Curr Med Chem. https://doi.org/10.2174/0929867325666180426164352

Fang, J., Beattie, D.S., 2003. Identification of a gene encoding a 54 kDa alternative NADH dehydrogenase in *Trypanosoma brucei*. Mol. Biochem. Parasitol. 127, 73–77.

Fang, J., Beattie, D.S., 2002. Novel FMN-containing rotenone-insensitive NADH dehydrogenase from *Trypanosoma brucei* mitochondria: isolation and characterization. Biochemistry 41, 3065–3072.

Fang, J., Wang, Y., Beattie, D.S., n.d. Isolation and characterization of complex I, rotenone-sensitive NADH:ubiquinone oxidoreductase, from the procyclic forms of *Trypanosoma brucei.* European Journal of Biochemistry 268, 3075–3082. https://doi.org/10.1046/j.1432-1327.2001.02205.x

Feagin, J.E., Jasmer, D.P., Stuart, K., 1987. Developmentally regulated addition of nucleotides within apocytochrome b transcripts in *Trypanosoma brucei.* Cell 49, 337–345.

Feagin, J.E., Stuart, K., 1988. Developmental aspects of uridine addition within mitochondrial transcripts of *Trypanosoma brucei*. Mol. Cell. Biol. 8, 1259–1265.

Fenn, K., Matthews, K.R., 2007. The cell biology of *Trypanosoma brucei* differentiation. Curr Opin Microbiol 10, 539–46. https://doi.org/10.1016/j.mib.2007.09.014

Ferguson, M.A., Homans, S.W., Dwek, R.A., Rademacher, T.W., 1988. Glycosyl-phosphatidylinositol moiety that anchors *Trypanosoma brucei* variant surface glycoprotein to the membrane. Science 239, 753–759. https://doi.org/10.1126/science.3340856

Ferrante, A., Allison, A.C., 1983. Alternative pathway activation of complement by African trypanosomes lacking a glycoprotein coat. Parasite Immunol. 5, 491–498.

Fèvre, E.M., Wissmann, B.V., Welburn, S.C., Lutumba, P., 2008a. The burden of human African trypanosomiasis. PLoS Negl Trop Dis 2, e333. https://doi.org/10.1371/journal.pntd.0000333

Fèvre, E.M., Wissmann, B. v., Welburn, S.C., Lutumba, P., 2008b. The Burden of Human African Trypanosomiasis. PLoS Negl Trop Dis 2. https://doi.org/10.1371/journal.pntd.0000333

Fiebig, M., Kelly, S., Gluenz, E., 2015. Comparative Life Cycle Transcriptomics Revises Leishmania mexicana Genome Annotation and Links a Chromosome Duplication with Parasitism of Vertebrates. PLoS Pathog. 11, e1005186. https://doi.org/10.1371/journal.ppat.1005186

Field, M.C., Horn, D., Fairlamb, A.H., Ferguson, M.A.J., Gray, D.W., Read, K.D., De Rycker, M., Torrie, L.S., Wyatt, P.G., Wyllie, S., Gilbert, I.H., 2017. Antitrypanosomatid drug discovery: an ongoing challenge and a continuing need. Nat Rev Microbiol 15, 217–231. https://doi.org/10.1038/nrmicro.2016.193

Franco, J.R., Cecchi, G., Priotto, G., Paone, M., Diarra, A., Grout, L., Mattioli, R.C., Argaw, D., 2017. Monitoring the elimination of human African trypanosomiasis: Update to 2014. PLOS Neglected Tropical Diseases 11, e0005585. https://doi.org/10.1371/journal.pntd.0005585

Franco, J.R., Simarro, P.P., Diarra, A., Jannin, J.G., 2014a. Epidemiology of human African trypanosomiasis. Clin Epidemiol 6, 257–75. https://doi.org/10.2147/CLEP.S39728

Franco, J.R., Simarro, P.P., Diarra, A., Ruiz-Postigo, J.A., Jannin, J.G., 2014b. The journey towards elimination of gambiense human African trypanosomiasis: not far, nor easy. Parasitology 141, 748–60. https://doi.org/10.1017/S0031182013002102

Furuya, T., Kessler, P., Jardim, A., Schnaufer, A., Crudder, C., Parsons, M., 2002. Glucose is toxic to glycosome-deficient trypanosomes. https://doi.org/10.1073/pnas.222454899

Futcher, B., Latter, G.I., Monardo, P., McLaughlin, C.S., Garrels, J.I., 1999. A sampling of the yeast proteome. Mol Cell Biol 19, 7357–68.

Gabriel, K., Buchanan, S.K., Lithgow, T., 2001. The alpha and the beta: protein translocation across mitochondrial and plastid outer membranes. Trends in biochemical sciences 26, 36–40.

Geiger, A., Simo, G., Grébaut, P., Peltier, J.-B., Cuny, G., Holzmuller, P., 2011. Transcriptomics and proteomics in human African trypanosomiasis: current status and perspectives. J Proteomics 74, 1625–1643. https://doi.org/10.1016/j.jprot.2011.01.016

Getahun, M.N., Cecchi, G., Seyoum, E., 2014. Population studies of Glossina pallidipes in Ethiopia: emphasis on cuticular hydrocarbons and wing morphometric analysis. Acta Trop 138, S12–S21. https://doi.org/10.1016/j.actatropica.2014.04.015

Gheiratmand, L., Brasseur, A., Zhou, Q., He, C.Y., 2013. Biochemical characterization of the bi-lobe reveals a continuous structural network linking the bi-lobe to other single-

copied organelles in *Trypanosoma brucei*. The Journal of biological chemistry 288, 3489–99. https://doi.org/10.1074/jbc.M112.417428

Gilkerson, R.W., Selker, J.M., Capaldi, R.A., 2003. The cristal membrane of mitochondria is the principal site of oxidative phosphorylation. FEBS letters 546, 355–8.

Giordani, F., Morrison, L.J., Rowan, T.G., HP, D.E.K., Barrett, M.P., 2016. The animal trypanosomiases and their chemotherapy: a review. Parasitology 143, 1862–1889. https://doi.org/10.1017/s0031182016001268

Girvin, M.E., Fillingame, R.H., 1995. Determination of local protein structure by spin label difference 2D NMR: the region neighboring Asp61 of subunit c of the F1F0 ATP synthase. Biochemistry 34, 1635–1645.

Gnipova, A., Panicucci, B., Paris, Z., Verner, Z., Horvath, A., Lukes, J., Zikova, A., 2012. Disparate phenotypic effects from the knockdown of various *Trypanosoma brucei* cytochrome c oxidase subunits. Molecular and biochemical parasitology 184, 90–8. https://doi.org/10.1016/j.molbiopara.2012.04.013

Goldstein, E.J., Citron, D.M., Tyrrell, K.L., Merriam, C.V., 2013. Comparative in vitro activities of GSK2251052, a novel boron-containing leucyl-tRNA synthetase inhibitor, against 916 anaerobic organisms. Antimicrobial agents and chemotherapy 57, 2401–4. https://doi.org/10.1128/aac.02580-12

Gooding, R.H., Krafsur, E.S., 2005. Tsetse genetics: contributions to biology, systematics, and control of tsetse flies. Annu Rev Entomol 50, 101–23. https://doi.org/10.1146/annurev.ento.50.071803.130443

Gottesdiener, K., Chung, H.M., Brown, S.D., Lee, M.G., Van der Ploeg, L.H., 1991. Characterization of VSG gene expression site promoters and promoter-associated DNA rearrangement events. Molecular and cellular biology 11, 2467–80.

Green, C.H., 1994. Bait Methods for Tsetse-Fly Control. Adv Parasit 34, 229–291. https://doi.org/10.1016/S0065-308x(08)60140-2

Grewal, J.S., McLuskey, K., Das, D., Myburgh, E., Wilkes, J., Brown, E., Lemgruber, L., Gould, M.K., Burchmore, R.J., Coombs, G.H., Schnaufer, A., Mottram, J.C., 2016. PNT1 Is a C11 Cysteine Peptidase Essential for Replication of the Trypanosome Kinetoplast. J. Biol. Chem. 291, 9492–9500. https://doi.org/10.1074/jbc.M116.714972

Guerra, D.G., Decottignies, A., Bakker, B.M., Michels, P.A.M., 2006. The mitochondrial FAD-dependent glycerol-3-phosphate dehydrogenase of Trypanosomatidae and the

glycosomal redox balance of insect stages of *Trypanosoma brucei* and *Leishmania spp.* Mol. Biochem. Parasitol. 149, 155–169. https://doi.org/10.1016/j.molbiopara.2006.05.006

Gunasekera, K., Wüthrich, D., Braga-Lagache, S., Heller, M., Ochsenreiter, T., 2012. Proteome remodelling during development from blood to insect-form *Trypanosoma brucei* quantified by SILAC and mass spectrometry. BMC Genomics 13, 556. https://doi.org/10.1186/1471-2164-13-556

Günzl, A., Bruderer, T., Laufer, G., Schimanski, B., Tu, L.-C., Chung, H.-M., Lee, P.-T., Lee, M.G.-S., 2003. RNA Polymerase I Transcribes Procyclin Genes and Variant Surface Glycoprotein Gene Expression Sites in *Trypanosoma brucei.* Eukaryotic Cell 2, 542–551. https://doi.org/10.1128/EC.2.3.542-551.2003

Haanstra, J.R., Gonzalez-Marcano, E.B., Gualdron-Lopez, M., Michels, P.A., 2016. Biogenesis, maintenance and dynamics of glycosomes in trypanosomatid parasites. Biochimica et biophysica acta 1863, 1038–48. https://doi.org/10.1016/j.bbamcr.2015.09.015

Haines, L.R., Hancock, R.E., Pearson, T.W., 2003. Cationic antimicrobial peptide killing of African trypanosomes and Sodalis glossinidius, a bacterial symbiont of the insect vector of sleeping sickness. Vector Borne Zoonotic Dis 3, 175–86. https://doi.org/10.1089/153036603322662165

Hajduk, S., Ochsenreiter, T., 2010. RNA editing in kinetoplastids. RNA Biol 7, 229–36.

Hall, B.S., Gabernet-Castello, C., Voak, A., Goulding, D., Natesan, S.K., Field, M.C., 2006. TbVps34, the trypanosome orthologue of Vps34, is required for Golgi complex segregation. J Biol Chem 281, 27600–12. https://doi.org/10.1074/jbc.M602183200

Hammarton, T.C., 2007. Cell cycle regulation in *Trypanosoma brucei.* Mol Biochem Parasitol 153, 1–8. https://doi.org/10.1016/j.molbiopara.2007.01.017

Hammarton, T.C., Engstler, M., Mottram, J.C., 2004. The *Trypanosoma brucei* cyclin, CYC2, is required for cell cycle progression through G1 phase and for maintenance of procyclic form cell morphology. J Biol Chem 279, 24757–64. https://doi.org/10.1074/jbc.M401276200

Harbers, M., Carninci, P., 2005. Tag-based approaches for transcriptome research and genome annotation. Nat. Methods 2, 495–502. https://doi.org/10.1038/nmeth768

Harsman, A., Schneider, A., 2017. Mitochondrial protein import in trypanosomes: Expect the unexpected. Traffic 18, 96–109. https://doi.org/10.1111/tra.12463

Hart, D.T., Misset, O., Edwards, S.W., Opperdoes, F.R., 1984. A comparison of the glycosomes (microbodies) isolated from *Trypanosoma brucei* bloodstream form and cultured procyclic trypomastigotes. Molecular and Biochemical Parasitology 12, 25–35. https://doi.org/10.1016/0166-6851(84)90041-0

Hartmann, C., Benz, C., Brems, S., Ellis, L., Luu, V.-D., Stewart, M., D'Orso, I., Busold, C., Fellenberg, K., Frasch, A.C.C., Carrington, M., Hoheisel, J., Clayton, C.E., 2007. Small Trypanosome RNA-Binding Proteins TbUBP1 and TbUBP2 Influence Expression of F-Box Protein mRNAs in Bloodstream Trypanosomes. Eukaryotic Cell 6, 1964–1978. https://doi.org/10.1128/EC.00279-07

Henriques, C., Sanchez, M.A., Tryon, R., Landfear, S.M., 2003. Molecular and functional characterization of the first nucleobase transporter gene from African trypanosomes. Mol. Biochem. Parasitol. 130, 101–110.

Herbert, W.J., Lumsden, W.H., 1976. *Trypanosoma brucei*: a rapid "matching" method for estimating the host's parasitemia. Exp. Parasitol. 40, 427–431.

Hertz-Fowler, C., Figueiredo, L.M., Quail, M.A., Becker, M., Jackson, A., Bason, N., Brooks, K., Churcher, C., Fahkro, S., Goodhead, I., Heath, P., Kartvelishvili, M., Mungall, K., Harris, D., Hauser, H., Sanders, M., Saunders, D., Seeger, K., Sharp, S., Taylor, J.E., Walker, D., White, B., Young, R., Cross, G.A., Rudenko, G., Barry, J.D., Louis, E.J., Berriman, M., 2008. Telomeric expression sites are highly conserved in *Trypanosoma brucei*. PloS one 3, e3527. https://doi.org/10.1371/journal.pone.0003527

Hirst, J., 2005. Energy transduction by respiratory complex I--an evaluation of current knowledge. Biochem. Soc. Trans. 33, 525–529. https://doi.org/10.1042/BST0330525

Hirumi, H., Hirumi, K., 1989. Continuous cultivation of *Trypanosoma brucei* blood stream forms in a medium containing a low concentration of serum protein without feeder cell layers. The Journal of parasitology 75, 985–9.

Horn, D., 2014. Antigenic variation in African trypanosomes. Molecular and biochemical parasitology 195, 123–9. https://doi.org/10.1016/j.molbiopara.2014.05.001

Horn, D., Cross, G.A., 1997. Analysis of *Trypanosoma brucei* vsg expression site switching in vitro. Molecular and biochemical parasitology 84, 189–201.

Horn, D., McCulloch, R., 2010. Molecular mechanisms underlying the control of antigenic variation in African trypanosomes. Curr Opin Microbiol 13, 700–5. https://doi.org/10.1016/j.mib.2010.08.009

Horváth, A., Horáková, E., Dunajcíková, P., Verner, Z., Pravdová, E., Slapetová, I., Cuninková, L., Lukes, J., 2005. Downregulation of the nuclear-encoded subunits of the complexes III and IV disrupts their respective complexes but not complex I in procyclic *Trypanosoma brucei.* Mol. Microbiol. 58, 116–130. https://doi.org/10.1111/j.1365-2958.2005.04813.x

Hug, M., Carruthers, V.B., Hartmann, C., Sherman, D.S., Cross, G.A.M., Clayton, C., 1993. A possible role for the 3'-untranslated region in developmental regulation in *Trypanosoma brucei*. Molecular and Biochemical Parasitology 61, 87–95. https://doi.org/10.1016/0166-6851(93)90161-P

Jacobs, R.T., Plattner, J.J., Nare, B., Wring, S.A., Chen, D., Freund, Y., Gaukel, E.G., Orr, M.D., Perales, J.B., Jenks, M., Noe, R.A., Sligar, J.M., Zhang, Y.K., Bacchi, C.J., Yarlett, N., Don, R., 2011. Benzoxaboroles: a new class of potential drugs for human African trypanosomiasis. Future Med Chem 3, 1259–78. https://doi.org/10.4155/fmc.11.80

Jain, S., Jacob, M., Walker, L., Tekwani, B., 2016. Screening North American plant extracts in vitro against Trypanosoma brucei for discovery of new antitrypanosomal drug leads. BMC Complement Altern Med 16, 131. https://doi.org/10.1186/s12906-016-1122-0

Jazwinski, S.M., 2013. The retrograde response: when mitochondrial quality control is not enough. Biochim. Biophys. Acta 1833, 400–409. https://doi.org/10.1016/j.bbamcr.2012.02.010

Jeacock, L., Faria, J., Horn, D., 2018. Codon usage bias controls mRNA and protein abundance in trypanosomatids, in: ELife. https://doi.org/10.7554/eLife.32496

Jensen, R.E., Englund, P.T., 2012. Network news: the replication of kinetoplast DNA. Annu Rev Microbiol 66, 473–91. https://doi.org/10.1146/annurev-micro-092611-150057

Joja, L.L., Okoli, U.A., 2001. Trapping the vector: community action to curb sleeping sickness in southern Sudan. Am J Public Health 91, 1583–5.

Kabani, S., Fenn, K., Ross, A., Ivens, A., Smith, T.K., Ghazal, P., Matthews, K., 2009. Genome-wide expression profiling of in vivo-derived bloodstream parasite stages and dynamic analysis of mRNA alterations during synchronous differentiation in *Trypanosoma brucei.* BMC genomics 10, 427. https://doi.org/10.1186/1471-2164-10-427

Kannan, S., Burger, G., 2008. Unassigned MURF1 of kinetoplastids codes for NADH dehydrogenase subunit 2. BMC Genomics 9, 455–455. https://doi.org/10.1186/1471-2164-9-455

Kaser, S., Oeljeklaus, S., Tyc, J., Vaughan, S., Warscheid, B., Schneider, A., 2016. Outer membrane protein functions as integrator of protein import and DNA inheritance in mitochondria. Proceedings of the National Academy of Sciences of the United States of America 113, E4467-75. https://doi.org/10.1073/pnas.1605497113

Käser, S., Oeljeklaus, S., Týč, J., Vaughan, S., Warscheid, B., Schneider, A., 2016. Outer membrane protein functions as integrator of protein import and DNA inheritance in mitochondria. Proc Natl Acad Sci U S A 113, E4467–E4475. https://doi.org/10.1073/pnas.1605497113

Kelly, S., Ivens, A., Mott, G.A., O'Neill, E., Emms, D., Macleod, O., Voorheis, P., Tyler, K., Clark, M., Matthews, J., Matthews, K., Carrington, M., 2017. An Alternative Strategy for Trypanosome Survival in the Mammalian Bloodstream Revealed through Genome and Transcriptome Analysis of the Ubiquitous Bovine Parasite *Trypanosoma (Megatrypanum) theileri.* Genome Biol Evol 9, 2093–2109. https://doi.org/10.1093/gbe/evx152

Kennedy, P.G., 2013. Clinical features, diagnosis, and treatment of human African trypanosomiasis (sleeping sickness). Lancet Neurol 12, 186–194. https://doi.org/10.1016/S1474-4422(12)70296-X

Kennedy, P.G., 2004. Human African trypanosomiasis of the CNS: current issues and challenges. J Clin Invest 113, 496–504. https://doi.org/10.1172/JCI21052

Kgori, P.M., Modo, S., Torr, S.J., 2006. The use of aerial spraying to eliminate tsetse from the Okavango Delta of Botswana. Acta Trop 99, 184–99. https://doi.org/10.1016/j.actatropica.2006.07.007

Kinabo, L.D.B., 1993. Pharmacology of Existing Drugs for Animal Trypanosomiasis. Acta Trop 54, 169–183. https://doi.org/10.1016/0001-706x(93)90091-O

Kirchman, P.A., Kim, S., Lai, C.Y., Jazwinski, S.M., 1999. Interorganelle signaling is a determinant of longevity in *Saccharomyces cerevisiae*. Genetics 152, 179–90.

Kleine, T., Leister, D., 2016. Retrograde signaling: Organelles go networking. Biochim. Biophys. Acta 1857, 1313–1325. https://doi.org/10.1016/j.bbabio.2016.03.017

Knorre, D.A., Sokolov, S.S., Zyrina, A.N., Severin, F.F., 2016. How do yeast sense mitochondrial dysfunction? Microbial Cell 3, 532–539. https://doi.org/10.15698/mic2016.11.537

Koch, H., Raabe, M., Urlaub, H., Bindereif, A., Preußer, C., 2016. The polyadenylation complex of *Trypanosoma brucei*: Characterization of the functional poly(A) polymerase. RNA Biol 13, 221–231. https://doi.org/10.1080/15476286.2015.1130208

Kohl, L., Robinson, D., Bastin, P., 2003. Novel roles for the flagellum in cell morphogenesis and cytokinesis of trypanosomes. The EMBO journal 22, 5336–46. https://doi.org/10.1093/emboj/cdg518

Kolev, N.G., Franklin, J.B., Carmi, S., Shi, H., Michaeli, S., Tschudi, C., 2010. The transcriptome of the human pathogen *Trypanosoma brucei* at single-nucleotide resolution. PLoS Pathog 6, e1001090. https://doi.org/10.1371/journal.ppat.1001090

Kotiadis, V.N., Duchen, M.R., Osellame, L.D., 2014. Mitochondrial quality control and communications with the nucleus are important in maintaining mitochondrial function and cell health. Biochim. Biophys. Acta 1840, 1254–1265. https://doi.org/10.1016/j.bbagen.2013.10.041

Kovarova, J., Horakova, E., Changmai, P., Vancova, M., Lukes, J., 2014. Mitochondrial and nucleolar localization of cysteine desulfurase Nfs and the scaffold protein Isu in *Trypanosoma brucei*. Eukaryotic cell 13, 353–62. https://doi.org/10.1128/ec.00235-13

Kuruma, Y., Suzuki, T., Ono, S., Yoshida, M., Ueda, T., 2012. Functional analysis of membranous Fo-a subunit of F1Fo-ATP synthase by in vitro protein synthesis. Biochem. J. 442, 631–638. https://doi.org/10.1042/BJ20111284

Lacomble, S., Vaughan, S., Gadelha, C., Morphew, M.K., Shaw, M.K., McIntosh, J.R., Gull, K., 2010. Basal body movements orchestrate membrane organelle division and cell morphogenesis in *Trypanosoma brucei*. Journal of cell science 123, 2884–91. https://doi.org/10.1242/jcs.074161

Lamont, G.S., Tucker, R.S., Cross, G.A., 1986. Analysis of antigen switching rates in Trypanosoma brucei. Parasitology 92 (Pt 2), 355–67.

Lamour, N., Riviere, L., Coustou, V., Coombs, G.H., Barrett, M.P., Bringaud, F., 2005. Proline metabolism in procyclic *Trypanosoma brucei* is down-regulated in the presence of glucose. J Biol Chem 280, 11902–10. https://doi.org/10.1074/jbc.M414274200

Lane-Serff, H., MacGregor, P., Peacock, L., Macleod, O.J., Kay, C., Gibson, W., Higgins, M.K., Carrington, M., 2016. Evolutionary diversification of the trypanosome haptoglobin-haemoglobin receptor from an ancestral haemoglobin receptor [WWW Document]. eLife. https://doi.org/10.7554/eLife.13044

Lanham, S.M., 1968. Separation of trypanosomes from the blood of infected rats and mice by anion-exchangers. Nature 218, 1273–1274.

Laun, P., Pichova, A., Madeo, F., Fuchs, J., Ellinger, A., Kohlwein, S., Dawes, I., Frohlich, K.U., Breitenbach, M., 2001. Aged mother cells of *Saccharomyces cerevisiae* show markers of oxidative stress and apoptosis. Molecular microbiology 39, 1166–73.

Lee, J.H., Jung, H.S., Günzl, A., 2009. Transcriptionally active TFIIH of the early-diverged eukaryote *Trypanosoma brucei* harbors two novel core subunits but not a cyclin-activating kinase complex. Nucleic Acids Res. 37, 3811–3820. https://doi.org/10.1093/nar/gkp236

Li, Z., 2012. Regulation of the cell division cycle in *Trypanosoma brucei*. Eukaryot Cell 11, 1180–90. https://doi.org/10.1128/EC.00145-12

Liang, X.H., Haritan, A., Uliel, S., Michaeli, S., 2003. trans and cis splicing in trypanosomatids: mechanism, factors, and regulation. Eukaryotic cell 2, 830–40.

Linstead, D.J., Klein, R.A., Cross, G.A., 1977. Threonine catabolism in *Trypanosoma brucei*. Journal of general microbiology 101, 243–51. https://doi.org/10.1099/00221287-101-2-243

MacGregor, P., Rojas, F., Dean, S., Matthews, K.R., 2013. Stable transformation of pleomorphic bloodstream form *Trypanosoma brucei*. Mol Biochem Parasitol 190, 60–62. https://doi.org/10.1016/j.molbiopara.2013.06.007

MacGregor, P., Savill, N.J., Hall, D., Matthews, K.R., 2011. Transmission stages dominate trypanosome within-host dynamics during chronic infections. Cell host & microbe 9, 310–8. https://doi.org/10.1016/j.chom.2011.03.013

Mahalingam, A., Geonnotti, A.R., Balzarini, J., Kiser, P.F., 2011. Activity and safety of synthetic lectins based on benzoboroxole-functionalized polymers for inhibition of HIV entry. Molecular pharmaceutics 8, 2465–75. https://doi.org/10.1021/mp2002957

Mair, G., Shi, H., Li, H., Djikeng, A., Aviles, H.O., Bishop, J.R., Falcone, F.H., Gavrilescu, C., Montgomery, J.L., Santori, M.I., Stern, L.S., Wang, Z., Ullu, E., Tschudi, C., 2000. A new twist in trypanosome RNA metabolism: cis-splicing of pre-mRNA. RNA 6, 163–9.

Majekodunmi, A.O., Fajinmi, A., Dongkum, C., Picozzi, K., Thrusfield, M.V., Welburn, S.C., 2013. A longitudinal survey of African animal trypanosomiasis in domestic cattle on the Jos Plateau, Nigeria: prevalence, distribution and risk factors. Parasit Vectors 6, 239. https://doi.org/10.1186/1756-3305-6-239

Makumi, J.N., Green, C., Baylis, M., 1998. Activity patterns in Glossina longipennis: a field study using different sampling methods. Medical and veterinary entomology 12, 399–406.

Mani, J., Meisinger, C., Schneider, A., 2016. Peeping at TOMs—Diverse Entry Gates to Mitochondria Provide Insights into the Evolution of Eukaryotes. Mol Biol Evol 33, 337–351. https://doi.org/10.1093/molbev/msv219

Mantilla, B.S., Paes, L.S., Pral, E.M., Martil, D.E., Thiemann, O.H., Fernandez-Silva, P., Bastos, E.L., Silber, A.M., 2015. Role of Delta1-pyrroline-5-carboxylate dehydrogenase supports mitochondrial metabolism and host-cell invasion of *Trypanosoma cruzi.* J Biol Chem 290, 7767–90. https://doi.org/10.1074/jbc.M114.574525

Markham, A., 2014. Tavaborole: first global approval. Drugs 74, 1555–8. https://doi.org/10.1007/s40265-014-0276-7

Martínez-Calvillo, S., Yan, S., Nguyen, D., Fox, M., Stuart, K., Myler, P.J., 2003. Transcription of *Leishmania major* Friedlin chromosome 1 initiates in both directions within a single region. Mol. Cell 11, 1291–1299.

Maslov, D.A., Simpson, L., 1992. The polarity of editing within a multiple gRNA-mediated domain is due to formation of anchors for upstream gRNAs by downstream editing. Cell 70, 459–67.

Maslov, D.A., Zíková, A., Kyselová, I., Lukes, J., 2002. A putative novel nuclear-encoded subunit of the cytochrome c oxidase complex in trypanosomatids. Mol. Biochem. Parasitol. 125, 113–125.

Matthews, K.R., 2005. The developmental cell biology of *Trypanosoma brucei*. J Cell Sci 118, 283–90. https://doi.org/10.1242/jcs.01649

Matthews, K.R., 1999. Developments in the differentiation of *Trypanosoma brucei*. Parasitol. Today (Regul. Ed.) 15, 76–80.

Matthews, K.R., Ellis, J.R., Paterou, A., 2004. Molecular regulation of the life cycle of African trypanosomes. Trends in Parasitology 20, 40–47. https://doi.org/10.1016/j.pt.2003.10.016

Matthews, K.R., Gull, K., 1998. Identification of stage-regulated and differentiation-enriched transcripts during transformation of the African trypanosome from its bloodstream to procyclic form. Mol. Biochem. Parasitol. 95, 81–95.

Matthews, K.R., Gull, K., 1994a. Cycles within cycles: the interplay between differentiation and cell division in *Trypanosoma brucei.* Parasitology today (Personal ed.) 10, 473–6.

Matthews, K.R., Gull, K., 1994b. Evidence for an interplay between cell cycle progression and the initiation of differentiation between life cycle forms of African trypanosomes. J. Cell Biol. 125, 1147–1156.

Matthews, K.R., McCulloch, R., Morrison, L.J., 2015. The within-host dynamics of African trypanosome infections. Philos Trans R Soc Lond B Biol Sci 370. https://doi.org/10.1098/rstb.2014.0288

Mayho, M., Fenn, K., Craddy, P., Crosthwaite, S., Matthews, K., 2006. Post-transcriptional control of nuclear-encoded cytochrome oxidase subunits in *Trypanosoma brucei*: evidence for genome-wide conservation of life-cycle stage-specific regulatory elements. Nucleic acids research 34, 5312–24. https://doi.org/10.1093/nar/gkl598

Mazet, M., Morand, P., Biran, M., Bouyssou, G., Courtois, P., Daulouede, S., Millerioux, Y., Franconi, J.M., Vincendeau, P., Moreau, P., Bringaud, F., 2013. Revisiting the central metabolism of the bloodstream forms of *Trypanosoma brucei*: production of acetate in the mitochondrion is essential for parasite viability. PLoS neglected tropical diseases 7, e2587. https://doi.org/10.1371/journal.pntd.0002587

McBride, H.M., Neuspiel, M., Wasiak, S., 2006. Mitochondria: more than just a powerhouse. Curr Biol 16, R551-60. https://doi.org/10.1016/j.cub.2006.06.054

McKean, P.G., 2003. Coordination of cell cycle and cytokinesis in *Trypanosoma brucei*. Current Opinion in Microbiology 6, 600–607. https://doi.org/10.1016/j.mib.2003.10.010

Mehta, V., Sen, R., Moshiri, H., Salavati, R., 2015. Mutational Analysis of *Trypanosoma brucei* RNA Editing Ligase Reveals Regions Critical for Interaction with KREPA2. PLOS ONE 10, e0120844. https://doi.org/10.1371/journal.pone.0120844

Menna-Barreto, R.F.S., de Castro, S.L., 2014. The Double-Edged Sword in Pathogenic Trypanosomatids: The Pivotal Role of Mitochondria in Oxidative Stress and Bioenergetics. Biomed Res Int 2014. https://doi.org/10.1155/2014/614014

Merritt, C., Stuart, K., 2013. Identification of Essential and Non-essential Protein Kinases by a Fusion PCR Method for Efficient Production of Transgenic *Trypanosoma brucei.* Mol Biochem Parasitol 190, 44–49. https://doi.org/10.1016/j.molbiopara.2013.05.002

Meyer, A., Holt, H.R., Selby, R., Guitian, J., 2016. Past and Ongoing Tsetse and Animal Trypanosomiasis Control Operations in Five African Countries: A Systematic Review. Plos Neglect Trop D 10. https://doi.org/10.1371/journal.pntd.0005247

Meyer, H., Porter, K.R., 1954. A study of *Trypanosoma cruzi* with the electron microscope. Parasitology 44, 16–23.

Michaeli, S., 2015. The response of trypanosomes and other eukaryotes to ER stress and the spliced leader RNA silencing (SLS) pathway in *Trypanosoma brucei*. Critical Reviews in Biochemistry and Molecular Biology 50, 256–267. https://doi.org/10.3109/10409238.2015.1042541

Michelotti, E.F., Hajduk, S.L., 1987. Developmental regulation of trypanosome mitochondrial gene expression. J. Biol. Chem. 262, 927–932.

Michels, P.A.M., Bringaud, F., Herman, M., Hannaert, V., 2006. Metabolic functions of glycosomes in trypanosomatids. Biochimica et Biophysica Acta (BBA) - Molecular Cell Research 1763, 1463–1477. https://doi.org/10.1016/j.bbamcr.2006.08.019

Misset, O., Bos, O.J., Opperdoes, F.R., 1986. Glycolytic enzymes of *Trypanosoma brucei*. Simultaneous purification, intraglycosomal concentrations and physical properties. European journal of biochemistry 157, 441–53.

Monk, S.L., Simmonds, P., Matthews, K.R., 2013. A short bifunctional element operates to positively or negatively regulate ESAG9 expression in different developmental forms of *Trypanosoma brucei*. J Cell Sci 126, 2294–2304. https://doi.org/10.1242/jcs.126011

Mony, B.M., MacGregor, P., Ivens, A., Rojas, F., Cowton, A., Young, J., Horn, D., Matthews, K., 2014. Genome-wide dissection of the quorum sensing signalling pathway in *Trypanosoma brucei.* Nature 505, 681–685. https://doi.org/10.1038/nature12864

Moore, S., Shrestha, S., Tomlinson, K.W., Vuong, H., 2012. Predicting the effect of climate change on African trypanosomiasis: integrating epidemiology with parasite and vector biology. J R Soc Interface 9, 817–830. https://doi.org/10.1098/rsif.2011.0654

Moreira-Leite, F.F., Sherwin, T., Kohl, L., Gull, K., 2001. A Trypanosome Structure Involved in Transmitting Cytoplasmic Information During Cell Division. Science 294, 610–612. https://doi.org/10.1126/science.1063775

Morris, J.C., Wang, Z., Drew, M.E., Englund, P.T., 2002. Glycolysis modulates trypanosome glycoprotein expression as revealed by an RNAi library. The EMBO journal 21, 4429–38.

Morrison, L.J., Vezza, L., Rowan, T., Hope, J.C., 2016. Animal African Trypanosomiasis: Time to Increase Focus on Clinically Relevant Parasite and Host Species. Trends Parasitol. 32, 599–607. https://doi.org/10.1016/j.pt.2016.04.012

Munday, J.C., Eze, A.A., Baker, N., Glover, L., Clucas, C., Aguinaga Andrés, D., Natto, M.J., Teka, I.A., McDonald, J., Lee, R.S., Graf, F.E., Ludin, P., Burchmore, R.J.S., Turner, C.M.R., Tait, A., MacLeod, A., Mäser, P., Barrett, M.P., Horn, D., De Koning, H.P., 2014. Trypanosoma brucei aquaglyceroporin 2 is a high-affinity transporter for pentamidine and melaminophenyl arsenic drugs and the main genetic determinant of resistance to these drugs. J. Antimicrob. Chemother. 69, 651–663. https://doi.org/10.1093/jac/dkt442

Naguleswaran, A., Doiron, N., Roditi, I., 2018. RNA-Seq analysis validates the use of culture-derived Trypanosoma brucei and provides new markers for mammalian and insect life-cycle stages. BMC Genomics 19. https://doi.org/10.1186/s12864-018-4600-6

Nare, B., Wring, S., Bacchi, C., Beaudet, B., Bowling, T., Brun, R., Chen, D., Ding, C., Freund, Y., Gaukel, E., Hussain, A., Jarnagin, K., Jenks, M., Kaiser, M., Mercer, L., Mejia, E., Noe, A., Orr, M., Parham, R., Plattner, J., Randolph, R., Rattendi, D., Rewerts, C., Sligar, J., Yarlett, N., Don, R., Jacobs, R., 2010. Discovery of novel orally bioavailable oxaborole 6-carboxamides that demonstrate cure in a murine model of late-stage central nervous system african trypanosomiasis. Antimicrobial agents and chemotherapy 54, 4379–88. https://doi.org/10.1128/aac.00498-10

Nargund, A.M., Pellegrino, M.W., Fiorese, C.J., Baker, B.M., Haynes, C.M., 2012. Mitochondrial import efficiency of ATFS-1 regulates mitochondrial UPR activation. Science 337, 587–590. https://doi.org/10.1126/science.1223560

Nett, I.R.E., Martin, D.M.A., Miranda-Saavedra, D., Lamont, D., Barber, J.D., Mehlert, A., Ferguson, M.A.J., 2009. The Phosphoproteome of Bloodstream Form *Trypanosoma brucei,* Causative Agent of African Sleeping Sickness. Mol Cell Proteomics 8, 1527–1538. https://doi.org/10.1074/mcp.M800556-MCP200

Neupert, W., 1997. Protein import into mitochondria. Annual review of biochemistry 66, 863–917. https://doi.org/10.1146/annurev.biochem.66.1.863

Neyrolles, O., Hernández-Pando, R., Pietri-Rouxel, F., Fornès, P., Tailleux, L., Barrios Payán, J.A., Pivert, E., Bordat, Y., Aguilar, D., Prévost, M.-C., Petit, C., Gicquel, B., 2006. Is adipose

tissue a place for *Mycobacterium tuberculosis* persistence? PLoS ONE 1, e43. https://doi.org/10.1371/journal.pone.0000043

Nilsson, D., Gunasekera, K., Mani, J., Osteras, M., Farinelli, L., Baerlocher, L., Roditi, I., Ochsenreiter, T., 2010. Spliced leader trapping reveals widespread alternative splicing patterns in the highly dynamic transcriptome of *Trypanosoma brucei.* PLoS pathogens 6, e1001037. https://doi.org/10.1371/journal.ppat.1001037

Novel Naphthalene-Based Inhibitors of *Trypanosoma brucei* RNA Editing Ligase 1, 2018. https://doi.org/10.1371/journal.pntd.0000803

Ochatt, C.M., Butikofer, P., Navarro, M., Wirtz, E., Boschung, M., Armah, D., Cross, G.A., 1999. Conditional expression of glycosylphosphatidylinositol phospholipase C in *Trypanosoma brucei*. Molecular and biochemical parasitology 103, 35–48.

Odeniran, P.O., Ademola, I.O., 2018. A meta-analysis of the prevalence of African animal trypanosomiasis in Nigeria from 1960 to 2017. Parasit Vectors 11, 280. https://doi.org/10.1186/s13071-018-2801-0

Ogbadoyi, E.O., Robinson, D.R., Gull, K., 2003. A high-order trans-membrane structural linkage is responsible for mitochondrial genome positioning and segregation by flagellar basal bodies in trypanosomes. Mol Biol Cell 14, 1769–79. https://doi.org/10.1091/mbc.E02-08-0525

Omolo, M.O., Hassanali, A., Mpiana, S., Esterhuizen, J., Lindh, J., Lehane, M.J., Solano, P., Rayaisse, J.B., Vale, G.A., Torr, S.J., Tirados, I., 2009. Prospects for Developing Odour Baits To Control Glossina fuscipes spp., the Major Vector of Human African Trypanosomiasis. Plos Neglect Trop D 3. https://doi.org/10.1371/journal.pntd.0000435

Opperdoes, F.R., 1987. Compartmentation of carbohydrate metabolism in trypanosomes. Annual review of microbiology 41, 127–51. https://doi.org/10.1146/annurev.mi.41.100187.001015

Opperdoes, F.R., Borst, P., Bakker, S., Leene, W., 1977. Localization of glycerol-3-phosphate oxidase in the mitochondrion and particulate NAD+-linked glycerol-3-phosphate dehydrogenase in the microbodies of the bloodstream form to *Trypanosoma brucei*. Eur. J. Biochem. 76, 29–39.

Opperdoes, F.R., Michels, P.A., 2008. Complex I of Trypanosomatidae: does it exist? Trends in parasitology 24, 310–7. https://doi.org/10.1016/j.pt.2008.03.013

Panigrahi, A.K., Allen, T.E., Stuart, K., Haynes, P.A., Gygi, S.P., 2003. Mass spectrometric analysis of the editosome and other multiprotein complexes in Trypanosoma brucei. J Am Soc Mass Spectrom 14, 728–735. https://doi.org/10.1016/S1044-0305(03)00126-0

Panigrahi, A.K., Ogata, Y., Zikova, A., Anupama, A., Dalley, R.A., Acestor, N., Myler, P.J., Stuart, K.D., 2009. A comprehensive analysis of Trypanosoma brucei mitochondrial proteome. Proteomics 9, 434–50. https://doi.org/10.1002/pmic.200800477

Pays, E., Vanhamme, L., Perez-Morga, D., 2004. Antigenic variation in *Trypanosoma brucei*: facts, challenges and mysteries. Current opinion in microbiology 7, 369–74. https://doi.org/10.1016/j.mib.2004.05.001

Pays, E., Vanhollebeke, B., Uzureau, P., Lecordier, L., Perez-Morga, D., 2014. The molecular arms race between African trypanosomes and humans. Nature reviews. Microbiology 12, 575–84. https://doi.org/10.1038/nrmicro3298

Peña-Diaz, P., Pelosi, L., Ebikeme, C., Colasante, C., Gao, F., Bringaud, F., Voncken, F., 2012. Functional Characterization of TbMCP5, a Conserved and Essential ADP/ATP Carrier Present in the Mitochondrion of the Human Pathogen *Trypanosoma brucei.* J Biol Chem 287, 41861–41874. https://doi.org/10.1074/jbc.M112.404699

Ploubidou, A., Robinson, D.R., Docherty, R.C., Ogbadoyi, E.O., Gull, K., 1999. Evidence for novel cell cycle checkpoints in trypanosomes: kinetoplast segregation and cytokinesis in the absence of mitosis. Journal of cell science 112 (Pt 24), 4641–50.

Pollard, V.W., Rohrer, S.P., Michelotti, E.F., Hancock, K., Hajduk, S.L., 1990. Organization of minicircle genes for guide RNAs in *Trypanosoma brucei*. Cell 63, 783–90.

Povelones, M.L., 2014. Beyond replication: division and segregation of mitochondrial DNA in kinetoplastids. Mol Biochem Parasitol 196, 53–60. https://doi.org/10.1016/j.molbiopara.2014.03.008

Priest, Hajduk, S., 1994. Developmental regulation of mitochondrial biogenesis in *Trypanosoma brucei*. J Bioenerg Biomembr 26, 179–191. https://doi.org/10.1007/BF00763067

Queiroz, R., Benz, C., Fellenberg, K., Hoheisel, J.D., Clayton, C., 2009. Transcriptome analysis of differentiating trypanosomes reveals the existence of multiple post-transcriptional regulons. BMC Genomics 10, 495. https://doi.org/10.1186/1471-2164-10-495

Qureshi, M.A., Haynes, C.M., Pellegrino, M.W., 2017. The mitochondrial unfolded protein response: Signaling from the powerhouse. J. Biol. Chem. 292, 13500–13506. https://doi.org/10.1074/jbc.R117.791061

Radwanska, M., Chamekh, M., Vanhamme, L., Claes, F., Magez, S., Magnus, E., de Baetselier, P., Büscher, P., Pays, E., 2002. The serum resistance-associated gene as a diagnostic tool for the detection of *Trypanosoma brucei rhodesiense*. Am. J. Trop. Med. Hyg. 67, 684–690.

Raper, J., Fung, R., Ghiso, J., Nussenzweig, V., Tomlinson, S., 1999. Characterization of a novel trypanosome lytic factor from human serum. Infect Immun 67, 1910–6.

Rastogi, V.K., Girvin, M.E., 1999. Structural changes linked to proton translocation by subunit c of the ATP synthase. Nature 402, 263–268. https://doi.org/10.1038/46224

Reinartz, J., Bruyns, E., Lin, J.-Z., Burcham, T., Brenner, S., Bowen, B., Kramer, M., Woychik, R., 2002. Massively parallel signature sequencing (MPSS) as a tool for in-depth quantitative gene expression profiling in all organisms. Brief Funct Genomic Proteomic 1, 95–104.

Rico, E., Jeacock, L., Kovářová, J., Horn, D., 2018. Inducible high-efficiency CRISPR-Cas9-targeted gene editing and precision base editing in African trypanosomes. Sci Rep 8. https://doi.org/10.1038/s41598-018-26303-w

Rijo-Ferreira, F., Carvalho, T., Afonso, C., Sanches-Vaz, M., Costa, R.M., Figueiredo, L.M., Takahashi, J.S., 2018. Sleeping sickness is a circadian disorder. Nat Commun 9. https://doi.org/10.1038/s41467-017-02484-2

Robinson, D.R., Gull, K., 1991. Basal body movements as a mechanism for mitochondrial genome segregation in the trypanosome cell cycle. Nature 352, 731–3. https://doi.org/10.1038/352731a0

Robinson, D.R., Sherwin, T., Ploubidou, A., Byard, E.H., Gull, K., 1995. Microtubule polarity and dynamics in the control of organelle positioning, segregation, and cytokinesis in the trypanosome cell cycle. J. Cell Biol. 128, 1163–1172.

Roditi, I., Furger, A., Ruepp, S., Schürch, N., Bütikofer, P., 1998. Unravelling the procyclin coat of *Trypanosoma brucei*. Mol. Biochem. Parasitol. 91, 117–130.

Roldan, A., Comini, M.A., Crispo, M., Krauth-Siegel, R.L., 2011. Lipoamide dehydrogenase is essential for both bloodstream and procyclic *Trypanosoma brucei.* Molecular microbiology 81, 623–39. https://doi.org/10.1111/j.1365-2958.2011.07721.x

Rolin, S., Hancocq-Quertier, J., Paturiaux-Hanocq, F., Nolan, D.P., Pays, E., 1998. Mild acid stress as a differentiation trigger in *Trypanosoma brucei*. Mol. Biochem. Parasitol. 93, 251–262.

Rosenberry, T.L., Krall, J.A., Dever, T.E., Haas, R., Louvard, D., Merrick, W.C., 1989. Biosynthetic incorporation of [3H]ethanolamine into protein synthesis elongation factor 1 alpha reveals a new post-translational protein modification. J. Biol. Chem. 264, 7096–7099.

Rotureau, B., Subota, I., Buisson, J., Bastin, P., 2012. A new asymmetric division contributes to the continuous production of infective trypanosomes in the tsetse fly. Development (Cambridge, England) 139, 1842–50. https://doi.org/10.1242/dev.072611

Ruepp, S., Furger, A., Kurath, U., Renggli, C.K., Hemphill, A., Brun, R., Roditi, I., 1997. Survival of *Trypanosoma brucei* in the Tsetse Fly Is Enhanced by the Expression of Specific Forms of Procyclin. J Cell Biol 137, 1369–79.

Sanchez, M.A., Drutman, S., van Ampting, M., Matthews, K., Landfear, S.M., 2004. A novel purine nucleoside transporter whose expression is up-regulated in the short stumpy form of the Trypanosoma brucei life cycle. Mol. Biochem. Parasitol. 136, 265–272.

Sanchez, M.A., Tryon, R., Green, J., Boor, I., Landfear, S.M., 2002. Six Related Nucleoside/Nucleobase Transporters from *Trypanosoma brucei* Exhibit Distinct Biochemical Functions. J. Biol. Chem. 277, 21499–21504. https://doi.org/10.1074/jbc.M202319200

Santi-Rocca, J., Chenouard, N., Fort, C., Lagache, T., Olivo-Marin, J.-C., Bastin, P., 2015. Chapter 23 - Imaging intraflagellar transport in trypanosomes, in: Basto, R., Marshall, W.F. (Eds.), Methods in Cell Biology, Methods in Cilia & Flagella. Academic Press, pp. 487–508. https://doi.org/10.1016/bs.mcb.2015.01.005

Schatz, G., Haslbrunner, E., Tuppy, H., 1964. Deoxyribonucleic Acid Associated with Yeast Mitochondria. Biochem Biophys Res Commun 15, 127–32.

Schimanski, B., Laufer, G., Gontcharova, L., Günzl, A., 2004. The *Trypanosoma brucei* spliced leader RNA and rRNA gene promoters have interchangeable TbSNAP50-binding elements. Nucleic Acids Res 32, 700–709. https://doi.org/10.1093/nar/gkh231

Schnaufer, A., Clark-Walker, G.D., Steinberg, A.G., Stuart, K., 2005. The F1-ATP synthase complex in bloodstream stage trypanosomes has an unusual and essential function. The EMBO journal 24, 4029–40. https://doi.org/10.1038/sj.emboj.7600862

Schnaufer, A., Domingo, G.J., Stuart, K., 2002. Natural and induced dyskinetoplastic trypanosomatids: how to live without mitochondrial DNA. International journal for parasitology 32, 1071–84.

Schnaufer, A., Panigrahi, A.K., Panicucci, B., Igo, R.P., Jr., Wirtz, E., Salavati, R., Stuart, K., 2001. An RNA ligase essential for RNA editing and survival of the bloodstream form of *Trypanosoma brucei.* Science (New York, N.Y.) 291, 2159–62. https://doi.org/10.1126/science.1058955

Schneider, A., 2001. Unique aspects of mitochondrial biogenesis in trypanosomatids. Int. J. Parasitol. 31, 1403–1415.

Schneider, A., Bouzaidi-Tiali, N., Chanez, A.L., Bulliard, L., 2007. ATP production in isolated mitochondria of procyclic *Trypanosoma brucei*. Methods in molecular biology (Clifton, N.J.) 372, 379–87. https://doi.org/10.1007/978-1-59745-365-3_27

Schneider, C.A., Rasband, W.S., Eliceiri, K.W., 2012. NIH Image to ImageJ: 25 years of image analysis. Nat. Methods 9, 671–675.

Schumann Burkard, G., Jutzi, P., Roditi, I., 2011. Genome-wide RNAi screens in bloodstream form trypanosomes identify drug transporters. Mol Biochem Parasitol 175, 91–4. https://doi.org/10.1016/j.molbiopara.2010.09.002

Schurch, N.J., Schofield, P., Gierliński, M., Cole, C., Sherstnev, A., Singh, V., Wrobel, N., Gharbi, K., Simpson, G.G., Owen-Hughes, T., Blaxter, M., Barton, G.J., 2016. How many biological replicates are needed in an RNA-seq experiment and which differential expression tool should you use? RNA 22, 839–851. https://doi.org/10.1261/rna.053959.115

Schwede, A., Carrington, M., 2010. Bloodstream form Trypanosome plasma membrane proteins: antigenic variation and invariant antigens. Parasitology 137, 2029–39. https://doi.org/10.1017/s0031182009992034

Serricchio, M., Bütikofer, P., 2011. *Trypanosoma brucei*: a model micro-organism to study eukaryotic phospholipid biosynthesis. The FEBS Journal 278, 1035–1046. https://doi.org/10.1111/j.1742-4658.2011.08012.x

Sharma, R., Gluenz, E., Peacock, L., Gibson, W., Gull, K., Carrington, M., 2009. The heart of darkness: growth and form of *Trypanosoma brucei* in the tsetse fly. Trends in parasitology 25, 517–24. https://doi.org/10.1016/j.pt.2009.08.001

Sharma, R., Peacock, L., Gluenz, E., Gull, K., Gibson, W., Carrington, M., 2008. Asymmetric cell division as a route to reduction in cell length and change in cell morphology in trypanosomes. Protist 159, 137–51. https://doi.org/10.1016/j.protis.2007.07.004

Sharma, S., Singha, U.K., Chaudhuri, M., 2010. Role of Tob55 on mitochondrial protein biogenesis in *Trypanosoma brucei*. Mol Biochem Parasit 174, 89–100. https://doi.org/10.1016/j.molbiopara.2010.07.003

Sherwin, T., Gull, K., 1989. The cell division cycle of *Trypanosoma brucei brucei:* timing of event markers and cytoskeletal modulations. Philosophical transactions of the Royal Society of London. Series B, Biological sciences 323, 573–88.

Shlomai, J., 2004. The structure and replication of kinetoplast DNA. Curr. Mol. Med. 4, 623–647.

Silva Pereira, S., Jackson, A.P., 2018. UDP-glycosyltransferase genes in trypanosomatid genomes have diversified independently to meet the distinct developmental needs of parasite adaptations. BMC Evol Biol 18. https://doi.org/10.1186/s12862-018-1149-6

Silvester, E., McWilliam, K.R., Matthews, K.R., 2017. The Cytological Events and Molecular Control of Life Cycle Development of *Trypanosoma brucei* in the Mammalian Bloodstream. Pathogens (Basel, Switzerland) 6. https://doi.org/10.3390/pathogens6030029

Simarro, P.P., Jannin, J., Cattand, P., 2008. Eliminating Human African Trypanosomiasis: Where Do We Stand and What Comes Next? PLOS Medicine 5, e55. https://doi.org/10.1371/journal.pmed.0050055

Simpson, R.M., Bruno, A.E., Chen, R., Lott, K., Tylec, B.L., Bard, J.E., Sun, Y., Buck, M.J., Read, L.K., 2017. Trypanosome RNA Editing Mediator Complex proteins have distinct functions in gRNA utilization. Nucleic Acids Res 45, 7965–7983. https://doi.org/10.1093/nar/gkx458

Spannagel, C., Vaillier, J., Arselin, G., Graves, P.V., Velours, J., 1997. The subunit f of mitochondrial yeast ATP synthase--characterization of the protein and disruption of the structural gene ATP17. Eur. J. Biochem. 247, 1111–1117.

Steinert, M., 1960. Mitochondria Associated with the Kinetonucleus of *Trypanosoma Mega*. J Biophys Biochem Cytol 8, 542–6.

Steinert, M., Van Assel, S., 1967. [Coordinated replication of nuclear and mitochondrial desoxyribonucleic acids in “Crithidia luciliae”]. Arch Int Physiol Biochim 75, 370–1.

Steverding, D., 2008. The history of African trypanosomiasis. Parasit Vectors 1, 3. https://doi.org/10.1186/1756-3305-1-3

Stewart, M.L., Burchmore, R.J.S., Clucas, C., Hertz-Fowler, C., Brooks, K., Tait, A., Macleod, A., Turner, C.M.R., De Koning, H.P., Wong, P.E., Barrett, M.P., 2010. Multiple genetic mechanisms lead to loss of functional TbAT1 expression in drug-resistant trypanosomes. Eukaryotic Cell 9, 336–343. https://doi.org/10.1128/EC.00200-09

Stich, A., Ponte-Sucre, A., Holzgrabe, U., 2013. Do we need new drugs against human African trypanosomiasis? Lancet Infect Dis 13, 733–4. https://doi.org/10.1016/S1473-3099(13)70191-9

Stock, D., Leslie, A.G., Walker, J.E., 1999. Molecular architecture of the rotary motor in ATP synthase. Science 286, 1700–1705.

Stuart, K.D., 1971. Evidence for the retention of kinetoplast DNA in an acriflavine-induced dyskinetoplastic strain of *Trypanosoma brucei* which replicates the altered central element of the kinetoplast. The Journal of cell biology 49, 189–95.

Surve, S., Heestand, M., Panicucci, B., Schnaufer, A., Parsons, M., 2012. Enigmatic Presence of Mitochondrial Complex I in *Trypanosoma brucei* Bloodstream Forms. Eukaryotic Cell 11, 183–193. https://doi.org/10.1128/ec.05282-11

Surve, S.V., Jensen, B.C., Heestand, M., Mazet, M., Smith, T.K., Bringaud, F., Parsons, M., Schnaufer, A., 2017. NADH dehydrogenase of *Trypanosoma brucei* is important for efficient acetate production in bloodstream forms. Mol Biochem Parasitol 211, 57–61. https://doi.org/10.1016/j.molbiopara.2016.10.001

Szöör, B., Haanstra, J.R., Gualdrón-López, M., Michels, P.A.M., 2014. Evolution, dynamics and specialized functions of glycosomes in metabolism and development of trypanosomatids. Curr. Opin. Microbiol. 22, 79–87. https://doi.org/10.1016/j.mib.2014.09.006

Szoor, B., Wilson, J., McElhinney, H., Tabernero, L., Matthews, K.R., 2006. Protein tyrosine phosphatase TbPTP1: A molecular switch controlling life cycle differentiation in trypanosomes. The Journal of cell biology 175, 293–303. https://doi.org/10.1083/jcb.200605090

Takeet, M.I., Fagbemi, B.O., De Donato, M., Yakubu, A., Rodulfo, H.E., Peters, S.O., Wheto, M., Imumorin, I.G., 2013. Molecular survey of pathogenic trypanosomes in naturally infected Nigerian cattle. Res Vet Sci 94, 555–61. https://doi.org/10.1016/j.rvsc.2012.10.018

Tasker, M., Timms, M., Hendriks, E., Matthews, K., 2001. Cytochrome oxidase subunit VI of *Trypanosoma brucei* is imported without a cleaved presequence and is developmentally regulated at both RNA and protein levels. Mol Microbiol 39, 272–285.

Taylor, J.E., Rudenko, G., 2006. Switching trypanosome coats: what's in the wardrobe? Trends Genet. 22, 614–620. https://doi.org/10.1016/j.tig.2006.08.003

Tchamdja, E., Kulo, A.E., Vitouley, H.S., Batawui, K., Bankole, A.A., Adomefa, K., Cecchi, G., Hoppenheit, A., Clausen, P.H., De Deken, R., Van Den Abbeele, J., Marcotty, T., Delespaux, V., 2017. Cattle breeding, trypanosomosis prevalence and drug resistance in Northern Togo. Veterinary parasitology 236, 86–92. https://doi.org/10.1016/j.vetpar.2017.02.008

Thomson, R., Samanovic, M., Raper, J., 2009. Activity of trypanosome lytic factor: a novel component of innate immunity. Future Microbiol 4, 789–96. https://doi.org/10.2217/fmb.09.57

Timms, M.W., van Deursen, F.J., Hendriks, E.F., Matthews, K.R., 2002. Mitochondrial development during life cycle differentiation of African trypanosomes: evidence for a kinetoplast-dependent differentiation control point. Mol. Biol. Cell 13, 3747–3759. https://doi.org/10.1091/mbc.e02-05-0266

Trikin, R., Doiron, N., Hoffmann, A., Haenni, B., Jakob, M., Schnaufer, A., Schimanski, B., Zuber, B., Ochsenreiter, T., 2016. TAC102 Is a Novel Component of the Mitochondrial Genome Segregation Machinery in Trypanosomes. PLoS pathogens 12, e1005586. https://doi.org/10.1371/journal.ppat.1005586

Trindade, S., Rijo-Ferreira, F., Carvalho, T., Pinto-Neves, D., Guegan, F., Aresta-Branco, F., Bento, F., Young, S.A., Pinto, A., Van Den Abbeele, J., Ribeiro, R.M., Dias, S., Smith, T.K., Figueiredo, L.M., 2016. *Trypanosoma brucei* Parasites Occupy and Functionally Adapt to the Adipose Tissue in Mice. Cell host & microbe 19, 837–48. https://doi.org/10.1016/j.chom.2016.05.002

Tu, X., Wang, C.C., 2004. The involvement of two cdc2-related kinases (CRKs) in *Trypanosoma brucei* cell cycle regulation and the distinctive stage-specific phenotypes caused by CRK3 depletion. J Biol Chem 279, 20519–28. https://doi.org/10.1074/jbc.M312862200

Turner, C.M., 1990. The use of experimental artefacts in African trypanosome research. Parasitology today (Personal ed.) 6, 14–7.

Tyler, K.M., Matthews, K.R., Gull, K., 2001. Anisomorphic cell division by African trypanosomes. Protist 152, 367–78. https://doi.org/10.1078/1434-4610-00074

Untergasser, A., Nijveen, H., Rao, X., Bisseling, T., Geurts, R., Leunissen, J.A.M., 2007. Primer3Plus, an enhanced web interface to Primer3. Nucleic Acids Res 35, W71–W74. https://doi.org/10.1093/nar/gkm306

Urwyler, S., Studer, E., Renggli, C.K., Roditi, I., 2007. A family of stage-specific alanine-rich proteins on the surface of epimastigote forms of *Trypanosoma brucei*. Molecular microbiology 63, 218–28. https://doi.org/10.1111/j.1365-2958.2006.05492.x

Vale, G.A., Lovemore, D.F., Flint, S., Cockbill, G.F., 1988. Odor-Baited Targets to Control Tsetse Flies, Glossina Spp (Diptera, Glossinidae), in Zimbabwe. B Entomol Res 78, 31–49. https://doi.org/10.1017/S0007485300016059

Van Den Abbeele, J., Claes, Y., van Bockstaele, D., Le Ray, D., Coosemans, M., 1999. *Trypanosoma brucei spp*. development in the tsetse fly: characterization of the post-mesocyclic stages in the foregut and proboscis. Parasitology 118 (Pt 5), 469–78.

Van den Bossche, P., Doran, M., Connor, R.J., 2000. An analysis of trypanocidal drug use in the Eastern Province of Zambia. Acta tropica 75, 247–58.

van Weelden, S.W.H., van Hellemond, J.J., Opperdoes, F.R., Tielens, A.G.M., 2005. New functions for parts of the Krebs cycle in procyclic *Trypanosoma brucei*, a cycle not operating as a cycle. J. Biol. Chem. 280, 12451–12460. https://doi.org/10.1074/jbc.M412447200

Vanhamme, L., lvanham@dbm.ulb.ac.be, Laboratory of Molecular Parasitology, I., Free University of Brussels, Rue des Professeurs Jeener et Brachet 12, B. 6041, Gosselies, Belgium, Pays, E., Laboratory of Molecular Parasitology, I., Free University of Brussels, Rue des Professeurs Jeener et Brachet 12, B. 6041, Gosselies, Belgium, McCulloch, R., Wellcome Centre for Molecular Parasitology, T.A.C., University of Glasgow, 56 Dumbarton Rd, Glasgow, UK G11 6NU, Barry, J.D., Wellcome Centre for Molecular Parasitology, T.A.C., University of Glasgow, 56 Dumbarton Rd, Glasgow, UK G11 6NU, 2001. An update on antigenic variation in African trypanosomes. Trends in Parasitology 17, 338–343. https://doi.org/10.1016/S1471-4922(01)01922-5

Vanhamme, L., Paturiaux-Hanocq, F., Poelvoorde, P., Nolan, D.P., Lins, L., Van Den Abbeele, J., Pays, A., Tebabi, P., Van Xong, H., Jacquet, A., Moguilevsky, N., Dieu, M., Kane, J.P., De Baetselier, P., Brasseur, R., Pays, E., 2003. Apolipoprotein L-I is the trypanosome lytic factor of human serum. Nature 422, 83–7. https://doi.org/10.1038/nature01461

VanHellemond, J.J., VanderMeer, P., Tielens, A.G.M., 1997. Leishmania infantum promastigotes have a poor capacity for anaerobic functioning and depend mainly on

respiration for their energy generation. Parasitology 114, 351–360. https://doi.org/10.1017/S0031182096008591

Vassella, E., Acosta-Serrano, A., Studer, E., Lee, S.H., Englund, P.T., Roditi, I., 2001a. Multiple procyclin isoforms are expressed differentially during the development of insect forms of *Trypanosoma brucei*. Journal of molecular biology 312, 597–607. https://doi.org/10.1006/jmbi.2001.5004

Vassella, E., Den Abbeele, J.V., Butikofer, P., Renggli, C.K., Furger, A., Brun, R., Roditi, I., 2000. A major surface glycoprotein of *Trypanosoma brucei* is expressed transiently during development and can be regulated post-transcriptionally by glycerol or hypoxia. Genes Dev 14, 615–26.

Vassella, E., Krämer, R., Turner, C.M., Wankell, M., Modes, C., van den Bogaard, M., Boshart, M., 2001b. Deletion of a novel protein kinase with PX and FYVE-related domains increases the rate of differentiation of *Trypanosoma brucei*. Mol. Microbiol. 41, 33–46.

Vassella, E., Probst, M., Schneider, A., Studer, E., Renggli, C.K., Roditi, I., 2004. Expression of a major surface protein of *Trypanosoma brucei* insect forms is controlled by the activity of mitochondrial enzymes. Molecular biology of the cell 15, 3986–93. https://doi.org/10.1091/mbc.E04-04-0341

Vassella, E., Reuner, B., Yutzy, B., Boshart, M., 1997. Differentiation of African trypanosomes is controlled by a density sensing mechanism which signals cell cycle arrest via the cAMP pathway. Journal of Cell Science 110, 2661–2671.

Vaughan, S., Gull, K., 2003. The trypanosome flagellum. Journal of cell science 116, 757–9.

Verner, Z., Basu, S., Benz, C., Dixit, S., Dobakova, E., Faktorova, D., Hashimi, H., Horakova, E., Huang, Z.Q., Paris, Z., Pena-Diaz, P., Ridlon, L., Tyc, J., Wildridge, D., Zikova, A., Lukes, J., 2015. Malleable Mitochondrion of *Trypanosoma brucei*. Int Rev Cel Mol Bio 315, 73–151. https://doi.org/10.1016/bs.ircmb.2014.11.001

Verner, Z., Cermáková, P., Skodová, I., Kriegová, E., Horváth, A., Lukes, J., 2011. Complex I (NADH:ubiquinone oxidoreductase) is active in but non-essential for procyclic *Trypanosoma brucei*. Mol. Biochem. Parasitol. 175, 196–200. https://doi.org/10.1016/j.molbiopara.2010.11.003

Verner, Z., Škodová, I., Poláková, S., Ďurišová-Benkovičová, V., Horváth, A., Lukeš, J., 2013. Alternative NADH dehydrogenase (NDH2): intermembrane-space-facing counterpart of

mitochondrial complex I in the procyclic *Trypanosoma brucei.* Parasitology 140, 328–337. https://doi.org/10.1017/S003118201200162X

Vickerman, K., 1978. Antigenic variation in trypanosomes. Nature 273, 613–7.

Vickerman Keith, 1965. Polymorphism and mitochondrial activity in sleeping sickness trypanosomes. Nature 208, 762. https://doi.org/10.1038/208762a0

Vincent, I.M., Creek, D., Watson, D.G., Kamleh, M.A., Woods, D.J., Wong, P.E., Burchmore, R.J., Barrett, M.P., 2010. A molecular mechanism for eflornithine resistance in African trypanosomes. PLoS pathogens 6, e1001204. https://doi.org/10.1371/journal.ppat.1001204

Vreysen, M.J., Seck, M.T., Sall, B., Bouyer, J., 2013. Tsetse flies: their biology and control using area-wide integrated pest management approaches. J Invertebr Pathol 112 Suppl, S15-25. https://doi.org/10.1016/j.jip.2012.07.026

Vreysen, M.J.B., Saleh, K.M., Ali, M.Y., Abdulla, A.M., Zhu, Z.R., Juma, K.G., Dyck, V.A., Msangi, A.R., Mkonyi, P.A., Feldmann, H.U., 2000. Glossina austeni (Diptera : Glossinidae) eradicated on the Island of Unguja, Zanzibar, using the sterile insect technique. J Econ Entomol 93, 123–135. https://doi.org/10.1603/0022-0493-93.1.123

Wang, Z., Gerstein, M., Snyder, M., 2009. RNA-Seq: a revolutionary tool for transcriptomics. Nat. Rev. Genet. 10, 57–63. https://doi.org/10.1038/nrg2484

Wedel, C., Forstner, K.U., Derr, R., Siegel, T.N., 2017. GT-rich promoters can drive RNA pol II transcription and deposition of H2A.Z in African trypanosomes. EMBO J 36, 2581–2594. https://doi.org/10.15252/embj.201695323

West, R.A., O'Doherty, O.G., Askwith, T., Atack, J., Beswick, P., Laverick, J., Paradowski, M., Pennicott, L.E., Rao, S.P.S., Williams, G., Ward, S.E., 2017. African trypanosomiasis: Synthesis & SAR enabling novel drug discovery of ubiquinol mimics for trypanosome alternative oxidase. Eur J Med Chem 141, 676–689. https://doi.org/10.1016/j.ejmech.2017.09.067

Wheeler, R.J., Gluenz, E., Gull, K., 2011. The cell cycle of Leishmania: morphogenetic events and their implications for parasite biology. Mol Microbiol 79, 647–662. https://doi.org/10.1111/j.1365-2958.2010.07479.x

WHO, 2013. . Geneva: World Health Organization.

Wiedemar, N., Graf, F.E., Zwyer, M., Ndomba, E., Kunz Renggli, C., Cal, M., Schmidt, R.S., Wenzler, T., Maser, P., 2018. Beyond immune escape: a variant surface glycoprotein causes suramin resistance in *Trypanosoma brucei*. Molecular microbiology 107, 57–67. https://doi.org/10.1111/mmi.13854

Woodward, R., Gull, K., 1990. Timing of nuclear and kinetoplast DNA replication and early morphological events in the cell cycle of *Trypanosoma brucei.* J Cell Sci 95 (Pt 1), 49–57.

Wurst, M., Robles, A., Po, J., Luu, V.-D., Brems, S., Marentije, M., Stoitsova, S., Quijada, L., Hoheisel, J., Stewart, M., Hartmann, C., Clayton, C., 2009. An RNAi screen of the RRM-domain proteins of *Trypanosoma brucei*. Mol. Biochem. Parasitol. 163, 61–65. https://doi.org/10.1016/j.molbiopara.2008.09.001

Xu, C.W., Hines, J.C., Engel, M.L., Russell, D.G., Ray, D.S., 1996. Nucleus-encoded histone H1-like proteins are associated with kinetoplast DNA in the trypanosomatid Crithidia fasciculata. Molecular and cellular biology 16, 564–76.

Yabu, Y., Takayanagi, T., 1988. Trypsin-stimulated transformation of *Trypanosoma brucei gambiense* bloodstream forms to procyclic forms in vitro. Parasitology research 74, 501–6.

Zhang, Y.K., Plattner, J.J., Easom, E.E., Zhou, Y.S., Akama, T., Bu, W., White, W.H., Defauw, J.M., Winkle, J.R., Balko, T.W., Guo, S.H., Xue, J., Cao, J.X., Zou, W.X., 2015. Discovery of an orally bioavailable isoxazoline benzoxaborole (AN8030) as a long acting animal ectoparasiticide. Bioorg Med Chem Lett 25, 5589–5593. https://doi.org/10.1016/j.bmcl.2015.10.044

Zhao, Z., Lindsay, M.E., Roy Chowdhury, A., Robinson, D.R., Englund, P.T., 2008. p166, a link between the trypanosome mitochondrial DNA and flagellum, mediates genome segregation. The EMBO journal 27, 143–54. https://doi.org/10.1038/sj.emboj.7601956

Zhu, J., Vinothkumar, K.R., Hirst, J., 2016. Structure of mammalian respiratory complex I. Nature 536, 354–358. https://doi.org/10.1038/nature19095

Zíková, A., Panigrahi, A.K., Uboldi, A.D., Dalley, R.A., Handman, E., Stuart, K., 2008. Structural and functional association of *Trypanosoma brucei* MIX protein with cytochrome c oxidase complex. Eukaryotic Cell 7, 1994–2003. https://doi.org/10.1128/EC.00204-08

Zíková, A., Verner, Z., Nenarokova, A., Michels, P.A.M., Lukeš, J., 2017. A paradigm shift: The mitoproteomes of procyclic and bloodstream *Trypanosoma brucei* are comparably complex. PLoS Pathog 13. https://doi.org/10.1371/journal.ppat.1006679

Zimmermann, H., Subota, I., Batram, C., Kramer, S., Janzen, C.J., Jones, N.G., Engstler, M., 2017. A quorum sensing-independent path to stumpy development in *Trypanosoma brucei*. PLOS Pathogens 13, e1006324. https://doi.org/10.1371/journal.ppat.1006324